

Examination of Kewaunee Cold Leg Steam Generator Tube R15C28

P. Kuchirka*, A. Madeyski, and M. Blaszkiewicz

Materials Reliability

*Waltz Mill, NSD

May 8, 1997

9709080028 970903
PDR . ADOCK 05000305
P PDR



Westinghouse STC
1310 Beulah Road
Pittsburgh, Pennsylvania 15235-5098

Examination of Kewaunee Cold Leg Steam Generator Tube R15C28


P. Kuchirka*, A. Madeyski, and M. Blaszkiewicz

Materials Reliability

*Waltz Mill, NSD

May 8, 1997

APPROVED:



D.M. Moon

Manager, Advanced Materials



Westinghouse STC
1310 Beulah Road
Pittsburgh, Pennsylvania 15235-5098

ABSTRACT

The first and second tube support plate crevice regions of cold leg Tube R15C28 from Steam Generator B of Kewaunee were examined by nondestructive and destructive examination techniques. Shallow, but extensively distributed, OD-origin intergranular corrosion was found contained in the tube support plate crevice regions of the mill annealed Alloy 600 tubing.

CONTENTS

Section	Page
ABSTRACT	iii
1. INTRODUCTION.....	1-1
2. NONDESTRUCTIVE EXAMINATION.....	2-1
2.1 Visual Data.....	2-1
2.2 Dimensional Data.....	2-2
2.3 X-ray Radiography	2-3
2.4 "UTEC" Ultrasonic Tests	2-4
2.5 Eddy Current Tests.....	2-7
3. BURST AND TENSILE TESTS.....	3-1
3.1 Burst Tests.....	3-1
3.2 Tensile Tests.....	3-2
4. DESTRUCTIVE EXAMINATION.....	4-1
4.1 Destructive Examination of the First Support Plate Crevice Region of Tube R15C28.....	4-1
4.2 Destructive Examination of the Second Support Plate Crevice Region of Tube R15C28.....	4-4
5. TUBE PROPERTIES	5-1
5.1 Sensitization Tests.....	5-1
5.2 Carbide Distribution in the Microstructure of Tube R15C28	5-1
6. DISCUSSION	6-1
6.1 Nondestructive Examination	6-1
6.2 Burst and Tensile Tests.....	6-2
6.3 Destructive Examination.....	6-2

6.4 Comparison of Field EC Data with Laboratory Destructive Examination Data.....	6-4
6.5 Tube Properties	6-4
7. CONCLUSIONS	7-1

LIST OF TABLES

	Page
2-1 Kewaunee NDE Results for Tube R15C28	2-10
3-1 Kewaunee Burst and Tensile Test Properties of Tube R15C28	3-3
4-1 Kewaunee SEM Fractographic Data for TSP Region Burst Specimens	4-9
4-2 Metallographic Data from Kewaunee Cold Leg Steam generator Tube R15C28...	4-11
5-1 Modified Huey Test Results.....	5-3
5-2 Vickers 500g Microhardness Test Results	5-4
6-1 Summary of the EDS Analyses of Surface Deposits on Tube R15C28	6-6
6-2 Comparison of Kewaunee Field EC and Laboratory DE Results for Tube R15C28	6-7

LIST OF FIGURES

- Figure 2-1 Photograph of the tubesheet top region of Tube R15C28, 0° face. Specimen 2B. Mag. 6.3X.
- Figure 2-2 Photograph of the tubesheet top region of Tube R15C28, 90° face. Specimen 2B. Mag. 6.3X.
- Figure 2-3 Photograph of the tubesheet top region of Tube R15C28, 180° face. Specimen 2B. Mag. 6.3X.
- Figure 2-4 Photograph of the tubesheet top region of Tube R15C28, 270° face. Specimen 2B. Mag. 6.3X.
- Figure 2-5 Photograph of the first support plate crevice region of Tube R15C28, 0° face. Specimen 4B. Mag. 6.3X.
- Figure 2-6 Photograph of the first support plate crevice region of Tube R15C28, 90° face. Specimen 4B. Mag. 6.3X.
- Figure 2-7 Photograph of the first support plate crevice region of Tube R15C28, 180° face. Specimen 4B. Mag. 6.3X.
- Figure 2-8 Photograph of the first support plate crevice region of Tube R15C28, 270° face. Specimen 4B. Mag. 6.3X.
- Figure 2-9 Photograph of the second support plate crevice region of Tube R15C28, 0° face. Specimen 6B. Mag. 6.3X.
- Figure 2-10 Photograph of the second support plate crevice region of Tube R15C28, 90° face. Specimen 6B. Mag. 6.3X.
- Figure 2-11 Photograph of the second support plate crevice region of Tube R15C28, 180° face. Specimen 6B. Mag. 6.3X.
- Figure 2-12 Photograph of the second support plate crevice region of Tube R15C28, 270° face. Specimen 6B. Mag. 6.3X.

- Figure 2-13 OD dimensional data obtained by laser micrometry of the tubesheet top region of Tube R15C28, showing radial data as a function of axial and circumferential position.
- Figure 2-14 OD dimensional data obtained by laser micrometry of the tubesheet top region of Tube R15C28, showing radial data as a function of axial and circumferential position, in form of a contour map.
- Figure 2-15 OD dimensional data obtained by laser micrometry of the tubesheet top region of Tube R15C28, showing diametrical data as a function of axial position, with circumferential information compressed.
- Figure 2-16 OD dimensional data obtained by laser micrometry of the first tube support plate region of Tube R15C28, showing radial data as a function of axial and circumferential position.
- Figure 2-17 OD dimensional data obtained by laser micrometry of the first tube support plate region of Tube R15C28, showing radial data as a function of axial and circumferential position, in form of a contour map.
- Figure 2-18 OD dimensional data obtained by laser micrometry of the first tube support plate region of Tube R15C28, showing diametrical data as a function of axial position, with circumferential information compressed.
- Figure 2-19 OD dimensional data obtained by laser micrometry of the second tube support plate region of Tube R15C28, showing radial data as a function of axial and circumferential position.
- Figure 2-20 OD dimensional data obtained by laser micrometry of the second tube support plate region of Tube R15C28, showing radial data as a function of axial and circumferential position, in form of a contour map.
- Figure 2-21 OD dimensional data obtained by laser micrometry of the second tube support plate region of Tube R15C28, showing diametrical data as a function of axial position, with circumferential information compressed.
- Figure 2-22 Typical display of UTEC ultrasonic test data. This is NOT a Kewaunee tube test result, but a figure used to explain the UTEC display system.
- Figure 2-23 Ultrasonic test UTEC display of the radial aim data obtained on the UT calibration standard, showing the flat bottom hole centered in the cruciform-shaped notch.

Figure 2-38 TSP1 crevice region of Tube R15C28. **Field** 3-coil probe circumferentially sensitive coil eddy current test data.....

Figure 2-39 TSP1 crevice region of Tube R15C28. **Field** 3-coil probe axially sensitive coil eddy current test data.....

Figure 2-40 TSP2 (second tube support plate) crevice region of Tube R15C28. **Field** bobbin probe eddy current test data.....

Figure 2-41 TSP2 crevice region of Tube R15C28. **Field** 3-coil probe pancake coil eddy current test data.....

Figure 2-42 TSP2 crevice region of Tube R15C28. **Field** 3-coil probe circumferentially sensitive coil eddy current test data.....

Figure 2-43 TSP2 crevice region of Tube R15C28. **Field** 3-coil probe axially sensitive coil eddy current test data.....

Figure 2-44 TST (tubesheet top) region of Tube R15C28. **Laboratory** bobbin probe eddy current test data.....

Figure 2-45 TST region of Tube R15C28. **Laboratory** 3-coil probe pancake coil eddy current test data.....

Figure 2-46 TST region of Tube R15C28. **Laboratory** +Point probe eddy current test data.....

Figure 2-47 TST region of Tube R15C28. **Laboratory** Cecco 5 probe eddy current test data strip chart.....

Figure 2-48 TSP1 (first tube support plate) crevice region of Tube R15C28. **Laboratory** bobbin probe eddy current test data.....

Figure 2-49 TSP1 crevice region of Tube R15C28. **Laboratory** bobbin probe eddy current test data.....

Figure 2-50 TSP1 crevice region of Tube R15C28. **Laboratory** 3-coil probe pancake coil eddy current test data.....

Figure 2-51 TSP1 crevice region of Tube R15C28. **Laboratory** 3-coil probe circumferentially sensitive coil eddy current test data.....

Figure 2-52 TSP1 crevice region of Tube R15C28. **Laboratory** 3-coil probe axially sensitive coil eddy current test data.....

Figure 2-24 Ultrasonic test UTEC display of the circumferential aim data obtained on the UT calibration standard, showing the axial notch and the edge of the flat bottom hole centered in the cruciform-shaped notch.....

Figure 2-25 Ultrasonic test UTEC display of the axial aim data obtained on the UT calibration standard, showing the circumferential notch and the edge of the flat bottom hole centered in the cruciform-shaped notch.....

Figure 2-26 Ultrasonic test UTEC display of the radial aim data obtained on the tubesheet top region of Tube R15C28.

Figure 2-27 Ultrasonic test UTEC display of the circumferential aim data obtained on the tubesheet top region of Tube R15C28.....

Figure 2-28 Ultrasonic test UTEC display of the axial aim data obtained on the tubesheet top region of Tube R15C28.

Figure 2-29 Ultrasonic test UTEC display of the radial aim data obtained on the first support plate crevice region of Tube R15C28.....

Figure 2-30 Ultrasonic test UTEC display of the circumferential aim data obtained on the first support plate crevice region of Tube R15C28.

Figure 2-31 Ultrasonic test UTEC display of the axial aim data obtained on the first support plate crevice region of Tube R15C28.....

Figure 2-32 Ultrasonic test UTEC display of the radial aim data obtained on the second support plate crevice region of Tube R15C28.....

Figure 2-33 Ultrasonic test UTEC display of the circumferential aim data obtained on the second support plate crevice region of Tube R15C28.....

Figure 2-34 Ultrasonic test UTEC display of the axial aim data obtained on the second support plate crevice region of Tube R15C28.....

Figure 2-35 TST (tubesheet top) region of Tube R15C28. **Field** bobbin probe eddy current test data.....

Figure 2-36 TSP1 (first tube support plate) crevice region of Tube R15C28. **Field** bobbin probe eddy current test data.

Figure 2-37 TSP1 crevice region of Tube R15C28. **Field** 3-coil probe pancake coil eddy current test data.....

- Figure 3-3 TSP1 crevice region Specimen 4B of Tube R15C28. Appearance of the 180° face after the burst test. Mag. 3X.....
- Figure 3-4 TSP1 crevice region Specimen 4B of Tube R15C28. Appearance of the 315° face after the burst test. Mag. 3X.....
- Figure 3-5 TSP2 crevice region Specimen 6B of Tube R15C28. Appearance of the 135° face after the burst test. Mag. 2.5X.....
- Figure 3-6 TSP2 crevice region Specimen 6B of Tube R15C28. Appearance of the 70° face after the burst test. Mag. 3X.....
- Figure 3-7 TSP2 crevice region Specimen 6B of Tube R15C28. Appearance of the 200° face after the burst test. Mag. 3X.....
- Figure 3-8 TSP2 crevice region Specimen 6B of Tube R15C28. Appearance of the 270° face after the burst test. Mag. 3X.....
- Figure 3-9 TSP2 crevice region Specimen 6B of Tube R15C28. Appearance of the 340° face after the burst test. Mag. 3X.....
- Figure 3-10 TSP1 crevice region Specimen 4B of Tube R15C28. Sketch showing the location of the burst opening and the approximate distribution of the small cracks. ...
- Figure 3-11 TSP2 crevice region Specimen 6B of Tube R15C28. Sketch showing the location of the burst opening and the approximate distribution of the small cracks. ...
- Figure 4-1 TSP1 crevice region Specimen 4B of Tube R15C28. Sketch showing the locations of the fractographic and metallographic samples used in the study of the crack distribution and morphology.
- Figure 4-2 TSP1 crevice region Specimen 4B-2D of Tube R15C28. Top view of the opened burst fracture. Areas 2 through 6 of the fracture are shown at higher magnifications in Figures 4-3 through 4-5. Areas 5 and 6 mark the ends of the intergranular corrosion cracking on the OD which started the burst fracture.....
- Figure 4-3 TSP1 crevice region Specimen 4B-2D of Tube R15C28. Areas 2 and 3 from Figure 4-2, showing the topography of the burst fracture at the location of the deepest corrosion penetration (30% throughwall).....

Figure 2-53 TSP1 crevice region of Tube R15C28. Laboratory +Point probe eddy current test data.....

Figure 2-54 TSP1 crevice region of Tube R15C28. Laboratory Cecco 5 probe eddy current test data Lissajous patterns.....

Figure 2-55 TSP1 crevice region of Tube R15C28. Laboratory Cecco 5 probe eddy current test data strip chart.

Figure 2-56 TSP2 (second tube support plate) crevice region of Tube R15C28. Laboratory bobbin probe eddy current test data.....

Figure 2-57 TSP2 crevice region of Tube R15C28. Laboratory bobbin probe eddy current test data.....

Figure 2-58 TSP2 crevice region of Tube R15C28. Laboratory 3-coil probe pancake coil eddy current test data.....

Figure 2-59 TSP2 crevice region of Tube R15C28. Laboratory 3-coil probe circumferentially sensitive coil eddy current test data.....

Figure 2-60 TSP2 crevice region of Tube R15C28. Laboratory 3-coil probe axially sensitive coil eddy current test data.....

Figure 2-61 TSP2 crevice region of Tube R15C28. Laboratory +Point probe eddy current test data.....

Figure 2-62 TSP2 crevice region of Tube R15C28. Laboratory +Point probe eddy current test data.....

Figure 2-63 TSP2 crevice region of Tube R15C28. Laboratory Cecco 5 probe eddy current test data Lissajous patterns.....

Figure 2-64 TSP2 crevice region of Tube R15C28. Laboratory Cecco 5 probe eddy current test data strip chart.

Figure 3-1 FS (control) Specimen 5B of Tube R15C28. Appearance of the 345° face after the burst test. Mag. 2X.....

Figure 3-2 TSP1 (first tube support plate) crevice region Specimen 4B of Tube R15C28. Appearance of the 225° face after the burst test. Mag. 2.5X.....

- Figure 4-13 TSP1 crevice region Specimen 4B-2C of Tube R15C28. Radial metallographic sample after flattening and polishing to a depth of 0.001 inch below the OD surface. Mount M2161. Mag. 3.25X.
- Figure 4-14 TSP1 crevice region Specimen 4B-2C of Tube R15C28. Radial metallographic sample after flattening and polishing to a depth of 0.001 inch below the OD surface. This montage is a higher magnification mirror image of Figure 4-13 because of the reversed optics of the two cameras. Mount M2161. Mag. 16X.....
- Figure 4-15 TSP1 crevice region Specimen 4B-2C of Tube R15C28. Radial metallographic sample after flattening and polishing to a depth of 0.001 inch below the OD surface. Examples of the corrosion crack pattern at this level of grinding and polishing. Mount M2161. Mag. 100X.....
- Figure 4-16 TSP1 crevice region Specimen 4B-2C of Tube R15C28. Radial metallographic sample after flattening and polishing to a depth of 0.001 inch below the OD surface. Examples of the corrosion crack pattern at this level of grinding and polishing. Mount M2161. Mag. 100X.....
- Figure 4-17 TSP1 crevice region Specimen 4B-2C of Tube R15C28. Radial metallographic sample after flattening and polishing to a depth of 0.001 inch below the OD surface. Examples of the corrosion crack pattern at this level of grinding and polishing. Mount M2161. Mag. 100X.....
- Figure 4-18 TSP1 crevice region Specimen 4B-2C of Tube R15C28. Radial metallographic sample after flattening and polishing to a depth of 0.005 inch below the OD surface. Mount M2161. Mag. 3.25X.
- Figure 4-19 TSP1 crevice region Specimen 4B-2C of Tube R15C28. Radial metallographic sample after flattening and polishing to a depth of 0.005 inch below the OD surface. This montage is a higher magnification mirror image of Figure 4-18 because of the reversed optics of the two cameras. Mount M2161. Mag. 16X.....
- Figure 4-20 TSP1 crevice region Specimen 4B-2C of Tube R15C28. Radial metallographic sample after flattening and polishing to a depth of 0.005 inch below the OD surface. Examples of the corrosion crack pattern at this level of grinding and polishing. Mount M2161. Mag. 100X.....
- Figure 4-21 TSP1 crevice region Specimen 4B-2C of Tube R15C28. Radial metallographic sample after flattening and polishing to a depth of 0.005 inch below the OD surface. Examples of the corrosion crack pattern at this level of grinding and polishing. Mount M2161. Mag. 100X.....

- Figure 4-4 TSP1 crevice region Specimen 4B-2D of Tube R15C28. Upper photograph: Area 4 from Figure 4-3 showing the boundary between the field corrosion crack at the point of deepest penetration and the laboratory fracture produced during the burst test. Lower photograph: Area 5 from Figure 4-2 showing the left end of field corrosion cracking on the burst test fracture.
- Figure 4-5 TSP1 crevice region Specimen 4B-2D of Tube R15C28. Area 6 from Figure 4-2 showing the right end of field corrosion cracking on the burst test fracture.
- Figure 4-6 TSP1 crevice region Specimen 4B-2D of Tube R15C28. Side view of the opened burst fracture showing OD corrosion cracks opened wider by the burst test. Area 7 on the OD surface is shown at progressively higher magnifications in Figures 4-7 through 4-9.
- Figure 4-7 TSP1 crevice region Specimen 4B-2D of Tube R15C28. Side view of the opened burst fracture showing OD corrosion cracks opened wider by the burst test. Area 7 on the OD surface from Figure 4-6, shown at a higher magnification.
- Figure 4-8 TSP1 crevice region Specimen 4B-2D of Tube R15C28. Side view of the opened burst fracture showing OD corrosion cracks opened wider by the burst test. Area 7 on the OD surface from Figure 4-6, shown at a higher magnification. Upper photograph: reflected electron image. Lower photograph: backscattered electron image of the same area.
- Figure 4-9 TSP1 crevice region Specimen 4B-2D of Tube R15C28. Side view of the opened burst fracture showing OD corrosion cracks opened wider by the burst test. Area 7 on the OD surface from Figure 4-6, shown at a higher magnification. Upper photograph: reflected electron image. Lower photograph: backscattered electron image of the same area.
- Figure 4-10 TSP1 crevice region Specimen 4B-2D of Tube R15C28. Side view of the opened burst fracture showing OD corrosion cracks opened wider by the burst test. Higher magnification photograph of Area 7 on the OD surface from Figure 4-6, showing the locations of Spots 1 and 2 which were analyzed using the energy dispersive X-ray spectroscopy (EDS) technique. The results of the analyses are shown in Figures 4-11 and 4-12.
- Figure 4-11 TSP1 crevice region Specimen 4B-2D of Tube R15C28. Results of the EDS analysis of Spot 1, Figure 4-10, on the OD surface at Area 7 from Figure 4-6.
- Figure 4-12 TSP1 crevice region Specimen 4B-2D of Tube R15C28. Results of the EDS analysis of Spot 2, Figure 4-10, on the OD surface at Area 7 from Figure 4-6.

Figure 4-22 TSP1 crevice region Specimen 4B-2C of Tube R15C28. Radial metallographic sample after flattening and polishing to a depth of 0.005 inch below the OD surface. Examples of the corrosion crack pattern at this level of grinding and polishing. Mount M2161. Mag. 100X.....

Figure 4-23 TSP1 crevice region Specimen 4B-2C of Tube R15C28. Radial metallographic sample after flattening and polishing to a depth of 0.010 inch below the OD surface. Mount M2161. Mag. 3.25X.

Figure 4-24 TSP1 crevice region Specimen 4B-2C of Tube R15C28. Radial metallographic sample after flattening and polishing to a depth of 0.010 inch below the OD surface. This montage is a higher magnification mirror image of Figure 4-23 because of the reversed optics of the two cameras. Mount M2161. Mag. 16X.....

Figure 4-25 TSP1 crevice region Specimen 4B-2C of Tube R15C28. Radial metallographic sample after flattening and polishing to a depth of 0.010 inch below the OD surface. Examples of the corrosion crack pattern at this level of grinding and polishing. Mount M2161. Mag. 100X.....

Figure 4-25 TSP1 crevice region Specimen 4B-2C of Tube R15C28. Radial metallographic sample after flattening and polishing to a depth of 0.010 inch below the OD surface. Example of the corrosion crack pattern at this level of grinding and polishing. Mount M2161. Mag. 100X.....

Figure 4-27 TSP1 crevice region Specimen 4B-2C of Tube R15C28. Radial metallographic sample after flattening and polishing to a depth of 0.015 inch below the OD surface. Note the absence of cracks at this level. Mount M2161. Mag. 3.25X.....

Figure 4-28 TSP1 crevice region Specimen 4B-2B of Tube R15C28. Transverse metallographic sample. Areas A through E are shown at a higher magnification in Figures 4-29 through 4-31. Mount M2160. Mag. 3.25X.....

Figure 4-29 TSP1 crevice region Specimen 4B-2B of Tube R15C28. Transverse metallographic sample. Areas A and B from Figure 4-28 showing OD surface cracks at a higher magnification. Mount M2160. Mag. 100X.....

Figure 4-30 TSP1 crevice region Specimen 4B-2B of Tube R15C28. Transverse metallographic sample. Areas C and D from Figure 4-28 showing OD surface cracks at a higher magnification. Mount M2160. Mag. 100X.....

Figure 4-31 TSP1 crevice region Specimen 4B-2B of Tube R15C28. Transverse metallographic sample. Area E from Figure 4-28 showing OD surface cracks at a higher magnification. Mount M2160. Mag. 100X.....

- Figure 4-32 TSP2 crevice region Specimen 6B of Tube R15C28. Sketch showing the locations of the fractographic and metallographic samples used in the study of the crack distribution and morphology.
- Figure 4-33 TSP2 crevice region Specimen 6B-2A of Tube R15C28. Top view of the opened burst fracture. Areas 2 through 6 of the fracture are shown at higher magnifications in Figures 4-34 through 4-36. Areas 5 and 6 mark the ends of the intergranular corrosion cracking on the OD which started the burst fracture.
- Figure 4-34 TSP2 crevice region Specimen 6B-2A of Tube R15C28. Areas 2 and 3 from Figure 4-33, showing the topography of the burst fracture at the location of the deepest corrosion penetration (31% throughwall).....
- Figure 4-35 TSP2 crevice region Specimen 6B-2A of Tube R15C28. Upper photograph: Area 4 from Figure 4-34 showing the boundary between the field corrosion crack at the point of deepest penetration and the laboratory fracture produced during the burst test. Lower photograph: Area 5 from Figure 4-33 showing the left end of field corrosion cracking on the burst test fracture.
- Figure 4-36 TSP2 crevice region Specimen 6B-2A of Tube R15C28: Area 6 from Figure 4-33 showing the right end of field corrosion cracking on the burst test fracture.
- Figure 4-37 TSP2 crevice region Specimen 6B-2A of Tube R15C28. Side view of the opened burst fracture showing OD corrosion cracks opened wider by the burst test. Areas 7 and 9 on the OD surface are shown at progressively higher magnifications in Figures 4-38 through 4-40.....
- Figure 4-38 TSP2 crevice region Specimen 6B-2A of Tube R15C28. Side view of the opened burst fracture showing OD corrosion cracks opened wider by the burst test. Areas 7 and 9 on the OD surface from Figure 4-37, shown at a higher magnification.50
- Figure 4-39 TSP2 crevice region Specimen 6B-2A of Tube R15C28. Side view of the opened burst fracture showing OD corrosion cracks opened wider by the burst test. Areas 7 and 9 on the OD surface from Figure 4-37 shown at a higher magnification. Upper photograph: reflected electron image. Lower photograph: backscattered electron image of the same area.....
- Figure 4-40 TSP2 crevice region Specimen 6B-2A of Tube R15C28. Side view of the opened burst fracture showing OD corrosion cracks opened wider by the burst test. Areas 7 and 9 on the OD surface from Figure 4-37, shown at a higher magnification. Upper photograph: reflected electron image. Lower photograph: backscattered electron image of the same area.....

Figure 4-41 TSP2 crevice region Specimen 6B-2A of Tube R15C28. Side view of the opened burst fracture showing OD corrosion cracks opened wider by the burst test. Higher magnification photographs of Areas 7 and 9 on the OD surface from Figure 4-37, showing the locations of Spots 1, 2, and 3 which were analyzed using the energy dispersive X-ray spectroscopy (EDS) technique. The results of the analyses are shown in Figures 4-42, 4-43, and 4-44.....

Figure 4-42 TSP2 crevice region Specimen 6B-2A of Tube R15C28. Results of the EDS analysis of Spot 1, Figure 4-41, on the OD surface at Area 9 from Figure 4-37.

Figure 4-43 TSP2 crevice region Specimen 6B-2A of Tube R15C28. Results of the EDS analysis of Spot 2, Figure 4-41, on the OD surface next to Area 9 from Figure 4-37.....

Figure 4-44 TSP2 crevice region Specimen 6B-2A of Tube R15C28. Results of the EDS analysis of Spot 3, Figure 4-41, on the OD surface at Area 7 from Figure 4-37.

Figure 4-45 TSP2 crevice region Specimen 6B-2D of Tube R15C28. Radial metallographic sample after flattening and polishing to a depth of 0.001 inch below the OD surface. Mount M2163. Mag. 3.25X.

Figure 4-46 TSP2 crevice region Specimen 6B-2D of Tube R15C28. Radial metallographic sample after flattening and polishing to a depth of 0.001 inch below the OD surface. This montage is a higher magnification mirror image of Figure 4-45 because of the reversed optics of the two cameras. Mount M2163. Mag. 16X.....

Figure 4-47 TSP2 crevice region Specimen 6B-2D of Tube R15C28. Radial metallographic sample after flattening and polishing to a depth of 0.001 inch below the OD surface. Examples of the corrosion crack pattern at this level of grinding and polishing. Mount M2163. Mag. 100X.....

Figure 4-48 TSP2 crevice region Specimen 6B-2D of Tube R15C28. Radial metallographic sample after flattening and polishing to a depth of 0.001 inch below the OD surface. Examples of the corrosion crack pattern at this level of grinding and polishing. Mount M2163. Mag. 100X.....

Figure 4-49 TSP2 crevice region Specimen 6B-2D of Tube R15C28. Radial metallographic sample after flattening and polishing to a depth of 0.001 inch below the OD surface. Examples of the corrosion crack pattern at this level of grinding and polishing. Mount M2163. Mag. 100X.....

Figure 4-50 TSP2 crevice region Specimen 6B-2D of Tube R15C28. Radial metallographic sample after flattening and polishing to a depth of 0.005 inch below the OD surface. Mount M2163. Mag. 3.25X.

Figure 4-51 TSP2 crevice region Specimen 6B-2D of Tube R15C28. Radial metallographic sample after flattening and polishing to a depth of 0.005 inch below the OD surface. This montage is a higher magnification mirror image of Figure 4-50 because of the reversed optics of the two cameras. Mount M2163. Mag. 16X.....

Figure 4-52 TSP2 crevice region Specimen 6B-2D of Tube R15C28. Radial metallographic sample after flattening and polishing to a depth of 0.005 inch below the OD surface. Examples of the corrosion crack pattern at this level of grinding and polishing. Mount M2163. Mag. 100X.....

Figure 4-53 TSP2 crevice region Specimen 6B-2D of Tube R15C28. Radial metallographic sample after flattening and polishing to a depth of 0.005 inch below the OD surface. Example of the corrosion crack pattern at this level of grinding and polishing. Mount M2163. Mag. 100X.....

Figure 4-54 TSP2 crevice region Specimen 6B-2D of Tube R15C28. Radial metallographic sample after flattening and polishing to a depth of 0.010 inch below the OD surface. Note the absence of cracks. Mount M2163. Mag. 3.25X.....

Figure 4-55 TSP2 crevice region Specimen 6B-2C of Tube R15C28. Transverse metallographic sample. Areas A through I are shown at a higher magnification in Figures 4-56 through 4-60. Mount M2162. Mag. 3.25X.....

Figure 4-56 TSP2 crevice region Specimen 6B-2C of Tube R15C28. Transverse metallographic sample. Areas A and B from Figure 4-55 showing OD surface cracks at a higher magnification. Mount M2162. Mag. 100X.....

Figure 4-57 TSP2 crevice region Specimen 6B-2C of Tube R15C28. Transverse metallographic sample. Areas C and D from Figure 4-55 showing OD surface cracks at a higher magnification. Mount M2162. Mag. 100X.....

Figure 4-58 TSP2 crevice region Specimen 6B-2C of Tube R15C28. Transverse metallographic sample. Areas E and F from Figure 4-55 showing OD surface cracks at a higher magnification. Mount M2162. Mag. 100X.....

Figure 4-59 TSP2 crevice region Specimen 6B-2C of Tube R15C28. Transverse metallographic sample. Areas G and H from Figure 4-55 showing OD surface cracks at a higher magnification. Mount M2162. Mag. 100X.....

Figure 4-60 TSP2 crevice region Specimen 6B-2C of Tube R15C28. Transverse metallographic sample. Area I from Figure 4-55 showing OD surface cracks at a higher magnification. Mount M2162. Mag. 100X.....

Figure 5-1 SEM photomicrographs showing the microstructure and carbide distribution of Tube R15C28. Mount M2146. Mag. 1000X.....

Figure 5-2 Higher magnification SEM photomicrographs showing the microstructure and carbide distribution of Tube R15C28. Mount M2146. Mag. 2020X.....

Figure 5-3 SEM photomicrographs showing the microstructure and carbide distribution of Tube R15C28. Mount M2146. Upper photomicrograph: Mag. 1000X. Lower photomicrograph: Mag. 2020X.....

INTRODUCTION

The Kewaunee Nuclear Power Plant Unit 1 of the Wisconsin Public Service Corporation has been in operation since March 1974. The primary to secondary side heat transfer in this plant occurs in two steam generators, A and B, that are of the Model 51 type manufactured by the Westinghouse Electric Corporation. The mill-annealed Alloy 600 steam generator tubes are nominally 0.875 inch in diameter, and have a wall thickness of 0.050 inch. The U-shaped tubes were mechanically expanded into the bottom 2.5 inches of the 21.2 inch thick tube sheet after passing through seven 0.75 inch thick tube support plates (TSPs). A bottom seal weld was made between each tube and the tubesheet bottom at both the hot and cold leg sides of the tubesheet. Forty nine and three quarters inches above the tubesheet top (TST) is the first tube support plate (TSP1). Similarly, the bottom of the second tube support plate, TSP2, is located 49.75 inches above the top of the TSP1. The nominal TSP hole is 0.893 inch in diameter, creating a 0.018 inch diametrical gap between the tube and the tube support plate.

The secondary side environment of the steam generators has used an all volatile treatment (AVT) water chemistry since the end of 1974. Note, however, that the plant started operation with a secondary side phosphate water treatment in March 1974. Boric acid was added to the secondary side water to act as a denting and stress corrosion cracking (SCC) inhibitor in 1988. (The first indication of SCC at TST and TSP hot leg crevice locations, along with minor denting, was observed in 1983).

During recent examinations, some steam generator tube support plate crevice locations had field eddy current indications suggestive of OD origin volumetric corrosion on the cold leg side of the steam generator B. To further characterize the probable corrosion at these locations, it was decided during the October 1966 outage to pull the first and the second cold leg support plate (TSP1 and TSP2) crevice regions of Tube R15C28 from steam generator (S/G) B. These locations had field eddy current signals indicating probable volumetric corrosion on the OD of the tube.

The removed tube specimens (including also the TST region) were sent to the Remote Metallographic Facility of the Westinghouse Science and Technology Center (STC) for examinations and tests, both nondestructive and destructive. The nondestructive evaluation (NDE) included visual, dimensional, eddy current (EC), ultrasonic (UT), and radiographic examinations and tests. The nondestructive portion of the investigation was followed by burst tests and tensile tests. No leak testing was performed because all the NDE indications were too shallow to produce any possible leakage. The burst

tested specimens were then fractographically examined with a scanning electron microscope (SEM). Deposits and oxides on the fractures and on the OD surfaces were analyzed using the energy-dispersive X-ray spectroscopy (EDS) technique, to help identify the local chemical environment. Metallographic specimens were also prepared and examined, to determine the microstructure of the tube material and the extent of the corrosion. In addition, a hardness test, an examination of the carbide distribution within the matrix, and a modified Huey test for sensitization were performed.

All the examinations and tests of this investigations were performed following required Quality Assurance (QA) provisions. Westinghouse STC provided products and services according to the Westinghouse Energy Systems Business Unit Quality Management System. This system meets the requirements of the United States Nuclear Regulatory Commission related to quality control and quality assurance, including the requirements set forth in 10 C.F.R. 50, Appendix B, and the standards set forth in ISO 9001. The STC QA files for this Kewaunee program are contained in the STC Data File 8TC5-KWCLD.

The following report describes the examinations and tests, and their results, as well as discusses the data obtained.

NONDESTRUCTIVE EXAMINATION

The total length of the cold leg portion of Tube R15C28 pulled from Steam Generator B was approximately 168.43 inches. This portion was cut¹ into 7 pieces with the following lengths:

- Pc. #1 10.62"
- Pc. #2 25.25" included tubesheet top (TST) region
- Pc. #3 22.50"
- Pc. #4 26.25" included first tube support plate (TSP1) region
- Pc. #5 29.50"
- Pc. #6 25.56" included second tube support plate (TSP2) region
- Pc. #7 28.00"

The pieces were submitted to the Westinghouse Remote Metallographic Facility for examination and tests. These pieces were subsequently cut into smaller specimens for individual tests. The designation of every specimen includes the number of the original piece. For instance, specimen 2B was cut from piece #2. In the following description of the tube specimens, 0° of each specimen faces the divider plate, and 90° is *clockwise* of 0° when looking in the downward (primary flow) direction. Unless otherwise stated, this orientation system is used throughout the report.

2.1 VISUAL DATA

After initial inspection of the tubes in the Hot Cells, which determined the locations of the tubesheet top (TST) and of the tube support plate (TSP) crevice regions, the pieces were cut and photographed to document the general condition of the oxides and of the surface deposits. Figures 2-1 through 2-12 show the crevice regions with deposits on the tube at the 0°, 90°, 180°, and 270° faces.

¹ The width of every one of the 6 cuts was approximately 0.125", with a total of about 0.75".

2.1.1 Surface Appearance of the TST Region (Specimen 2B)

The tubesheet top region of Tube R15C28 is shown in Figures 2-1 through 2-4. The deposit/oxide film "bathtub ring" that marks the TST location is clearly visible. The patchy deposits in the top part of the tubesheet crevice were mostly gray to black. The deposits were apparently not very thick, because the polishing marks on the tube OD surface are visible in many islands among the deposit patches, and even in some deposit areas (e.g., Figure 2-1, 0° face). The tube surface above the TST showed some non-uniformly distributed, thin, gray colored, deposits, with occasional white spots, and some evidence of smearing in the tube pulling process (e.g., Figure 2-4, 270° face).

2.1.2 Surface Appearance of the TSP1 Crevice Region (Specimen 4B)

The first tube support plate crevice region of Tube R15C28 is illustrated in Figures 2-5 through 2-8. The location of the TSP1 is reasonably well delineated by a mostly thin, grayish-brown, deposit, showing evidence of abrasion and smearing in the tube pulling process. The tube polishing marks are visible in many areas. However, in other areas the deposit is thicker and heavily spalled, revealing relatively clean tube surface underneath (e.g., Figures 2-5 and 2-6, 0° and 90° faces, respectively). The OD surface areas outside the TSP1 crevice show occasional scratches from the tube pulling (e.g., Figure 2-5, 0° face). Some of the scratches may be also seen within the TSP1 ring (e.g., Figure 2-7, 180° face).

2.1.3 Surface Appearance of the TSP2 Crevice Region (Specimen 6B)

The second tube support plate crevice region of Tube R15C28 may be seen in Figures 2-9 through 2-12. Again, the location of the crevice ring on the tube surface is reasonably well defined. The grayish-brown deposit at TSP2 is similar to slightly thicker than at TSP1. There are fewer areas showing the tube polishing marks. Some areas have occasional white spots (e.g., Figure 2-10, 90° face). Long scratches are visible on the 270° face, Figure 2-12. The areas outside the TSP2 crevice appear to have relatively thick deposits.

2.2 DIMENSIONAL DATA

OD laser micrometry was performed on the three crevice regions, TST, TSP1, and TSP2, to characterize the tube dimensionally. In interpreting the results of these measurements it must be remembered that tube pulling operations frequently introduce into the tube dings and dents at the tubesheet and tube support plate locations that can be misleading when assessing the laboratory micrometry test data. Geometrical variations at these locations should be trusted only if the field bobbin probe eddy current data indicate that such variations were present prior to the tube pull. The effect

of surface deposits of variable thickness must be also considered. In the case of the Kewaunee Tube R15C28, the OD dimensional characterization by laser micrometry suggested that 0.001 to 0.002 inch dents existed at the top edge of the TSP1 region and at the bottom edge of the TSP2 region. However, the field NDE results indicated that these dents were not present prior to the tube pull. Furthermore, the surface deposits in the two TSP regions were heavily spalled, presumably due to the tube pull, which also affected the laser micrometry data.

Figures 2-13 through 2-21 present plots of the OD laser micrometry data for the TST, TSP1, and TSP2 regions. The raw data were in the form of radial distance from a mathematically averaged centerline of the tube section. For any given location, the data are presented in the following manner: the first figure shows the radial data in the form of a three dimensional plot of the tube radius versus axial position versus circumferential position; the second figure presents a two dimensional plot of the same data as a contour map (this form is best for revealing the presence of uneven surface deposits and spalling); the third figure is a "compressed" two dimensional plot of the tube diameter (with an expanded scale) versus the axial position, which can clearly reveal possible presence of local dents in the tube.

2.2.1 Dimensional Data for the TST Region

Figures 2-13 through 2-15 present the radial laser profilometry data for the tubesheet top region of Tube R15C28.

2.2.2 Dimensional Data for the TSP1 Region

Figures 2-16 through 2-18 present the radial laser profilometry data for the first tube support plate region of Tube R15C28.

2.2.3 Dimensional Data for the TSP2 Region

Figures 2-19 through 2-21 present the radial laser profilometry data for the second tube support plate region of Tube R15C28.

2.3 X-RAY RADIOGRAPHY

X-ray radiography was performed on the Specimens 2B, 4B, and 6B, representing the tubesheet top region, first tube support plate crevice region, and second tube support plate crevice region, respectively. No radiographic indications were detected, suggesting that the cracking was still relatively tightly bound.

2.4 "UTEC" ULTRASONIC TESTS

The Westinghouse NDE Center, located at the Science and Technology Center, performed multiple element ultrasonic tests (UT) of Tube R15C28 at the tubesheet top region (Specimen 2B), first tube support plate region (Specimen 4B), and second tube support plate region (Specimen 6B). The examinations were made at the Remote Metallographic Laboratory, using field worthy UTEC transducers, instrumentation, and techniques, including acquisition and display software.

2.4.1 *Ultrasonic Inspection System*

The UTEC probe has three individually focused UT transducer elements, mounted in a single body along with a Rotating Pancake Coil (RPC) eddy current probe. The first UT transducer is a high frequency, spherically focused element, which directs sound in the radial direction. This transducer is used for attenuation measurements and to detect thickness changes characteristic of pitting or wall loss damage. The second transducer is a cylindrically focused search unit which directs sound around the circumference of the tube, and is sensitive to discontinuities oriented in the radial-axial direction. The third transducer is spherically focused and directs sound energy along the tube axis at a 45 degree angle. This search unit is particularly sensitive to flaws oriented in the radial-circumferential direction.

2.4.2 *Ultrasonic Data Acquisition and Display*

The ultrasonic transducers are interfaced to field style ultrasonic instrumentation. A Sonic (Stavely) ultrasonic instrument, consisting of three stacked Mark IIs, comprises the electronic package. Gated signal responses are captured, along with position information, by the computer data acquisition package.

The data acquisition system consists of a motor driven probe scanner equipped with a rotary encoder. A lead screw is used to accurately move the probe over a 5 inch axial inspection path. The screw is connected to an axial encoder which provides position information with respect to the transducers. A rotation speed of about 20 RPM is used during the examination. The encoders and ultrasonic gates are connected to a Gateway 2000 computer which is used to both gather and display the ultrasonic data. Data acquisition software gathers gated UT information every one degree (0.006 inch) around the tube circumference from every transducer, as well as the angular and the axial positions where the data were gathered.

Once the data are captured, they are graphically displayed, showing angular position, axial position, and signal amplitude. Data from every transducer element are displayed separately for evaluation. To enhance signal interpretation, color plots of signal amplitude can be made at different color levels. The display of the UTEC system for the

ultrasonic data consists of five image areas, as illustrated in Figure 2-22¹. These areas permit the ultrasonic data to be simultaneously viewed in three different fashions, to achieve optimum data analysis.

The first display mode, shown in Area 1 in Figure 2-22, is the ultrasonic "a-scan". This is a time-amplitude plot of the ultrasonic response. This constitutes the "raw" data from which the remaining display images are constructed. The data for one of these images are stored for every ultrasonic transducer for every degree of probe rotation.

The images found in the subsequent display areas are constructed in various manners from these a-scan records. Within Area 1, two time selectable gating locations can be established. These are shown as "broad" horizontal lines in the display. The maximum amplitude of the ultrasonic signal within these gates is converted into a color which is used to construct the pseudo-color "c-scan" display of Area 2. A c-scan image is constructed by plotting a color corresponding to the amplitude within the gate in a box corresponding to the rotary and axial location of the transducer. Thus, the c-scan is a two dimensional image of the ultrasonic response, where the relative amplitude of the response can be determined from the color.

Within Area 2 there are two cursor lines. One is horizontal, corresponding to a particular axial location of the probe. The other, vertical, corresponds to a specific azimuthal location around the tube. The intersection of the two lines is the data location for the displayed a-scan in Area 1. These cursor lines also determine the content of the images in the remaining three display areas.

Areas 3 and 4 are "b-scan" images, constructed along either the horizontal or vertical cursor lines of display Area 2. A pseudo-color b-scan is constructed by converting the a-scan in Area 1 to a line of colors where every color corresponds to the amplitude of the ultrasonic signal for that particular time. By stacking successive b-scans together, an image of the response either as the probe rotates around the tube (Area 3), or moves down the axis of the tube at one azimuthal location (Area 4), can be constructed. The images of Area 3 or Area 4 reveal the apparent motion of the ultrasonic responses as the probe moves through the tube. This information contributes to determining the significance of a particular response.

The final display, Area 5, is user-selectable, to be either a magnified c-scan (around the intersection of the cursor lines of Area 2), or a magnified b-scan (around the vertical cursor location of Area 3).

¹ Figure 2-22 is NOT a Kewaunee test result, but a typical figure used to explain the UTEC display system for ultrasonic test data.

Combining the information contained in these images with those obtained from the images produced by the other ultrasonic transducers, and also with eddy current data, allows a complete assessment of the tube condition.

2.4.3 Ultrasonic Test Reference Tube Standard

A single reference tube standard was used to calibrate the UTEC ultrasonic and eddy current test system. The reference tube contains an OD "cruciform" flaw. The flaw consists of bisecting axial and circumferential EDM (electrical discharge machine) notches, with a 0.0625 inch flat bottom hole located at the intersection. Each of the notches, and the hole, are machined to a 20% of the tube wall depth. This "cruciform" standard is used to monitor the detection capability of the system, and to assist in flaw characterization. Normally, the radial aim transducer detects the presence of the flat bottom hole. The circumferentially directed shear beam detects the axial notch and the edge of the hole, while the axial aim search unit detects the circumferential notch and the edge of the hole.

Figures 2-23, 2-24, and 2-25 document the ultrasonic calibration test results of the UTEC system prior to the Kewaunee tube testing.

2.4.4 Ultrasonic Test UTEC Data for the TST Region of Tube R15C28

The radial aim data, Figure 2-26, showed only some helical markings and axial scratches on the tube. The circumferential and axial aim data, Figures 2-27 and 2-28, respectively, did not show any detectable degradation, either.

2.4.5 Ultrasonic Test UTEC Data for the TSP1 Crevice Region of Tube R15C28

All three aim data revealed dents. However, as will be seen in the field eddy current test data shown in the next part of this report, there were no dents in the tube at the TSP1 and TSP2 crevice regions prior to the tube pull. Therefore, it has been concluded that the dents were produced by the tube pull.

The radial aim data, Figure 2-29, showed possible indications around 150° and 320°. The circumferential and axial aim data, Figures 2-30 and 2-31, confirmed the presence of numerous, short, shallow ($\leq 20\%$ deep), indications at the OD, located mostly in two patches: one centered near 320°, and the other near 150° (with an axial extent of about 0.2 inch). Also, some axial scratches were shown by the circumferential aim data, Figure 2-30.

2.4.6 Ultrasonic Test UTEC Data for the TSP2 Crevice Region of Tube R15C28

Similarly to the first support plate region, the second support plate region also showed dents in all three aim data. Again, as explained above, the dents are considered to have been made during the tube pull.

All three aim test data showed multiple indications at the OD. The circumferential aim test data revealed a network of indications located from 93° to 167°, with a 0.34 inch axial extent, as well as a network of indications located from 239° to 337°, with a 0.27 inch axial extent. The deepest penetration in either of the networks did not exceed 30%.

The axial aim test data pointed out to a network of indications located from 85° to 122°, with a 0.1 inch axial extent, and a network of indications located from 168° to 258°, with a 0.17 inch axial extent. None of the indications in either network exceeded 20% in depth.

In the assessment of these data it has been concluded that, basically, in the TSP2 crevice region there were multiple, short, shallow ($\leq 30\%$ deep), indications shown by both the circumferential and the axial aim scans, and that most of them were located in two patches: one centered near 120°, and the other near 290°. The indications were suggestive of either two dimensional intergranular cellular corrosion (ICC) or a three dimensional intergranular attack (IGA).

2.5 EDDY CURRENT TESTS

Prior to the pull of Tube R15C28 it was examined in the steam generator using the eddy current (EC) test technique. A bobbin and a 3-coil probe were used in the examination of the tubesheet top (TST), first tube support plate (TSP1), and the second tube support plate (TSP2) regions of the tube. The 3-coil probe consists of a pancake coil, circumferentially sensitive coil, and an axially sensitive coil. No Cecco 5 or +Point probes were used in the pre-pull tests. The results of this examination are reported below as "Field Tests".

After the tube was pulled, the same regions of the tube were eddy current examined in the Hot Cell area of the Westinghouse Remote Metallographic Facility, using a bobbin, 3-coil probe, + Point probe, and Cecco 5 probe. The data obtained in this examination are reported below as "Laboratory Tests".

2.5.1 Field Eddy Current Test Data

2.5.1.1 Field Eddy Current Test Data for the TST Region of Tube R15C28

The field EC test data for the tubesheet top region of Tube R15C28 are shown in Figure 2-35¹. The data were obtained with a bobbin probe, which showed a 5.17 Vpp (Volts peak-to-peak) dent indication. The 3-coil probe data, not displayed, showed no detectable degradation (NDD) of the tube in this region.

2.5.1.2 Field Eddy Current Test Data for the TSP1 Crevice Region of Tube R15C28

The field EC test data for the first tube support plate crevice region of Tube R15C28 are shown in Figures 2-36 through 2-39. They were obtained using the bobbin, as well as the pancake coil, the circumferentially sensitive coil, and the axially sensitive coil of the 3-coil probe. The bobbin probe showed a 1.14 Vpp indication, less than 20% deep. The 3-coil probe revealed a 0.50 Vpp volumetric indication, extending over a distance of 0.30 inch axially and 150° circumferentially. The responses of the axially sensitive and circumferentially sensitive coils were approximately equal, shallow, and non-quantifiable.

2.5.1.3 Field Eddy Current Test Data for the TSP2 Crevice Region of Tube R15C28

Figures 2-40 through 2-43 show the field EC test data for the second tube support plate crevice region of Tube R15C28. The bobbin probe showed a 1.49 Vpp indication, less than 20% deep. The 3-coil probe revealed a 0.11 Vpp volumetric indication, extending over a distance of 0.30 inch axially and 193° circumferentially. Again, the responses of the axially sensitive and circumferentially sensitive coils were approximately equal, shallow, and non-quantifiable.

2.5.2 Laboratory Eddy Current Test Data

2.5.2.1 Laboratory Eddy Current Test Data for the TST Region of Tube R15C28

The laboratory EC test data for the tubesheet top region of Tube R15C28 are shown in Figures 2-44 through 2-47. The data were obtained with a bobbin probe, 3-coil probe pancake coil, + Point probe, and Cecco 5 probe. The bobbin probe indicated a 46.52

¹ In the caption of this figure and of the following figures showing the EC data the words **Field** and **Laboratory** are printed in bold letters to show clearly where the data were obtained.

Vpp dent in this region of the tube. The remaining probes showed no detectable degradation (NDD).

2.5.2.2 Laboratory Eddy Current Test Data for the TSP1 Region of Tube R15C28

Figures 2-48 through 2-55 show the laboratory EC test data for the first tube support plate crevice region of Tube R15C28. The bobbin test results, illustrated in Figures 2-48 and 2-49, showed a 2.14 Vpp distorted indication in a 9.15 Vpp dent. The 3-coil test data revealed a 0.56 Vpp volumetric indication, extending over a distance of 0.57 inch axially and 140° circumferentially. Two relatively large, localized dent signals (not present in the field) are clearly visible in Figures 2-50, and 2-51. There was an approximately equal response on the axially and circumferentially sensitive coils of the 3-coil probe. The + Point probe data, Figure 2-53, showed one region of nominally axial indication, 0.15 Vpp, spanning about 100°. The signal did not have a distinctive volumetric character, and was shallow. The Cecco 5 test data, presented as Lissajous patterns in Figure 2-54, and a strip chart in Figure 2-55, showed possible indications over about 105° of tube circumference, with an estimated depth of less than 20% of the wall.

2.5.2.3 Laboratory Eddy Current Test Data for the TSP2 Region of Tube R15C28

The laboratory EC test data for the second tube support plate crevice region of Tube R15C28 are shown in Figures 2-56 through 2-64. The bobbin probe, Figures 2-56 and 2-57, showed a 2.94 Vpp indication distorted by a 23.37 Vpp dent. The 3-coil probe data, obtained by the pancake coil, (Figure 2-58), circumferentially sensitive coil (Figure 2-59), and axially sensitive coil (Figure 2-60), showed a 0.45 Vpp volumetric indication, with a 0.45 inch x 240° extent. Four relatively large dent indications (not present in the field) are clearly visible in the above figures. There was approximately equal response on the circumferentially and axially sensitive coils (shallow indications). The + Point probe, Figures 2-61 and 2-62, revealed two regions of nominally axial indications, 0.13 Vpp and 0.12 Vpp, spanning about 240°, but shallow, with no distinctive volumetric character. Figures 2-63 and 2-64 present the Cecco 5 probe data, which showed two regions of possible indications over about 90° and 45° of circumference, with a 30° region without indications in between. The estimated depth was 30%.

The results of the non-destructive tests and examinations are summarized in Table 2-1.

Table 2-1 Kewaunee NDE Results For Tube R15C28

Location	Field E/C	Lab E/C	Lab UT	Lab X-Ray
TTS	Bobbin: 5.17V dent 3-Coil: NDD	Bobbin: 46.52V dent 3-Coil: NDD +Point: NDD Cecco-5: NDD	NDD	NDD
TSP1	Bobbin: 1.14V Ind, <20% deep 3-Coil: 0.50V volumetric Ind (0.3"x150 ⁰)	Bobbin: 2.14V distorted Ind in 9.15V dent 3-Coil: 0.56V volumetric Ind, (0.57"x140 ⁰), dent signals (not present in field) +Point: 0.15V axial Ind with 100 ⁰ involvement, but no distinctive volumetric character, shallow. Cecco-5: Possible Inds over 105 ⁰ of circumference, <20% deep	Numerous short, shallow ($\leq 20\%$ deep), Inds in both circumferential and axial aim scans; most located in two patches, one centered near 320 ⁰ & one near 150 ⁰ . Dent signals also present.	NDD
TSP2	Bobbin: 1.49V Ind, <20% deep 3-Coil: 0.11V volumetric Ind (0.3"x190 ⁰)	Bobbin: 2.94V distorted Ind in 23.37V dent 3-Coil: 0.45V volumetric Ind, (0.45"x240 ⁰), dent signals (not present in field) +Point: 0.12V & 0.13V axial Inds with 240 ⁰ of involvement, but no distinctive volumetric character, shallow. Cecco-5: Two areas with possible Inds over 90 ⁰ and 45 ⁰ of circumference, ~30% deep	Multiple short, shallow ($\leq 30\%$ deep), Inds in both circumferential and axial aim scans; most located in two patches, one centered near 120 ⁰ & one near 290 ⁰ .	NDD

FIGURES FOR SECTION 2

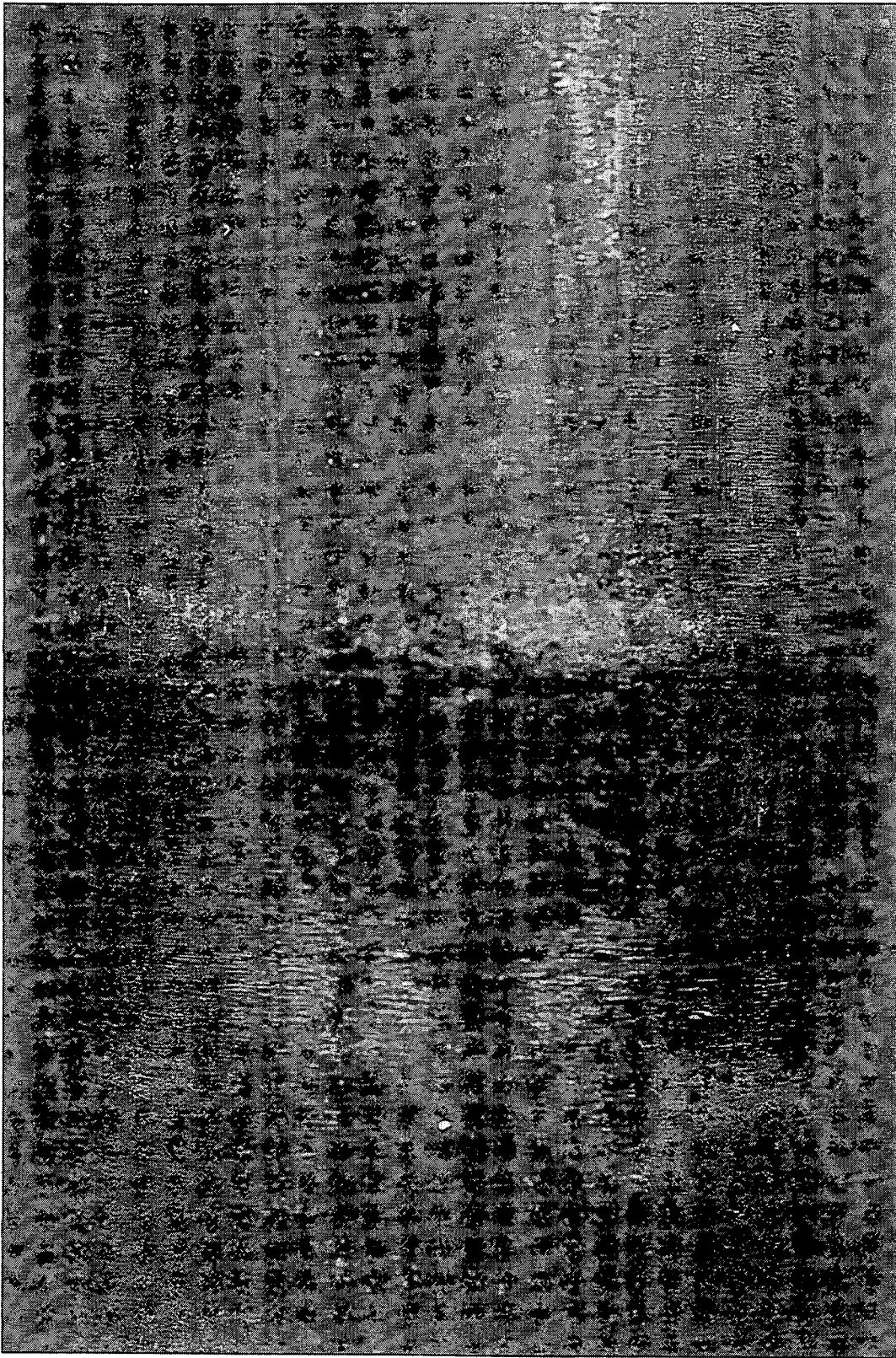


Figure 2-1 Photograph of the tubesheet top region of Tube R15C28, 0° face. Specimen 2B. Mag. 6.3X.

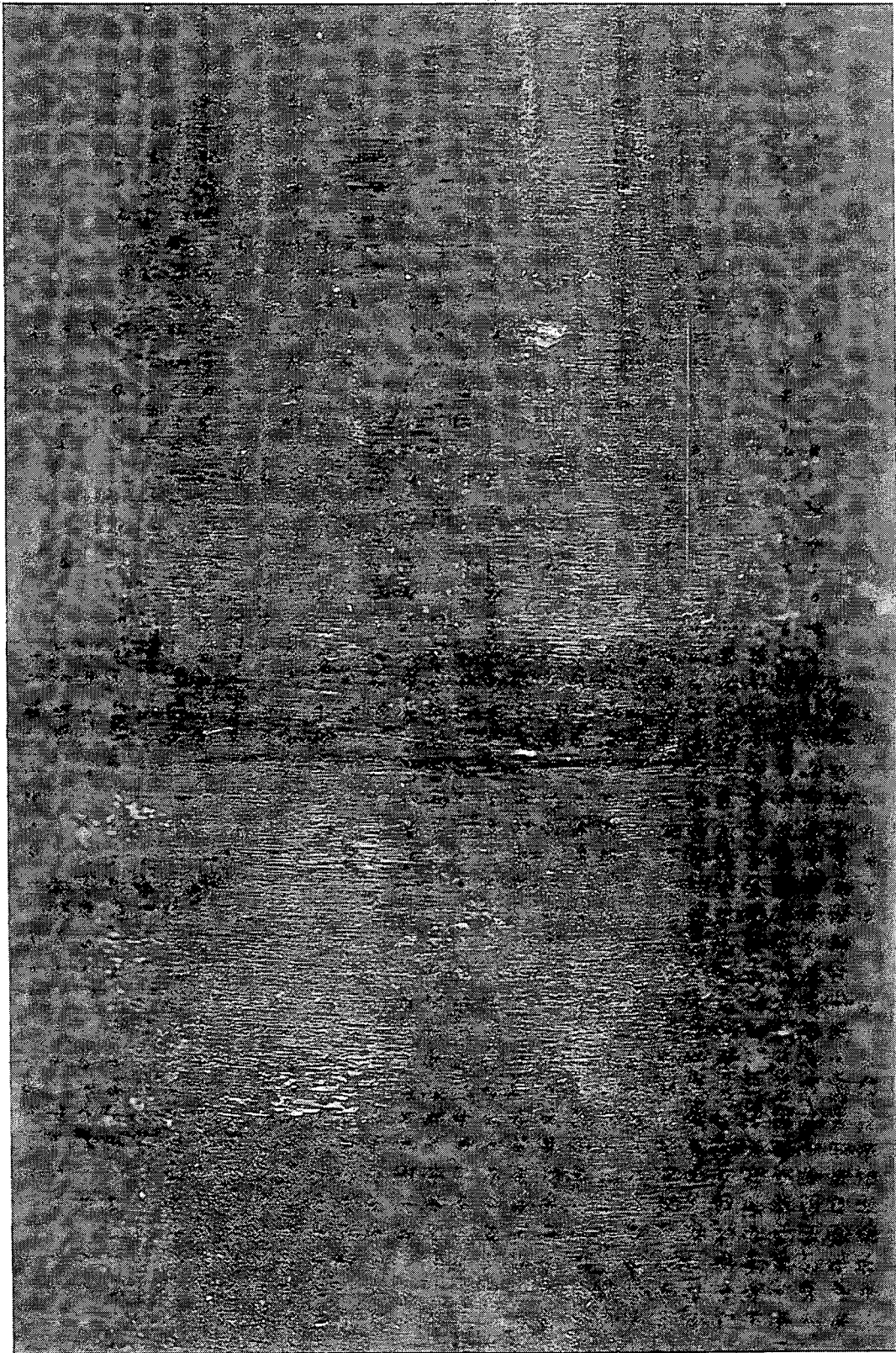


Figure 2-2 Photograph of the tubesheet top region of Tube R15C28, 90° face. Specimen 2B. Mag. 6.3X.

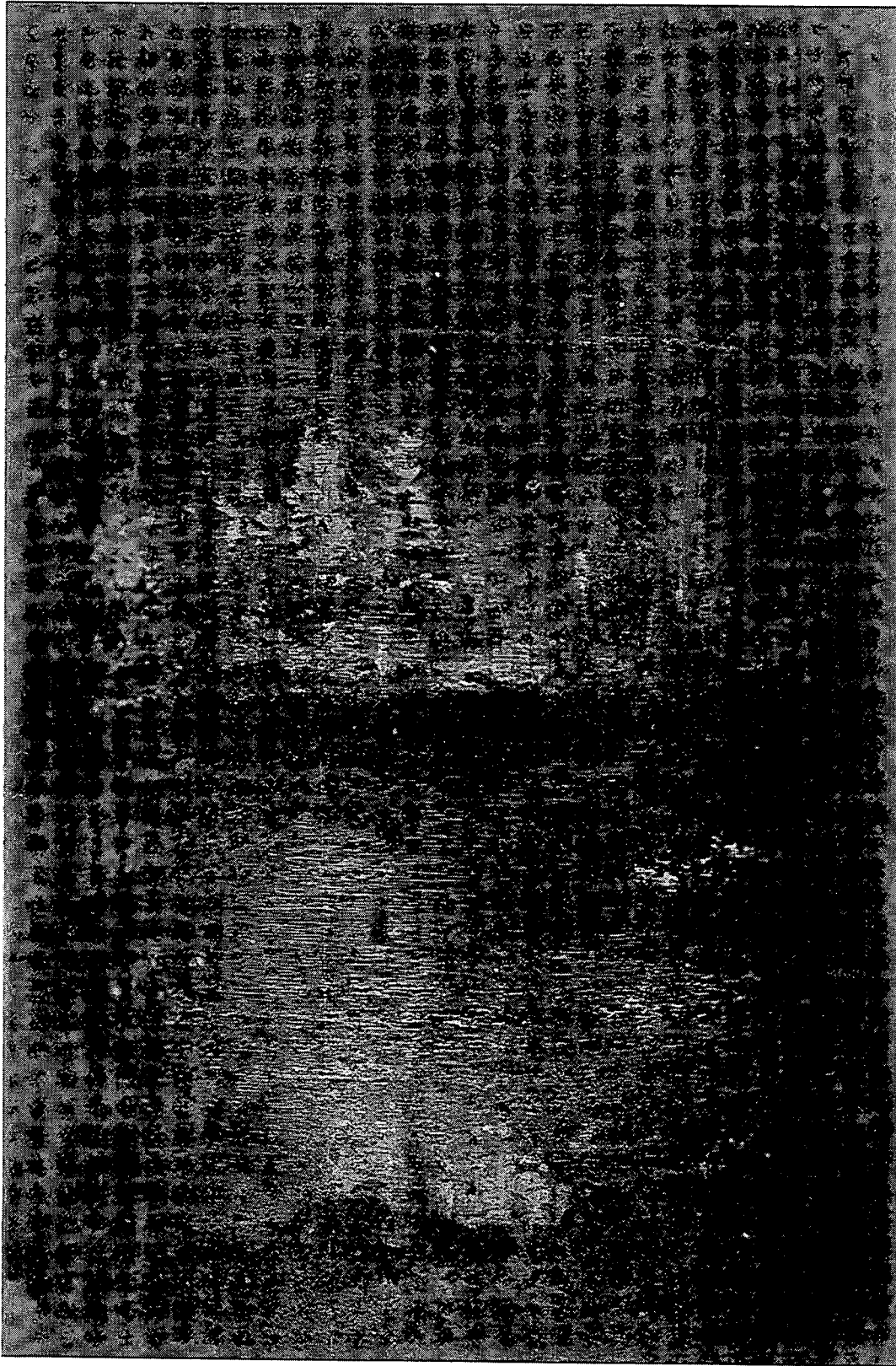


Figure 2-3 Photograph of the tubesheet top region of Tube R15C28, 180° face. Specimen 2B. Mag. 6.3X.

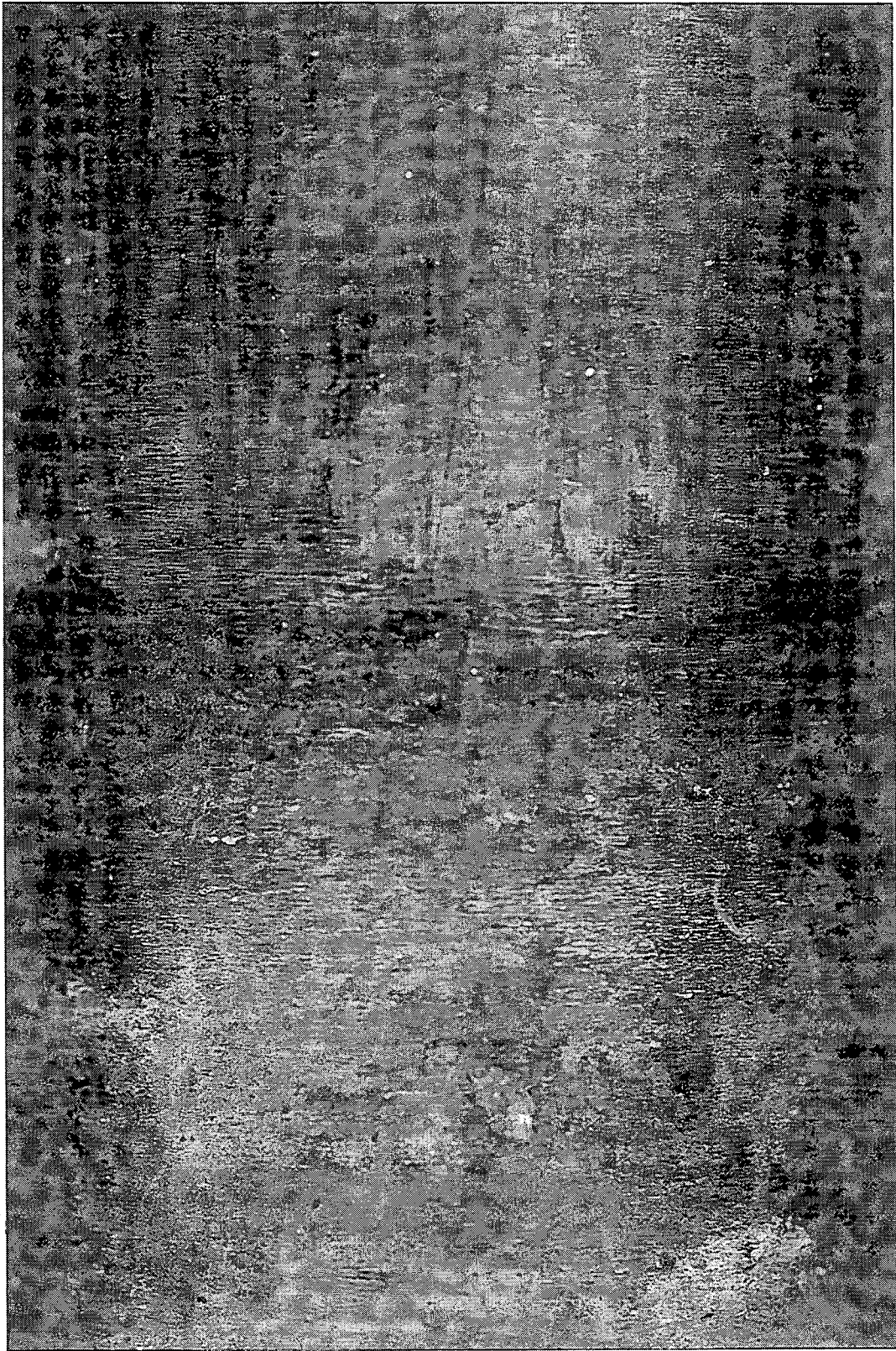


Figure 2-4 Photograph of the tubesheet top region of Tube R15C28, 270° face. Specimen 2B. Mag. 6.3X.

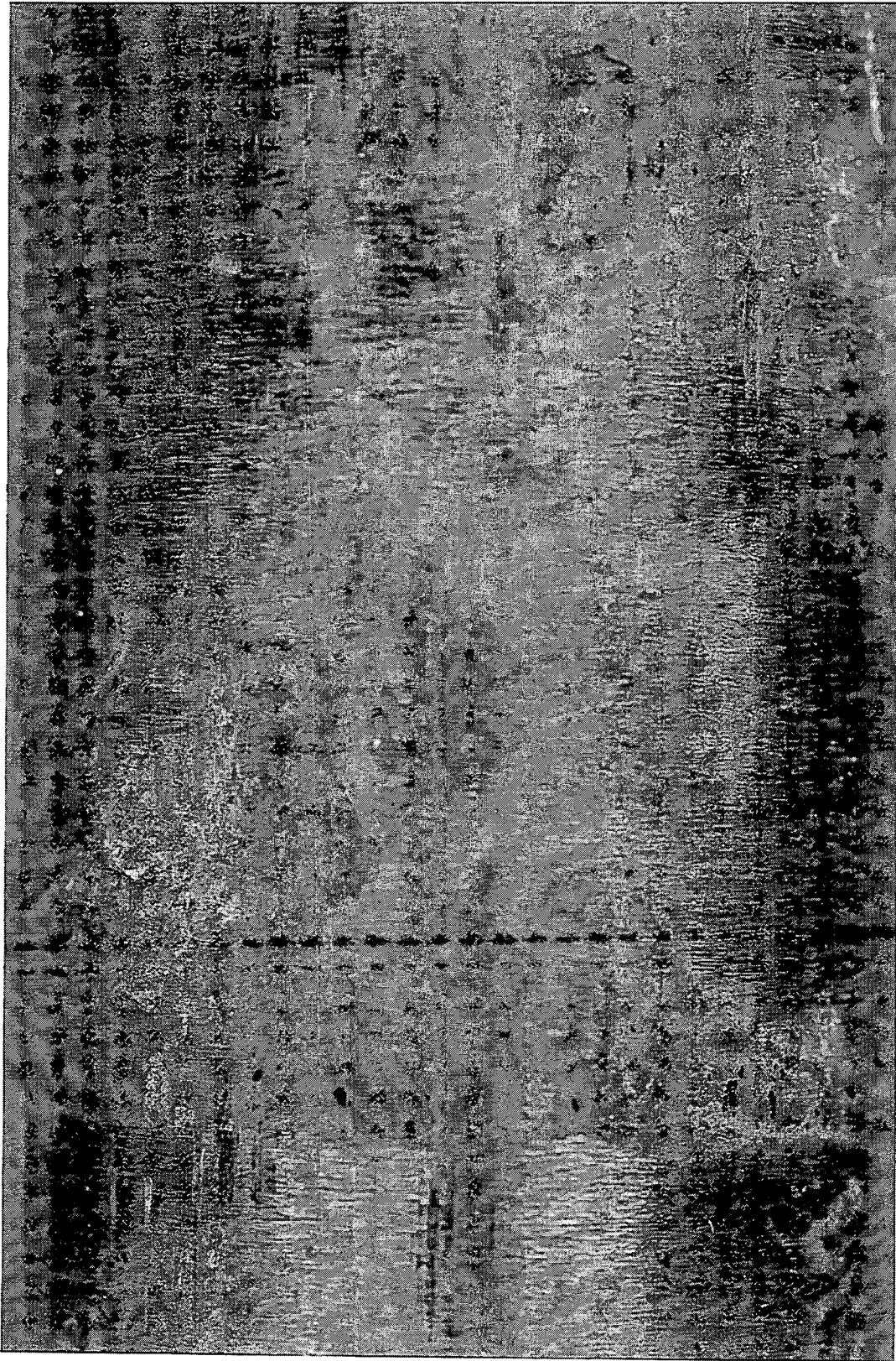


Figure 2-5 Photograph of the first support plate crevice region of Tube R15C28, 0° face.
Specimen 4B. Mag. 6.3X.

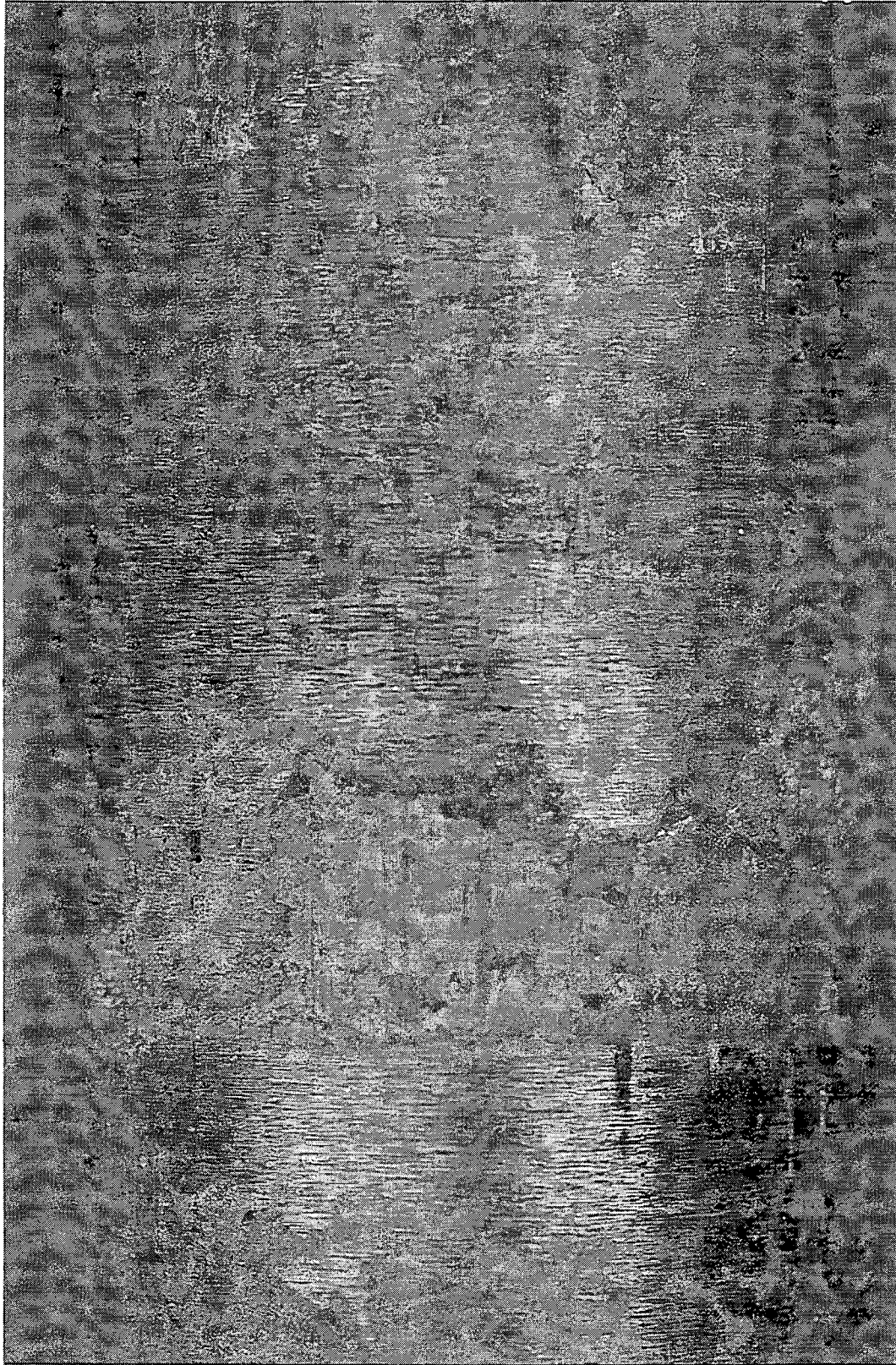


Figure 2-6 Photograph of the first support plate crevice region of Tube R15C28, 90° face. Specimen 4B. Mag. 6.3X.

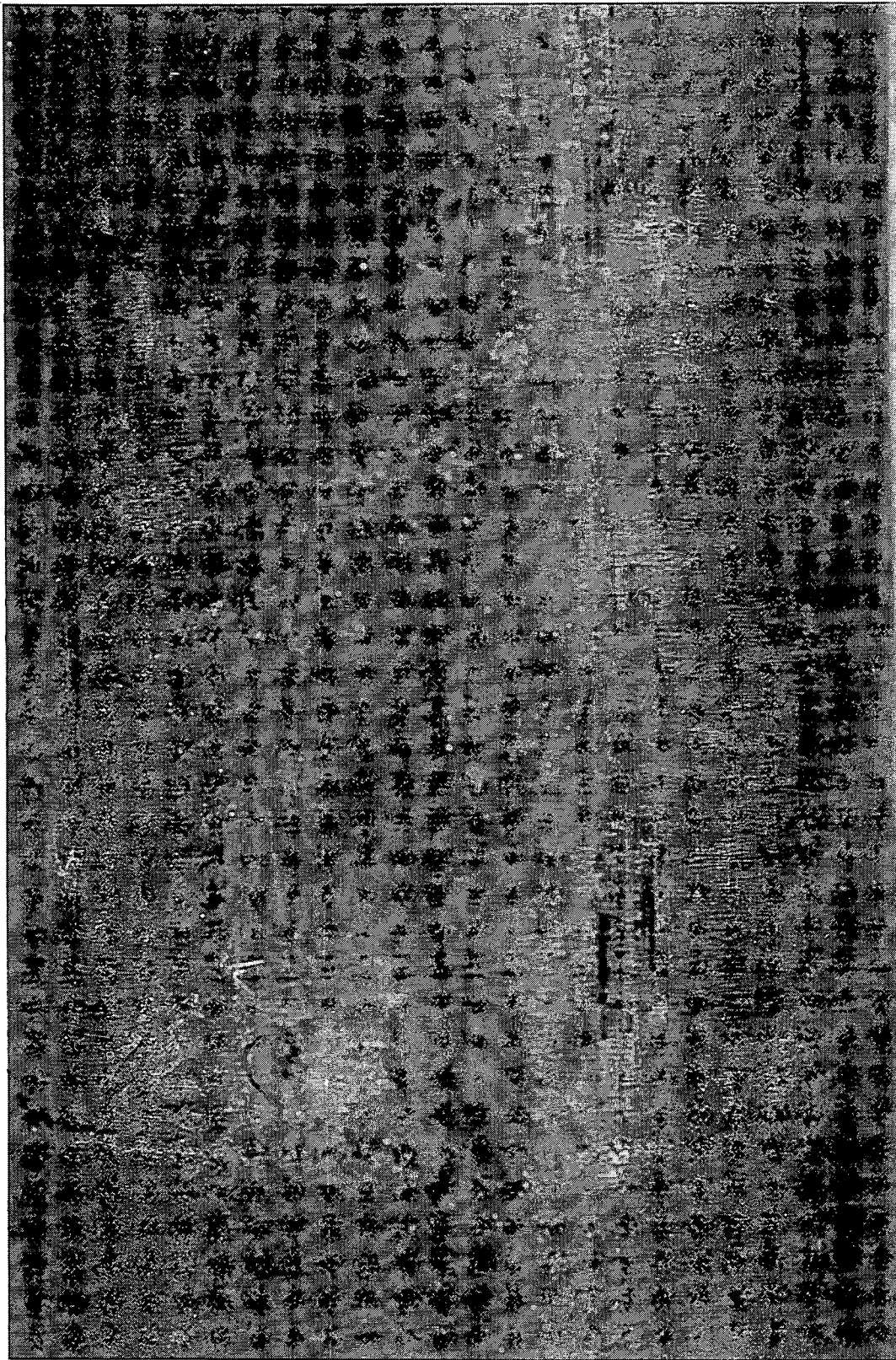


Figure 2-7 Photograph of the first support plate crevice region of Tube R15C28, 180° face. Specimen 4B. Mag. 6.3X.

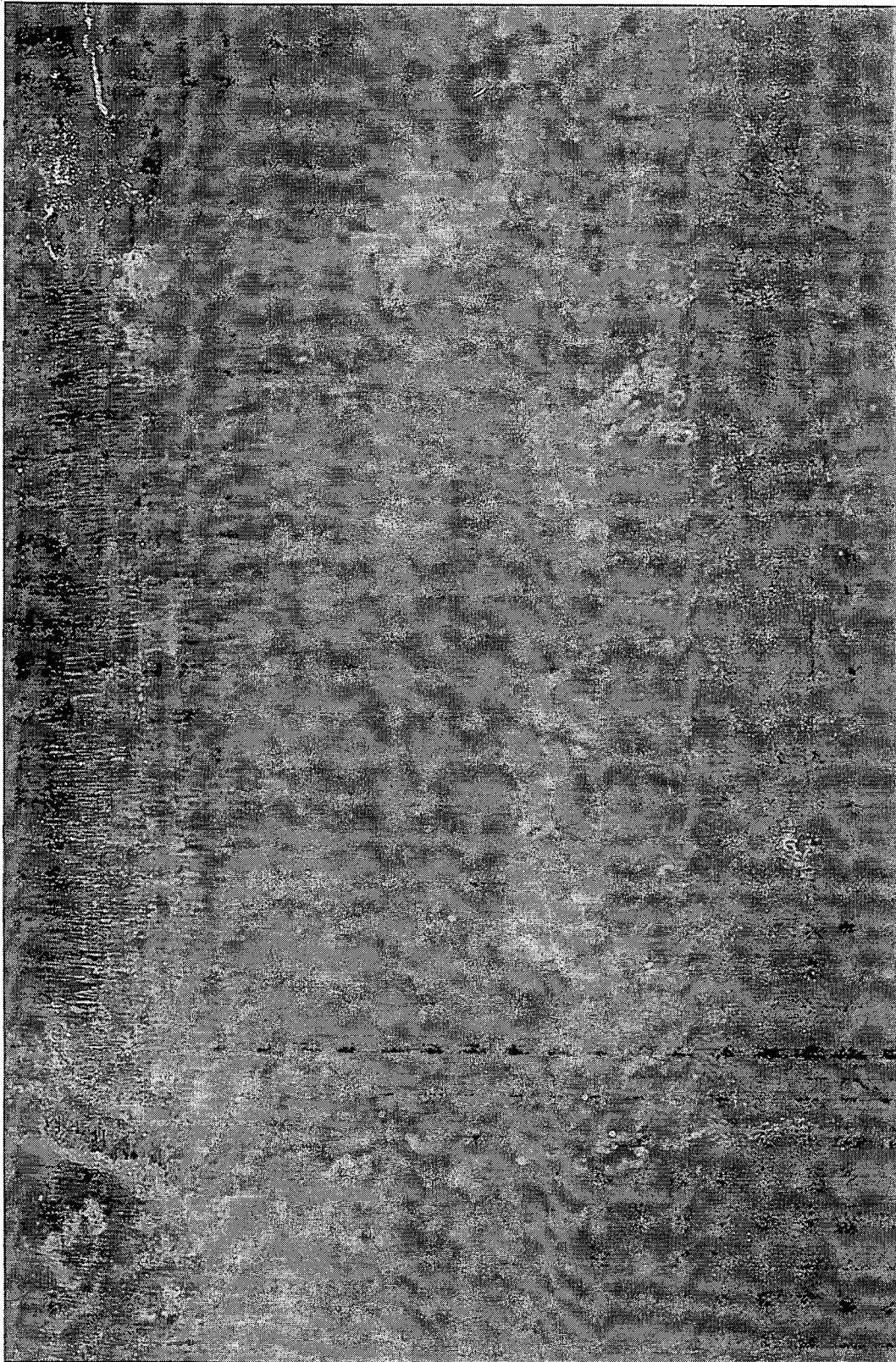


Figure 2-8 Photograph of the first support plate crevice region of Tube R15C28, 270° face. Specimen 4B. Mag. 6.3X.

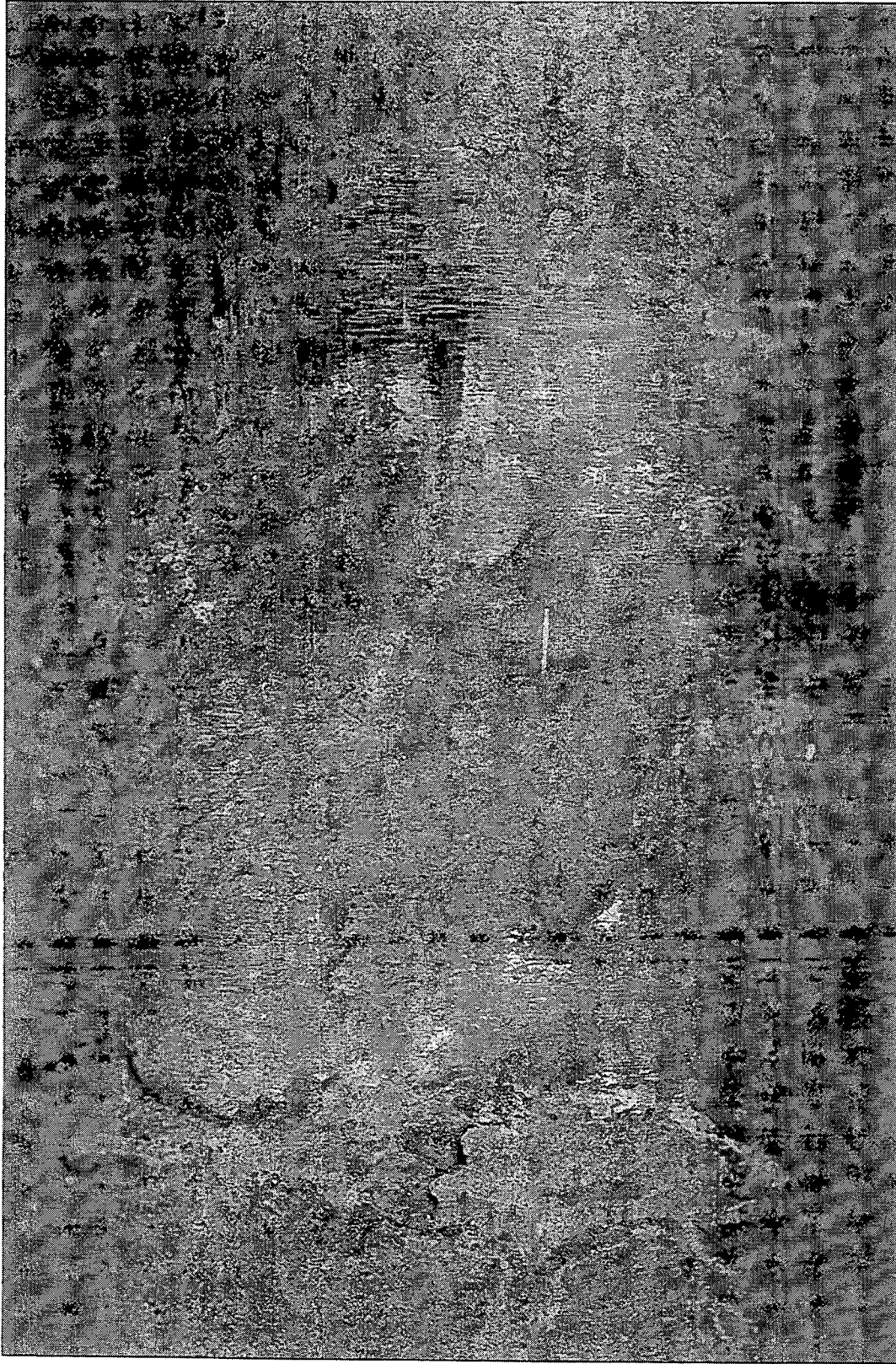


Figure 2-9 Photograph of the second support plate crevice region of Tube R15C28, 0° face. Specimen 6B. Mag. 6.3X.



Figure 2-10 Photograph of the second support plate crevice region of Tube R15C28, 90° face. Specimen 6B. Mag. 6.3X.

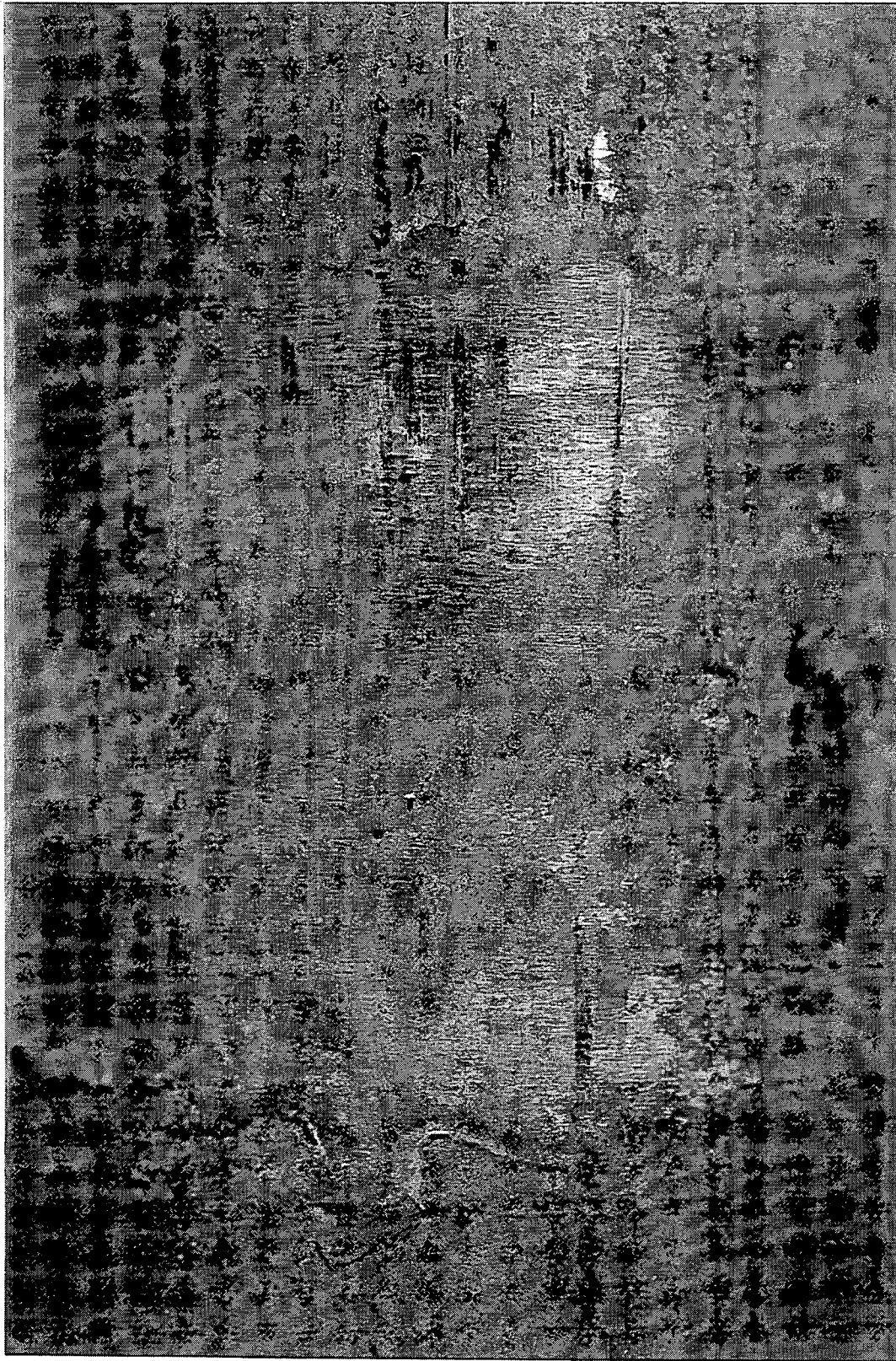


Figure 2-11 Photograph of the second support plate crevice region of Tube R15C28, 180° face. Specimen 6B. Mag. 6.3X.

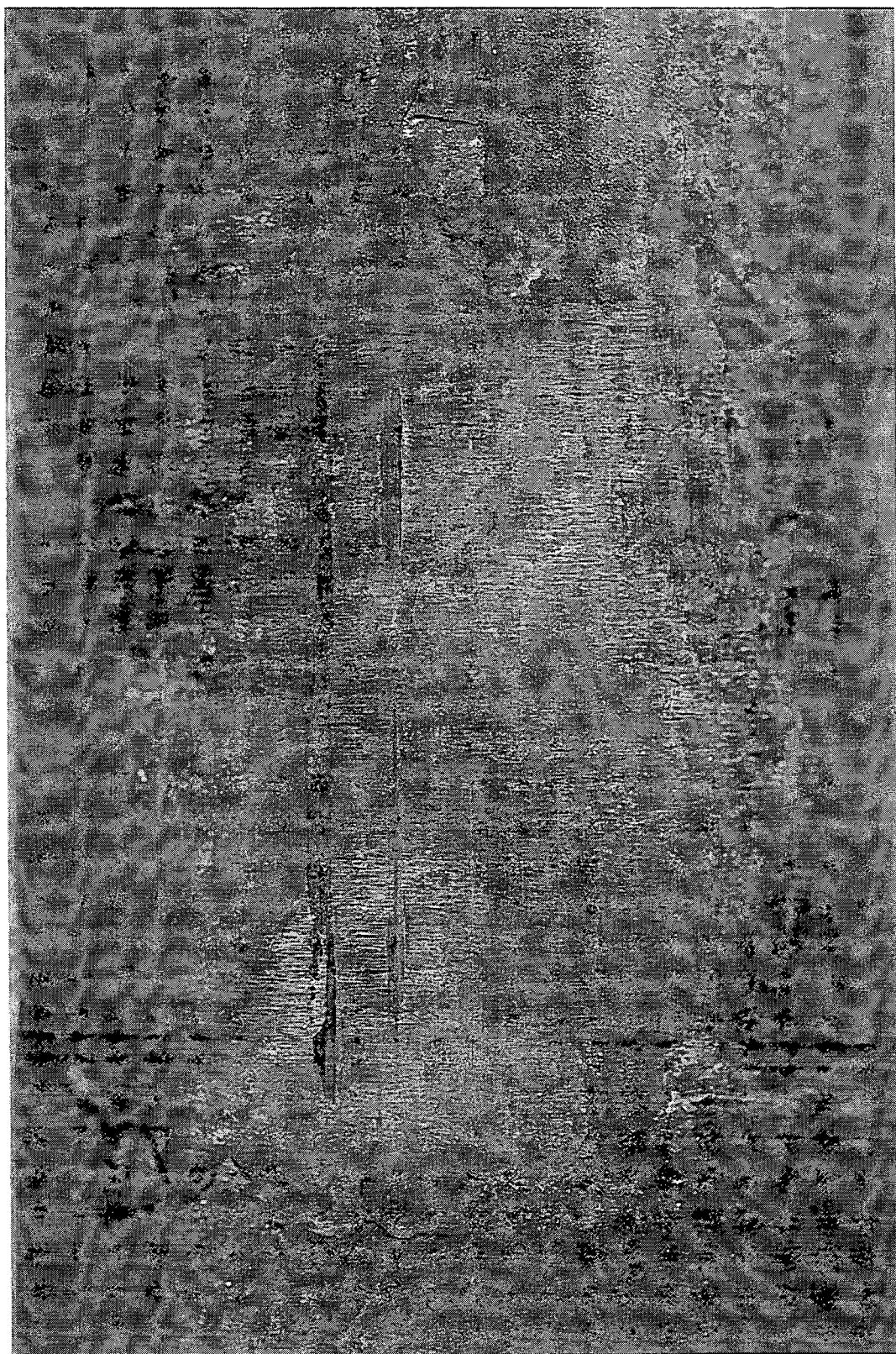


Figure 2-12 Photograph of the second support plate crevice region of Tube R15C28, 270° face. Specimen 6B. Mag. 6.3X.

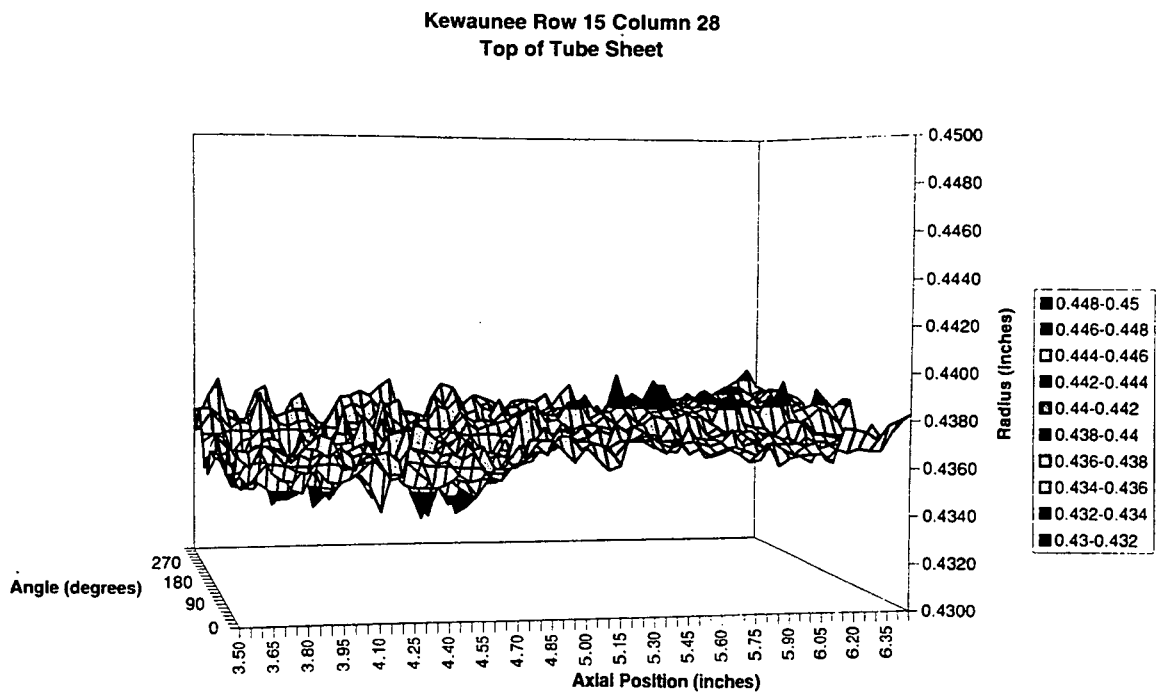


Figure 2-13 OD dimensional data obtained by laser micrometry of the tubesheet top region of Tube R15C28, showing radial data as a function of axial and circumferential position.

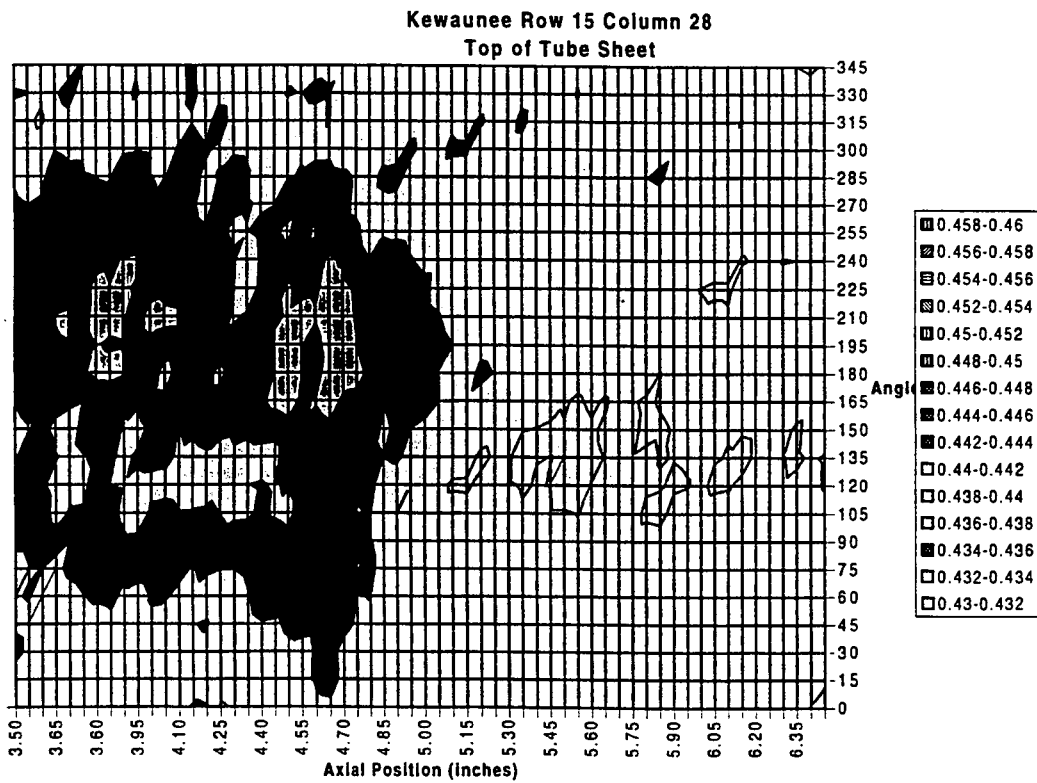


Figure 2-14 OD dimensional data obtained by laser micrometry of the tubesheet top region of Tube R15C28, showing radial data as a function of axial and circumferential position, in form of a contour map.

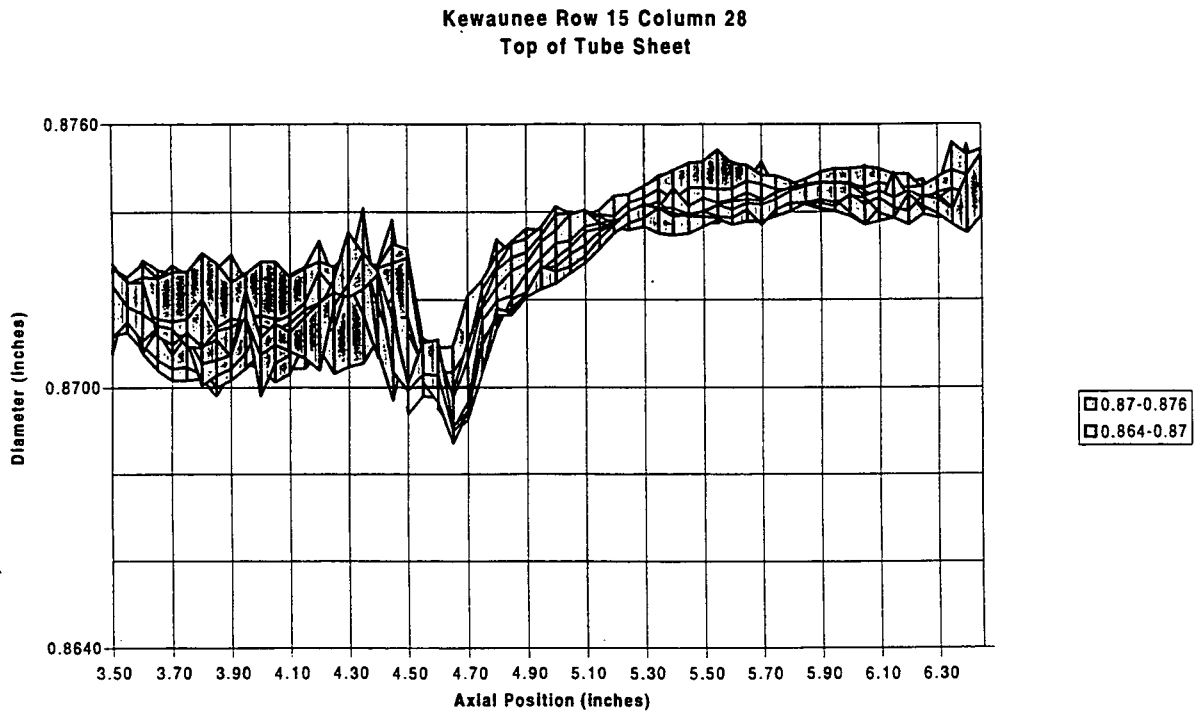


Figure 2-15 OD dimensional data obtained by laser micrometry of the tubesheet top region of Tube R15C28, showing diametrical data as a function of axial position, with circumferential information compressed.

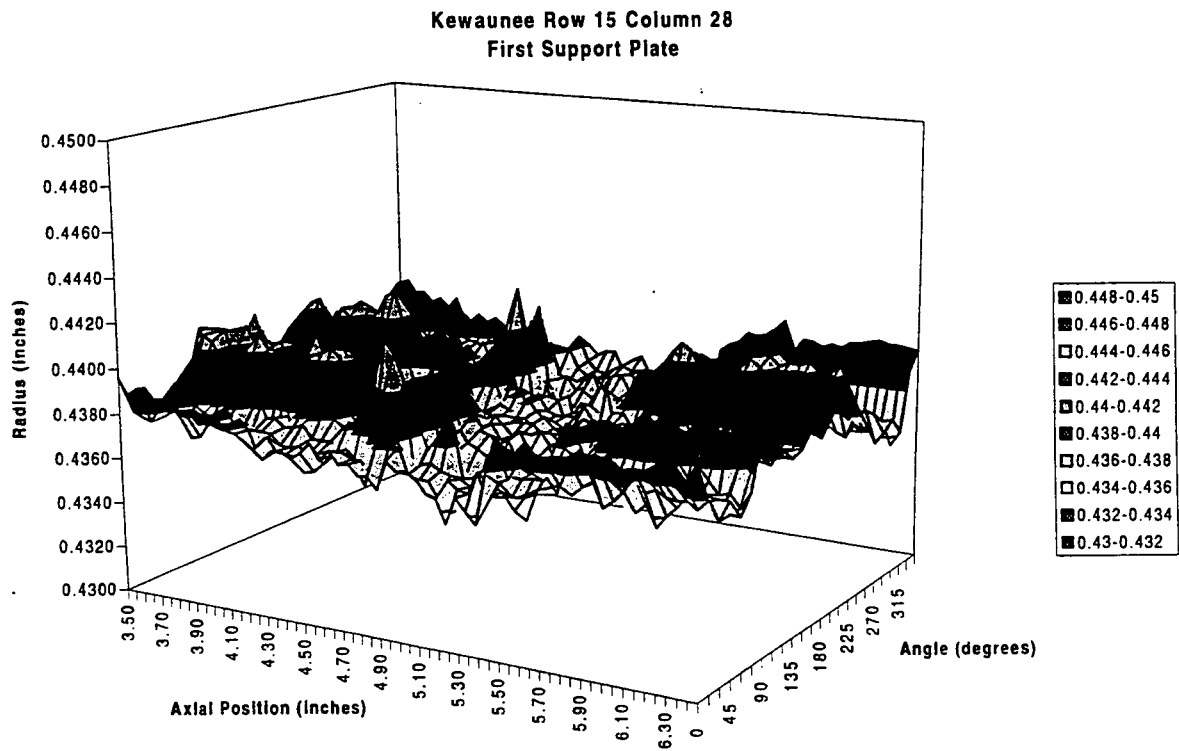


Figure 2-16 OD dimensional data obtained by laser micrometry of the first tube support plate region of Tube R15C28, showing radial data as a function of axial and circumferential position.

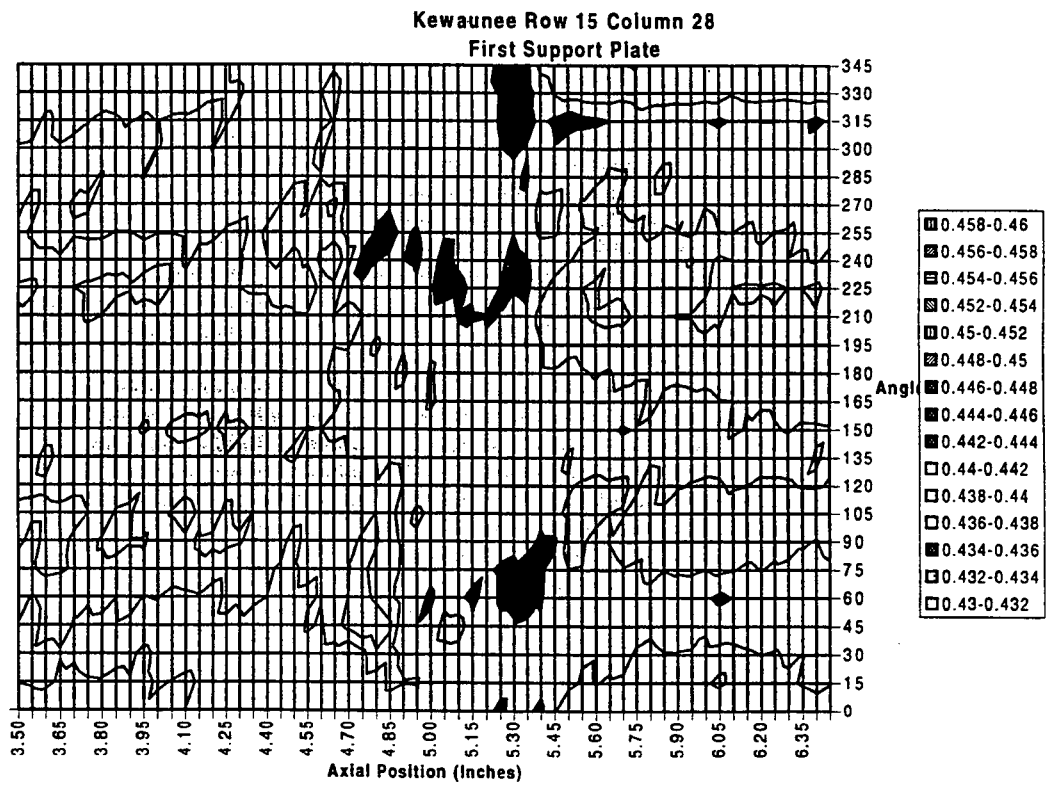


Figure 2-17 OD dimensional data obtained by laser micrometry of the first tube support plate region of Tube R15C28, showing radial data as a function of axial and circumferential position, in form of a contour map.

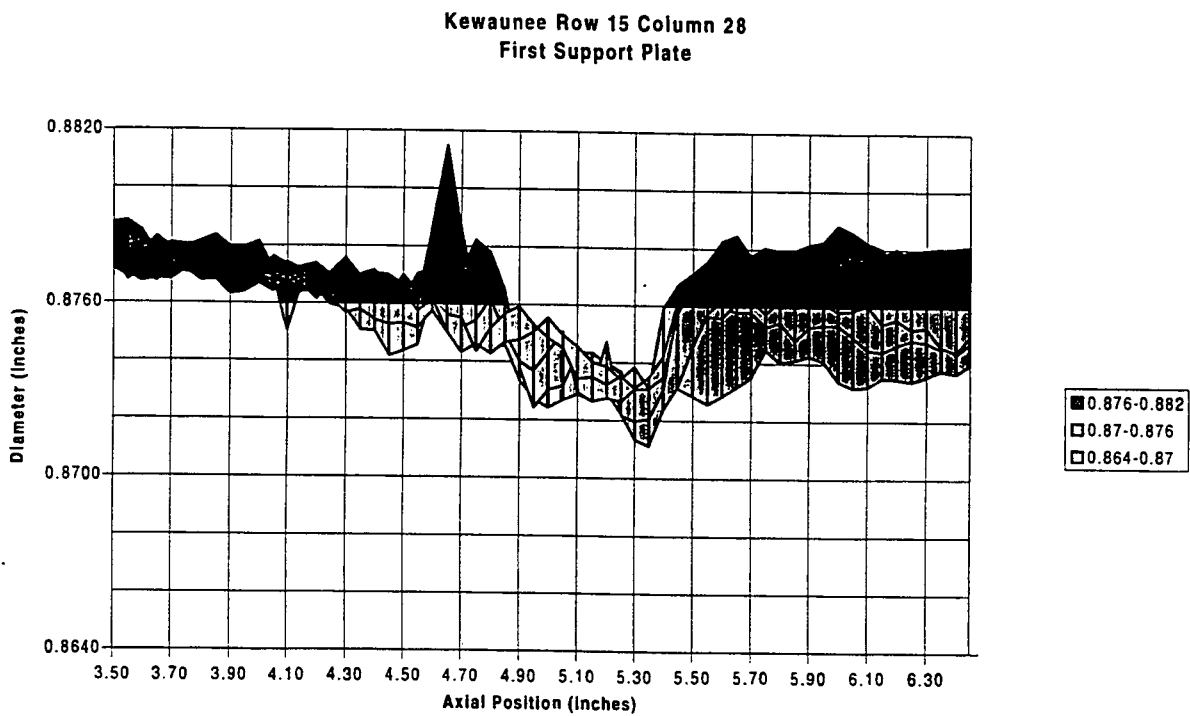


Figure 2-18 OD dimensional data obtained by laser micrometry of the first tube support plate region of Tube R15C28, showing diametrical data as a function of axial position, with circumferential information compressed.

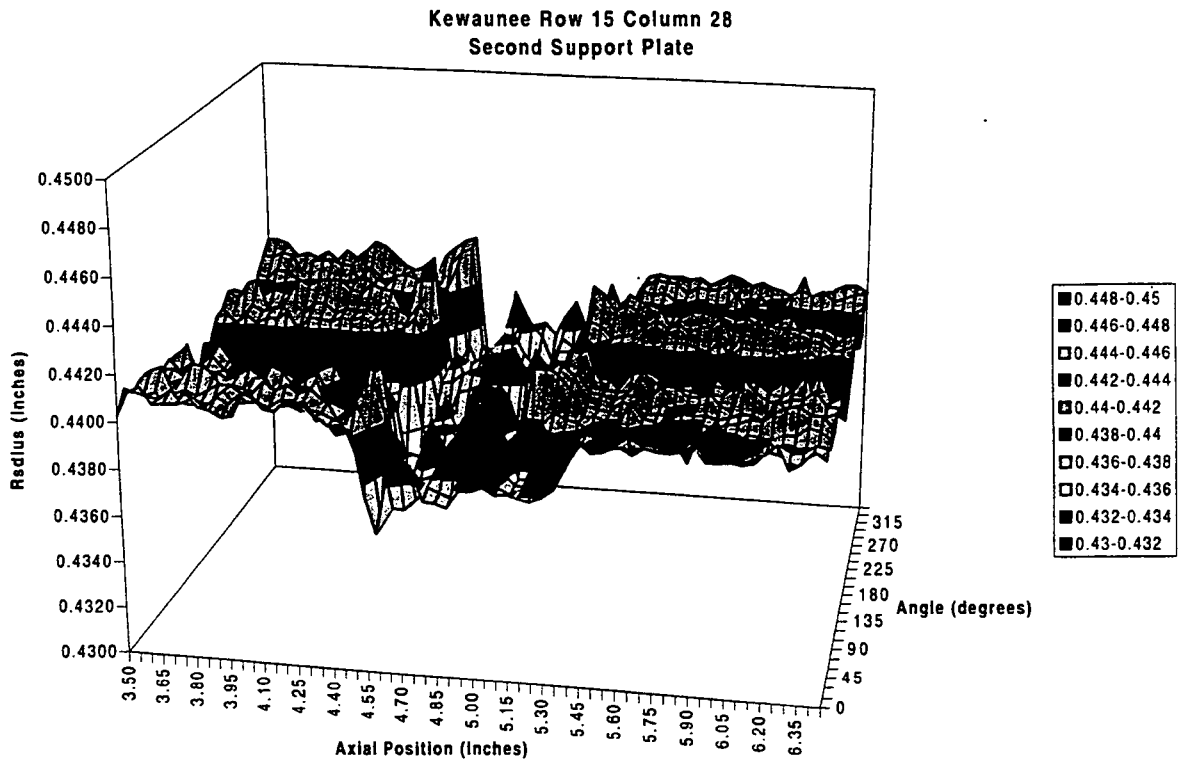


Figure 2-19 OD dimensional data obtained by laser micrometry of the second tube support plate region of Tube R15C28, showing radial data as a function of axial and circumferential position.

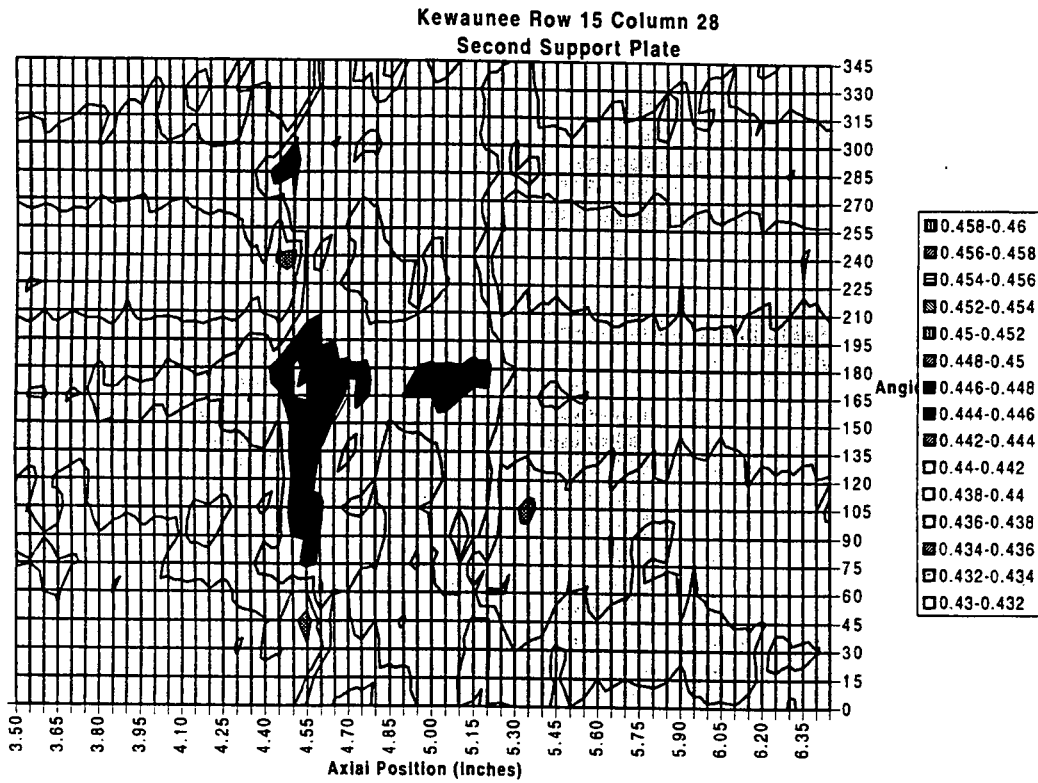


Figure 2-20 OD dimensional data obtained by laser micrometry of the second tube support plate region of Tube R15C28, showing radial data as a function of axial and circumferential position, in form of a contour map.

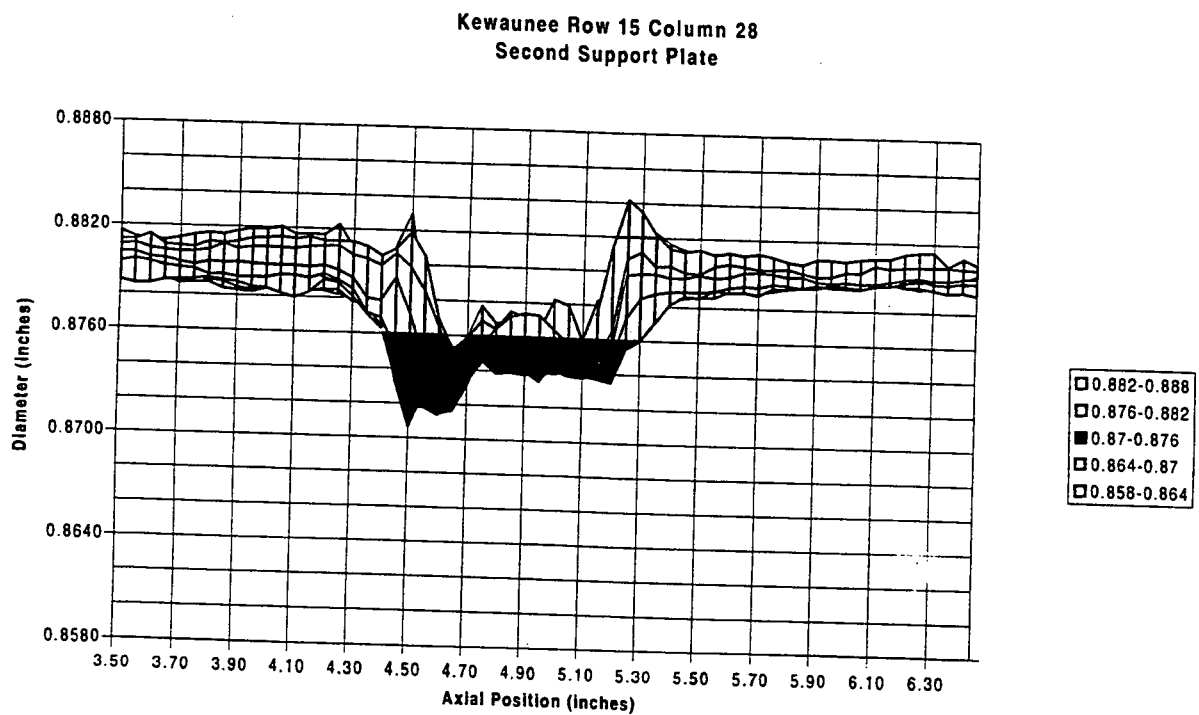


Figure 2-21 OD dimensional data obtained by laser micrometry of the second tube support plate region of Tube R15C28, showing diametrical data as a function of axial position, with circumferential information compressed.

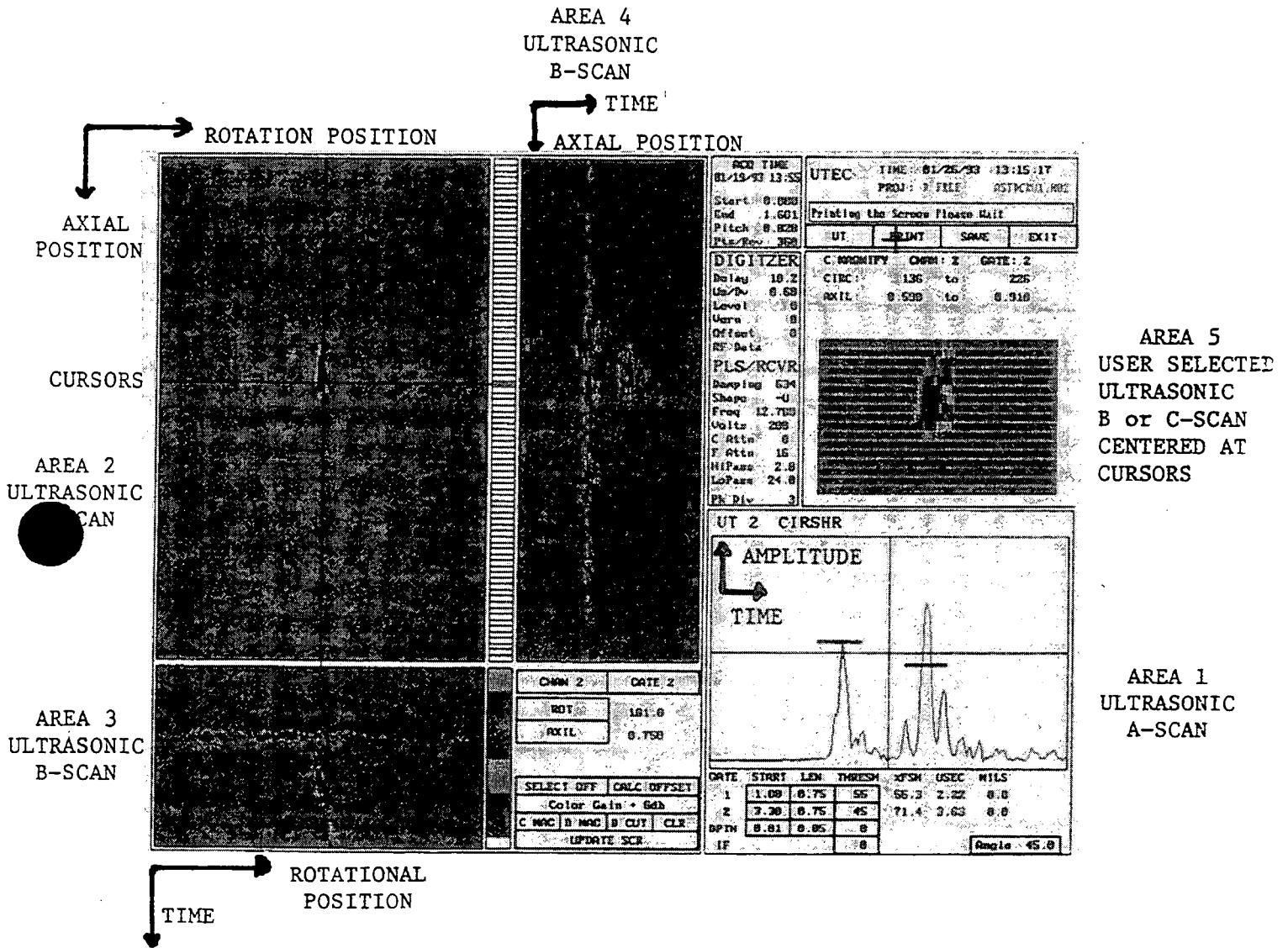


Figure 2-22 Typical display of UTEC ultrasonic test data. This is NOT a Kewaunee tube test result, but a figure used to explain the UTEC display system.

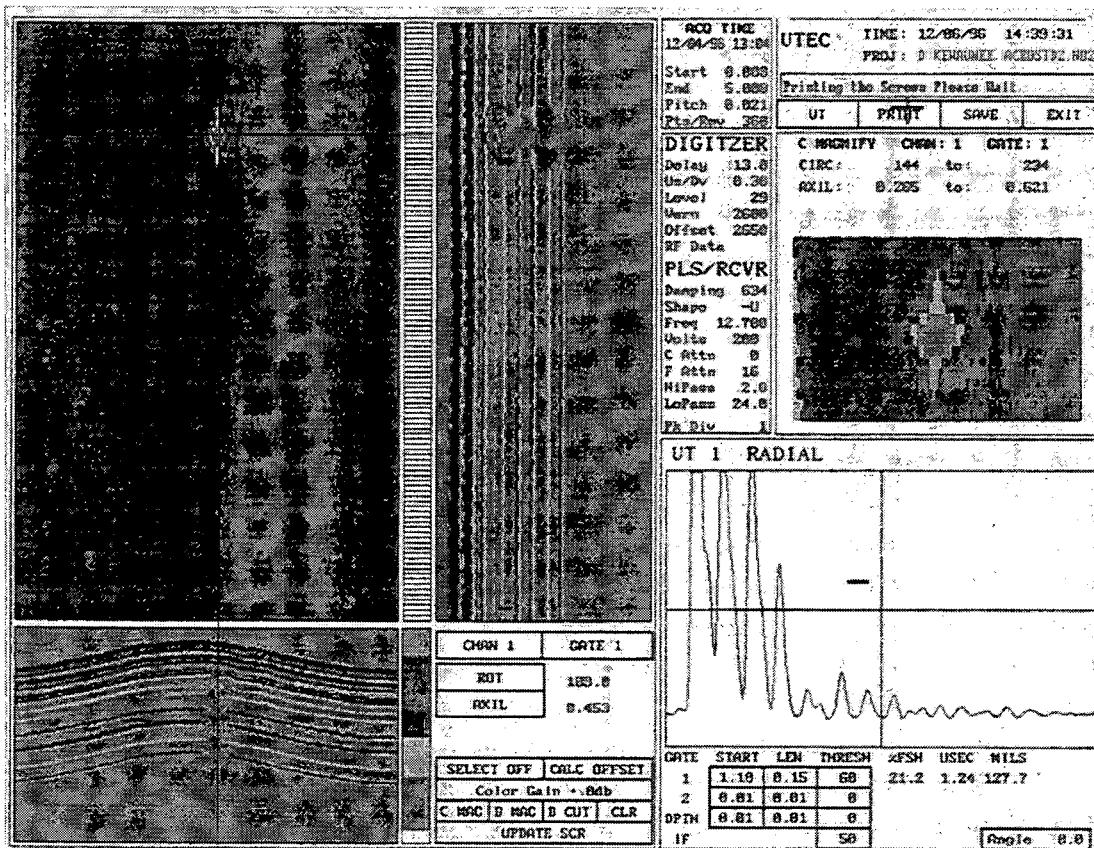


Figure 2-23 Ultrasonic test UTEC display of the radial aim data obtained on the UT calibration standard, showing the flat bottom hole centered in the cruciform-shaped notch.

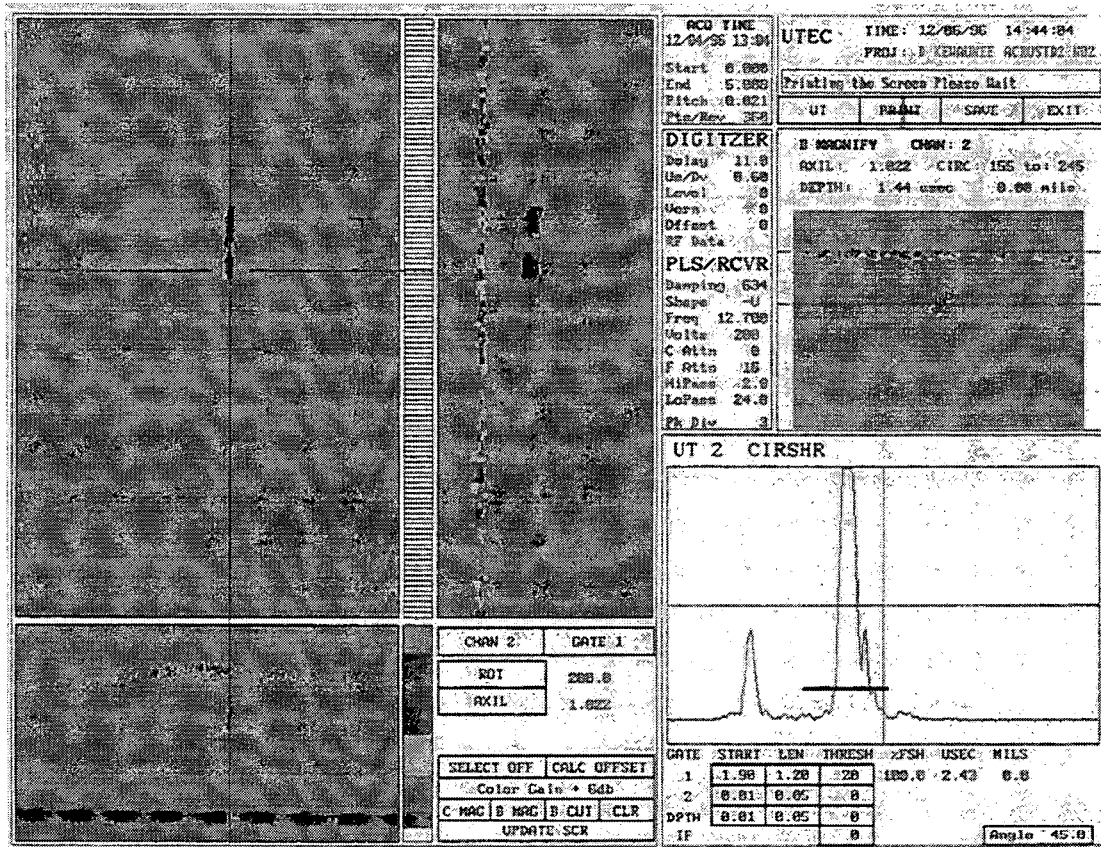


Figure 2-24 Ultrasonic test UTEC display of the circumferential aim data obtained on the UT calibration standard, showing the axial notch and the edge of the flat bottom hole centered in the cruciform-shaped notch.

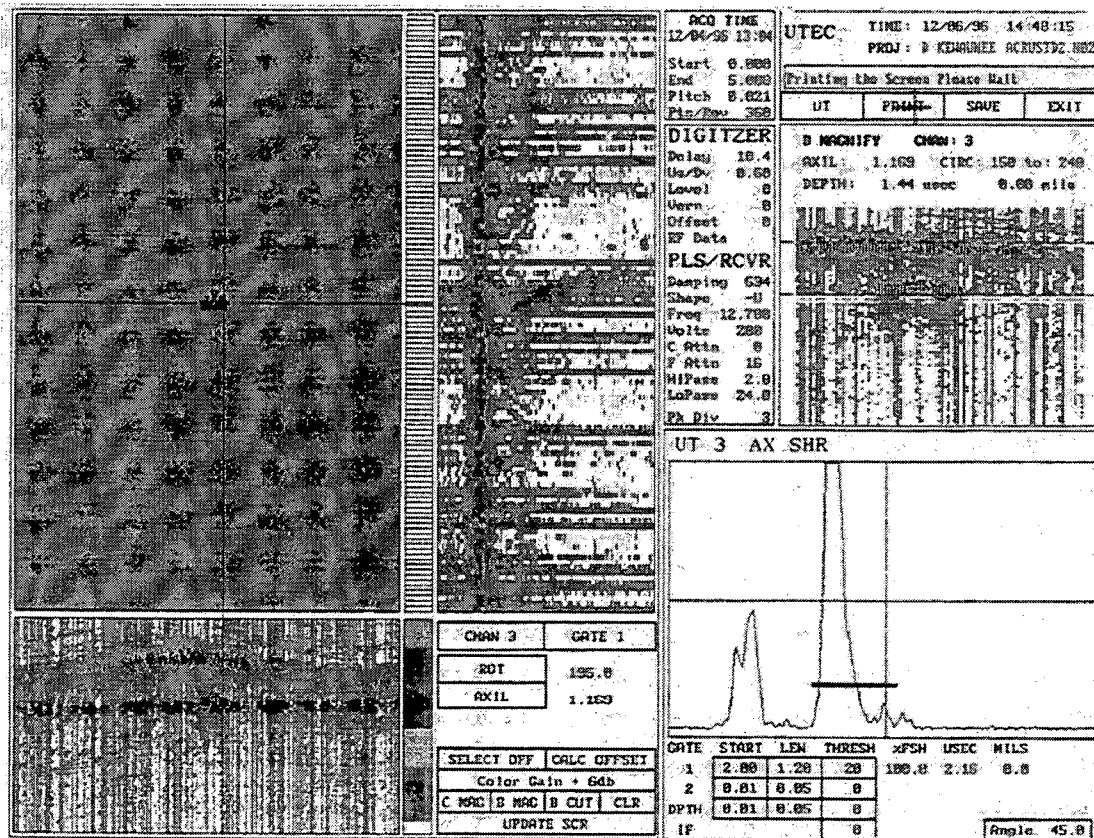


Figure 2-25 Ultrasonic test UTEC display of the axial aim data obtained on the UT calibration standard, showing the circumferential notch and the edge of the flat bottom hole centered in the cruciform-shaped notch.

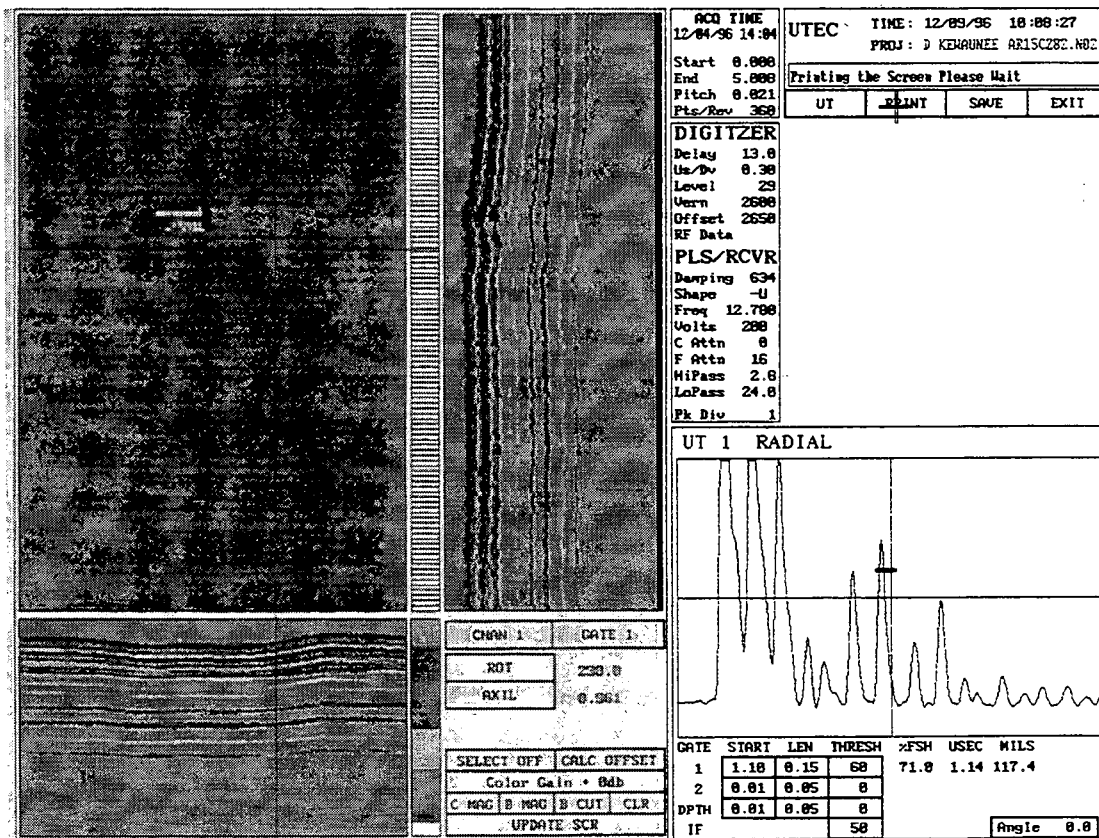


Figure 2-26 Ultrasonic test UTEC display of the radial aim data obtained on the tubesheet top region of Tube R15C28.

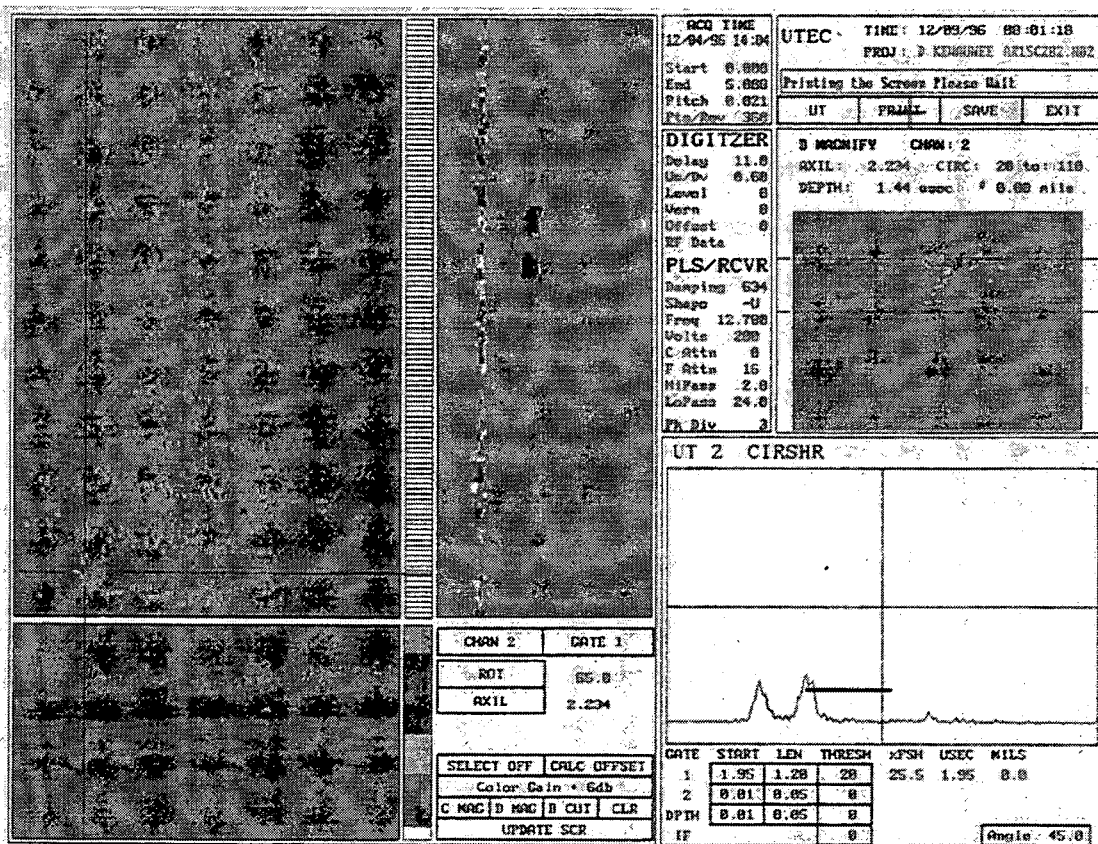


Figure 2-27 Ultrasonic test UTEC display of the circumferential aim data obtained on the tubesheet top region of Tube R15C28.

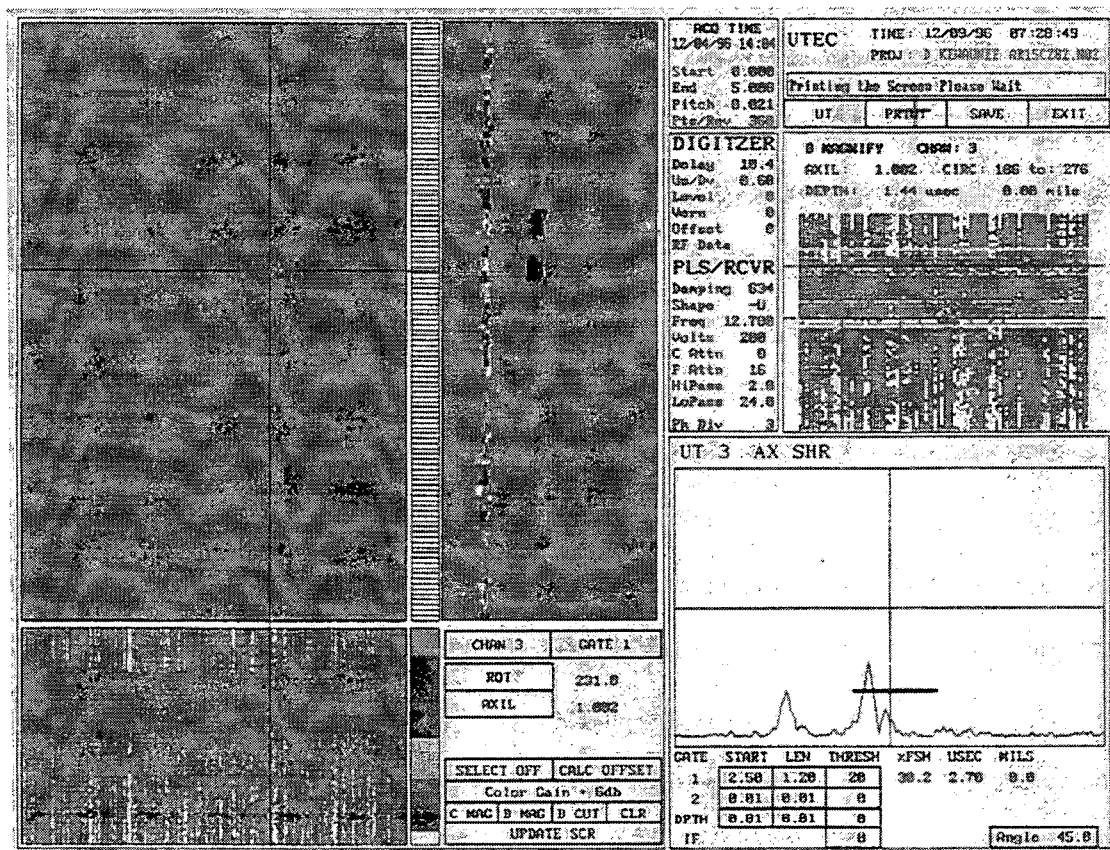


Figure 2-28 Ultrasonic test UTEC display of the axial aim data obtained on the tubesheet top region of Tube R15C28.

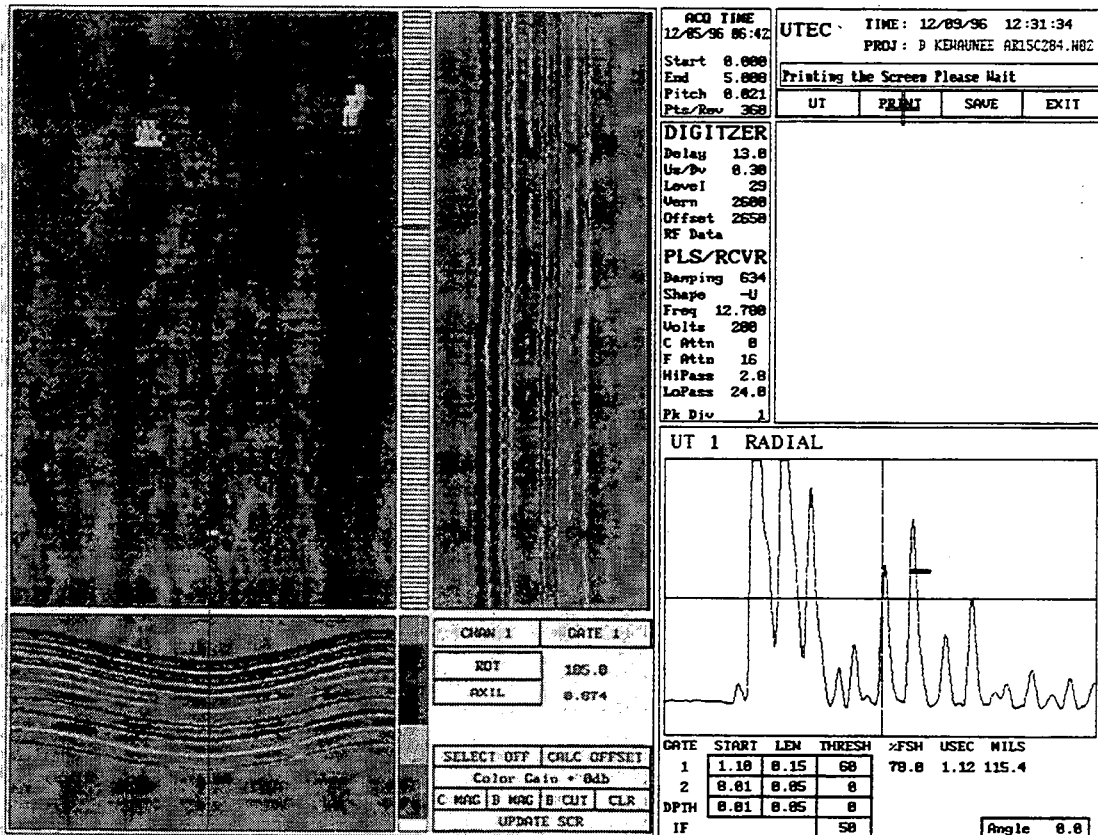


Figure 2-29 Ultrasonic test UTEC display of the radial aim data obtained on the first support plate crevice region of Tube R15C28.

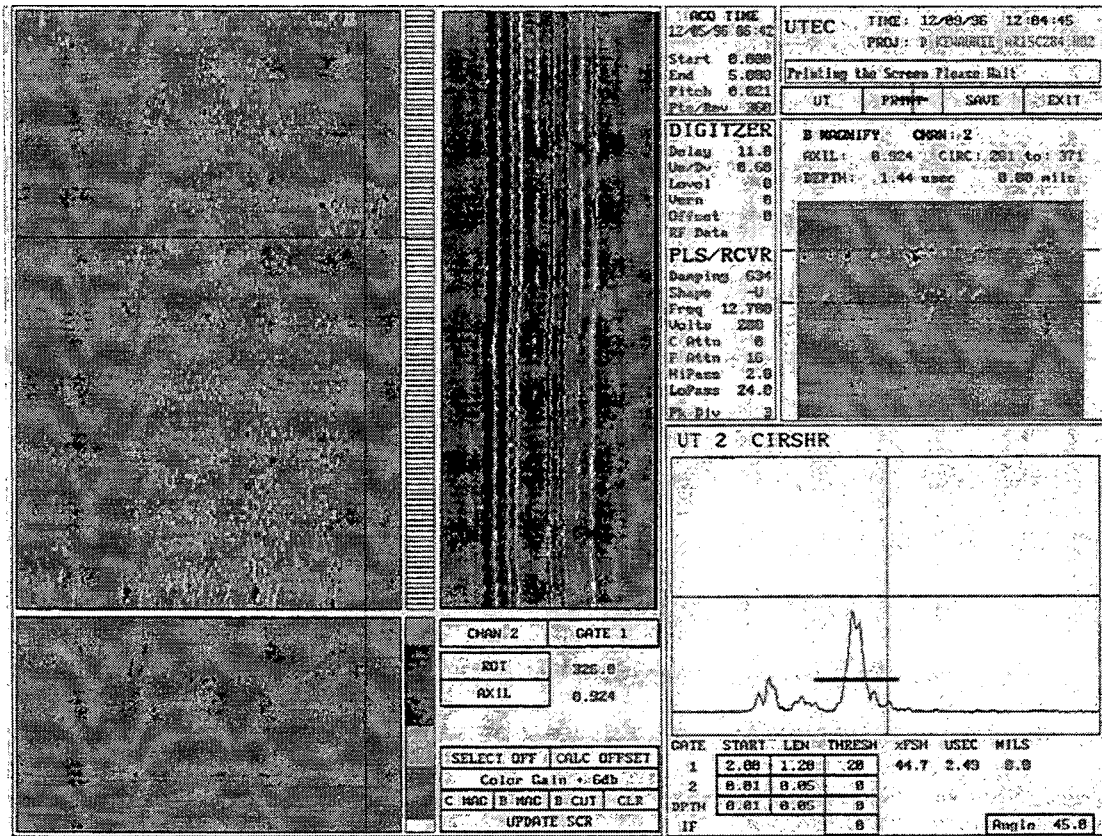


Figure 2-30 Ultrasonic test UTEC display of the circumferential aim data obtained on the first support plate crevice region of Tube R15C28.

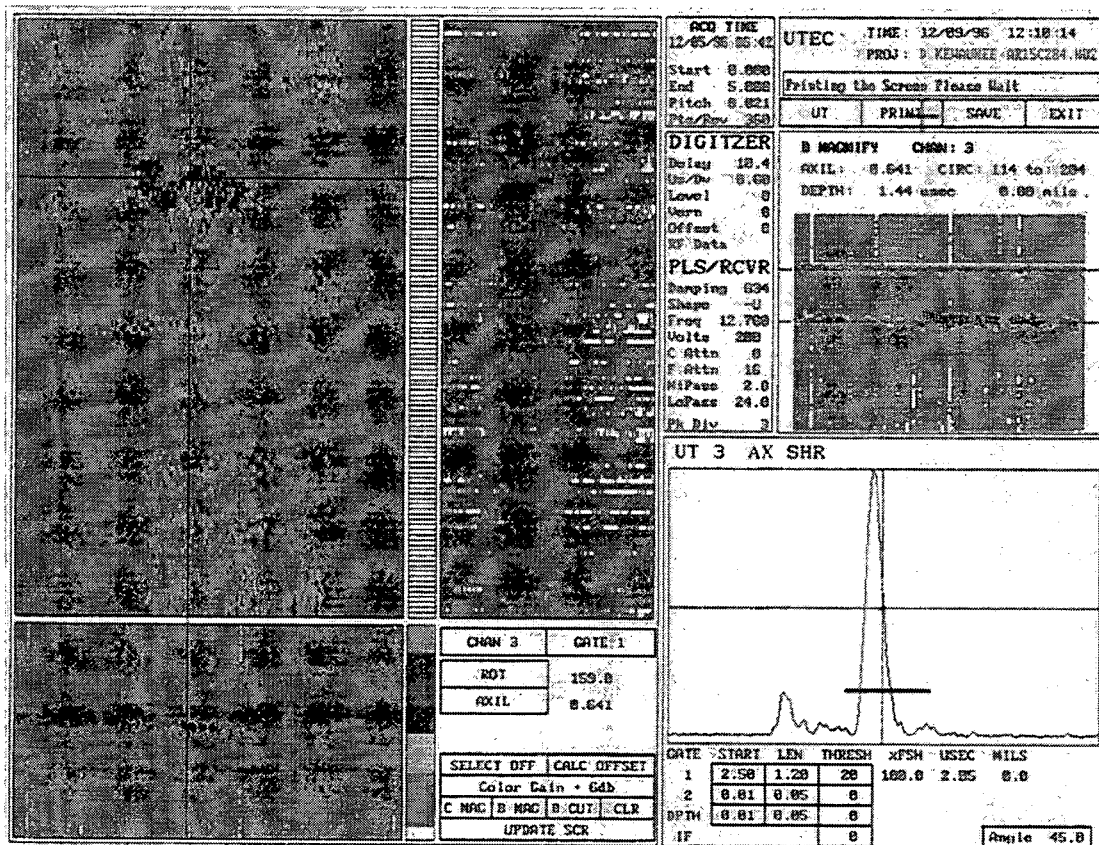


Figure 2-31 Ultrasonic test UTEC display of the axial aim data obtained on the first support plate crevice region of Tube R15C28.

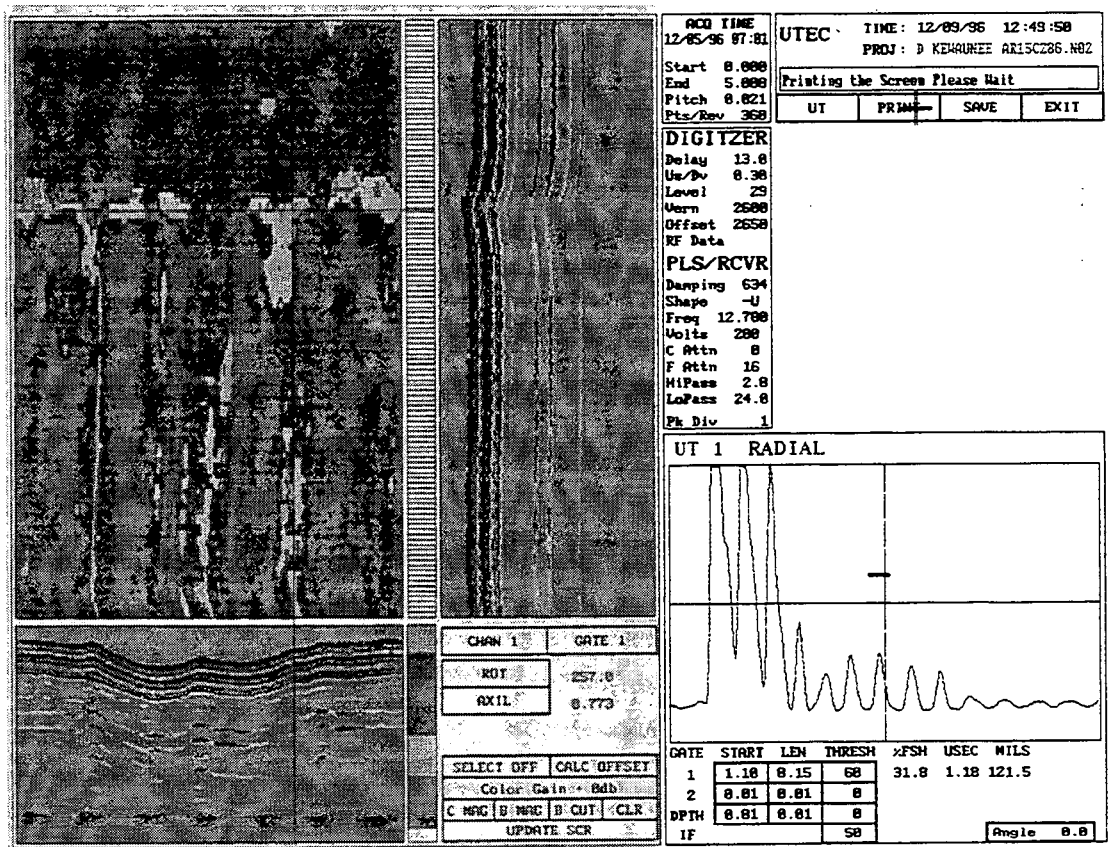


Figure 2-32 Ultrasonic test UTEC display of the radial aim data obtained on the second support plate crevice region of Tube R15C28.

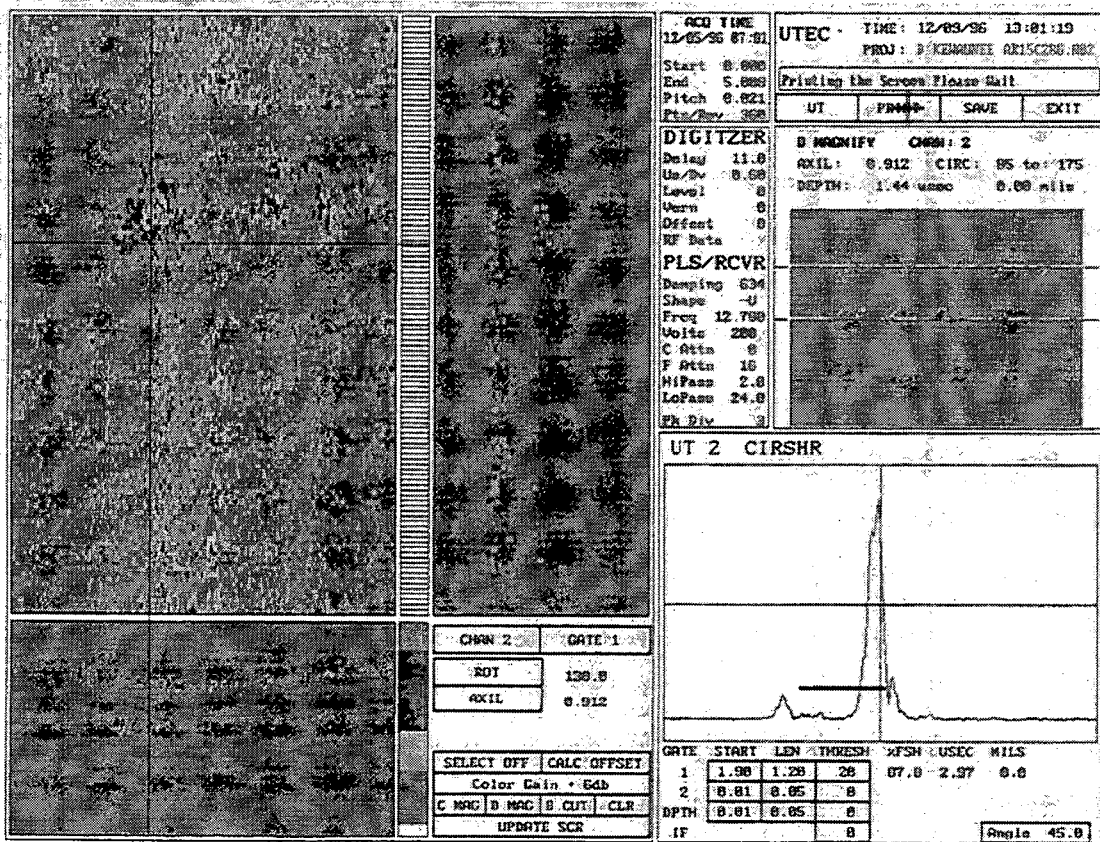


Figure 2-33 Ultrasonic test UTEC display of the circumferential aim data obtained on the second support plate crevice region of Tube R15C28.

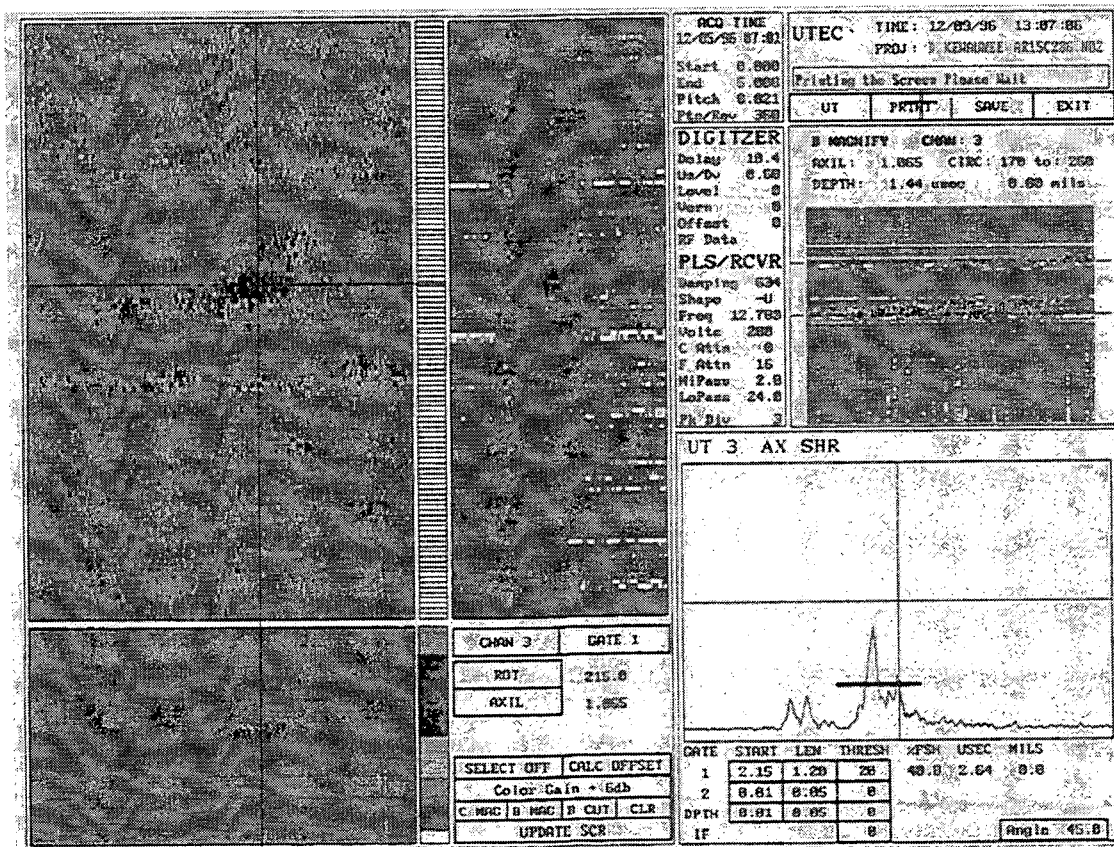


Figure 2-34 Ultrasonic test UTEC display of the axial aim data obtained on the second support plate crevice region of Tube R15C28.

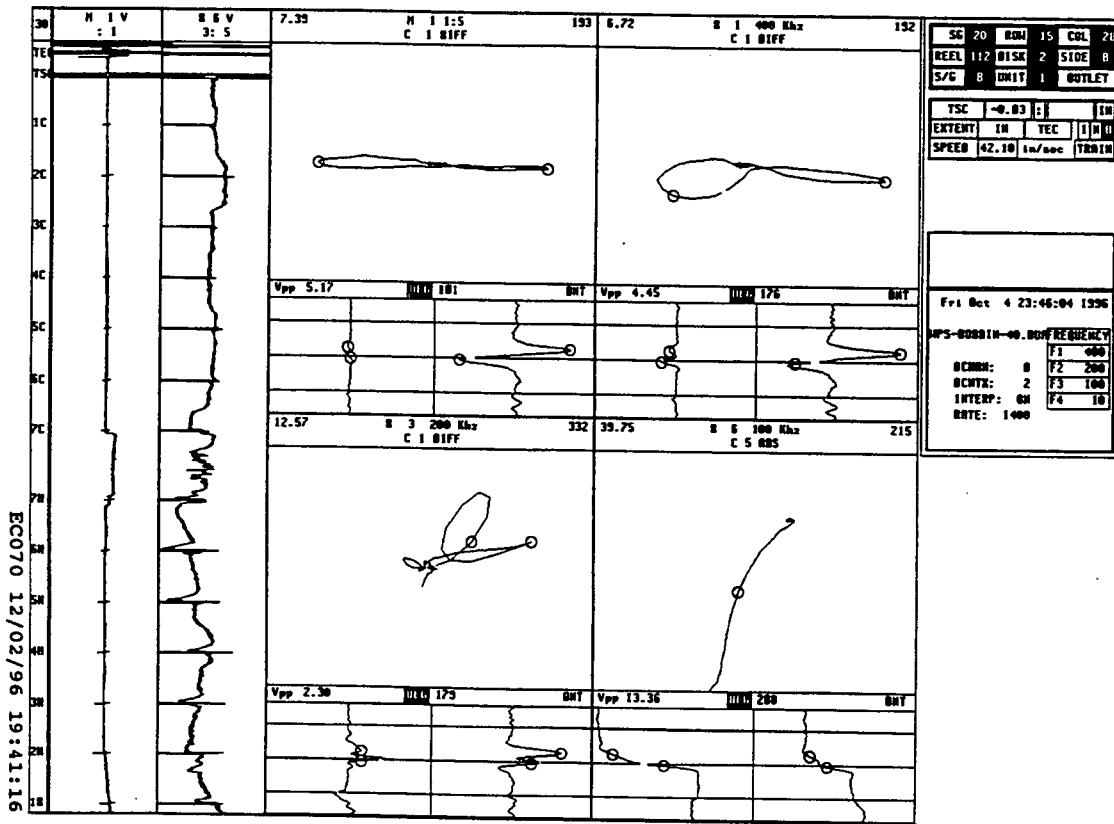


Figure 2-35 TST (tubesheet top) region of Tube R15C28. Field bobbin probe eddy current test data.

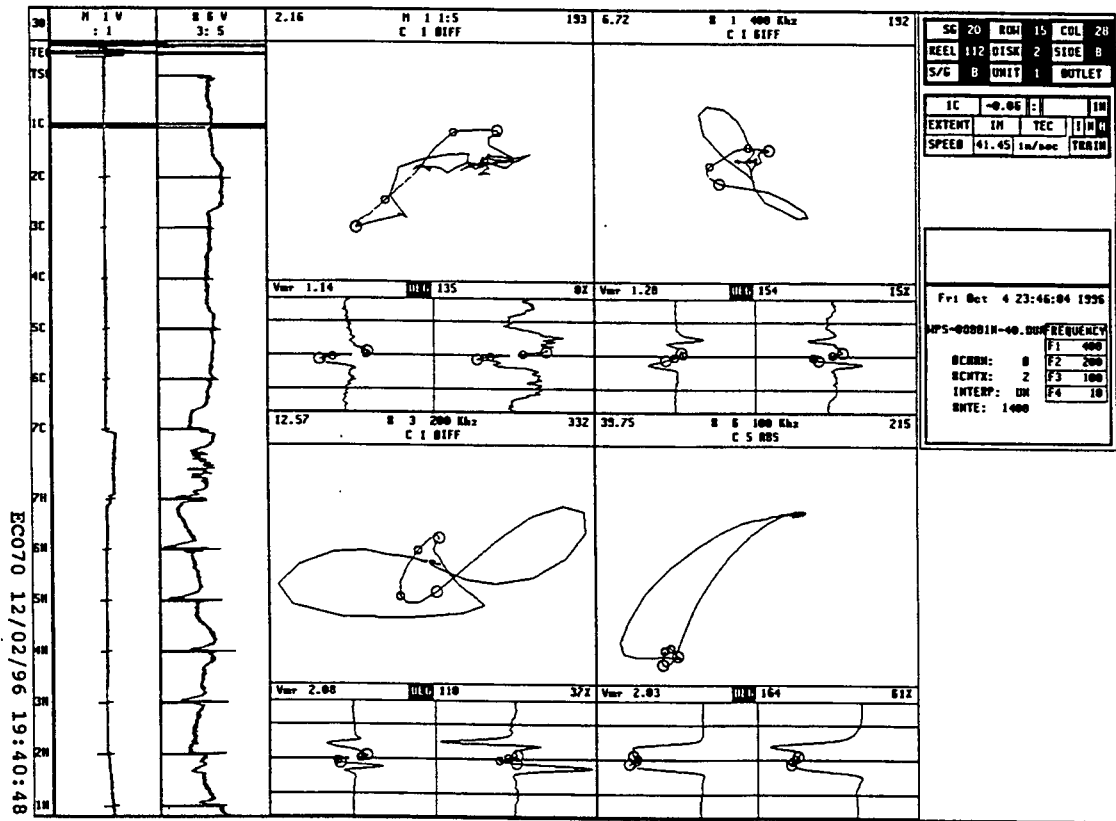


Figure 2-36 TSP1 (first tube support plate) crevice region of Tube R15C28. Field bobbin probe eddy current test data.

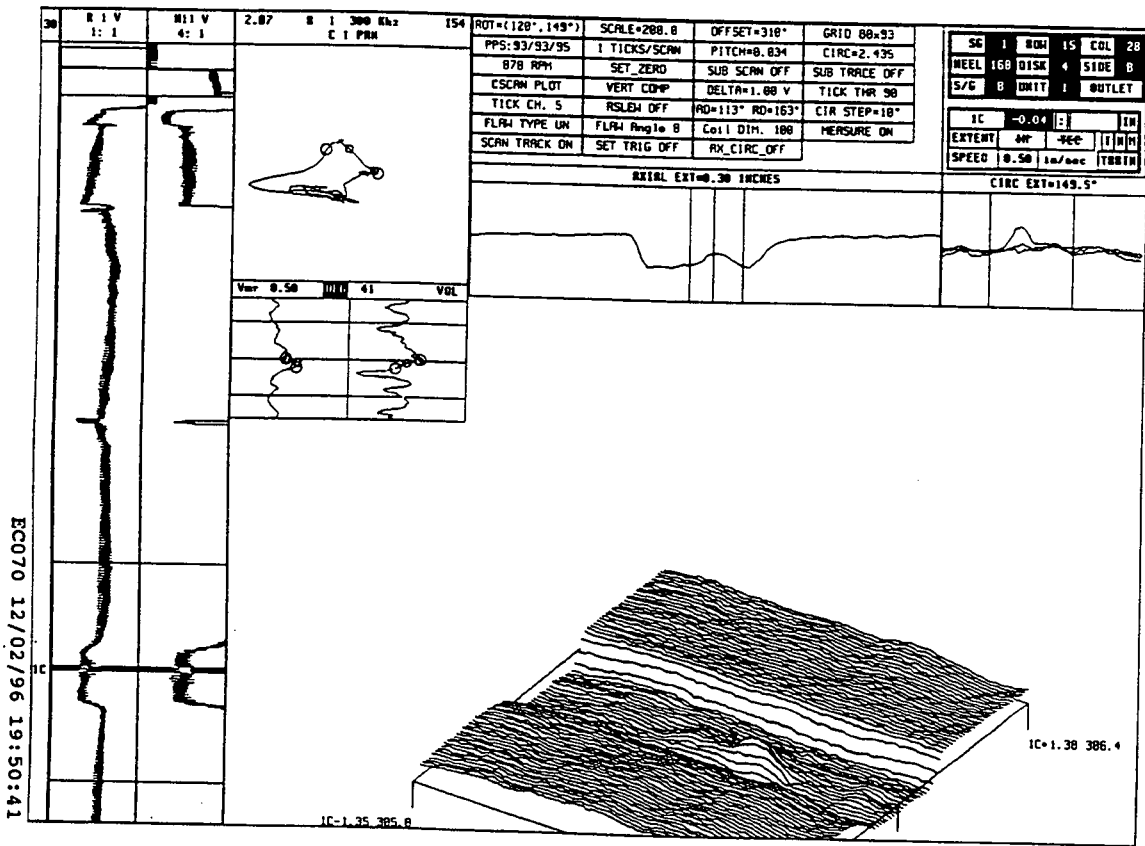


Figure 2-37 TSP1 crevice region of Tube R15C28. Field 3-coil MRPC probe pancake coil eddy current test data.

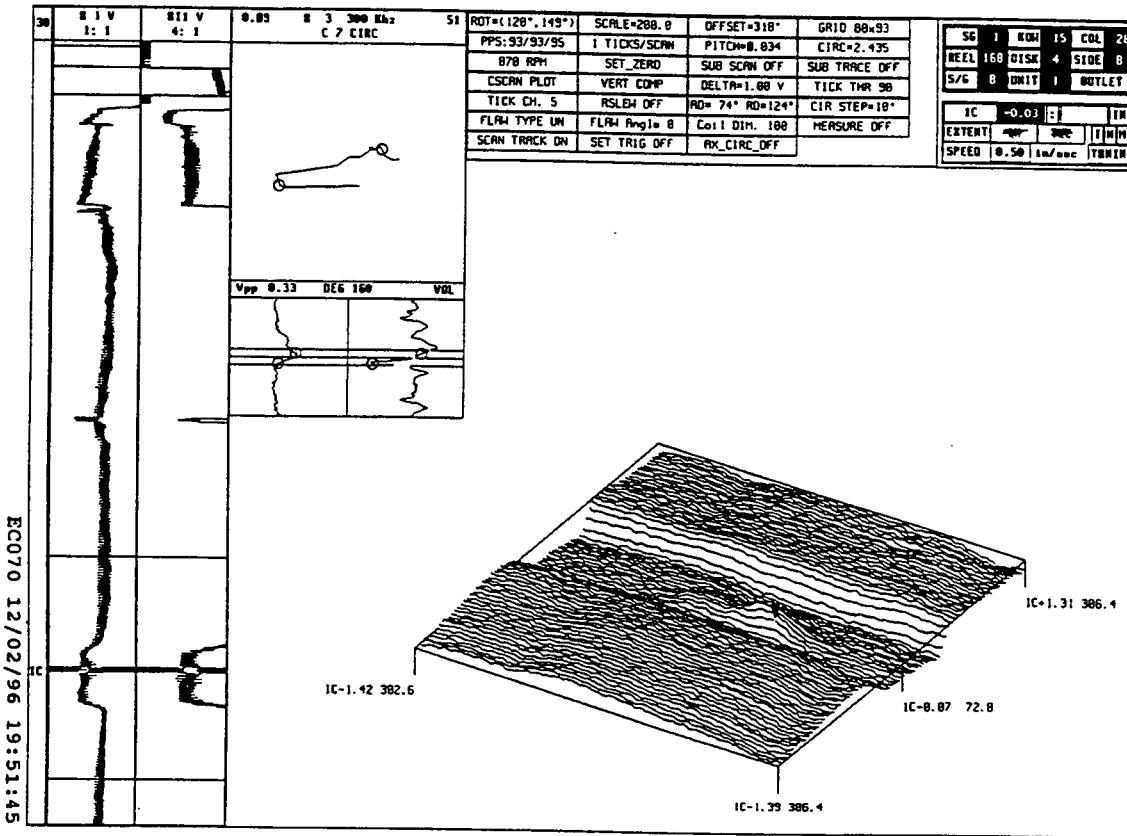


Figure 2-38 TSP1 crevice region of Tube R15C28. Field 3-coil MRPC probe circumferentially sensitive coil eddy current test data.

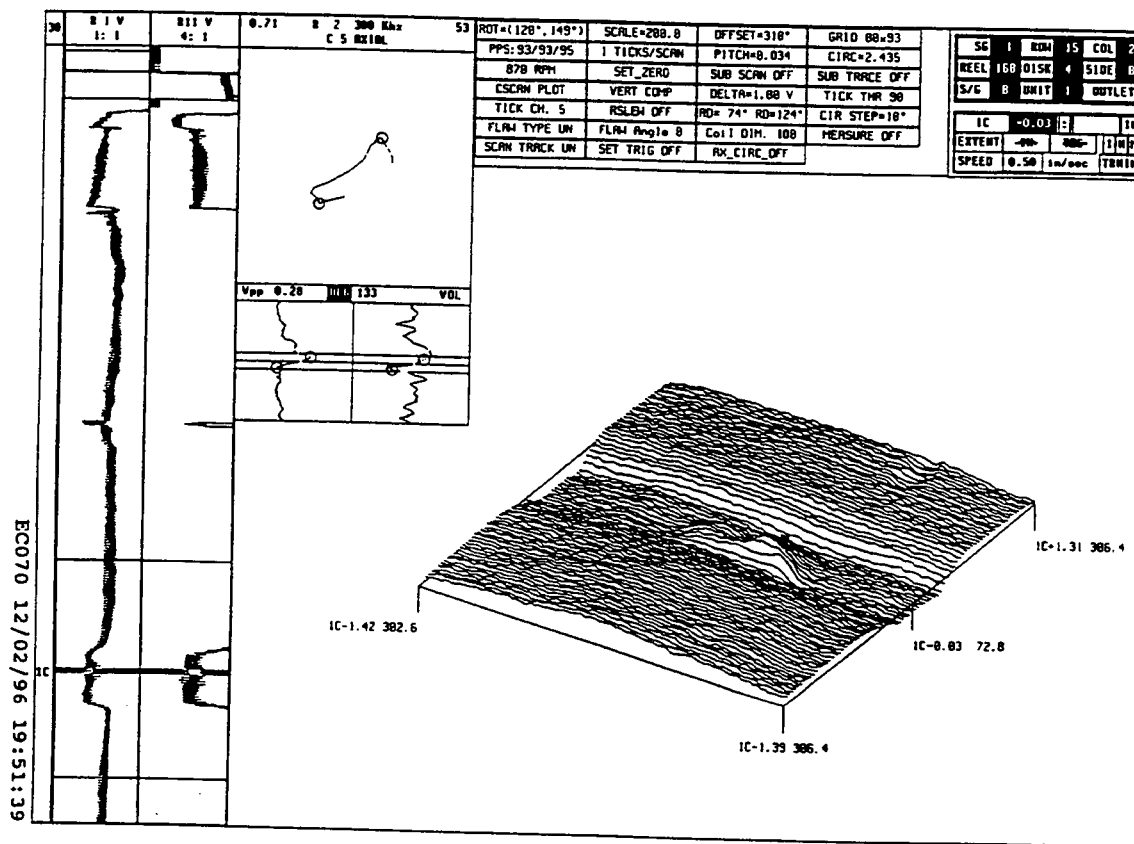


Figure 2-39 TSP1 crevice region of Tube R15C28. Field 3-coil MRPC probe axially sensitive coil eddy current test data.

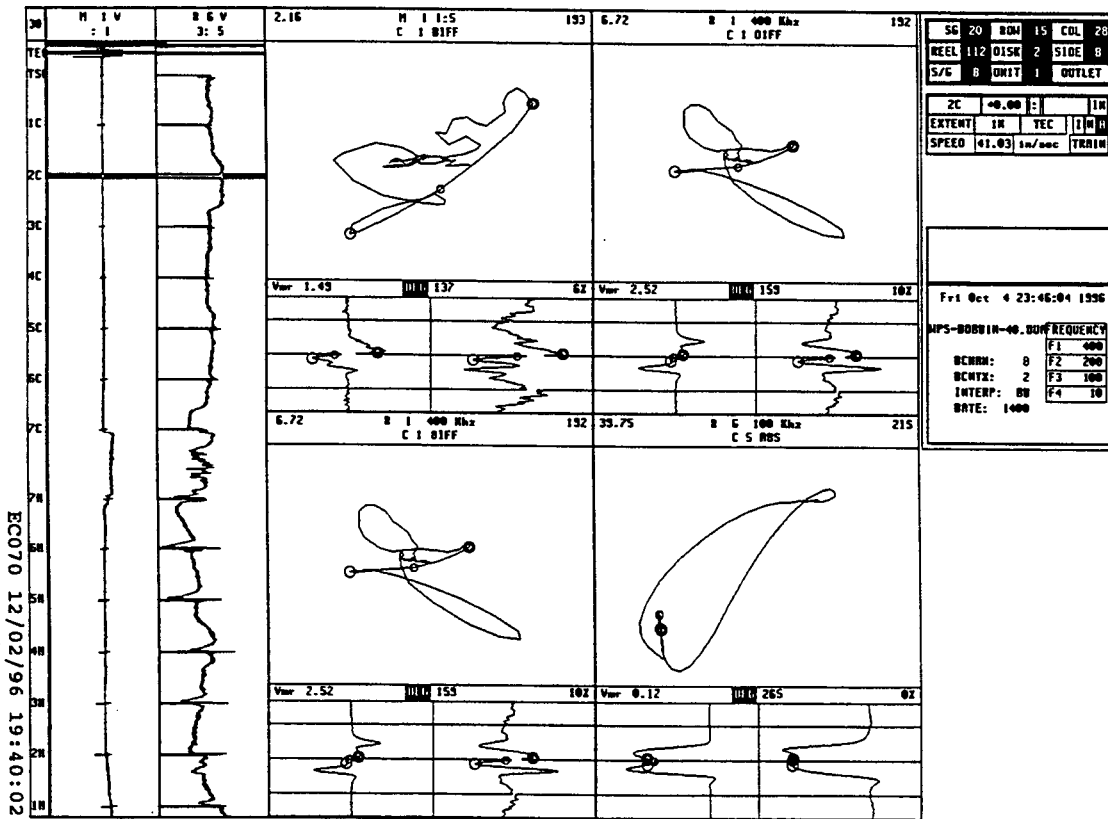


Figure 2-40 TSP2 (second tube support plate) crevice region of Tube R15C28. Field bobbin probe eddy current test data.

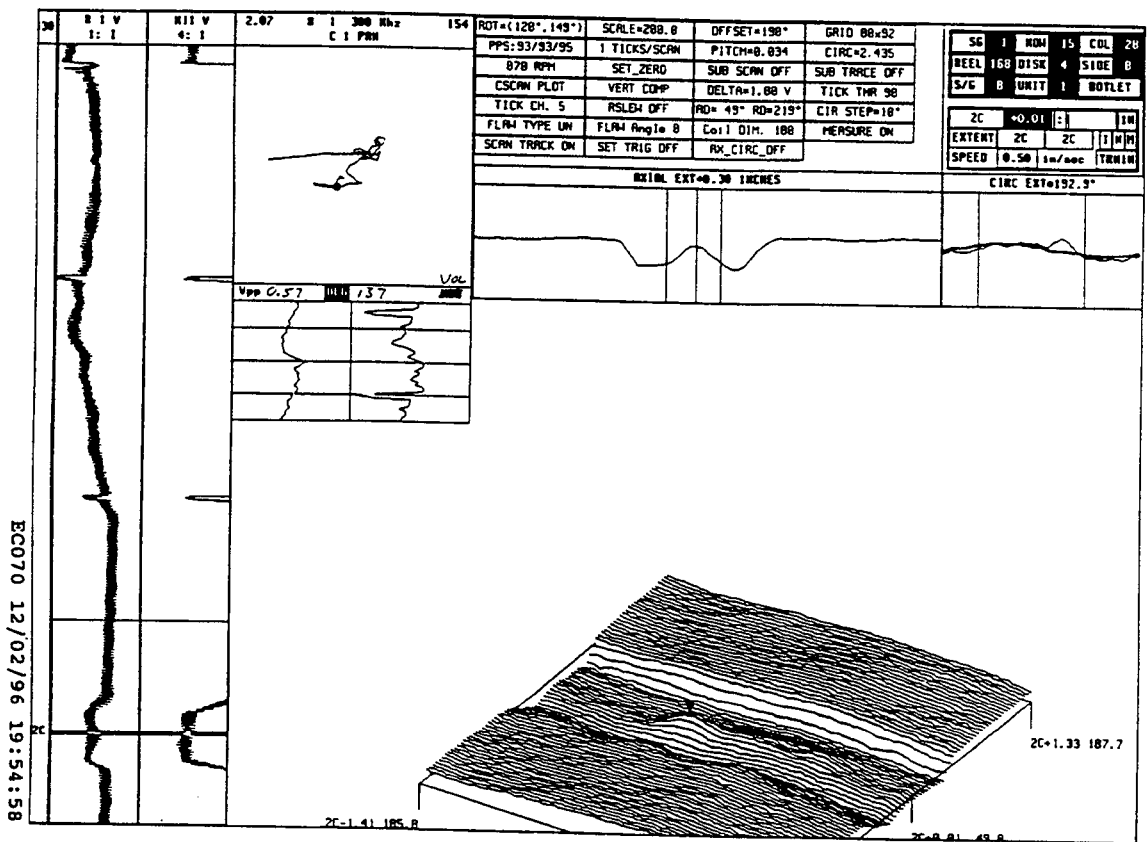


Figure 2-41 TSP2 crevice region of Tube R15C28. Field 3-coil MRPC probe pancake coil eddy current test data.

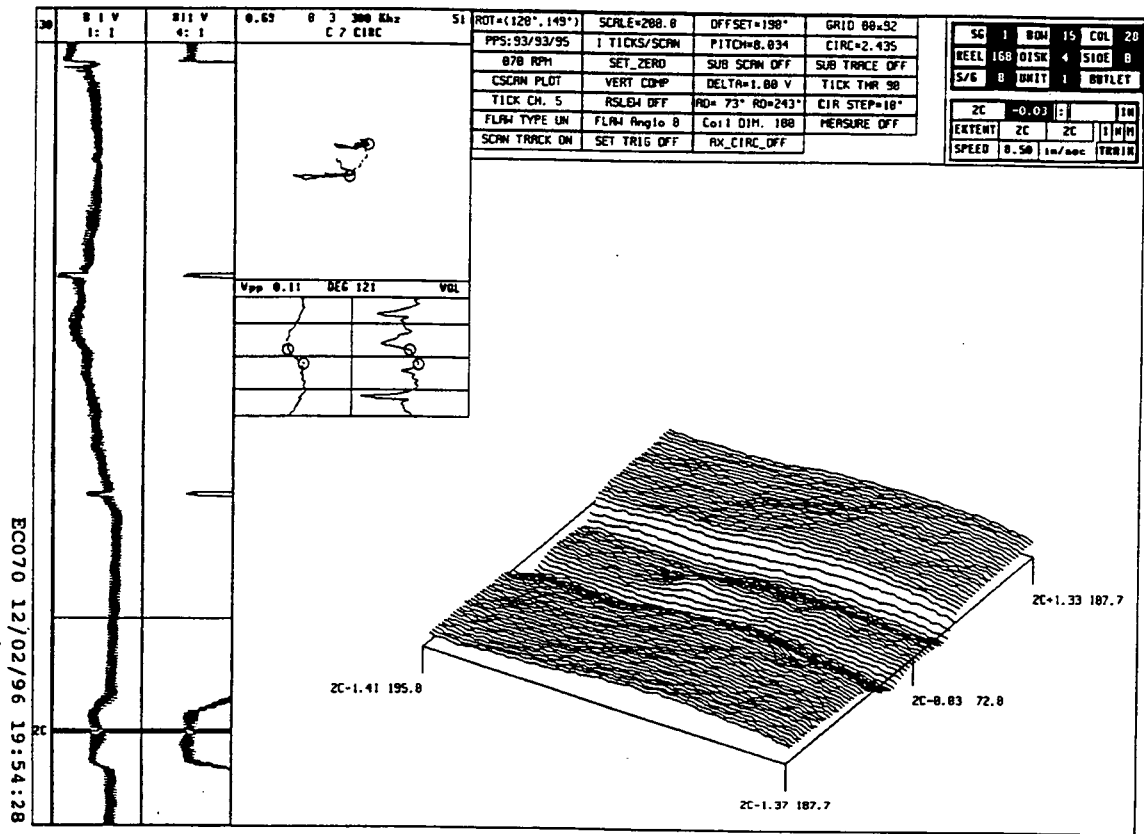


Figure 2-42 TSP2 crevice region of Tube R15C28. Field 3-coil MRPC probe circumferentially sensitive coil eddy current test data.

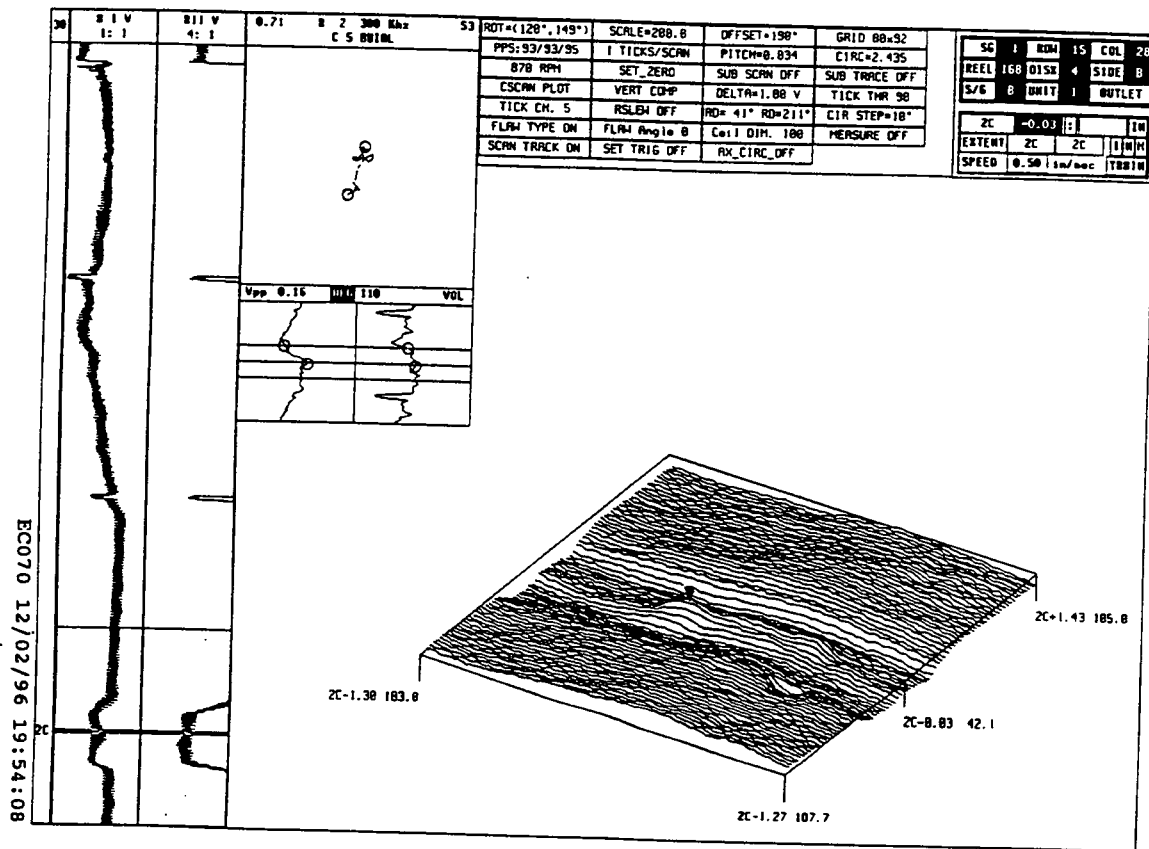


Figure 2-43 TSP2 crevice region of Tube R15C28. Field 3-coil MRPC probe axially sensitive coil eddy current test data.

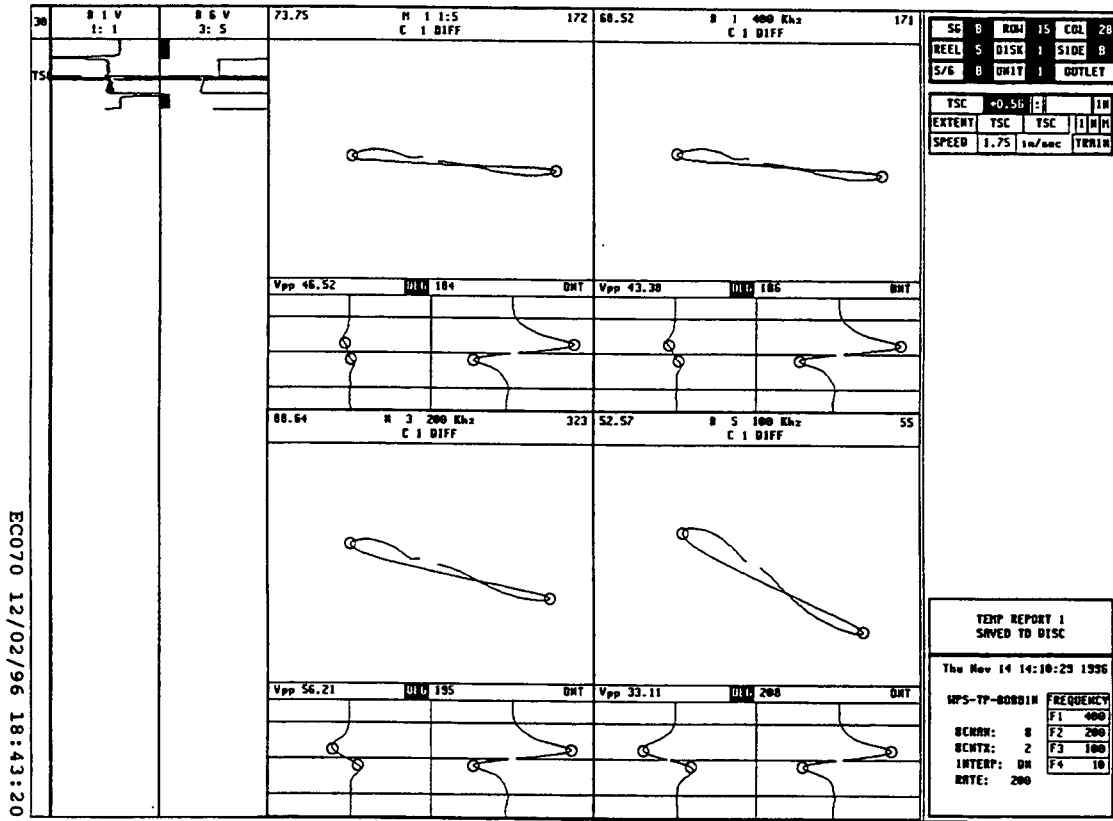


Figure 2-44 TST (tubesheet top) region of Tube R15C28. Laboratory bobbin probe eddy current test data.

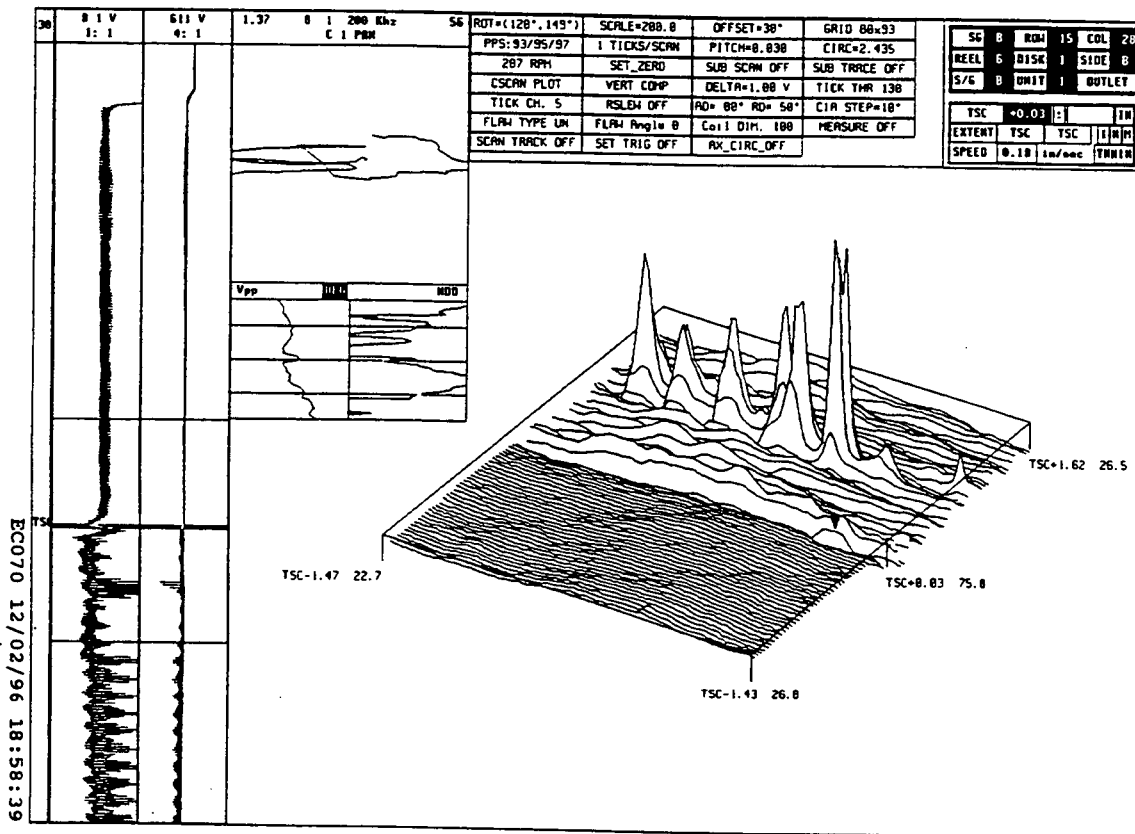


Figure 2-45 TST region of Tube R15C28. Laboratory 3-coil MRPC probe pancake coil eddy current test data, showing only numerous lift-off signals.

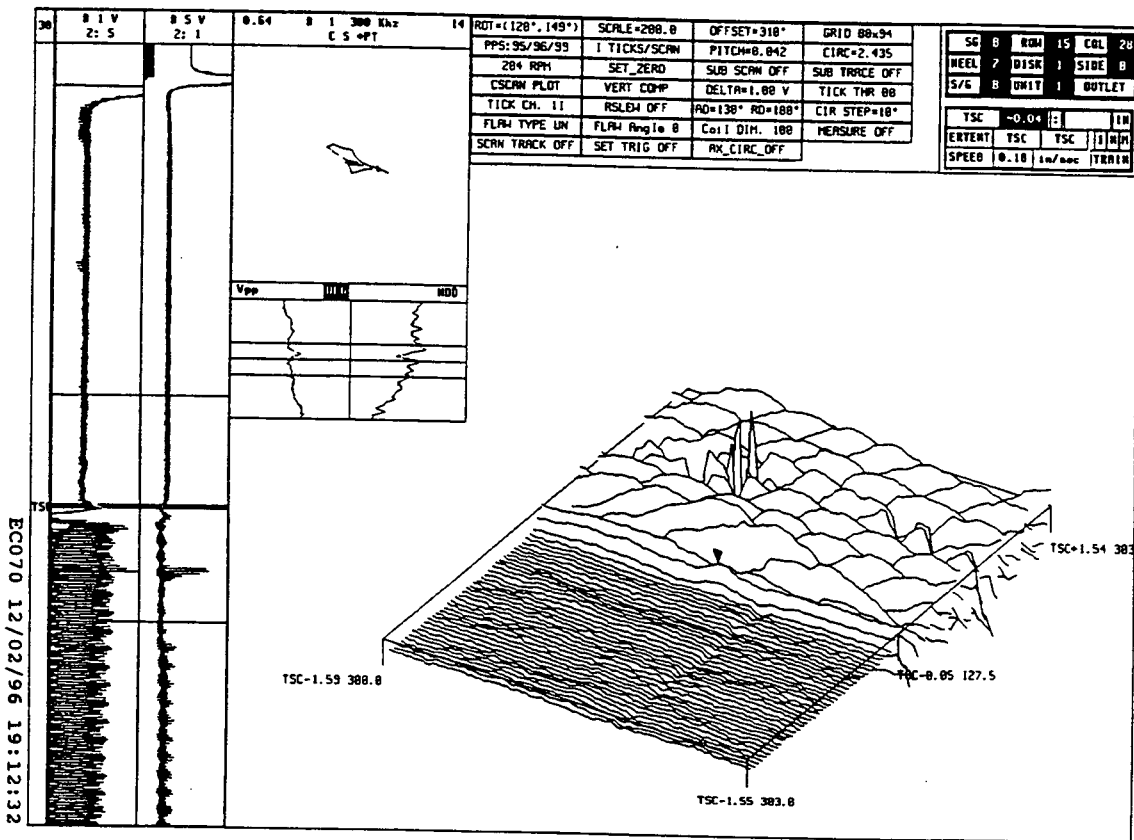


Figure 2-46 TST region of Tube R15C28. Laboratory +Point probe eddy current test data, showing only a few lift-off signals.

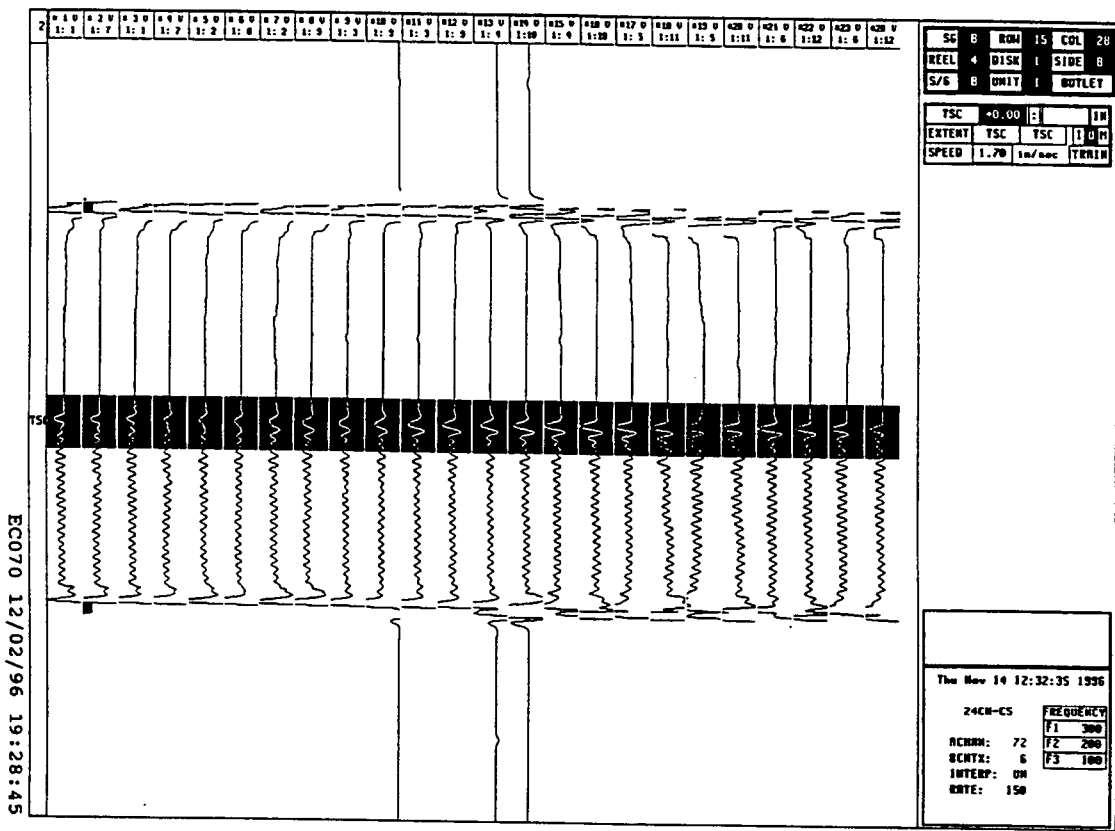


Figure 2-47 TST region of Tube R15C28. Laboratory Cecco 5 probe eddy current test data strip chart.

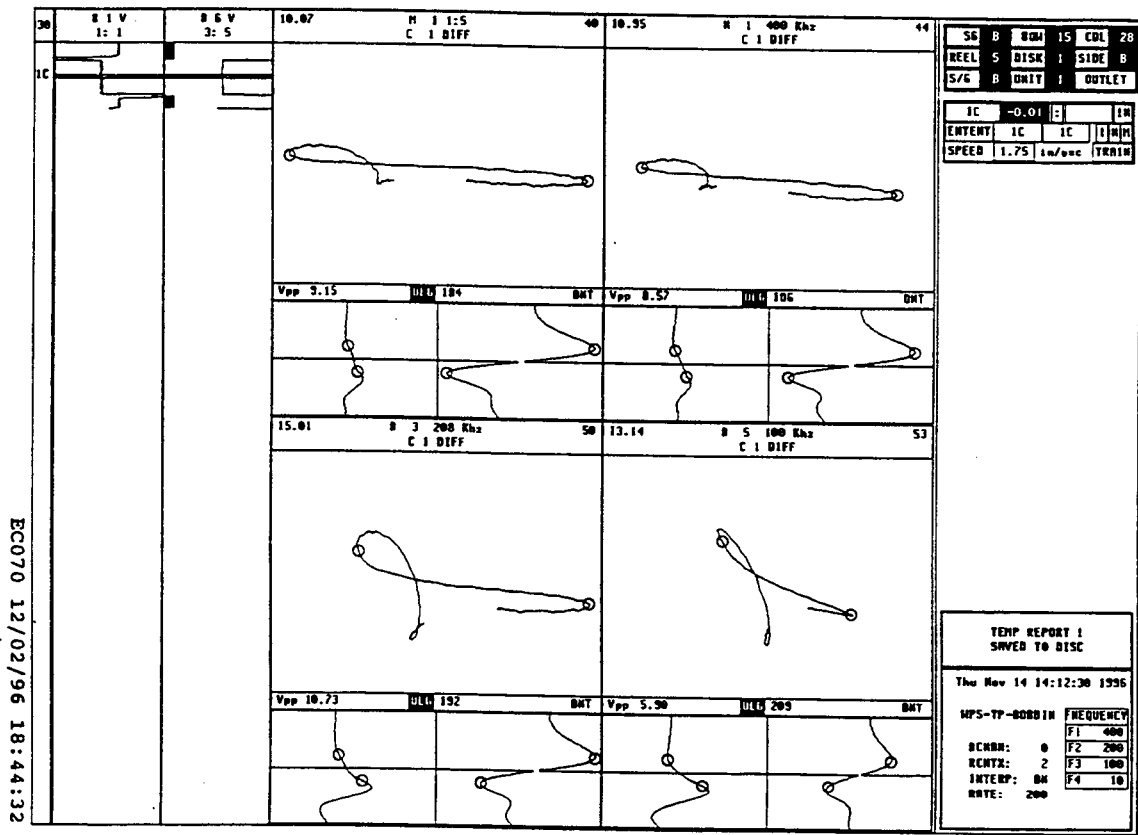


Figure 2-48 TSP1 (first tube support plate) crevice region of Tube R15C28. Laboratory bobbin probe eddy current test data, showing a dent signal.

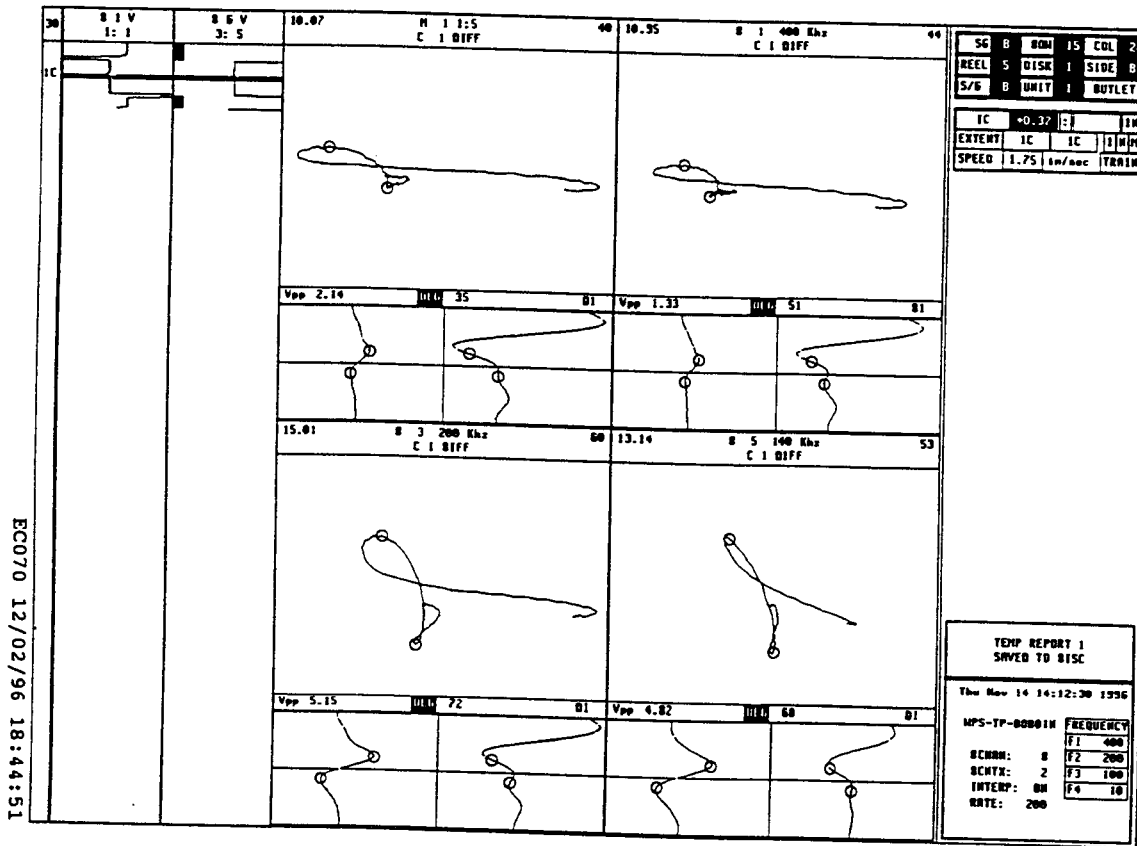


Figure 2-49 TSP1 crevice region of Tube R15C28. Laboratory bobbin probe eddy current test data, showing a distorted indication in the previous dent signal.

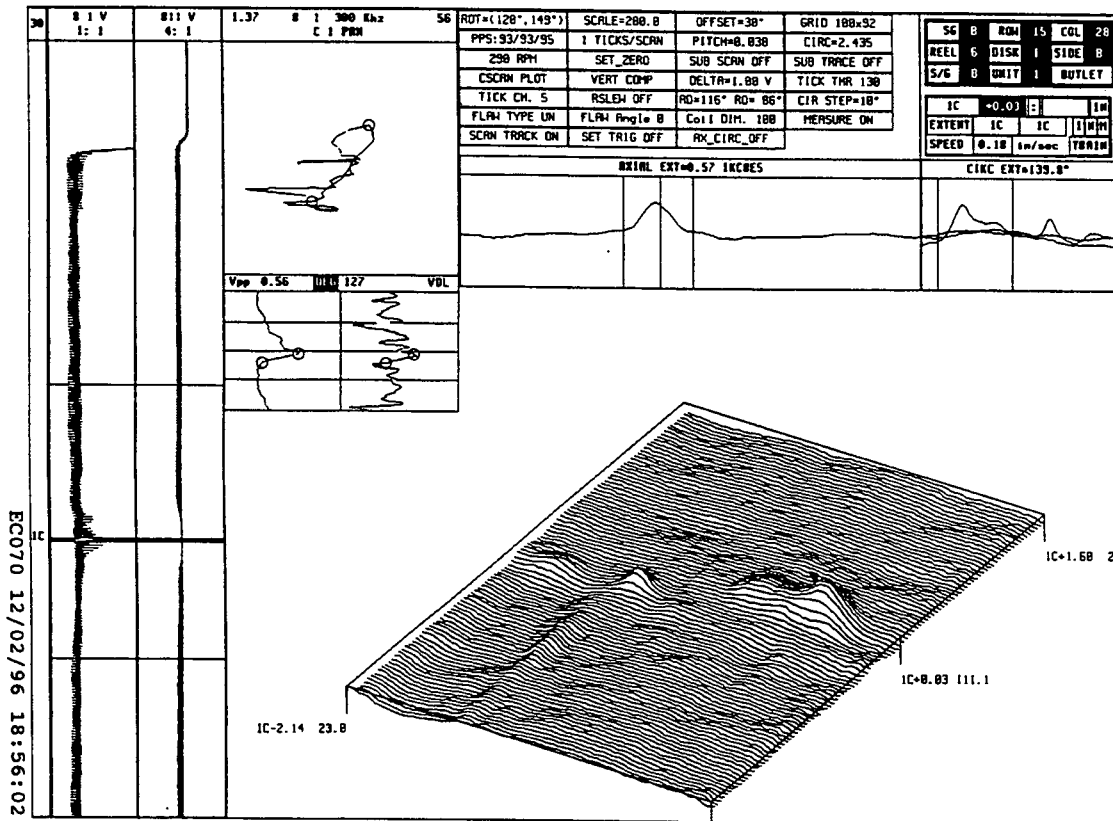


Figure 2-50 TSP1 crevice region of Tube R15C28. Laboratory 3-coil probe pancake coil eddy current test data.

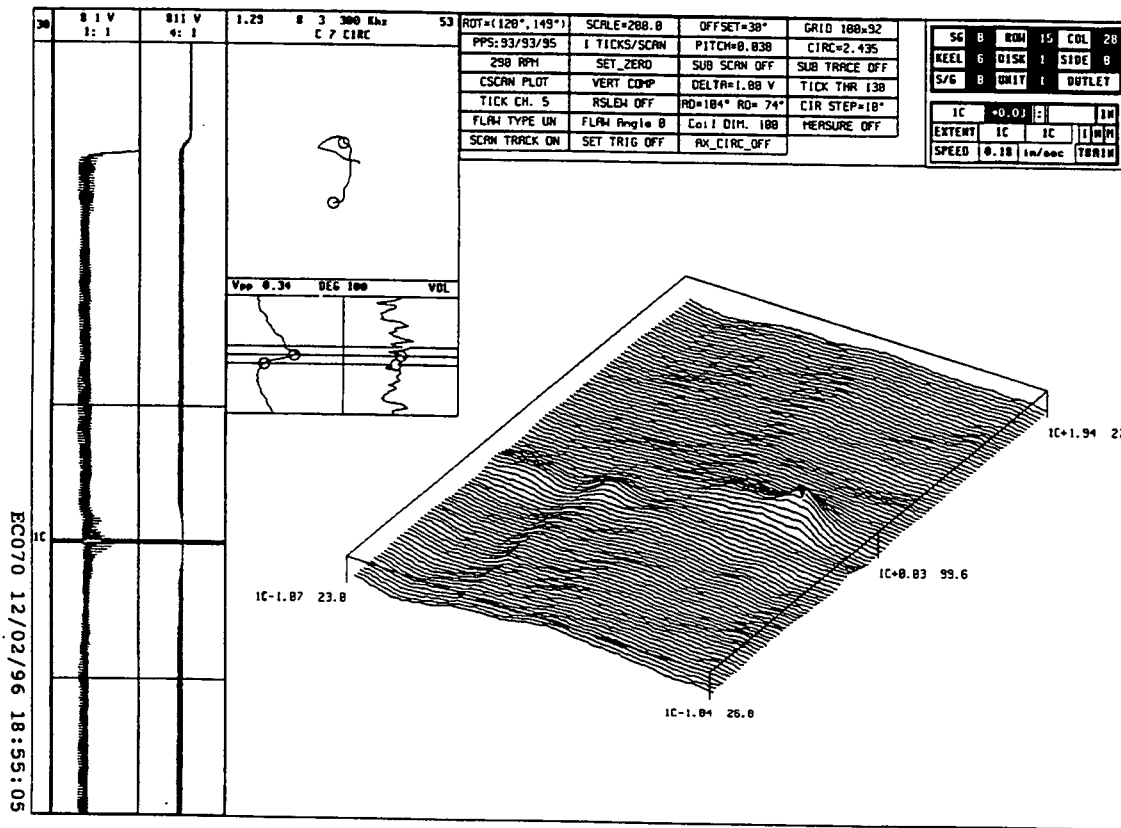


Figure 2-51 TSP1 crevice region of Tube R15C28. Laboratory 3-coil probe circumferentially sensitive coil eddy current test data.

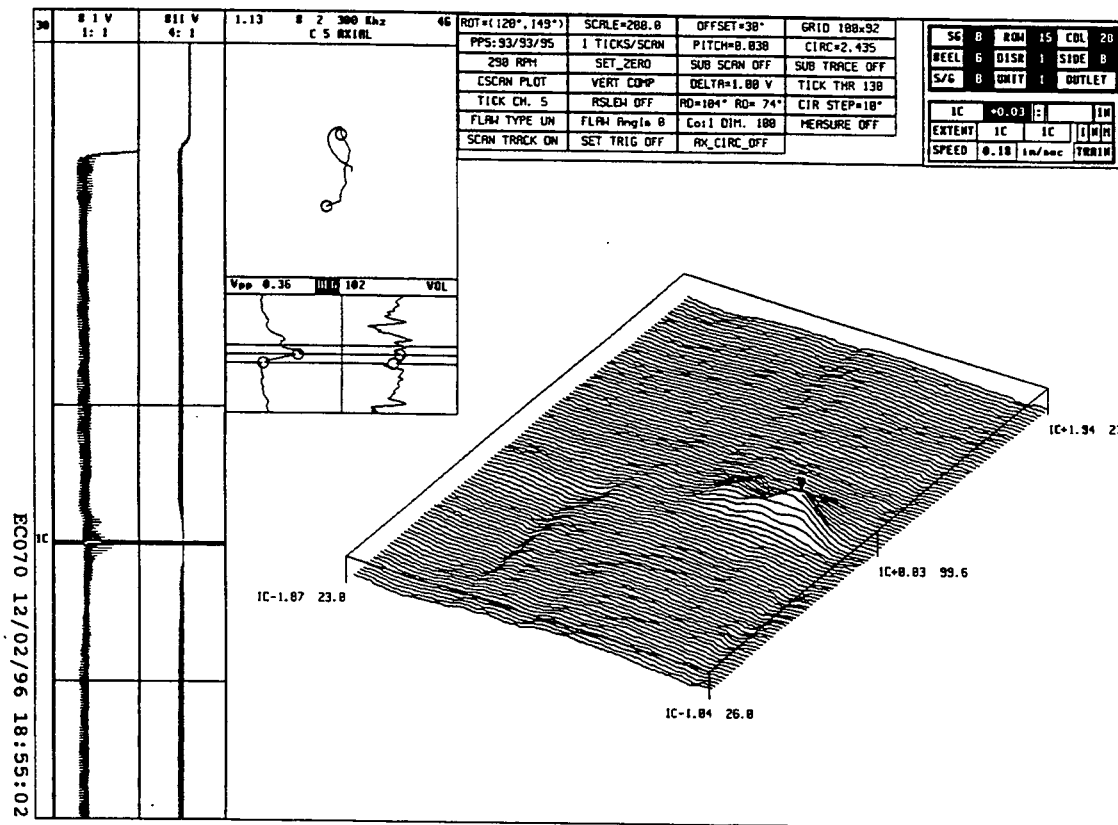


Figure 2-52 TSP1 crevice region of Tube R15C28. Laboratory 3-coil probe axially sensitive coil eddy current test data.

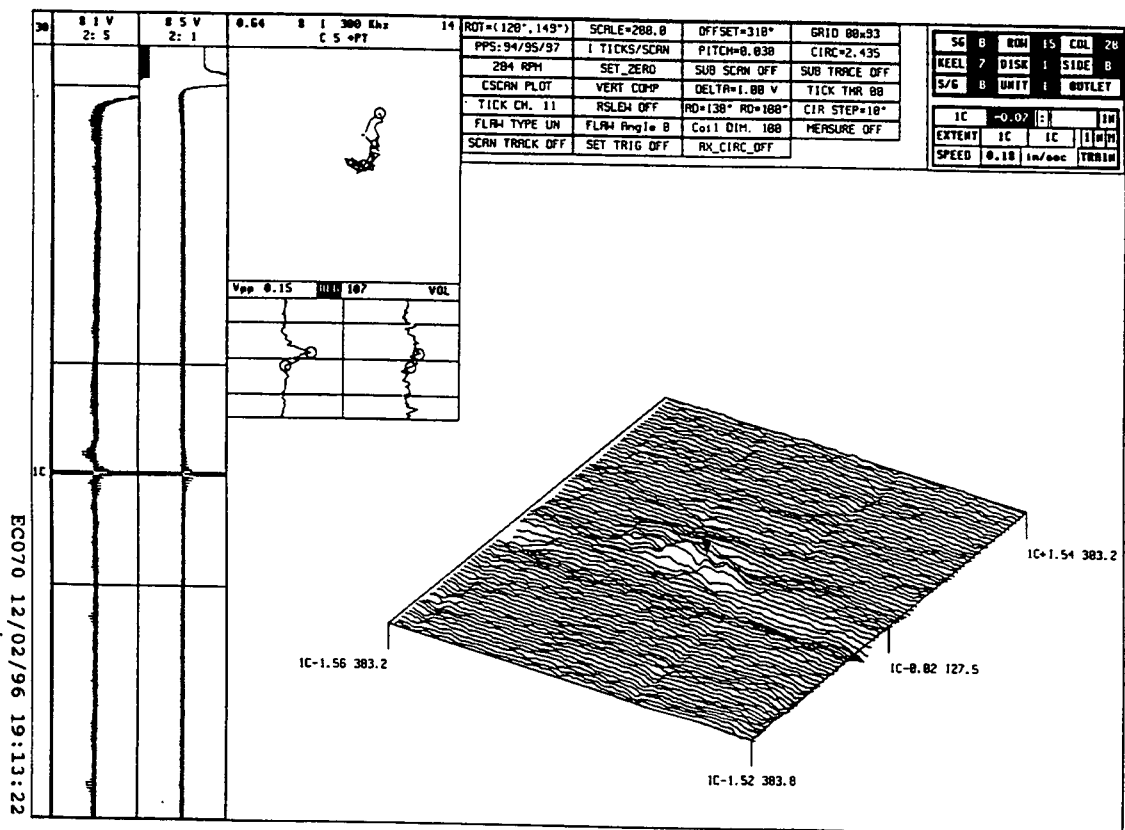


Figure 2-53 TSP1 crevice region of Tube R15C28. Laboratory +Point probe eddy current test data.

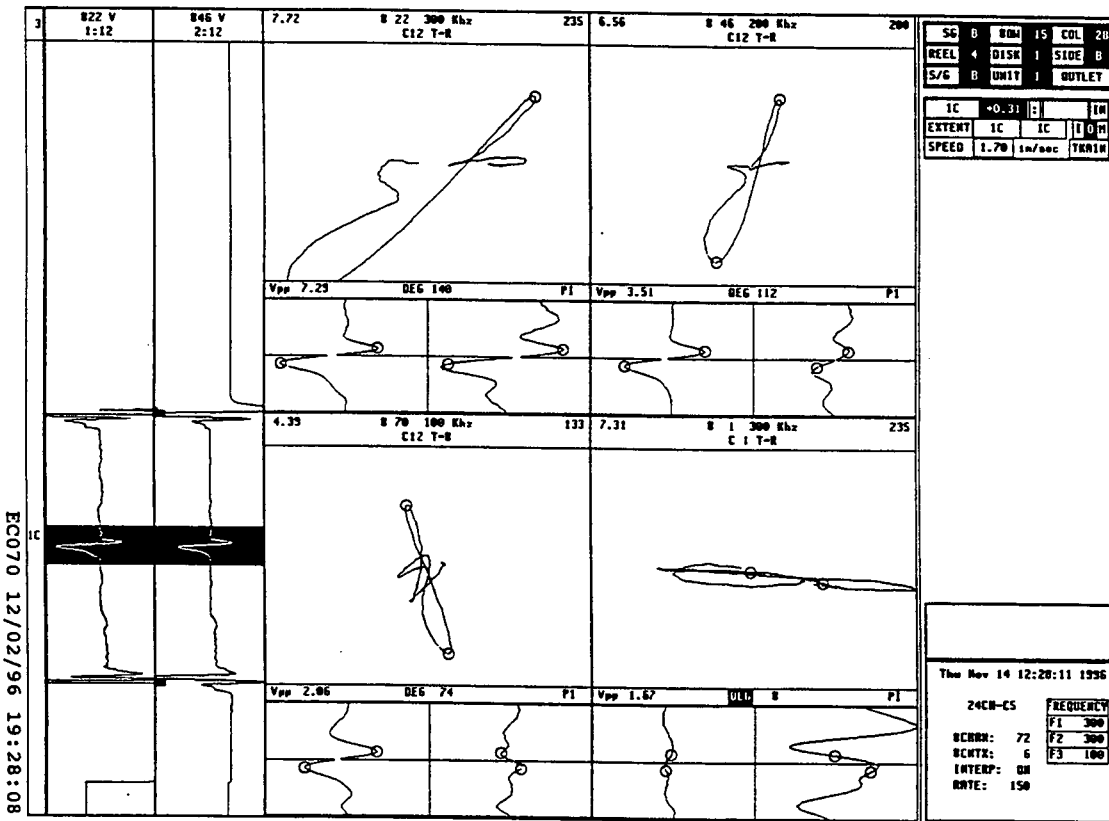


Figure 2-54 TSP1 crevice region of Tube R15C28. Laboratory Cecco 5 probe eddy current test data Lissajous patterns.

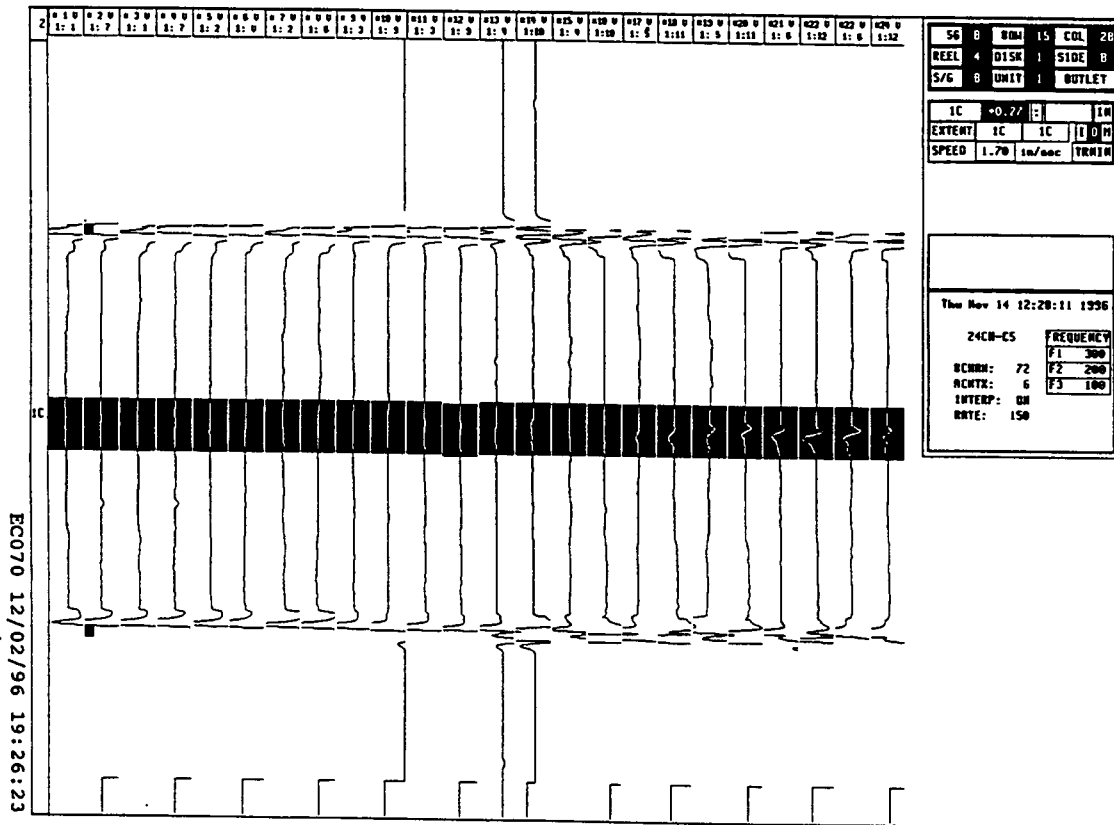


Figure 2-55 TSP1 crevice region of Tube R15C28. Laboratory Cecco 5 probe eddy current test data strip chart.

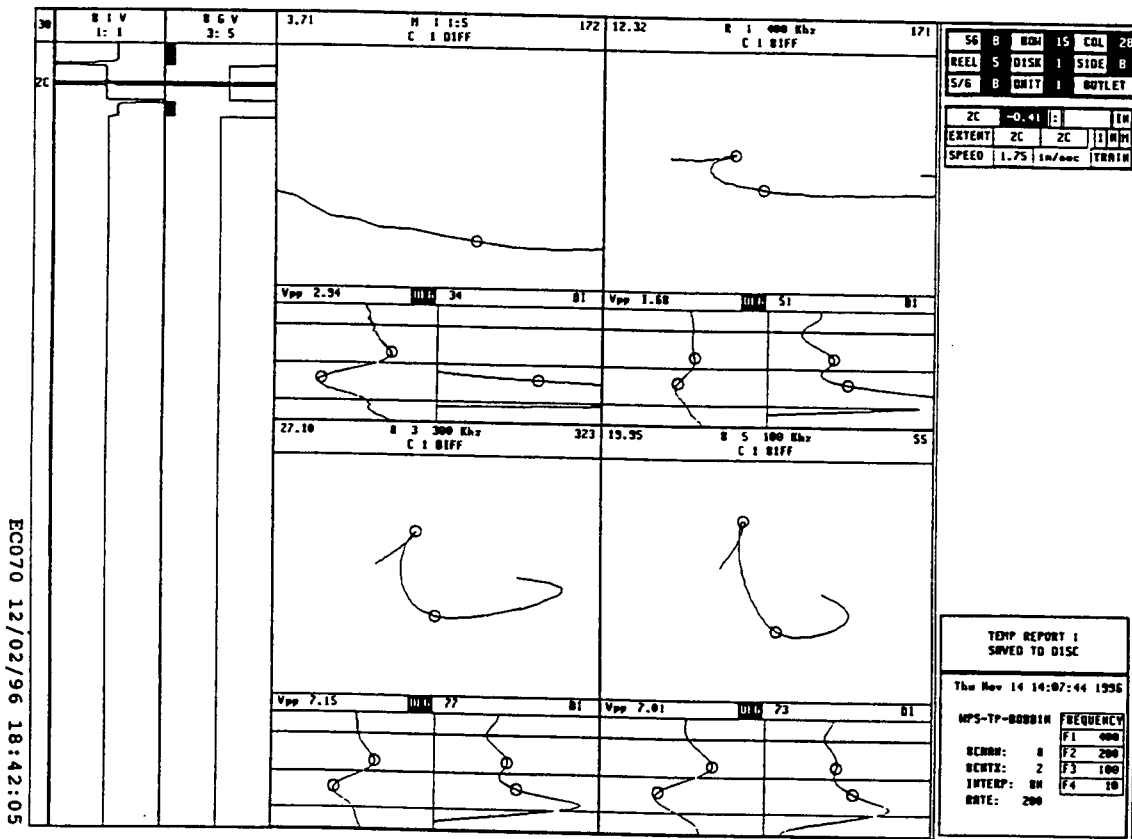
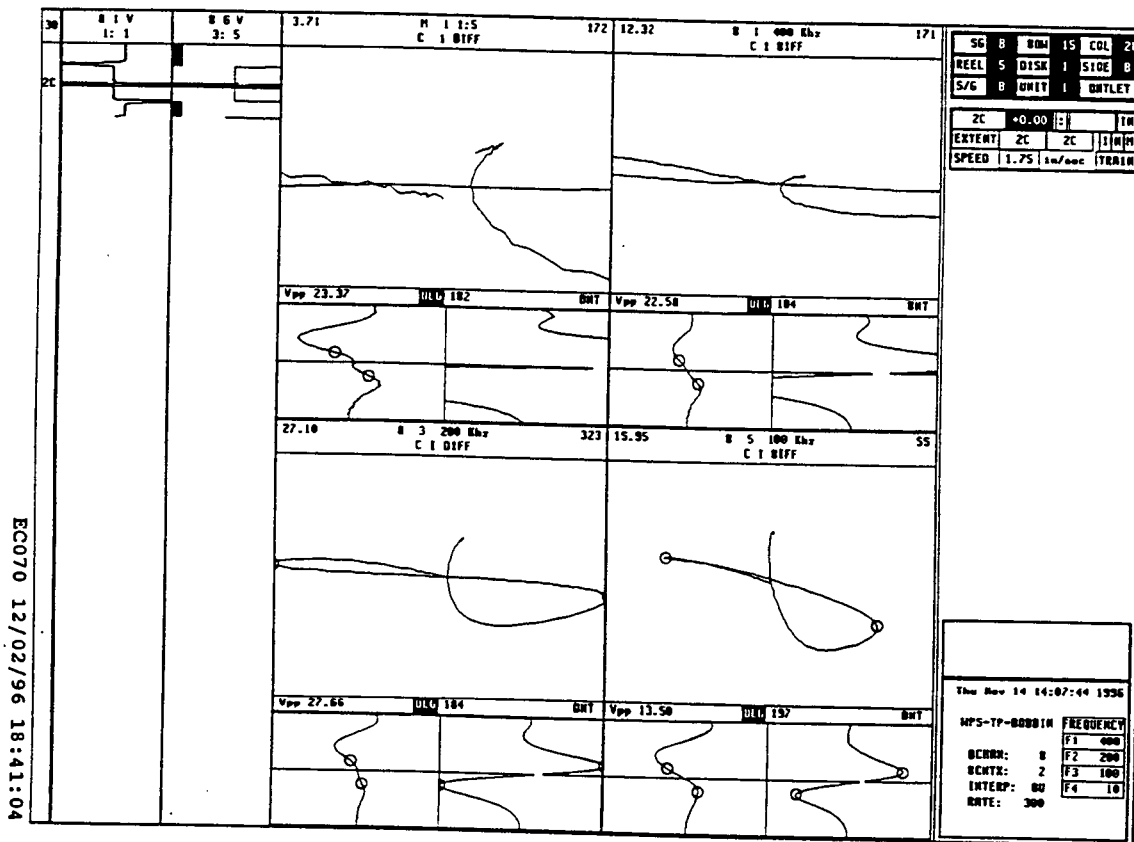


Figure 2-57 TSP2 crevice region of Tube R15C28. Laboratory bobbin probe eddy current test data, showing a distorted indication in the previous dent signal.



EC070 12/02/96 18:41:04

Figure 2-56 TSP2 (second tube support plate) crevice region of Tube R15C28. Laboratory bobbin probe eddy current test data, showing a dent signal.

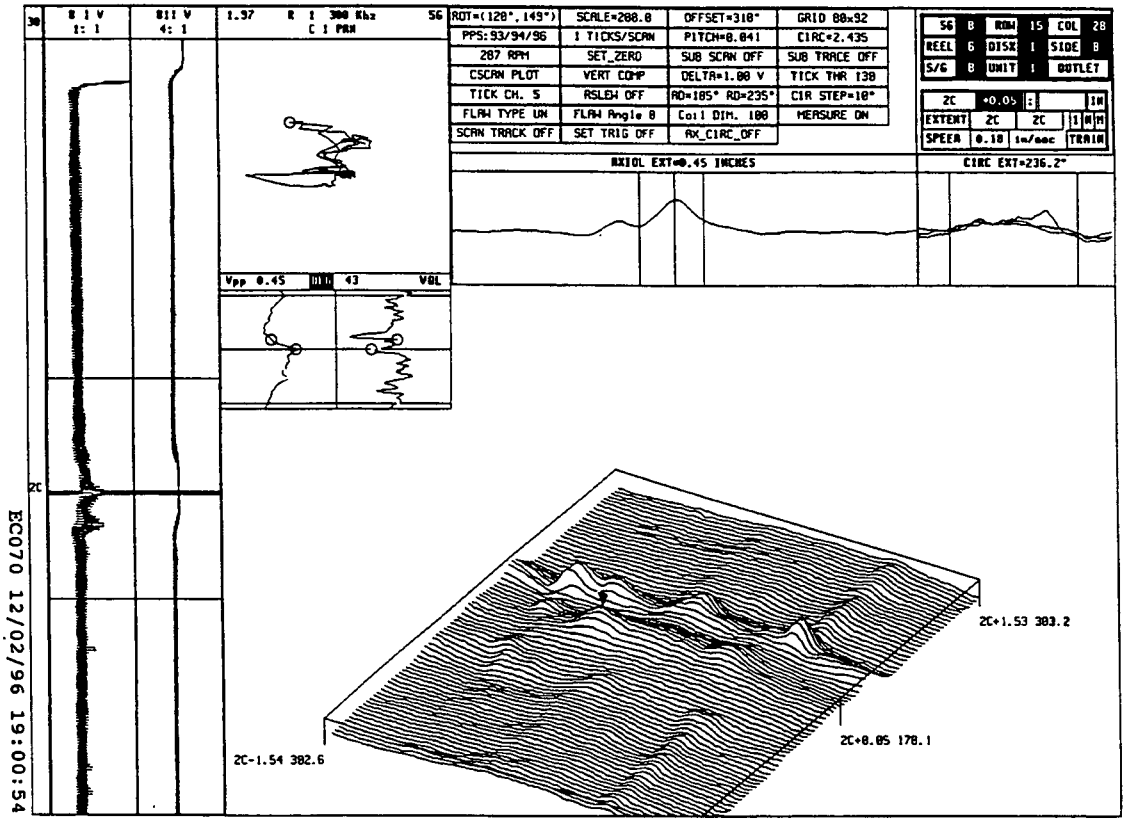


Figure 2-58 TSP2 crevice region of Tube R15C28. Laboratory 3-coil probe pancake coil eddy current test data.

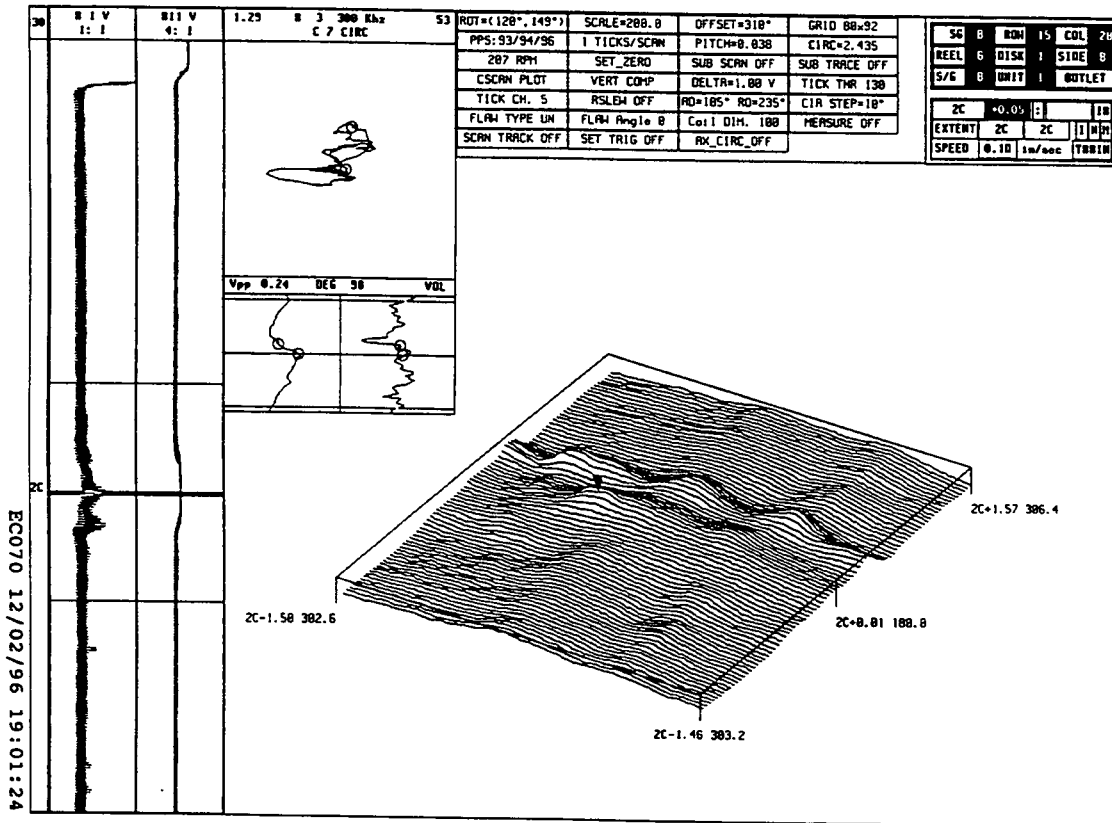


Figure 2-59 TSP2 crevice region of Tube R15C28. Laboratory 3-coil probe circumferentially sensitive coil eddy current test data.

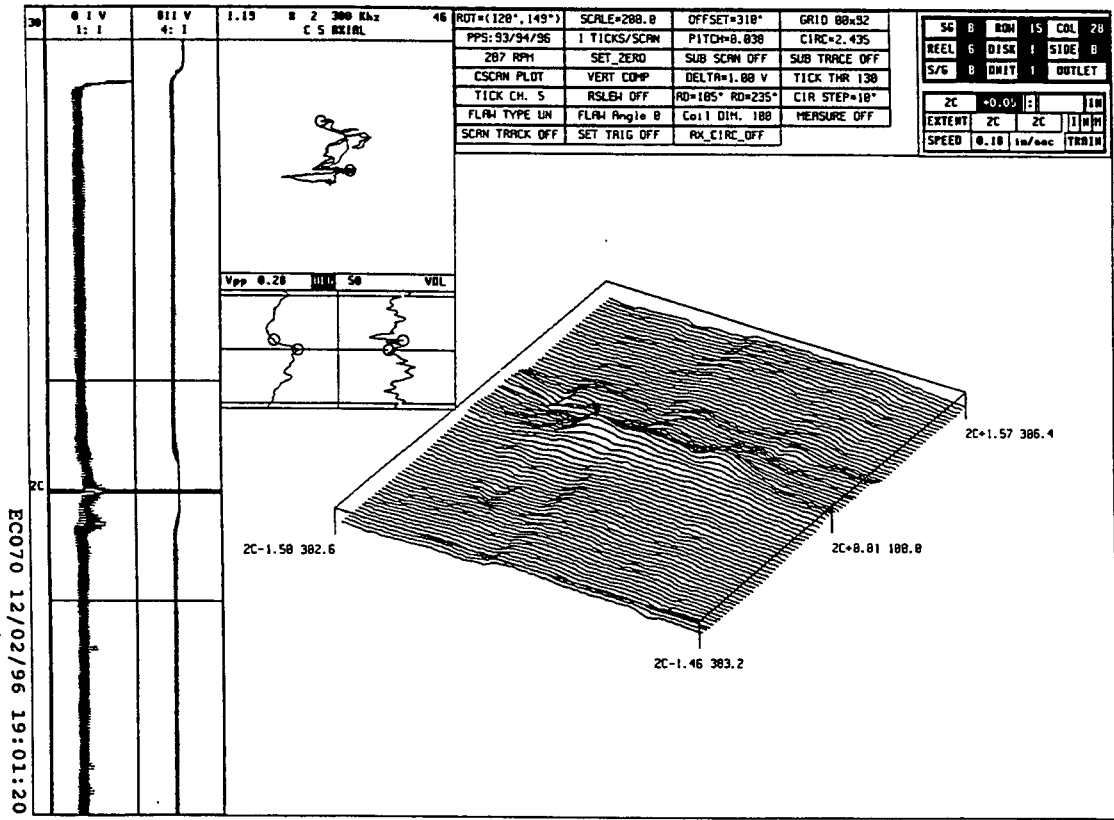


Figure 2-60 TSP2 crevice region of Tube R15C28. Laboratory 3-coil probe axially sensitive coil eddy current test data.

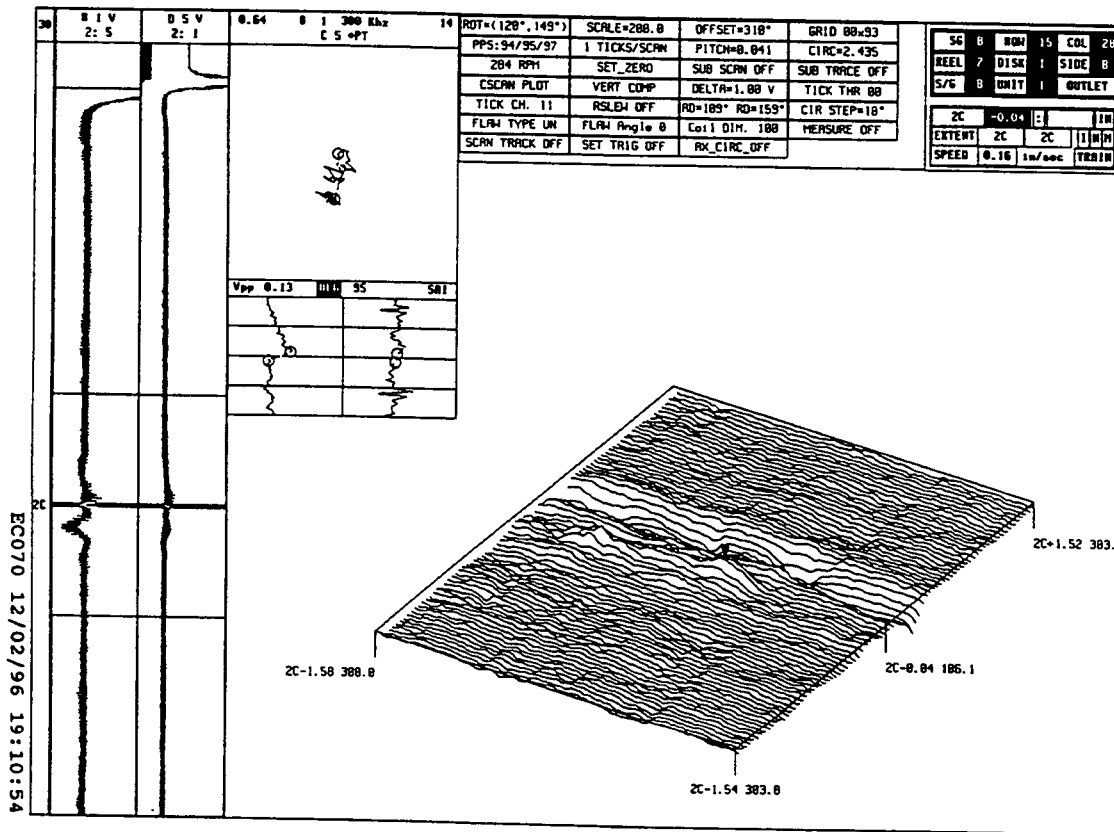


Figure 2-61 TSP2 crevice region of Tube R15C28. Laboratory +Point probe eddy current test data.

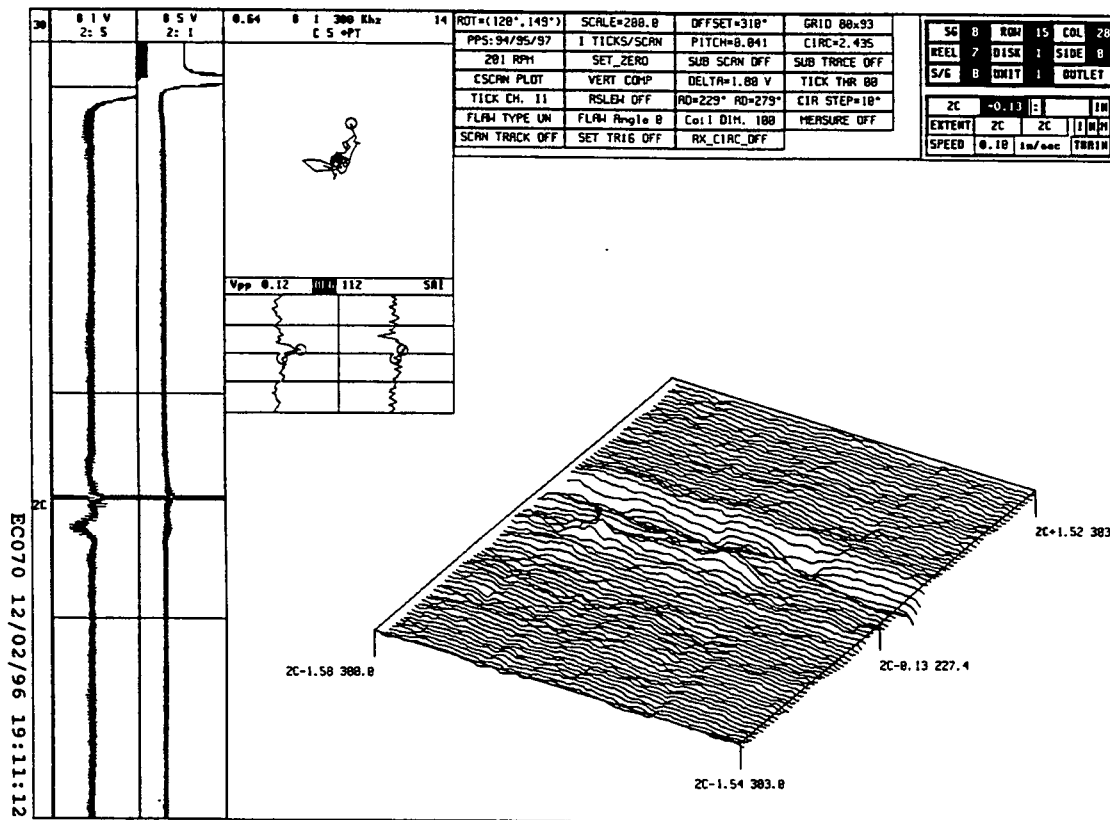


Figure 2-62 TSP2 crevice region of Tube R15C28. Laboratory +Point probe eddy current test data.

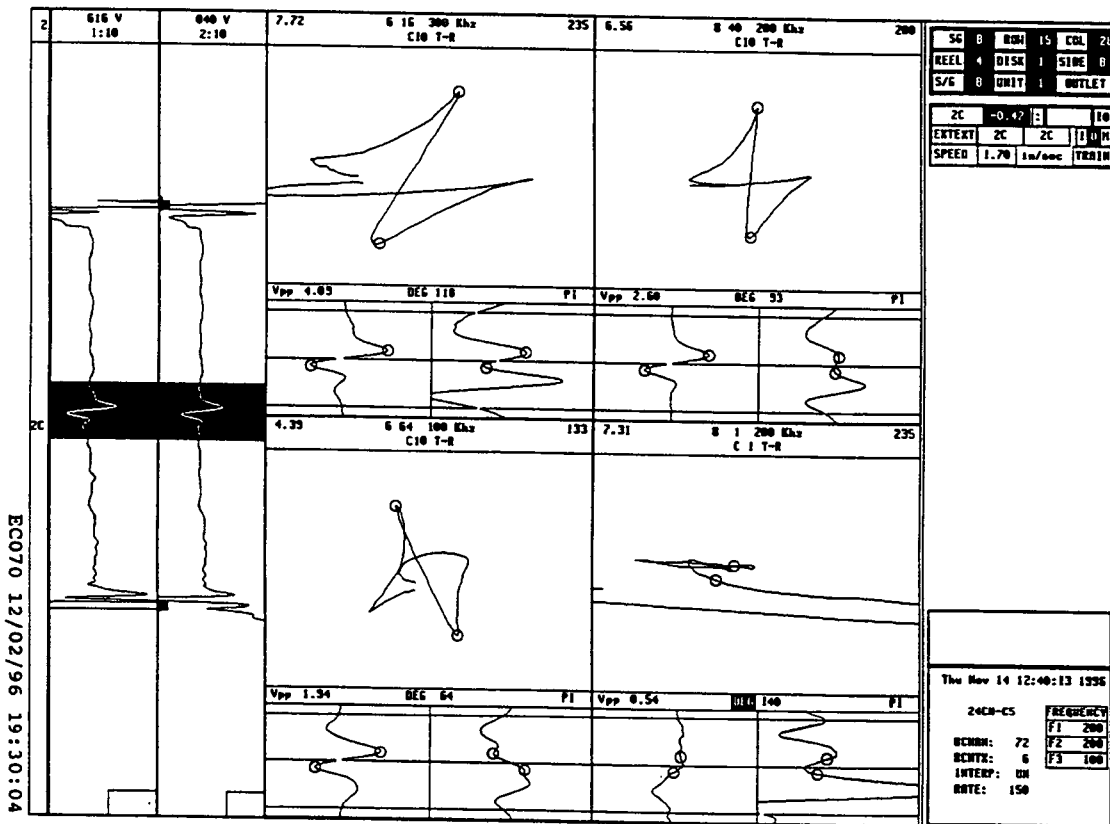


Figure 2-63 TSP2 crevice region of Tube R15C28. Laboratory Cecco 5 probe eddy current test data Lissajous patterns.

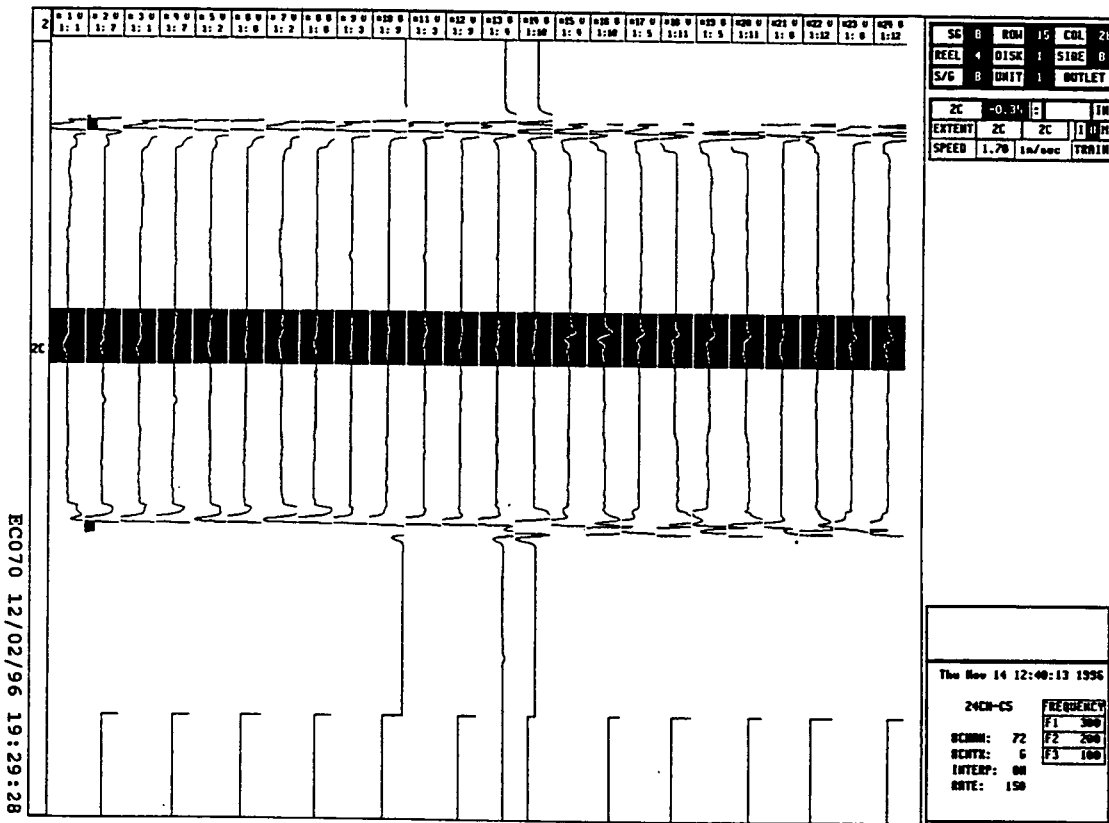


Figure 2-64 TSP2 crevice region of Tube R15C28. Laboratory Cecco 5 probe eddy current test data strip chart.

BURST AND TENSILE TESTS

3.1 BURST TESTS

Following the non-destructive examination (NDE), the first and the second tube support plate crevice regions (TSP1 and TSP2, Specimens 4B and 6B, respectively) of the cold leg of Tube R15C28 were burst tested. In addition, burst testing was also performed on a free span (FS) section of the tube as a control specimen (Specimen 5B). The burst tests were performed at room temperature, with the pressurization rate of 2000 psi per second. No foils, bladders, or restraint conditions were used, because the corrosion depths at the crevice regions were shallow, as indicated by the nondestructive examination (NDE) data. The burst test results listed in Table 3-1 show, in fact, that the effects of the cracks on the burst pressures were minor. The tube support crevice regions of Tube R15C28 burst at pressures of 9000 psi (TSP1) and 8700 psi (TSP2), which were 97% and 94%, respectively, of the nondegraded free span (FS) control specimen burst pressure of 9300 psi. The burst pressure of the FS control specimen was lower than those typically seen in undegraded steam generator tubes from other plants, but it was fairly typical for the Kewaunee steam generator tubing. In any case, the burst pressures of the tested tube support plate crevice region specimens were still above the pressures required to satisfy Reg. Guide 1.121.

The appearance of the burst openings of specimens 5B (FS), 4B (TSP1), and 6B (TSP2) is shown in Figures 3-1 through 3-9. Visual inspection of the fractures at 30X after the burst tests showed that no corrosion was present in the FS specimen, confirming that it was not degraded, and therefore it was valid as a control specimen. Axial corrosion, with intergranular cellular corrosion (ICC) characteristics, was found on approximately half of the central crevice region of TSP1 and on most of the central crevice region locations of TSP2. All corrosion was confined to the crevice regions. More detailed observations of the corrosion morphology, using a scanning electron microscope (SEM) at higher magnifications, are covered in the Destructive Examination section of this report.

The burst tests opened numerous smaller, secondary cracks within the crevice regions, with highest density concentrated near the burst openings. The cracking patterns observed (with adjustments made from later metallographic observations) are sketched

in Figures 3-10 and 3-11. The sketches show the locations of the cracks found and their overall appearance, but not the exact number of cracks nor their detailed morphology. It may be seen that the cracking was confined to the crevice regions of TSP1 and TSP2. The cracks extended around the entire circumference of the tube in the TSP2 crevice region, but only over a little more than half of the circumference in the TSP1 crevice region.

3.2 TENSILE TESTS

A free span (FS) section of Tube R15C28, taken from Piece 5, was tensile tested at room temperature to determine the mechanical properties. The tensile specimen was 12 inches long, with a free span between the grips of 8 inches. The test was performed according to the ASTM Standard E8. The strength and the elongation values, listed in Table 3-1, were within the range specified for Westinghouse Alloy 600 tubing of this vintage, but the strength was lower than normally found in Westinghouse tubing of later vintage.

Table 3-1 Kewaunee Burst and Tensile Test Properties of Tube R15C28

Location	Burst Pressure, psig	Burst Ductility, %	Burst Length, inches	Burst Width, inches	0.2% Offset Yield Strength, psi	Tensile Ultimate Strength, psi	Tensile Elongation, %
FS	9300	35	1.792	0.348	43500	93800	35.8
TSP1	9000	30	1.569	0.42			
TSP2	8700	33	1.536	0.352			

FIGURES FOR SECTION 3

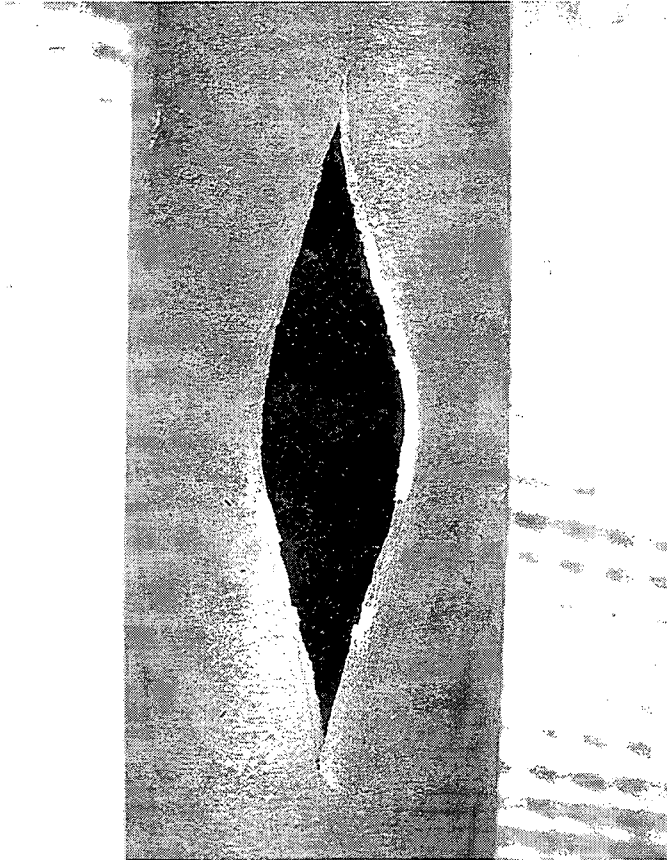


Figure 3-1 FS (control) Specimen 5B of Tube R15C28. Appearance of the 345° face after the burst test. Mag. 2X.



Figure 3-2 TSP1 (first tube support plate) crevice region Specimen 4B of Tube R15C28.
Appearance of the 225° face after the burst test. Mag. 2.5X.



Figure 3-3 TSP1 crevice region Specimen 4B of Tube R15C28. Appearance of the 180° face after the burst test. Mag. 3X.

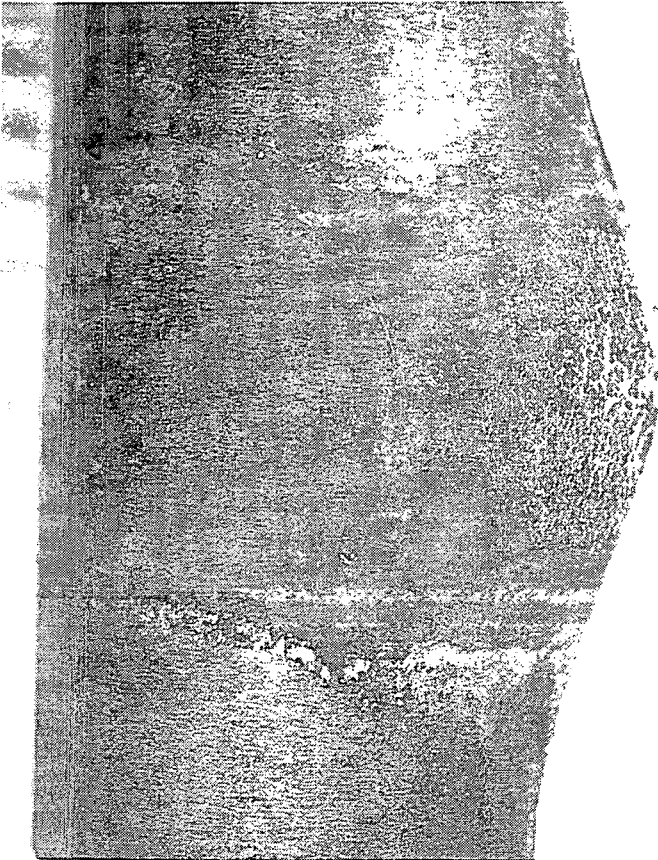


Figure 3-4 TSP1 crevice region Specimen 4B of Tube R15C28. Appearance of the 315° face after the burst test. Mag. 3X.

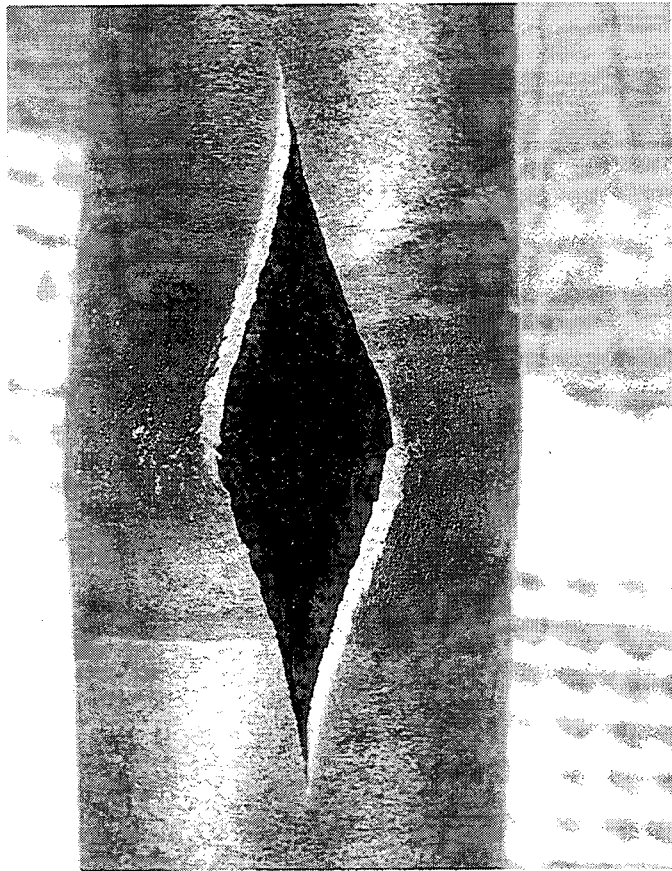


Figure 3-5 TSP2 crevice region Specimen 6B of Tube R15C28. Appearance of the 135° face after the burst test. Mag. 2.5X.

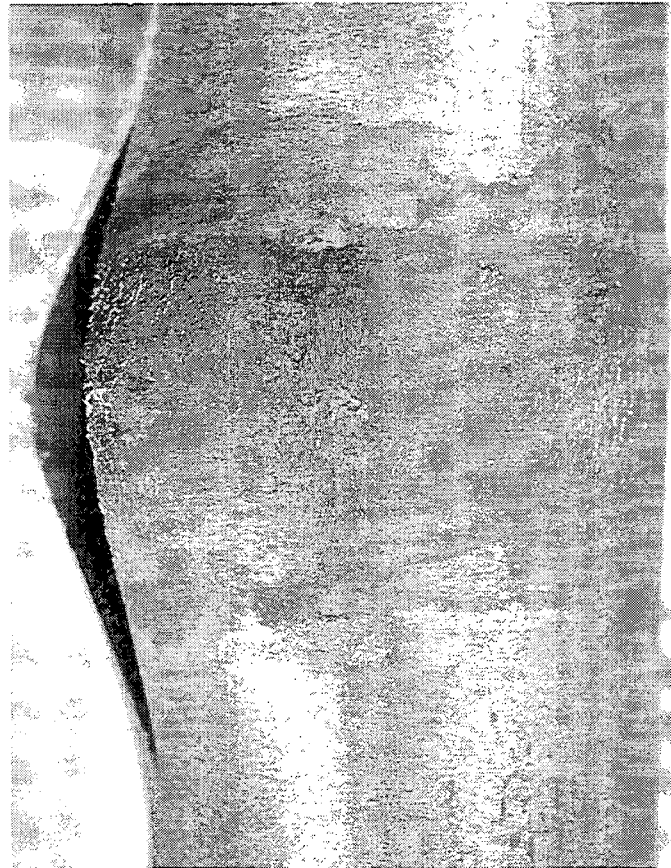


Figure 3-6 TSP2 crevice region Specimen 6B of Tube R15C28. Appearance of the 70° face after the burst test. Mag. 3X.



Figure 3-7 TSP2 crevice region Specimen 6B of Tube R15C28. Appearance of the 200° face after the burst test. Mag. 3X.



Figure 3-8 TSP2 crevice region Specimen 6B of Tube R15C28. Appearance of the 270° face after the burst test. Mag. 3X.



Figure 3-9 TSP2 crevice region Specimen 6B of Tube R15C28. Appearance of the 340° face after the burst test. Mag. 3X.

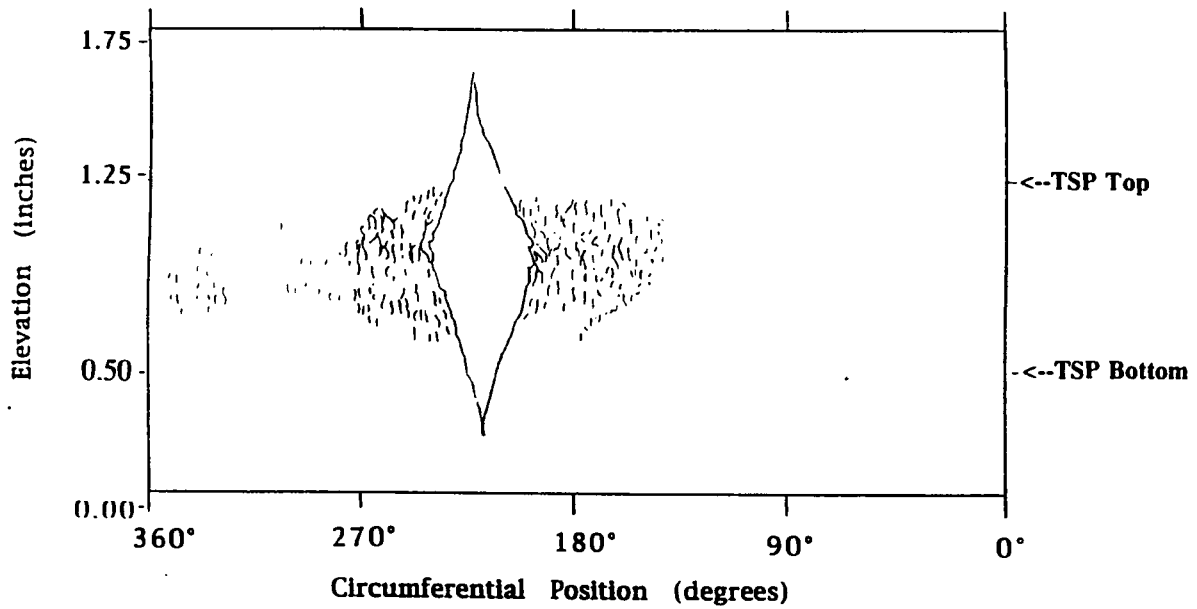


Figure 3-10 TSP1 crevice region Specimen 4B of Tube R15C28. Sketch showing the location of the burst opening and the approximate distribution of the small cracks.

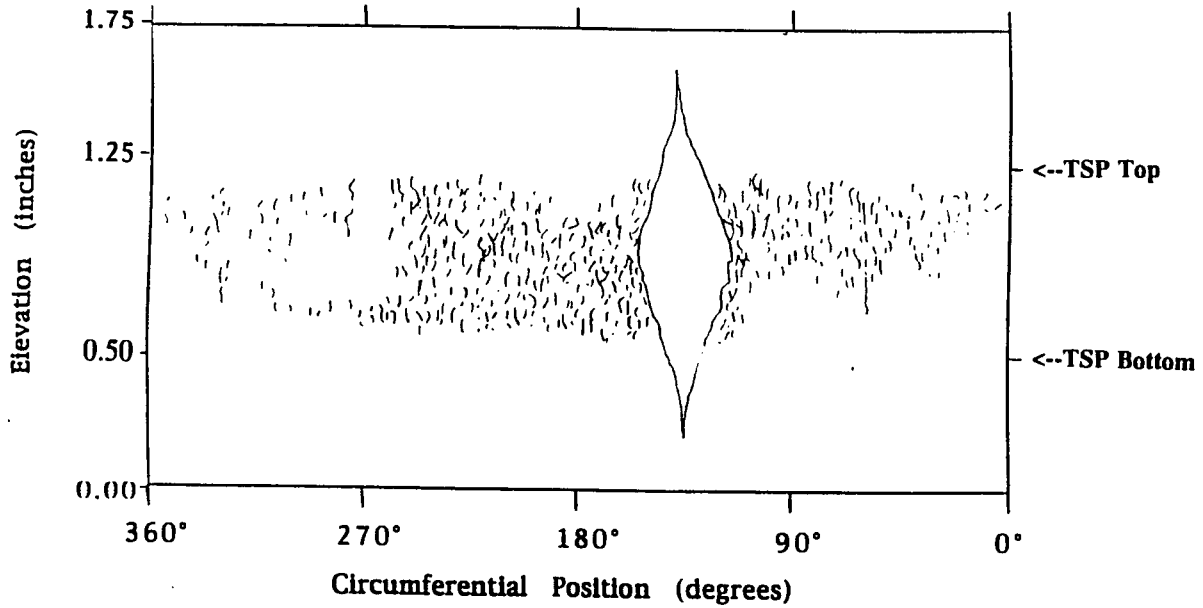


Figure 3-11 TSP2 crevice region Specimen 6B of Tube R15C28. Sketch showing the location of the burst opening and the approximate distribution of the small cracks.

FIGURES FOR SECTION 4

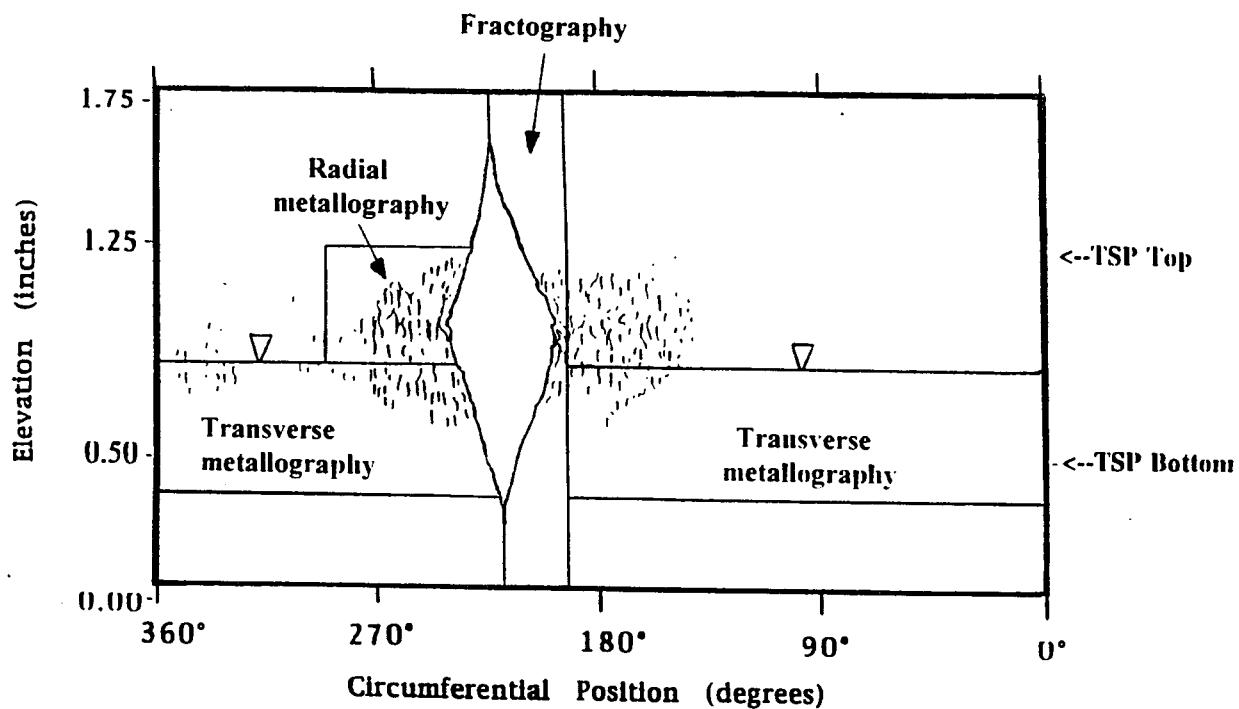


Figure 4-1 TSP1 crevice region Specimen 4B of Tube R15C28. Sketch showing the locations of the fractographic and metallographic samples used in the study of the crack distribution and morphology.

DESTRUCTIVE EXAMINATION

The burst tested sections were subsequently cut into smaller pieces and the major burst cracks were opened for fractography. Other areas of the tube support plate (TSP) regions were examined in detail by metallographic techniques. Scanning electron microscopy (SEM) was used for fractography, and light microscopy (LM) was employed in the metallographic examinations. The results of the destructive examinations are shown below.

4.1 DESTRUCTIVE EXAMINATION OF THE FIRST SUPPORT PLATE CREVICE REGION OF TUBE R15C28

The locations of the fractographic and metallographic samples on the burst test Specimen 4B are shown on the sketch of Figure 4-1.

4.1.1 *Fractography and EDS Analyses of the TSP1 Crevice Region of Tube R15C28*

4.1.1.1 *Fractography of the TSP1 Crevice Region of Tube R15C28*

The fractographic sample of the opened burst crack was examined in a scanning electron microscope (SEM). Figure 4-2 is a photographic montage of the top view of the burst fracture. Areas 2 to 4, 5, and 6¹ are shown at higher magnifications in Figures 4-3 through 4-5. It may be seen that the burst fracture started from a series of small intergranular OD corrosion microcracks which joined together forming an essentially continuous macrocrack from Area 5 to Area 6 (Figure 4-2). Areas 2 to 4 include the point of highest penetration of the intergranular corrosion (30% throughwall), which is also located approximately in the middle of the burst opening and, therefore, may be considered to be the initiation point of the burst fracture. The average depth of the corrosion penetration was 17%. The depth profile of the macrocrack at various positions is shown in Table 4-1. The macrocrack was 0.368 inches long and was confined to the crevice region of the first tube support plate.

¹ Every Area number corresponds to the number at the lower right corner of the photograph where the Area is shown at a higher magnification.

It is interesting to note that the ligaments between the microcracks were also intergranular, which is not typical of shallow IGSCC originating at the OD surface. It indicates that not all the microcracks were axial, but some were also part of an intergranular cellular corrosion (ICC) network, as was mentioned in Section 3 of this report. The ICC features will be seen also in the side view of the burst fracture and in radial metallography.

Figure 4-6 presents a side view of the opened burst fracture, showing OD corrosion cracks opened wider by the burst test. Area 7 of the OD surface is shown at progressively higher magnifications in Figures 4-7 through 4-9. The character of the intergranular cellular corrosion is clearly illustrated in these photographs, both in the reflected electron images and in the backscattered electron images¹.

4.1.1.2 EDS Analyses of the TSP1 Crevice Region of Tube R15C28

Two spots on the OD surface in Area 7 were analyzed using the energy dispersive X-ray spectroscopy (EDS) technique. The EDS system used was capable of detecting elements of atomic number 3 or higher. The depth of the analyzed material below the OD surface depends on the voltage of the SEM accelerating the primary electron beam. For the voltage used in this case the depth was about 2 micrometers. The locations of the analyzed spots, marked 1 and 2, are shown in Figure 4-10. Spot 2 appears to have had a somewhat thicker deposit than Spot 1. The results of the EDS analyses are presented in Figures 4-11 and 4-12, both as spectra and as numerical tables. The second column in each table lists the weight percent of every element, while the last column shows the equivalent atomic percent. The estimated weight percent error range values are shown in the third column of each table.

Oxygen was the most abundant element in the analyses of Area 7, indicating that most of the other elements were present either as oxides, or oxygen-containing compounds. Elements Ni, Cr, and Fe are part of the Alloy 600 composition. High concentrations of Fe on the tube surface are generally associated with thicker deposits that had an external origin (e.g., oxides from the tube support plate). The concentrations of Fe at Spots 1 and 2 were about equal, and fairly typical. The percentages of Ni and Cr at Spot 2 were much lower than at Spot 1, which is logical because with a thicker deposit less of

¹A reflected electron image presents a better view of the physical topography of the examined fracture or surface, with an almost three-dimensional quality. A backscattered electron image differentiates between areas of different chemical composition, because elements with higher atomic numbers appear brighter in this image. Furthermore, cracks are often better visible in the backscattered electron image.

the substrate is included in the analysis. The second group of elements found in the deposits, Ca, Mg, Si, and Al, can influence the cohesiveness and morphology of the crevice and sludge pile deposits, but these elements are not believed to directly contribute to corrosion degradation of the tubes. However, they help to provide a more dense deposit structure for the concentration of deleterious elements. All the elements of this group were present in the analyses of Area 7, with the concentrations at Spot 2 being much higher because of the thicker deposit at this location. The next group of elements, Cu, Pb, S, and P, could possibly contribute to corrosion or suggest a corrosion degradation mechanism. Copper (Cu), if present as an oxide, can accelerate intergranular corrosion by acting as an oxidant. Copper was present at both spots of Area 7, but not at high concentrations (less than 1 wt. %). Lead (Pb) was somewhat higher at Spot 1 (1.277 wt. %) than at Spot 2 (0.976 wt. %), but these concentrations are not unusually high. Sulfur (S) was not present in the analyses. Phosphorus (P) was relatively high at Spot 2 (6.121 wt. %), but less than 1 wt. % at Spot 1 (0.466 wt. %). In addition, Mn and Zn were also observed in the deposit. Zinc (Zn) was present at both spots, while manganese (Mn) was found only at Spot 2. Neither element is believed to contribute to corrosion degradation.

4.1.2 Metallography of the TSP1 Crevice Region of Tube R15C28

As indicated on the sketch of Figure 4-1, two metallographic samples were cut from Specimen 4B: sample for radial metallography, identified later as Specimen 4B-2C, and sample for transverse metallography, identified later as Specimen 4B-2B. The sample for radial metallography was flattened and mounted. It was then ground in 4 successive steps of gradually increasing depth. At every step the sample was polished, etched, and microscopically examined. The sample for transverse metallography was mounted, ground, polished, etched, and metallographically examined at the cross-section plane marked with ∇ in Figure 4-1. The radial metallography is shown in Figures 4-13 through 4-27, and the transverse metallography is presented in Figures 4-28 through 4-31. The results of metallography are summarized in Table 4-2.

The radial metallography Specimen 4B-2C was first polished to a depth of 0.001 inch below the OD surface. Figures 4-13 and 4-14 show the specimen at this stage. These two figures are reversed left to right with respect to each other because of the different optics of the corresponding cameras. A large number of corrosion cracks may be seen near the burst fracture. Also, a cavity is present inside the specimen, where a group of grains surrounded by cracks fell out in the specimen preparation. Typical cracks visible at this level are shown at a higher magnification in Figures 4-15, 4-16, and 4-17. Both axial IGSCC and cellular ICC crack morphology is observed. The specimen was then polished an additional 0.004 inch to a total depth of 0.005 inch below the OD surface. At this stage the crack morphology appears to be a little more axial, although some cellular character is still retained. The third polishing, of 0.005 inch, brought the total depth of the examined plane of the specimen to 0.010 inch below the OD surface

(Figures 4-23 through 4-26). The number of visible cracks was much smaller at this level, and they were predominantly axial IGSCC. Finally, the last polishing of 0.005 inch (total depth of 0.010 inch) removed the rest of the cracks, as may be seen in Figure 4-27.

Metallography of the transverse Specimen 4B-2B is illustrated in Figures 4-28 through 4-31. Figure 4-28 shows the whole specimen. Areas A through E, marked in this figure, are shown at a higher magnification in Figures 4-29 through 4-31, where the profiles and depths of the cracks may be observed. These micrographs show clusters of very shallow, axially oriented stress corrosion cracks originating at the OD surface. The deepest crack observed by transverse metallography was 8% throughwall.

The grains of the cold leg of Tube R15C28 were essentially equiaxed, with some duplex characteristics. The grain size was relatively large: ASTM No. 8.5 for the smallest grains, 7.0 for the average, and 1.5 to 2.0 for some of the largest grains. Modern Westinghouse typical mill annealed Alloy 600 steam generator tubing has average grain size of about 8.5 to 10.0.

4.2 DESTRUCTIVE EXAMINATION OF THE SECOND SUPPORT PLATE CREVICE REGION OF TUBE R15C28

The locations of the fractographic and metallographic samples on the burst test Specimen 6B are shown on the sketch of Figure 4-32.

4.2.1 *Fractography and EDS Analyses of the TSP2 Crevice Region of Tube R15C28*

4.2.1.1 *Fractography of the TSP2 Crevice Region of Tube R15C28*

The fractographic sample 6B-2A of the opened burst crack of the TSP2 region was examined in a scanning electron microscope (SEM) in the same manner as the TSP1 region sample. Figure 4-33 is a photographic montage of the top view of the burst fracture. Areas 2 to 4, 5, and 6 are shown at higher magnifications in Figures 4-34 through 4-36. Similarly to TSP1, it may be seen that the burst fracture at the TSP2 region started from a series of small intergranular OD corrosion microcracks which joined together forming an essentially continuous macrocrack from Area 5 to Area 6 (Figure 4-33). Areas 2 to 4, Figures 4-34 and 4-35, include the point of deepest penetration of the intergranular corrosion (31% throughwall, which is very close to the 30% observed at TSP1). The average depth of the corrosion penetration at TSP2 was 16%, again almost equal to the 17% found at TSP1. The depth profile of the macrocrack at various positions is shown in Table 4-1. The macrocrack was 0.480 inch long

(compared to 0.368 inch for TSP1), and was also confined to the crevice region of the tube support plate.

As was observed in the TSP1 region, the ligaments between the microcracks in the burst test macrocrack of the TSP2 region were also intergranular, which indicates that not all the microcracks were axial, but some were also part of an intergranular cellular corrosion (ICC) network. The ICC features will be seen also in the side view of the burst fracture and in radial metallography of the TSP2 region.

Figure 4-37 presents a side view of the opened burst fracture, showing OD corrosion cracks opened wider by the burst test. Areas 7 and 9 of the OD surface are shown at progressively higher magnifications in Figures 4-38 through 4-40. The character of the intergranular cellular corrosion is clearly illustrated in these photographs, both in the reflected electron images and in the backscattered electron images. Again, there appears to be very little difference between Figures 4-6 and 4-37 illustrating the TSP1 and TSP2 regions, respectively.

4.2.1.2 EDS Analyses of the TSP2 Crevice Region of Tube R15C28

Three spots on the OD surface in Areas 7 and 9, and their vicinity, were analyzed using the energy dispersive X-ray spectroscopy (EDS) technique. The locations of the analyzed spots, marked 1, 2 and 3, are shown in Figure 4-41. It may be seen that Spot 1 was in Area 9. Spot 2 had a thicker deposit than Spot 1. This deposit appears to be the same as in Area 7. In the backscattered electron image Spot 3 was a bright particle in Area 7, suggesting the presence of a different element than in the rest of the deposit in this area. The results of the EDS analyses are presented in Figures 4-42 through 4-44, both as spectra and as numerical tables. The second column in each table lists the weight percent of every element, while the last column shows the equivalent atomic percent. The estimated weight percent error range values are shown in the third column of each table.

Again, oxygen was the most abundant element in all the EDS analyses of the TSP2 region on the tube (at least in atomic %), indicating that most of the other elements were present either as oxides or oxygen-containing compounds. Elements Ni, Cr, and Fe are part of the Alloy 600 composition, although Fe in thicker deposits might have had an external origin. In the TSP2 region, the concentration of Fe at Spot 2, with a thicker deposit, was the highest ($\cong 38$ wt.%) compared to Spots 1 and 3 ($\cong 13$ and 3 wt.%, respectively). (The TSP1 region analyses showed about 23 - 27 wt.% Fe). The percentages of Ni and Cr at Spots 2 and 3 were much lower than at Spot 1, which is logical because with a thicker deposit less of the substrate is included in the analysis.

The second group of elements found in the deposits, Ca, Mg, Si, and Al, can influence the cohesiveness and morphology of the crevice and sludge pile deposits, but these

elements are not believed to directly contribute to corrosion degradation of the tubes, as was mentioned before. All the elements of this group were present in the analyses of Spots 1 and 2, but only Ca and Si were found at Spot 3. Their concentrations at all the spots were relatively low, mostly around 1 wt.%, and not exceeding 3 wt.%. (At the TSP1 region, at Spot 2, Mg reached about 5 wt.%, Ca about 9 wt.%, and Si about 4 wt.%). The next group of elements, Cu, Pb, S, and P, could possibly contribute to corrosion or suggest a corrosion degradation mechanism. Copper (Cu) was present at both Spots 1 and 2, but not at high concentrations (only around 1 wt.%). Cu was absent at Spot 3, but S was present there at about 2 wt.%. (S was not found in the TSP1 region analyses). Lead (Pb) and phosphorus (P) were relatively low at Spots 1 and 2 (less than 1 wt.% of each), and they were absent at Spot 3.

The last group of elements, Zn and Mn, is believed not to contribute to corrosion degradation. Zinc (Zn) was observed in the deposits at all three spots in quantities of about 1 to 4 wt.%. Manganese (Mn) was found only at Spots 1 and 2, in concentrations around 1 wt.%.

The little particle at Spot 3 contained a very high concentration (\cong 53 wt.%) of barium (Ba), which apparently came from an atypical small contamination in the secondary water. The source of this contamination is not certain, but it is known that barium sulfide can be found in the effluents from paper mills.

4.2.2 Metallography of the TSP2 Crevice Region of Tube R15C28

The metallographic examination of the TSP2 region of Tube R15C28 was performed essentially in the same way as that of the TSP1 region. As indicated on the sketch of Figure 4-32, two metallographic samples were cut from Specimen 6B: sample for radial metallography, identified later as Specimen 6B-2D, and sample for transverse metallography, identified later as Specimen 6B-2C. The sample for radial metallography was flattened and mounted. It was then ground in 3 successive steps of gradually increasing depth. At every step the sample was polished, etched, and microscopically examined. The sample for transverse metallography was mounted, ground, polished, etched, and metallographically examined at the cross-section plane marked with ∇ in Figure 4-32. The radial metallography is shown in Figures 4-45 through 4-54, and the transverse metallography is presented in Figures 4-55 through 4-60.

The radial metallography Specimen 6B-2D was first polished to a depth of 0.001 inch below the OD surface. Figures 4-45 and 4-46 show the specimen at this stage. These two figures are reversed left to right with respect to each other because of the different optics of the corresponding cameras. A large number of corrosion cracks may be seen near the burst fracture. Typical cracks visible at this level are shown at a higher magnification in Figures 4-47, 4-48, and 4-49. Both axial IGSCC and cellular ICC crack

morphology is observed, although axially seems to predominate. The specimen was then polished an additional 0.004 inch to a total depth of 0.005 inch below the OD surface (Figures 4-50 and 4-51). At this stage the cracks were less numerous and their morphology appears to be even more axial, although some cellular character was still retained, as may be seen in Figures 4-52 and 4-53. The third polishing, of 0.005 inch, brought the total depth of the examined plane of the specimen to 0.010 inch below the OD surface. This last polishing removed the rest of the cracks, as may be seen in Figure 4-54.

Metallography of the transverse Specimen 6B-2C is illustrated in Figures 4-55 through 4-60. Figure 4-55 shows the whole specimen. Areas A through I, marked in this figure, are shown at a higher magnification in Figures 4-56 through 4-60, where the profiles and depths of the OD cracks in these areas can be observed. These micrographs show clusters of relatively shallow, axially oriented intergranular cracks originating at the OD surface, which opened up during the burst test. Some of the opening of the cracks was also caused by falling out of the grains, or clusters of grains, which were entirely surrounded by grain boundary cracking. This is indicated by the fact that in many cases the two sides of an open crack do not match each other. The deepest crack observed by transverse metallography, 31% throughwall, is shown in Area B, Figure 4-56. Some plastic deformation at the tip of this crack, apparently produced by the burst test strain, may be also seen in this photomicrograph. Similar slip bands are visible also in Area E, Figure 4-58.

In general, it may be said that the dominant OD corrosion morphology was axial intergranular stress corrosion cracking (IGSCC). Some intergranular cellular corrosion (ICC) was also observed, but it was not predominant and it tended to be less pronounced in deeper layers below the surface. In high density crack areas, the corrosion morphology approached the appearance of intergranular attack (IGA). However, IGSCC became more dominant with increasing depth below the OD surface, and the IGA tended to disappear quickly.

Corrosion morphology can be characterized also by crack density and by the degree that IGA components are associated with IGSCC, frequently measured by the ratio of the crack depth to its width at the mid-depth (D/W)¹. The TSP2 region had about twice the crack density of the TSP1 region: a high TSP2 crack density (~140 cracks around the midcrevice region) versus a moderate TSP1 crack density (~75 cracks around the midcrevice region). (A high crack density is defined as greater than 100 cracks around the circumference; a moderate crack density as 25 to 100 cracks; and a low crack density as less than 25 cracks around the circumference). Both TSP regions had a moderate

¹ In measuring the widths of the cracks efforts have been made to compensate as much as possible for the effects of the burst test strain.

association of IGA with the IGSCC, since their D/W ratios were 6 to 9. (D/W ratios less than 3 suggest a high association of IGA with IGSCC; D/W ratios in the range of 3 to 20 point out to a moderate association of IGA with IGSCC; and D/W ratios greater than 20 are considered to show a low association of IGA with IGSCC). The examination has also shown that the area of cracking at the TSP2 crevice region was more extensive than that of the TSP1 crevice region (compare Figures 4-32 and 4-1).

Table 4-1 Kewaunee SEM Fractographic Data for TSP Region Burst Specimens

Tube, Specimen	Length vs. Depth (inches/% throughwall)	Positional Information	Comments
R15C28, 4B-2D Cold Leg, TSP1	0.000/00	<=Top of Macrocrack	The OD origin, axially oriented macrocrack had no ductile ligaments with dimple rupture features occurring over more than 50% of their lengths. Wall thickness is 0.050 inch.
	0.016/09		
	0.032/16		
	0.048/09		
	0.064/19		
	0.080/20		
	0.096/22		
	0.112/25		
	0.128/25		
	(0.138/30)<=(Max. Depth = 30%)		
	0.144/24		
	0.160/22		
	0.176/24		
	0.192/20		
	0.208/20		
	0.224/22		
	0.240/16		
	0.256/19		
	0.272/16		
	0.288/13		
0.304/13			
0.320/16			
0.336/09			
0.352/09			
0.368/00 (Avg. Depth = 17%)	<=Bottom of Macrocrack		

Table 4-1 (Continued) Kewaunee SEM Fractographic Data for TSP Region Burst Specimens

Tube, Specimen	Length vs. Depth (inches/% throughwall)	Positional Information	Comments
R15C28, 6B-2A Cold Leg, TSP2	0.000/00	<=Top of Macrocrack	The OD origin, axially oriented macrocrack had no ductile ligaments with dimple rupture features occurring over more than 50% of their lengths. Wall thickness is 0.050 inch.
	0.016/06		
	0.032/16		
	0.048/22		
	0.064/19		
	0.080/19		
	0.096/22		
	0.112/20		
	0.128/25		
	0.144/31 <=(Max. Depth = 31%)		
	0.160/25		
	0.176/24		
	0.192/25		
	0.208/22		
	0.224/24		
	0.240/22		
	0.256/20		
	0.272/14		
	0.288/19		
	0.304/11		
	0.320/14		
	0.336/13		
0.352/13			
0.368/11			
0.384/16			
0.400/09			
0.416/11			
0.432/13			
0.448/08			
0.464/08			
0.480/00 (Avg. Depth = 16%)	<=Bottom of Macrocrack		

Table 4-2 Metallographic Data from Kewaunee Cold Leg Steam Generator Tube R15C28

Specimen Location	Section Type	Number of Cracks	Section Length (inch)	Cracks per Inch	Estimated Maximum Number of Cracks at Mid-Crevice Location	Max/Avg Depth (%Throughwall)	Max. Depth of ICC Oblique and Axial Components (%Throughwall in Radial Section)	Avg D/W Ratio from Transverse Section
R15C28, TSP1	Transverse	8*	2.75	3*	75*	8/7 depth = 2% depth = 10% depth = 20% depth = 30%	10% < Oblique < 20% 20% < Axial < 30%	~ 6
	Radial	23	0.36	63				
	Radial	14	0.37	37				
	Radial	7	0.38	18				
	Radial	0	0.39	0				
R15C28, TSP2	Transverse	32*	2.75	12*	140*	31/13 depth = 2% depth = 10% depth = 20%	10% < Oblique < 20% 10% < Axial < 20%	~9
	Radial	63	0.54	117				
	Radial	37	0.55	67				
	Radial	0	0.55	0				

* Ignores cracks less than 5% throughwall.

ANSTEC
APERTURE
CARD

Also Available on
Aperture Card

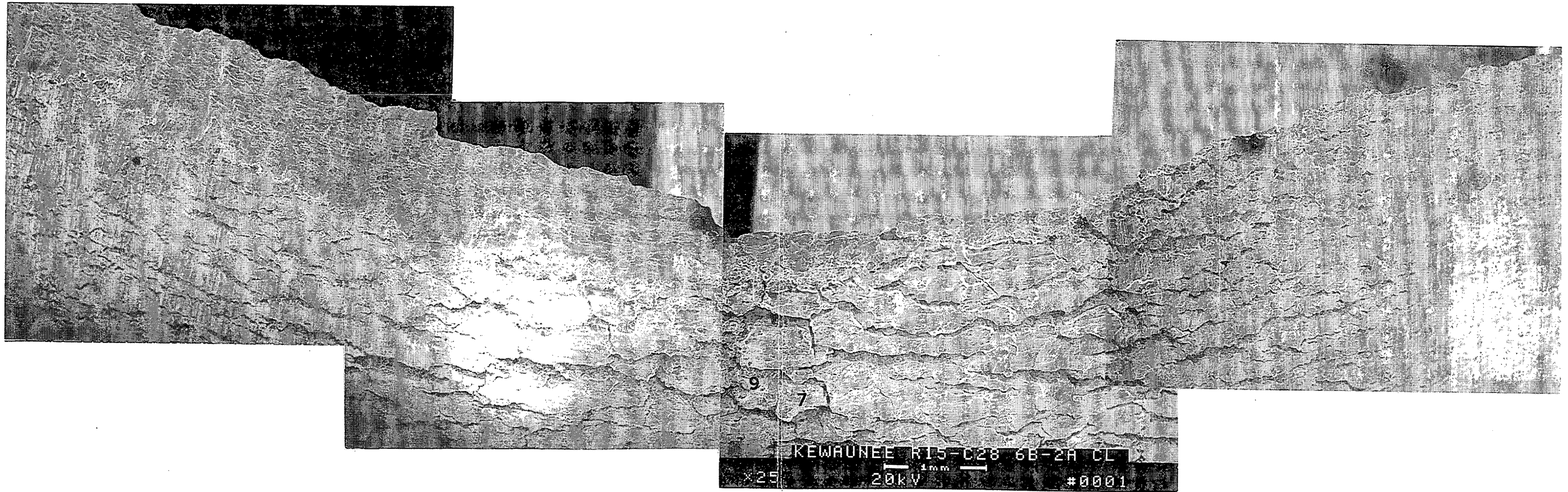


Figure 4-37 TSP2 crevice region Specimen 6B-2A of Tube R15C28. Side view of the opened burst fracture showing OD corrosion cracks opened wider by the burst test. Areas 7 and 9 on the OD surface are shown at progressively higher magnifications in Figures 4-38 through 4-40.

9709080028-04

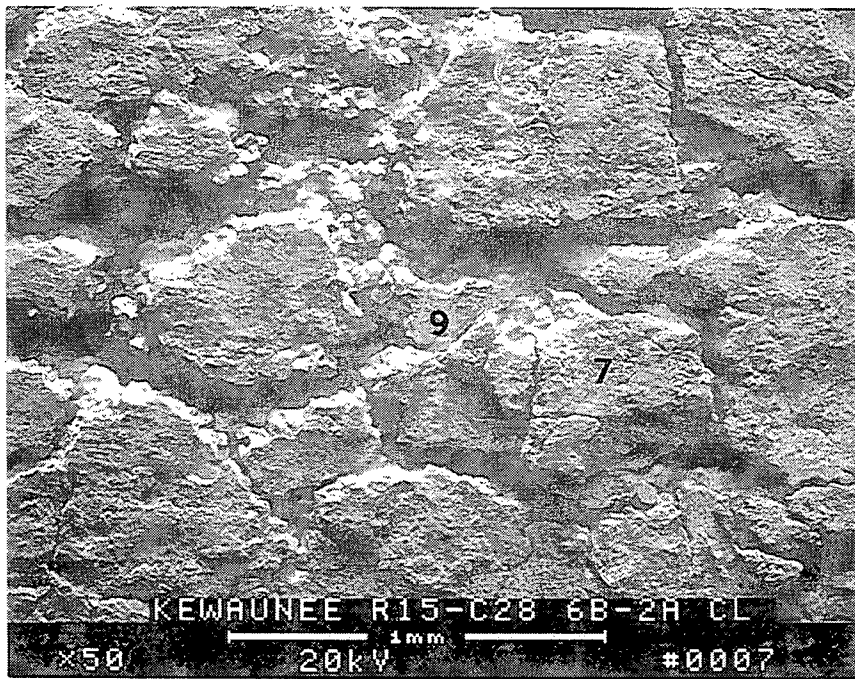


Figure 4-38 TSP2 crevice region Specimen 6B-2A of Tube R15C28. Side view of the opened burst fracture showing OD corrosion cracks opened wider by the burst test. Areas 7 and 9 on the OD surface from Figure 4-37, shown at a higher magnification.

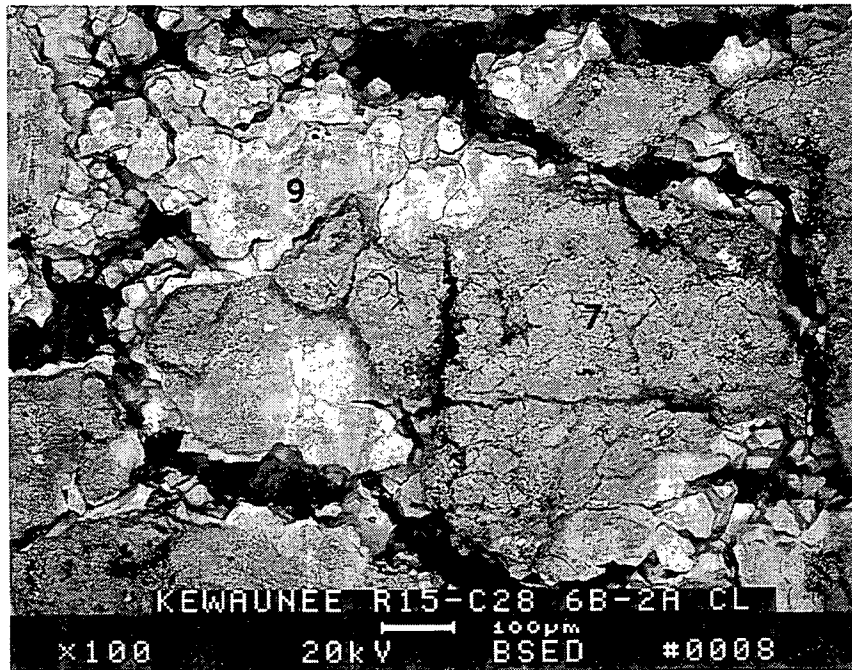
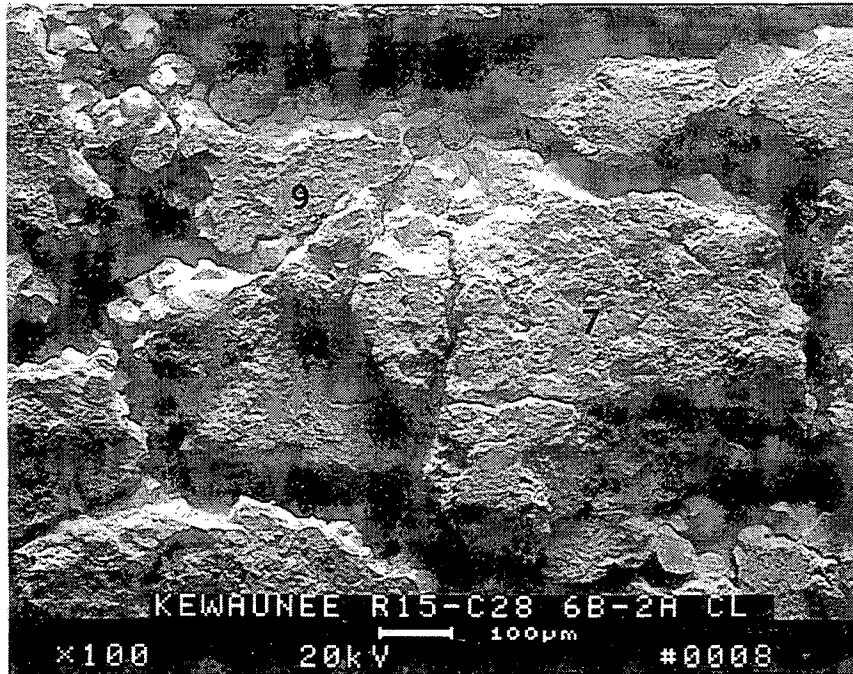


Figure 4-39 TSP2 crevice region Specimen 6B-2A of Tube R15C28. Side view of the opened burst fracture showing OD corrosion cracks opened wider by the burst test. Areas 7 and 9 on the OD surface from Figure 4-37 shown at a higher magnification. Upper photograph: reflected electron image. Lower photograph: backscattered electron image of the same area.

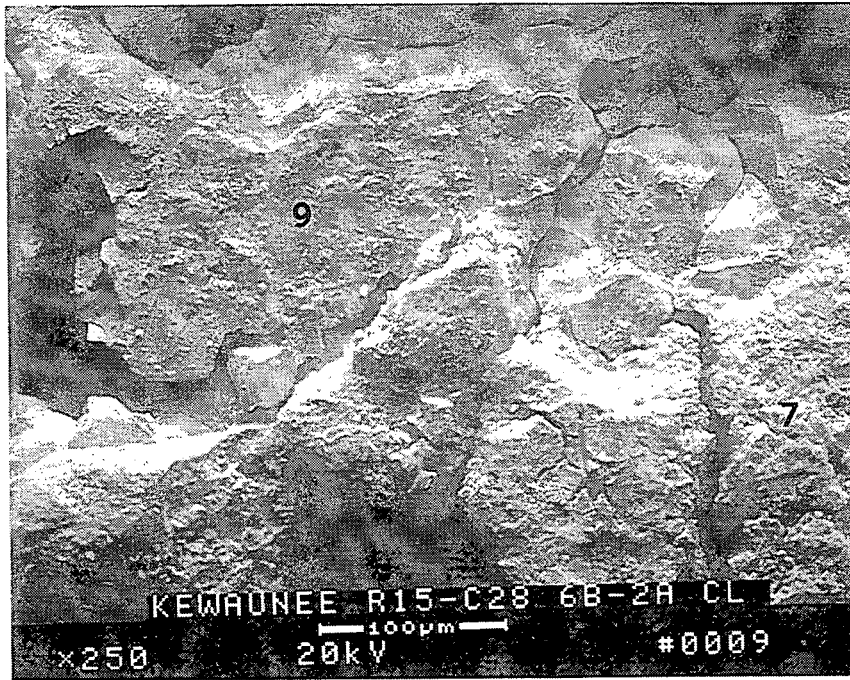


Figure 4-40 TSP2 crevice region Specimen 6B-2A of Tube R15C28. Side view of the opened burst fracture showing OD corrosion cracks opened wider by the burst test. Areas 7 and 9 on the OD surface from Figure 4-37, shown at a higher magnification. Upper photograph: reflected electron image. Lower photograph: backscattered electron image of the same area.

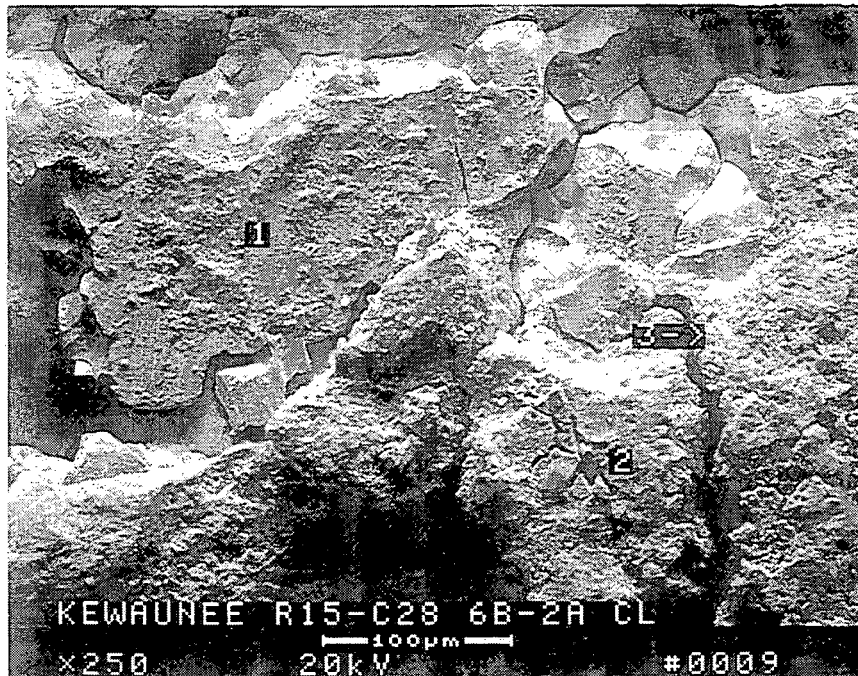
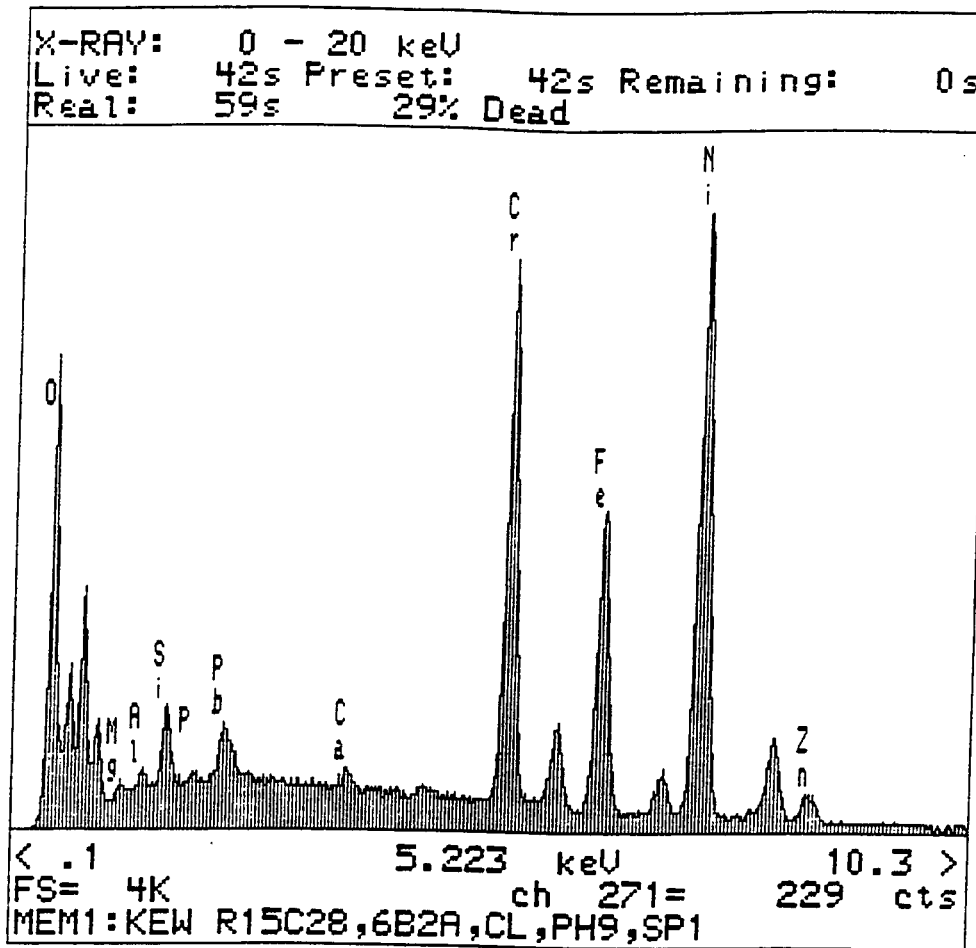


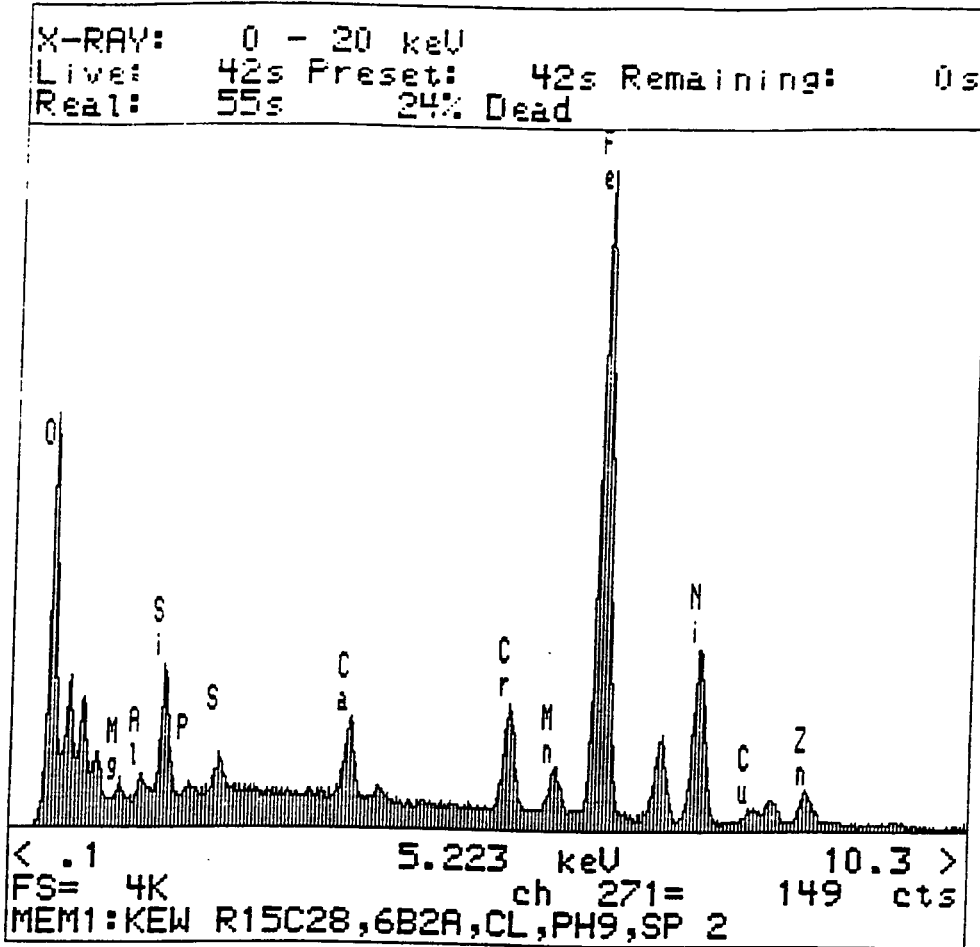
Figure 4-41 TSP2 crevice region Specimen 6B-2A of Tube R15C28. Side view of the opened burst fracture showing OD corrosion cracks opened wider by the burst test. Higher magnification photographs of Areas 7 and 9 on the OD surface from Figure 4-37, showing the locations of Spots 1, 2, and 3 which were analyzed using the energy dispersive X-ray spectroscopy (EDS) technique. The results of the analyses are shown in Figures 4-42, 4-43, and 4-44.

DESTRUCTIVE EXAMINATION



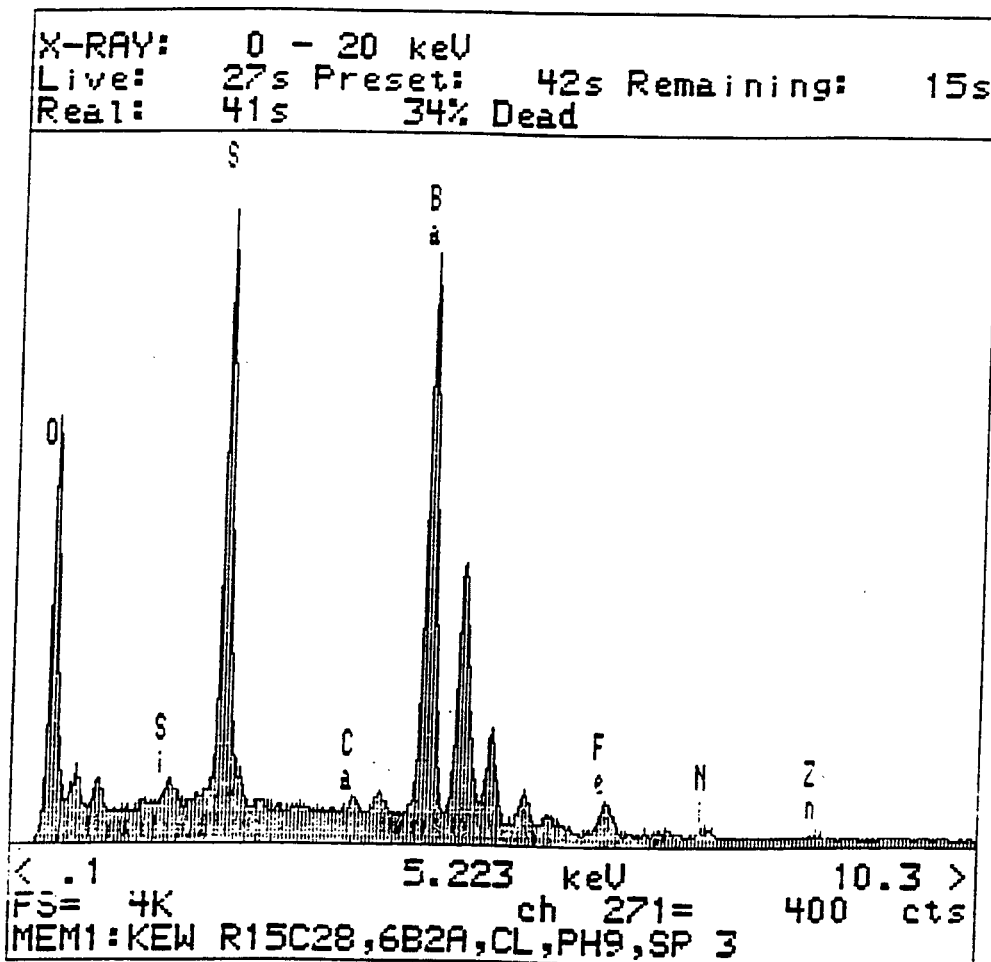
ELMT	%ELMT	+/-	Error	ATOM. %
O K	21.777	+/-	.334	49.377
MgK	.661	+/-	.162	.987
P K	.165	+/-	.068	.193
CaK	.219	+/-	.045	.198
ZnK	2.188	+/-	.237	1.214
PbM	2.416	+/-	.215	.423
AlK	.370	+/-	.072	.498
SiK	1.209	+/-	.067	1.561
CrK	16.135	+/-	.208	11.256
MnK	.481	+/-	.146	.318
FeK	13.115	+/-	.235	8.519
NiK	40.355	+/-	.485	24.936
CuK	.909	+/-	.245	.519
TOTAL	100.000			100.000

Figure 4-42 TSP2 crevice region Specimen 6B-2A of Tube R15C28. Results of the EDS analysis of Spot 1, Figure 4-41, on the OD surface at Area 9 from Figure 4-37.



ELMT	%ELMT	+-	Error	ATOM. %
O K	26.338	+-	.441	54.402
MgK	1.210	+-	.197	1.645
P K	.226	+-	.082	.241
CaK	1.532	+-	.069	1.263
ZnK	3.634	+-	.300	1.837
PbM	1.197	+-	.241	.191
AlK	.529	+-	.088	.648
SiK	2.589	+-	.091	3.046
CrK	4.179	+-	.151	2.656
MnK	1.825	+-	.168	1.098
FeK	38.447	+-	.431	22.750
NiK	16.546	+-	.410	9.314
CuK	1.750	+-	.293	.910
TOTAL	100.001			100.000

Figure 4-43 TSP2 crevice region Specimen 6B-2A of Tube R15C28. Results of the EDS analysis of Spot 2, Figure 4-41, on the OD surface next to Area 9 from Figure 4-37.



ELMT	%ELMT	+-	Error	ATOM. %
O K	38.549	+-	.582	80.498
CaK	.480	+-	.082	.400
ZnK	1.074	+-	.333	.549
BaL	52.698	+-	.549	12.820
SiK	.651	+-	.114	.774
S K	2.421	+-	.046	2.523
FeK	2.992	+-	.267	1.790
NiK	1.136	+-	.296	.647
TOTAL	100.000			100.000

Figure 4-44 TSP2 crevice region Specimen 6B-2A of Tube R15C28. Results of the EDS analysis of Spot 3, Figure 4-41, on the OD surface at Area 7 from Figure 4-37.

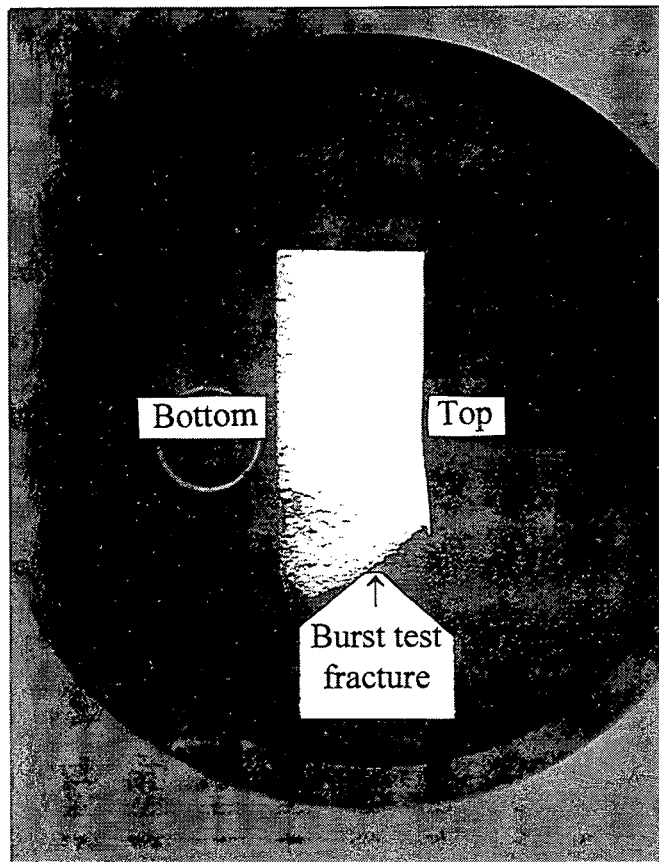


Figure 4-45 TSP2 crevice region Specimen 6B-2D of Tube R15C28. Radial metallographic sample after flattening and polishing to a depth of 0.001 inch below the OD surface. Mount M2163. Mag. 3.25X.

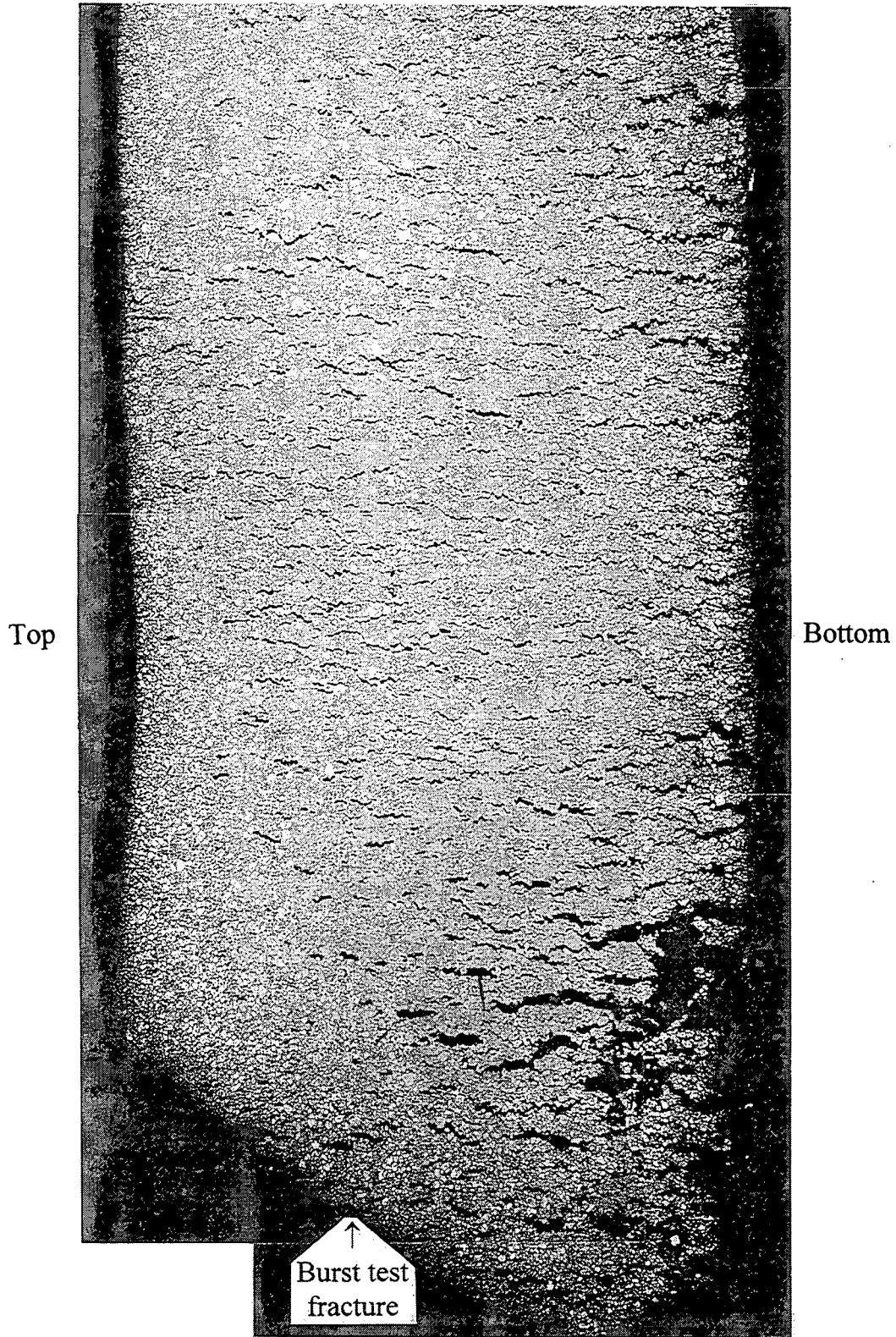
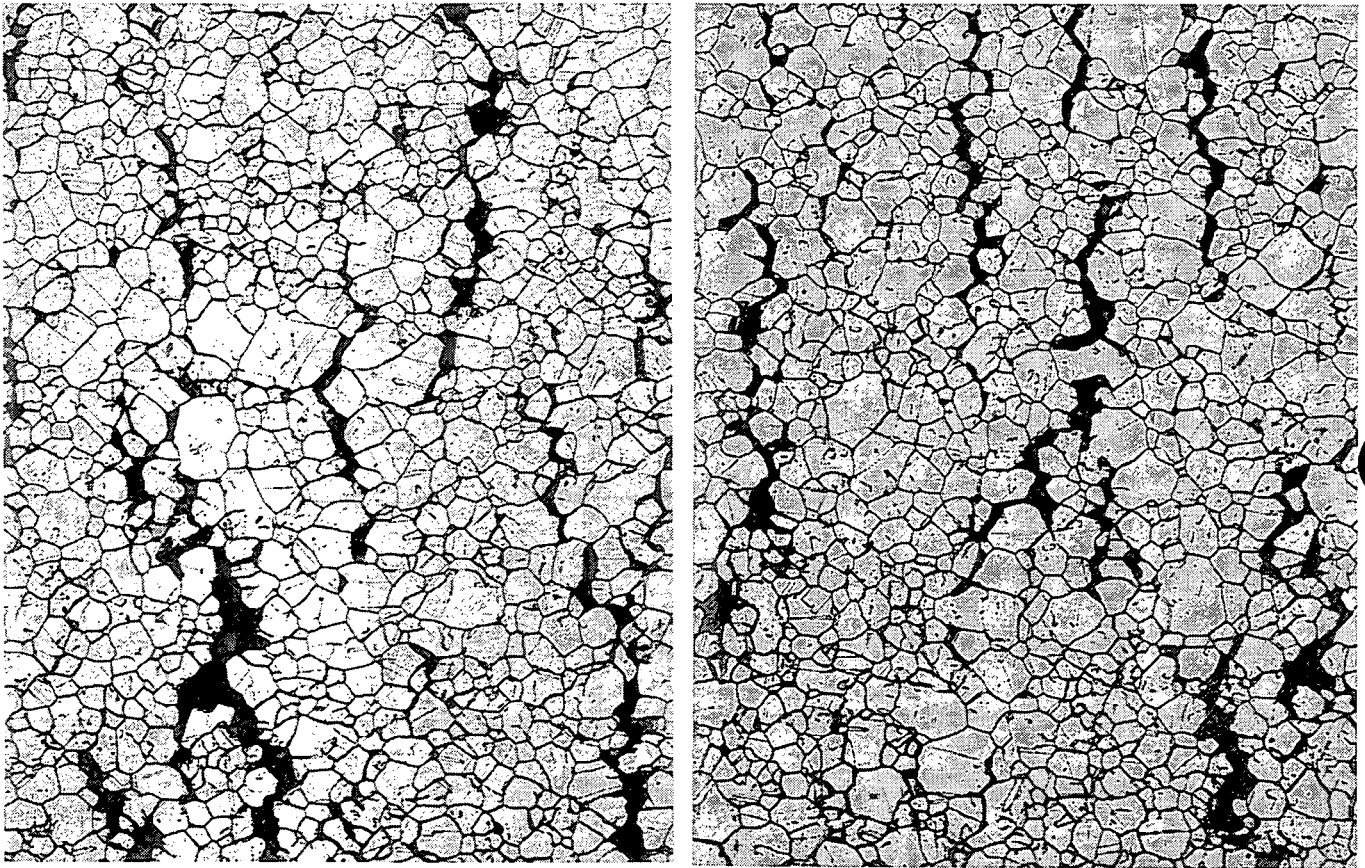


Figure 4-46 TSP2 crevice region Specimen 6B-2D of Tube R15C28. Radial metallographic sample after flattening and polishing to a depth of 0.001 inch below the OD surface. This montage is a higher magnification mirror image of Figure 4-45 because of the reversed optics of the two cameras. Mount M2163. Mag. 16X.

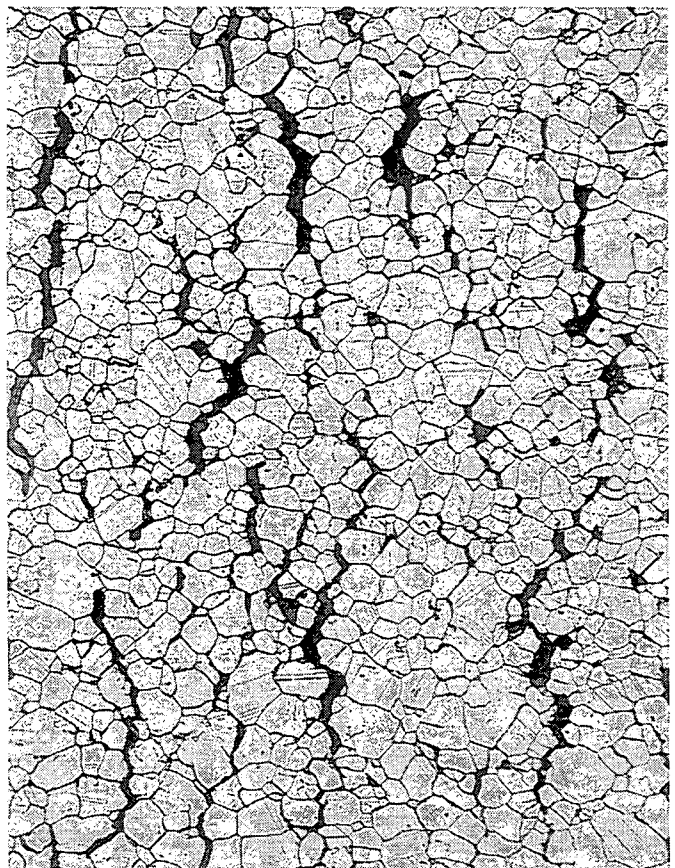
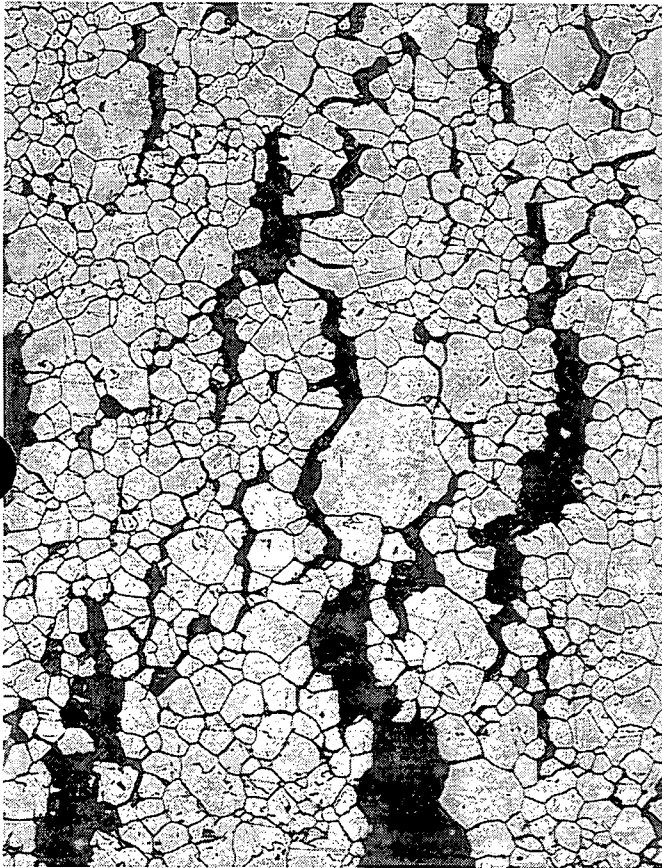
Top



Bottom

Figure 4-47 TSP2 crevice region Specimen 6B-2D of Tube R15C28. Radial metallographic sample after flattening and polishing to a depth of 0.001 inch below the OD surface. Examples of the corrosion crack pattern at this level of grinding and polishing. Mount M2163. Mag. 100X.

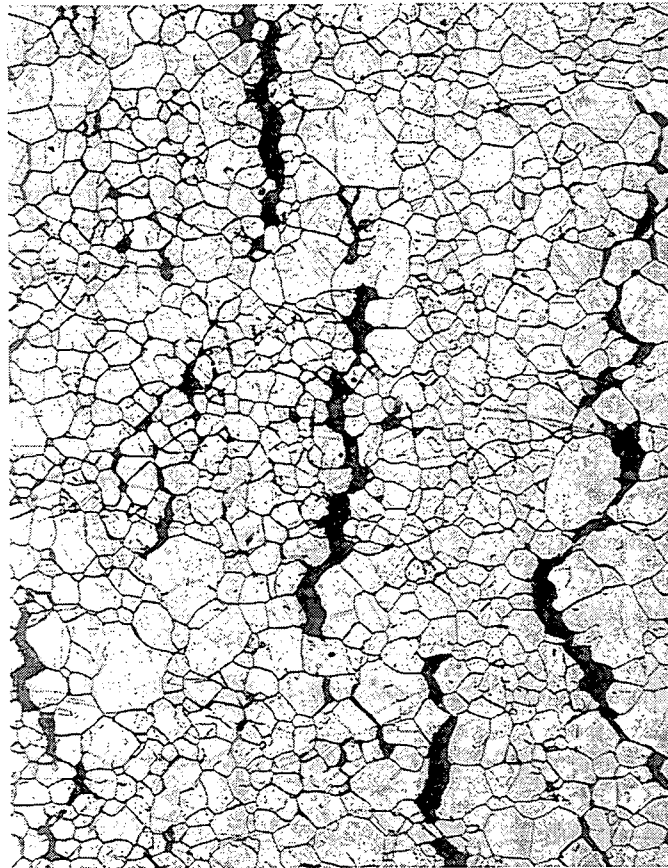
Top



Bottom

Figure 4-48 TSP2 crevice region Specimen 6B-2D of Tube R15C28. Radial metallographic sample after flattening and polishing to a depth of 0.001 inch below the OD surface. Examples of the corrosion crack pattern at this level of grinding and polishing. Mount M2163. Mag. 100X.

Top



Bottom

Figure 4-49 TSP2 crevice region Specimen 6B-2D of Tube R15C28. Radial metallographic sample after flattening and polishing to a depth of 0.001 inch below the OD surface. Examples of the corrosion crack pattern at this level of grinding and polishing. Mount M2163. Mag. 100X.

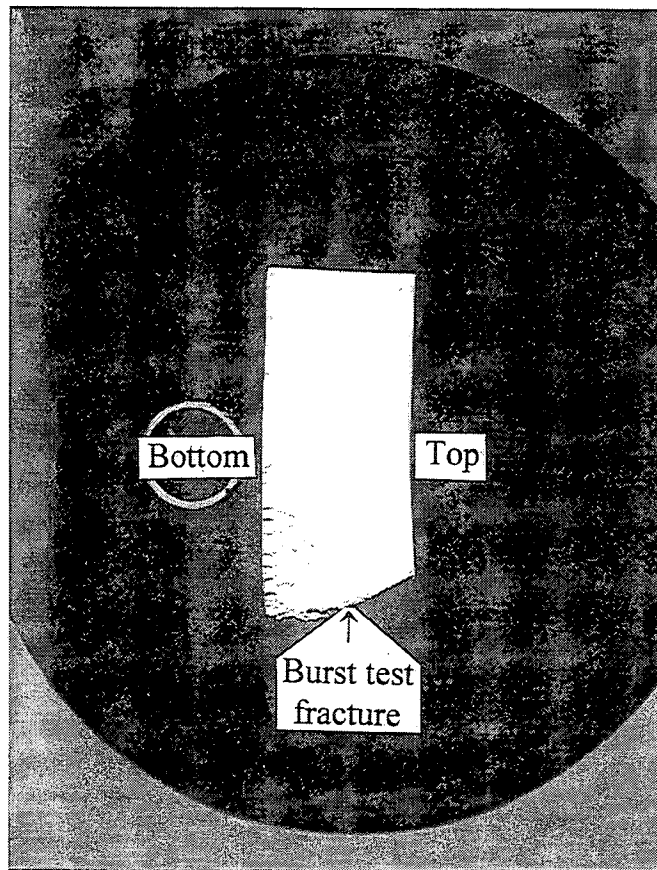


Figure 4-50 TSP2 crevice region Specimen 6B-2D of Tube R15C28. Radial metallographic sample after flattening and polishing to a depth of 0.005 inch below the OD surface. Mount M2163. Mag. 3.25X.

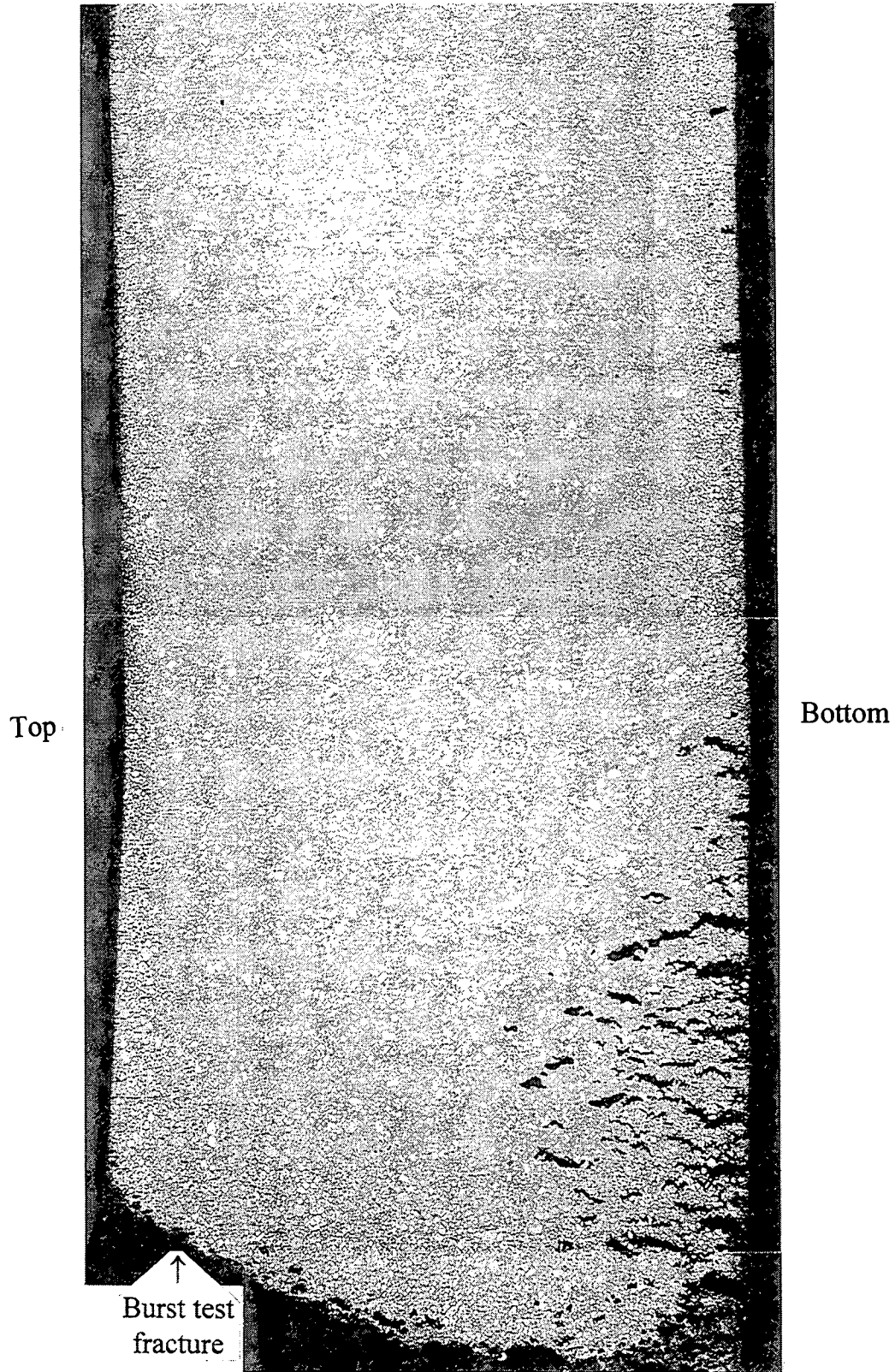
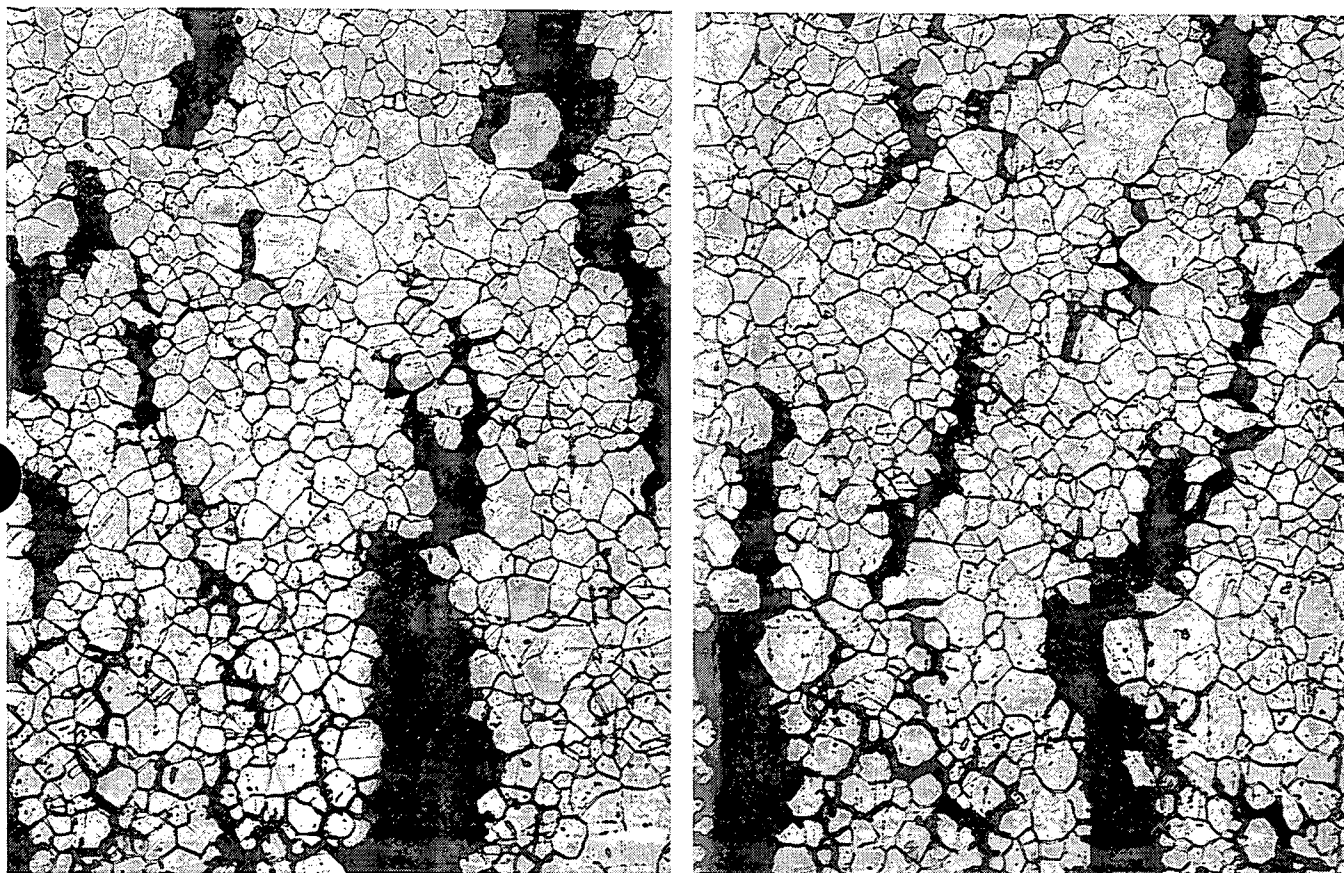


Figure 4-51 TSP2 crevice region Specimen 6B-2D of Tube R15C28. Radial metallographic sample after flattening and polishing to a depth of 0.005 inch below the OD surface. This montage is a higher magnification mirror image of Figure 4-50 because of the reversed optics of the two cameras. Mount M2163. Mag. 16X.

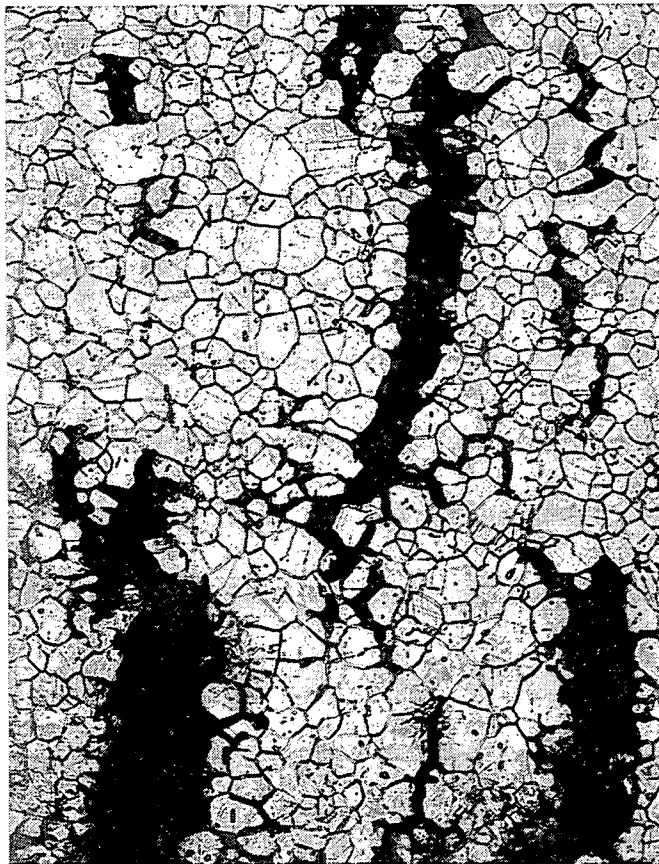
Top



Bottom

Figure 4-52 TSP2 crevice region Specimen 6B-2D of Tube R15C28. Radial metallographic sample after flattening and polishing to a depth of 0.005 inch below the OD surface. Examples of the corrosion crack pattern at this level of grinding and polishing. Mount M2163. Mag. 100X.

Top



Bottom

Figure 4-53 TSP2 crevice region Specimen 6B-2D of Tube R15C28. Radial metallographic sample after flattening and polishing to a depth of 0.005 inch below the OD surface. Example of the corrosion crack pattern at this level of grinding and polishing. Mount M2163. Mag. 100X.

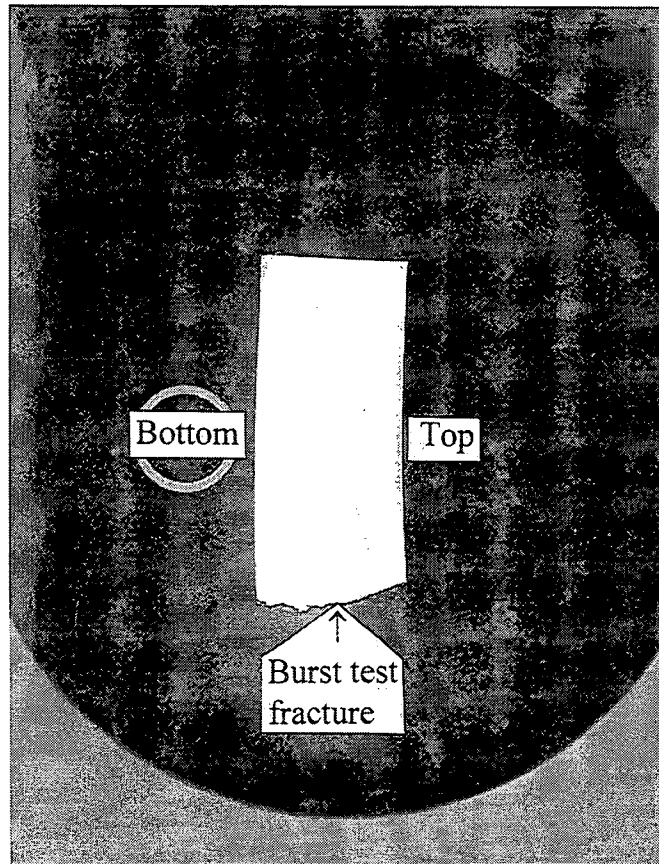


Figure 4-54 TSP2 crevice region Specimen 6B-2D of Tube R15C28. Radial metallographic sample after flattening and polishing to a depth of 0.010 inch below the OD surface. Note the absence of cracks. Mount M2163. Mag. 3.25X.

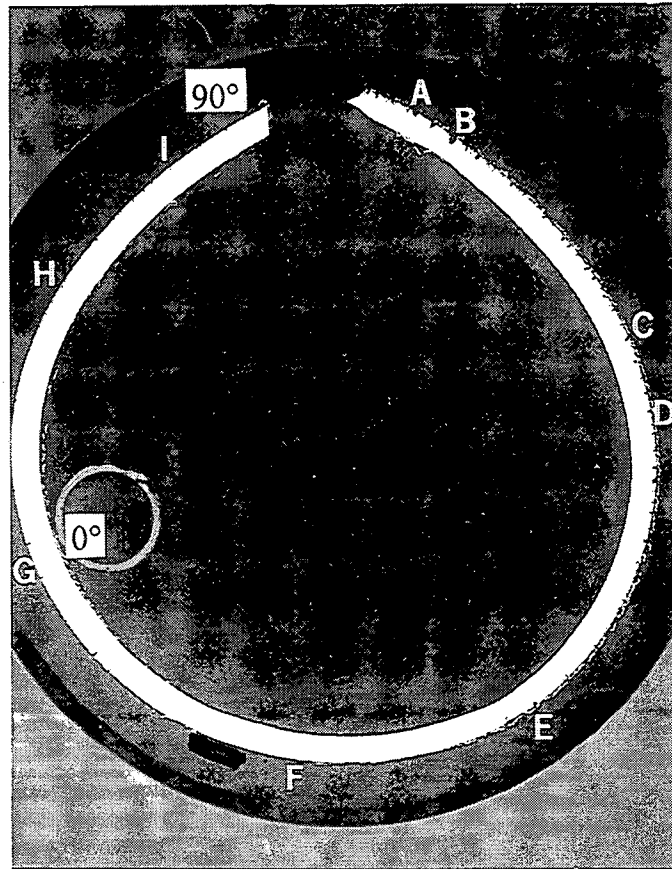


Figure 4-55 TSP2 crevice region Specimen 6B-2C of Tube R15C28. Transverse metallographic sample. Areas A through I are shown at a higher magnification in Figures 4-56 through 4-60. Mount M2162. Mag. 3.25X.

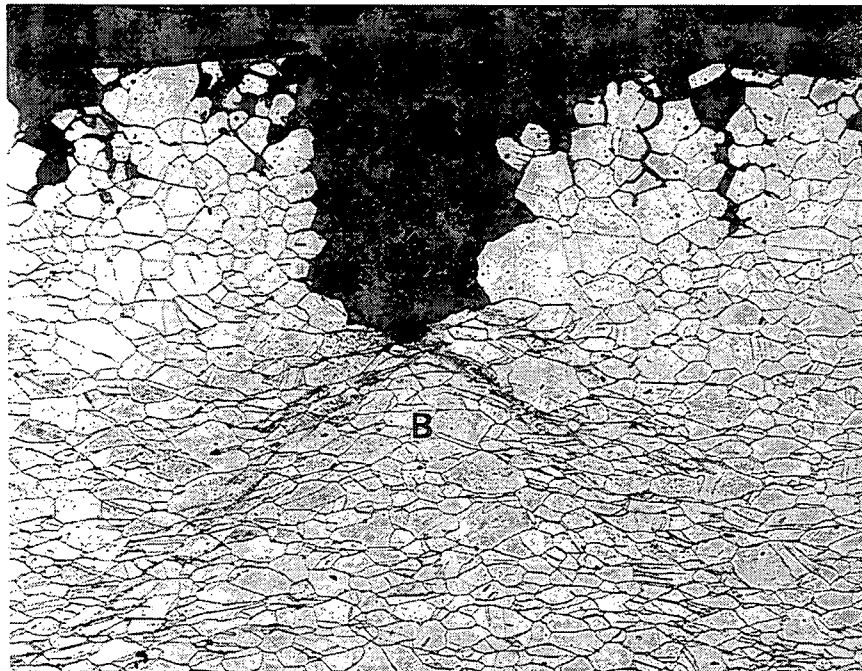
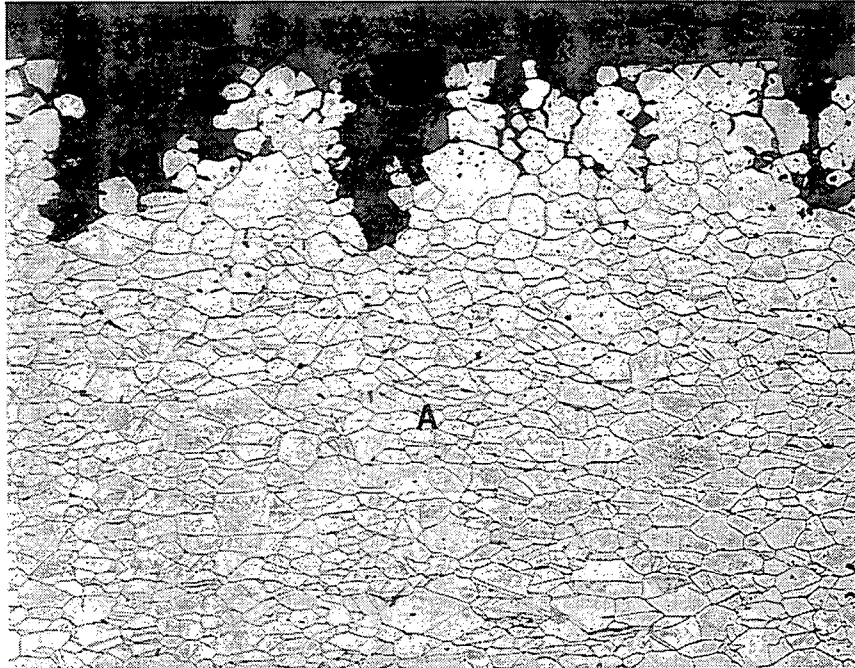


Figure 4-56 TSP2 crevice region Specimen 6B-2C of Tube R15C28. Transverse metallographic sample. Areas A and B from Figure 4-55 showing OD surface cracks at a higher magnification. Mount M2162. Mag. 100X.

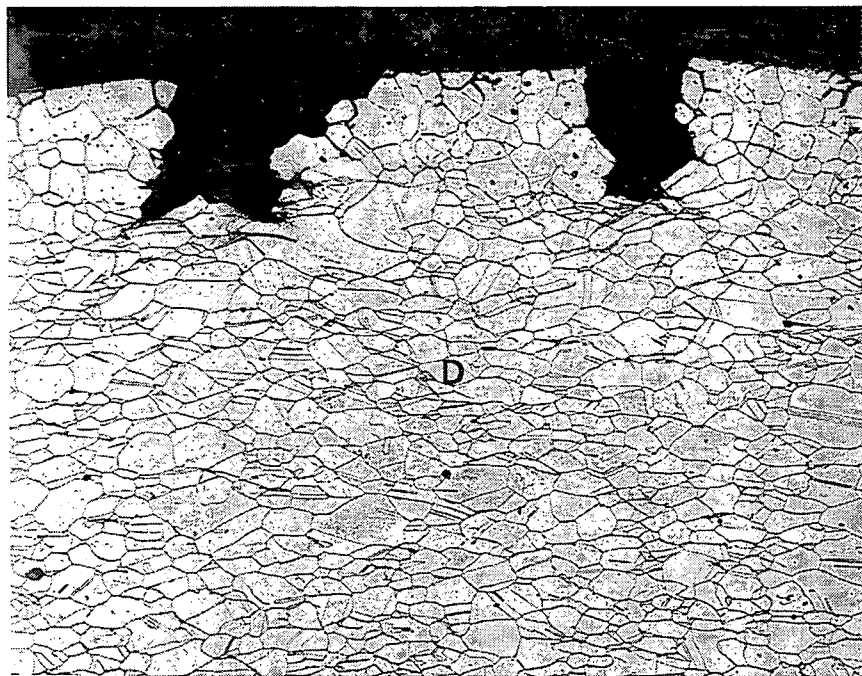
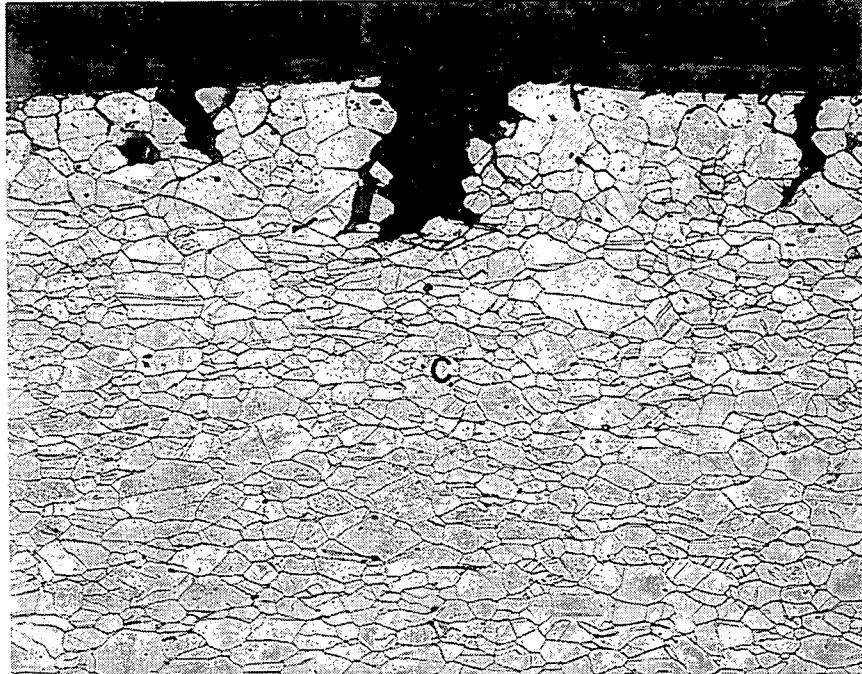


Figure 4-57 TSP2 crevice region Specimen 6B-2C of Tube R15C28. Transverse metallographic sample. Areas C and D from Figure 4-55 showing OD surface cracks at a higher magnification. Mount M2162. Mag. 100X.

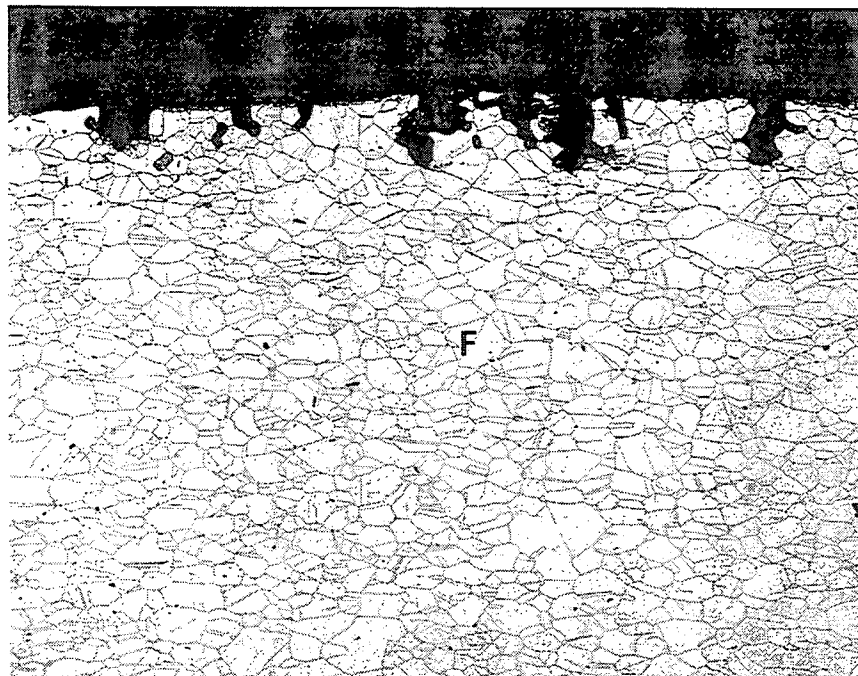


Figure 4-58 TSP2 crevice region Specimen 6B-2C of Tube R15C28. Transverse metallographic sample. Areas E and F from Figure 4-55 showing OD surface cracks at a higher magnification. Mount M2162. Mag. 100X.

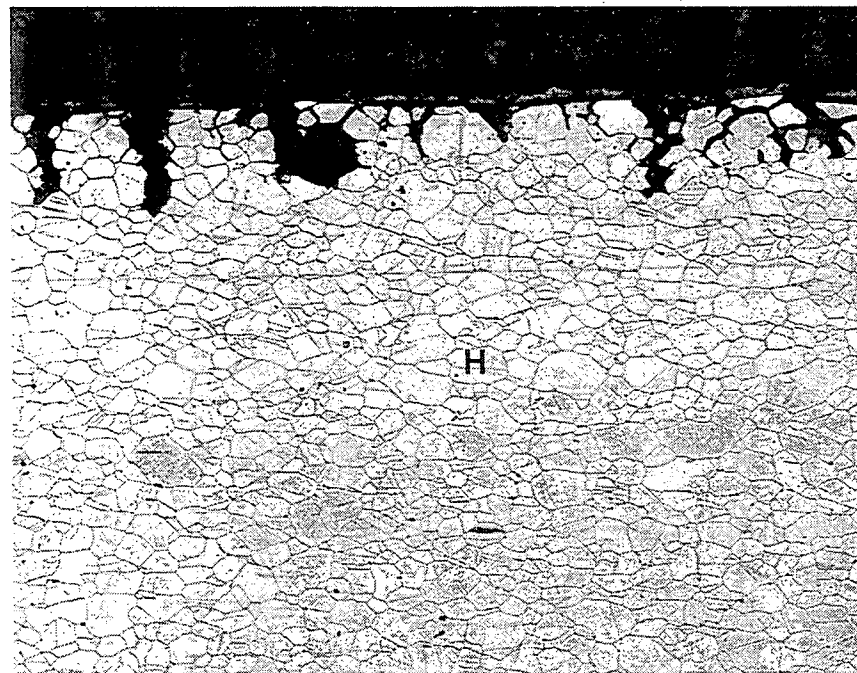
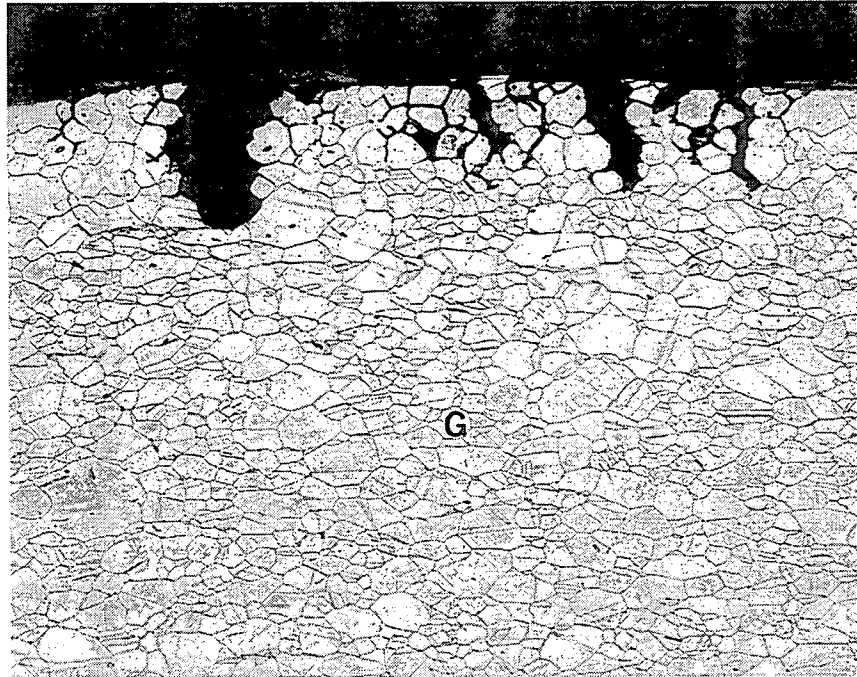


Figure 4-59 TSP2 crevice region Specimen 6B-2C of Tube R15C28. Transverse metallographic sample. Areas G and H from Figure 4-55 showing OD surface cracks at a higher magnification. Mount M2162. Mag. 100X.

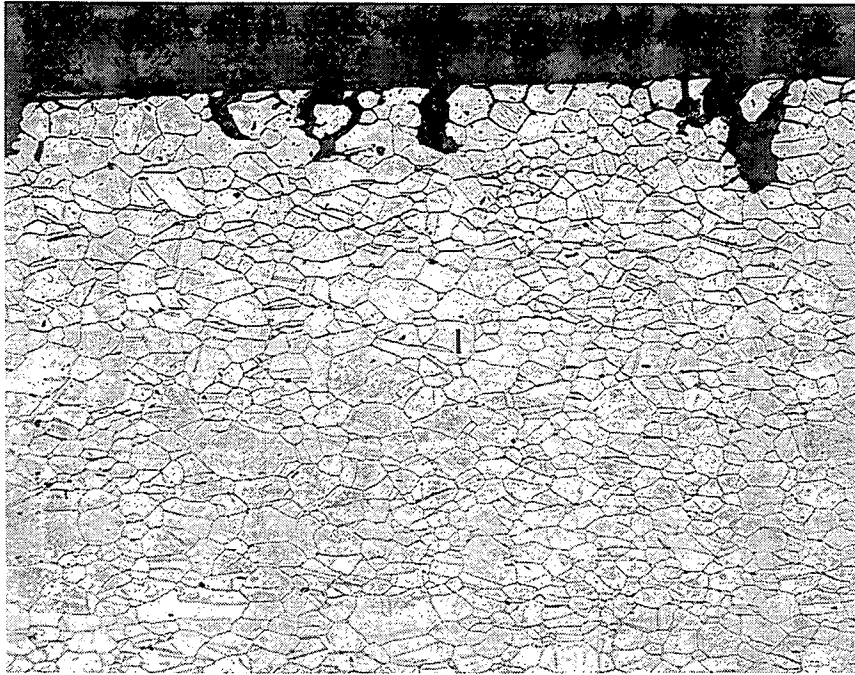


Figure 4-60 TSP2 crevice region Specimen 6B-2C of Tube R15C28. Transverse metallographic sample. Area I from Figure 4-55 showing OD surface cracks at a higher magnification. Mount M2162. Mag. 100X.

TUBE PROPERTIES

5.1 SENSITIZATION TEST

To determine the sensitization level of Tube R15C28, a modified Huey test was performed. The test consists in exposing a sample of the tubing to a 25% solution of nitric acid for 48 hours. The sample, identified as Specimen 5A-3, was taken from Piece 5 of Tube R15C28 (see Section 2 of this report). A control sample of typical Westinghouse Alloy 600 steam generator tubing was tested along with Specimen 5A-3. The results of the sensitization test are shown in Table 5-1. It may be seen that Specimen 5A-3 lost only 43.908 mg/dm²/day of its weight. This means that it was not sensitized, because a weight loss of 200 mg/dm²/day or greater is required before a tube is considered to be sensitized. Highly sensitized samples produce weight losses of many thousands of mg/dm²/day. In general, Westinghouse-produced mill annealed Alloy 600 material shows negligible weight losses in the nitric acid testing.

5.2 CARBIDE DISTRIBUTION IN THE MICROSTRUCTURE OF TUBE R15C28

The carbide distribution in Tube R15C28 was determined by an SEM examination of a metallographic sample of the tube etched in bromine methanol. The results are shown in Figures 5-1, 5-2, and 5-3. The photomicrographs in these figures demonstrate that the microstructure of this tubing contained a small amount of spherical carbides randomly distributed throughout the microstructure, with practically none at the grain boundaries. As determined before, the average grain size of Tube R15C28 was approximately ASTM 7. This grain size is larger than normally found in Westinghouse steam generator tubing.

The stress corrosion behavior of Alloy 600 is known to vary with grain boundary carbide precipitation and heat treatment. The large grain size of Tube R15C28 suggests that the mill annealing temperature was high (above 1700°F). This would explain also why some of the grains grew to very large sizes, without carbides pinning down the grain boundaries. In general, high temperature heat treatment is beneficial to stress corrosion cracking (SCC) resistance, but in this case the absence of intergranular carbides suggests that the carbon content of the material was low, since little or no solid solution carbon was apparently available for precipitation along the grain boundaries. This type of microstructure is less corrosion resistant to primary and secondary water in

steam generators than a microstructure with semi-continuous or continuous grain boundary carbide precipitates.

5.3 HARDNESS TESTS

Vickers microhardness (VH) tests with a 500 g weight were performed on the metallographic Specimen 5A-2 (Mount M2164) from Piece 5 of Tube R15C28. The indentations were spaced approximately 0.010 inch apart from the OD to the ID of the tube wall cross-section. Prior to the tests, the instrument was calibrated with a standard block. The results of the microhardness tests are listed in Table 5-2. It may be noticed that the hardness of the tube was slightly higher next to the ID (166 VHN) and next to the OD (164 VHN) compared to the center of the wall (149 - 151 VHN). The average hardness was 157 VHN. This is a relatively low value for mill annealed Alloy 600 steam generator tubing and is in line with the large grain size and low carbide density seen in the tube. It is also in agreement with a relatively low tensile strength of Tube R15C28 shown in Section 3 of this report.

Table 5-1 Modified Huey Test Results

Sample	OD (inch)	ID (inch)	Length (inch)	Area (dm²)	Weight before (g)	Weight after (g)	Weight loss rate mg/dm²/ day
Kewaunee R15C28 Spec.5A-3	0.874	0.769	0.526	0.192	9.456	9.439	43.908
Control Inconel 600	0.688	0.604	0.443	0.127	4.862	4.855	28.369

Table 5-2 Vickers 500g Microhardness Test Results
(Tube R15C28, Specimen 5A2, Mount M2164)

Location of the indentation (inches from OD)	VHN
0 (near OD edge)	164
0.010	154
0.020	149
0.030	151
0.040	156
0.050 (near ID edge)	166

Mean value: 157 VHN

FIGURES FOR SECTION 5

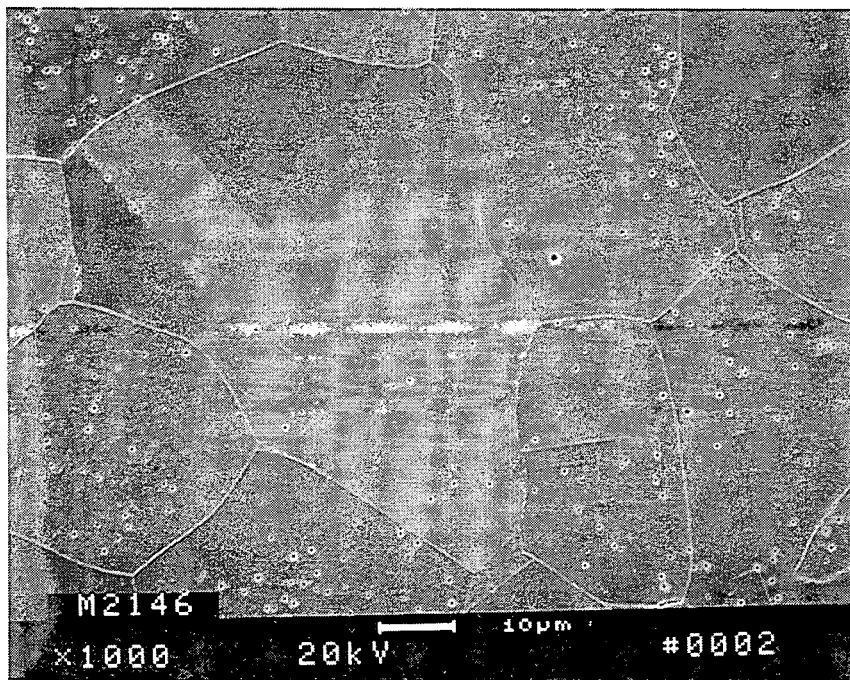
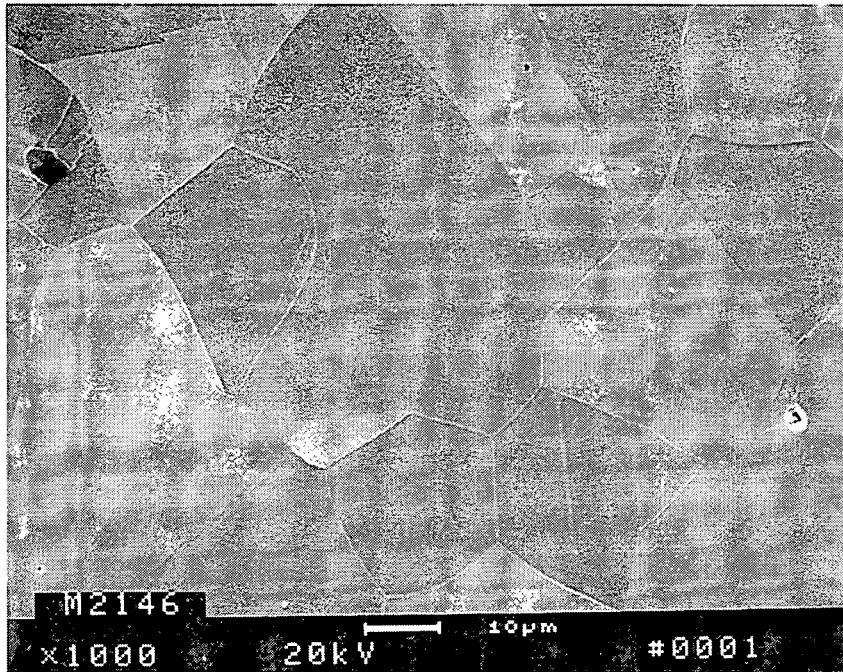


Figure 5-1 SEM photomicrographs showing the microstructure and carbide distribution of Tube R15C28. Mount M2146. Mag. 1000X.

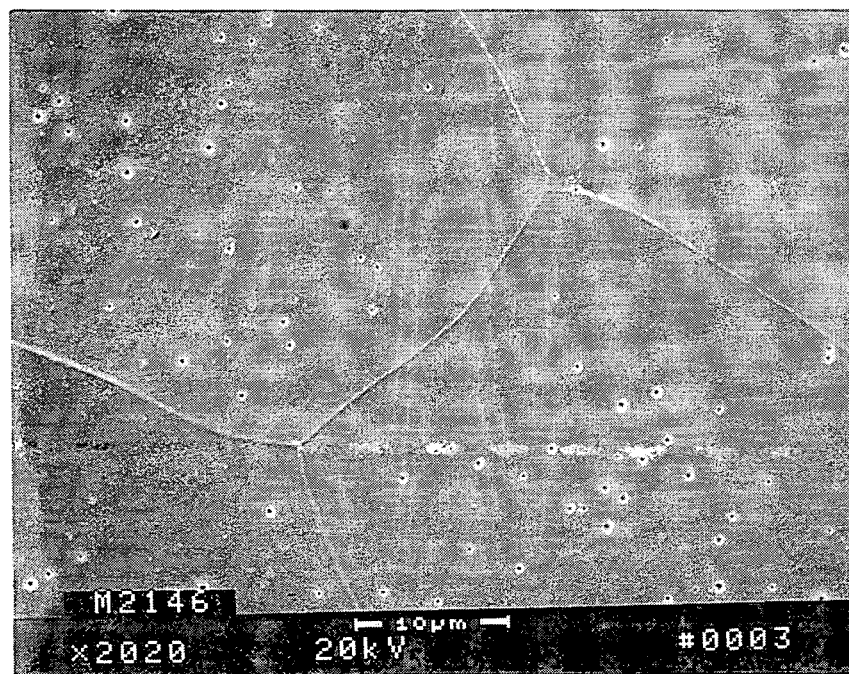
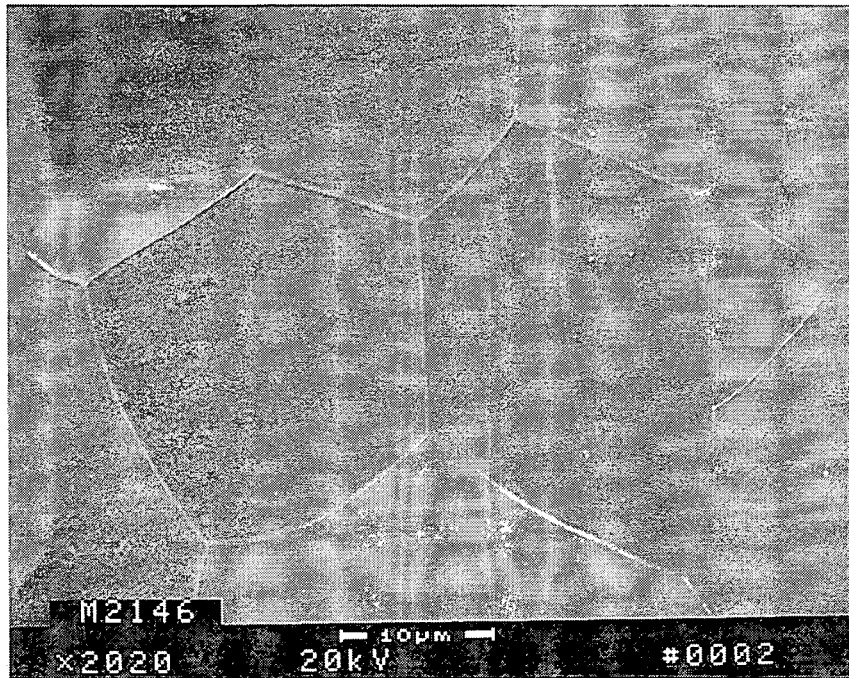


Figure 5-2 Higher magnification SEM photomicrographs showing the microstructure and carbide distribution of Tube R15C28. Mount M2146. Mag. 200X.

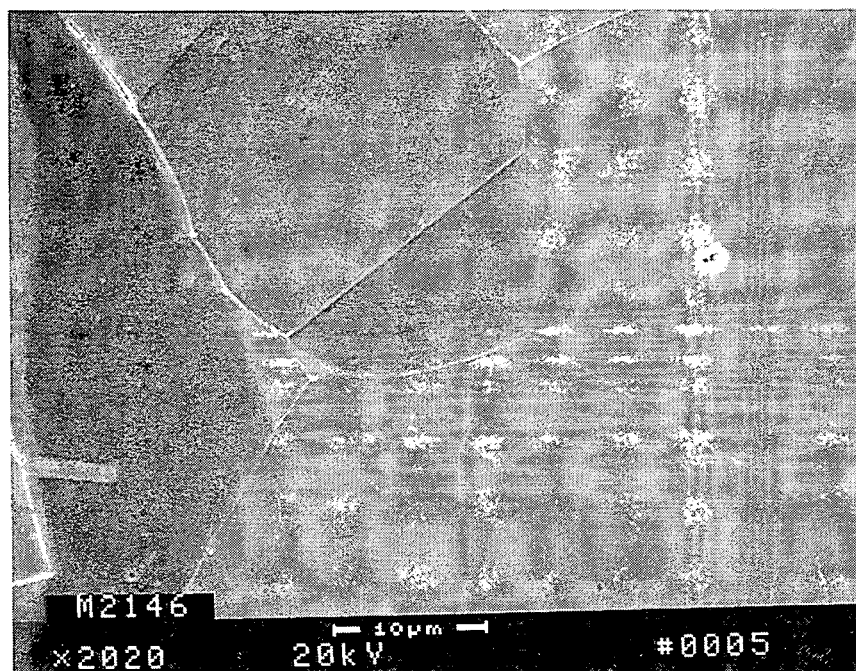
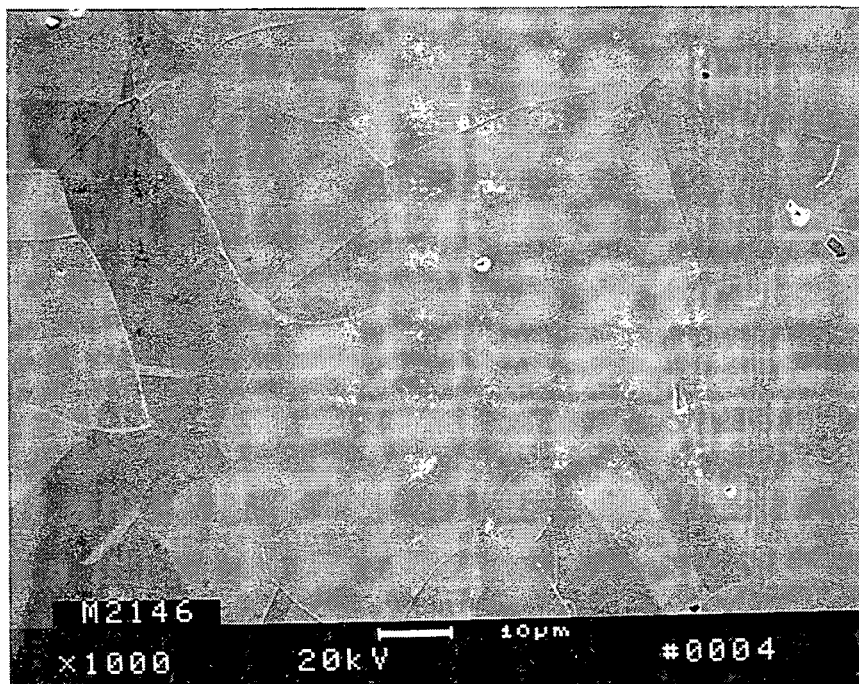


Figure 5-3 SEM photomicrographs showing the microstructure and carbide distribution of Tube R15C28. Mount M2146. Upper photomicrograph: Mag. 1000X. Lower photomicrograph: Mag. 2020X.

DISCUSSION

6.1 NONDESTRUCTIVE EXAMINATION

The tubesheet top (TST) and the first and second tube support plate (TSP1 and TSP2) regions of cold leg Tube R15C28 from S/G B were characterized by nondestructive examination. The field and laboratory NDE data were comparable, except for some dent signals which had been introduced by the tube pull. For example, the bobbin eddy current signal from a dent in the TST region of Tube R15C28 was 5.17V in the field, and 46.52 V in the laboratory, indicating that the dent in this region was increased by the tube pull. No bobbin dent signals from the TSP1 and TSP2 regions were recorded in the field, but 9.15V and 23.37V dent signals, respectively, were observed in the laboratory examination. This demonstrates that the dents in these regions did not exist until they were introduced during the tube pull.

The field eddy current (EC) data were obtained with bobbin and 3-coil MRPC probes. The laboratory EC examination employed four probes: a bobbin, a 3-coil MRPC, a + Point, and a Cecco 5. No corrosion cracking indications were found in the TST region either in the field or in the laboratory NDE data. The TSP1 and TSP2 regions had OD-origin indications (0.5-3V) which were confined to the crevice regions. These EC indications had considerable width in the RPC data and in the laboratory UT data suggesting the presence of intergranular cellular corrosion (ICC) or three dimensional intergranular attack (IGA) in addition to and in association with axial cracking. The presence of some ICC, with shallow IGA, but with predominant and deeper axial intergranular stress corrosion cracking (IGSCC), was later verified by destructive examination.

In the field EC test data there were low voltage, shallow depth, bobbin TSP indications that appeared volumetric in the 3-coil MRPC data. In the laboratory EC data the bobbin indications increased in strength by a factor of 2, presumably due to the tube pull causing the tight cracks to open up somewhat. The 3-coil MRPC probe showed volumetric indications again, while the + Point probe showed axial indications with a large area involvement, but with no distinctive volumetric characteristics. The laboratory Cecco 5 probe also had discrete areas with possible shallow indications.

The ultrasonic test (UT) examination results were essentially in agreement with the eddy current test observations. The UT showed numerous short, shallow ($\leq 20\%$ deep for TSP1, and $\leq 30\%$ deep for TSP2) indications in both circumferential and axial aim scans. In both TSP regions the indications were located mostly in two patches around

the circumference of the tube. No radiographic (X-ray) indications were observed, suggesting that any cracking present was tight and/or very shallow.

The OD surface deposits in the two TSP regions were heavily spalled in the crevice regions, presumably due to the tube pull. Laboratory OD dimensional characterization by laser micrometry suggested that 0.001 to 0.002 inch dents were present at the top edge of the TSP1 region and at the bottom edge of the TSP2 region. As mentioned before, these dents were not present prior to the tube pull.

6.2 BURST AND TENSILE TESTS

The TSP1 and TSP2 region specimens were burst tested at room temperature with a pressurization rate of 2000 psi per second. A sample from a free span (FS) section of the same tube was also burst tested as a non-corroded control specimen. No foils, bladders or restraint conditions were utilized in the burst tests, because the corrosion depths at the crevice regions were shallow, as indicated by the NDE data. The burst test results listed in Table 3-1 show, in fact, that the effects of the cracks on the burst pressures were minor: the burst pressures of the TSP1 and TSP2 region specimens were 97% and 94%, respectively, of that of the non-degraded FS control specimen. The burst pressure of the FS control specimen (9300 psi) was slightly lower than those typically seen in undegraded steam generator tubes from other plants, but it was fairly typical for the Kewaunee steam generator tubing. In any case, the burst pressures of the tested TSP crevice region specimens were significantly above the pressures required to satisfy Reg. Guide 1.121.

Visual inspection at 30X of the burst test fractures and of the OD cracks after the tests revealed that intergranular axial corrosion (IGSCC) with local cellular (ICC) characteristics was present on approximately half of the tube circumference in the central crevice region of TSP1, and on most of the circumference in the central crevice region of TSP2. All corrosion was confined to the crevice regions.

Room temperature tensile test data listed in Table 3-1, obtained on a non-corroded FS section of Tube R15C28, showed typical tensile properties for the Kewaunee steam generator tubing: a 43.5 ksi yield strength and a 93.8 tensile strength. These values, while typical for Westinghouse tubing in Kewaunee steam generators, show that the tubes were relatively low in strength. The strength normally found in Westinghouse tubing of later vintage is slightly higher.

6.3 DESTRUCTIVE EXAMINATION

SEM fractography was performed on the burst openings from the TSP crevice regions. Table 4-1 presented a summary of the OD-origin corrosion data. The TSP1 region had an intergranular corrosion macrocrack that was composed of numerous intergranular

microcracks, all of which were connected by ledges with intergranular features. This indicated that all the microcracks had grown together by intergranular corrosion prior to the burst testing. The macrocrack was 0.368 inch long, and 17% deep on the average, with a maximum depth of 30%. The TSP2 region had nearly identical results, where the macrocrack was 0.480 inch long, had an average depth of 16%, and a maximum depth of 31%.

Metallographic examinations showed that the corrosion morphology consisted primarily of axial intergranular stress corrosion cracking (IGSCC), with some intergranular cellular corrosion (ICC) components, and some superficial intergranular attack (IGA) involvement. The overall contributions of the ICC and of the IGA components to the corrosion morphology decreased as a function of depth below the OD surface, where the IGA tended to disappear quickly, and the ICC persisted a little longer. Table 4-2 presented a summary of the metallographic data.

Corrosion morphology can be characterized also by crack density, and by the degree that IGA components are associated with IGSCC, frequently measured by the ratio of the depth of a crack to its width at mid-depth (D/W). The TSP2 region had about twice the crack density (~140 cracks around the tube circumference at the midcrevice level) versus a moderate TSP1 crack density (~75 cracks around the tube circumference at the midcrevice level)¹. However, since the TSP1 region cracks were concentrated mostly in about one half of the circumference of the tube, their local density can still be considered relatively high. Both TSP regions had a moderate association of IGA with the IGSCC, since their D/W ratios were 6 to 9².

The grains of the cold leg of Tube R15C28 were essentially equiaxed, with some duplex characteristics. The grain size was relatively large: ASTM No. 8.5 for the smallest grains, 7.0 for the average, and 1.5 to 2.0 for some of the largest grains. Westinghouse typical mill annealed Alloy 600 steam generator tubing has average grain size of about 8.5 to 10.0.

Two spots on the OD surface in the TSP1 crevice region, and three spots in the TSP2 crevice region of Tube R15C28 were analyzed using the energy dispersive X-ray spectroscopy (EDS) technique. Oxygen was one of the most abundant elements in all the analyses, indicating that many of the other surface deposit elements were present

¹ A high crack density is defined as greater than 100 cracks around the tube circumference; a moderate crack density as 25 to 100 cracks; and a low crack density as less than 25 cracks around the circumference.

² D/W ratios less than 3 suggest a high association of IGA with IGSCC; D/W ratios in the range of 3 to 20 point out to a moderate association of IGA with IGSCC; and D/W ratios greater than 20 are considered to show low association of IGA with IGSCC.

either as oxides or as oxygen-containing compounds. Elements nickel (Ni), chromium (Cr), and iron (Fe) are part of the Alloy 600 composition and were also found in abundant concentrations in the EDS analyses. They partially appeared in the EDS data because part of the substrate was included in the analysis, although some of them might have been present as surface oxides. In particular, high concentrations of Fe (relative to Ni and Cr) on the tube surface are generally associated with thicker deposits which had an external origin (e.g., rust from the tube support plate). Such high concentrations of Fe were observed. Calcium (Ca), magnesium (Mg), silicon (Si), and aluminum (Al), were found in low to moderate concentrations. They can influence the cohesiveness and morphology of the crevice and sludge pile deposits, but these elements are not believed to directly contribute to corrosion degradation of the tubes. However, they help to provide a more dense deposit structure for the concentration of deleterious elements. Elements found which can contribute to corrosion included copper (Cu), lead (Pb), sulfur (S), and phosphorus (P). However, no conclusion regarding the corrosion mechanism could be made from the limited chemistry data.

The results of the EDS analyses have been summarized in Table 6-1, where the concentrations of the elements in the deposits have been rounded off to full percentage values for clarity.

6.4 COMPARISON OF FIELD EC DATA WITH LABORATORY DESTRUCTIVE EXAMINATION DATA

Table 6-2 presents a comparison of the field EC data with the laboratory destructive examination (DE) data. There is general good agreement between EC and DE results.

The field bobbin voltages (approximately 1 - 1.5V) seem unusually high for the shallow indications (31% throughwall maximum IGSCC depth, as demonstrated by DE). It is probable that the high voltages were associated with the absence of uncorroded ligaments between the microcracks that formed the burst test macrocrack, and with the large extent of shallow cracking around the tube circumference.

6.5 TUBE PROPERTIES

The modified Huey test, designed to detect possible sensitization of the tube material, revealed that no sensitization was present. The specimen lost only about 43 mg/dm²/day in the test, while a loss in excess of 200 mg/dm²/day denotes a sensitized material.

Metallographic etching of the tube material with bromine methanol demonstrated that the microstructure of Tube R15C28 contained only a small amount of randomly distributed spherical carbides, with practically none at the grain boundaries.

The stress corrosion behavior of Alloy 600 is known to vary with grain boundary carbide precipitation and heat treatment. The large grain size of Tube R15C28 suggests that the mill annealing temperature was high (above 1700°F). This would explain also why some of the grains grew to very large sizes, without carbides pinning down the grain boundaries. In general, high temperature heat treatment is beneficial to stress corrosion cracking (SCC) resistance, but in this case the absence of intergranular carbides suggests that the carbon content of the material was low, since little or no solid solution carbon was apparently available for precipitation along the grain boundaries. This type of microstructure is less corrosion resistant to primary and, to a lesser extent, secondary water in steam generators than a microstructure with semi-continuous or continuous grain boundary carbide precipitates.

Vickers microhardness tests have shown that the average hardness of Tube R15C28 material was 157 VHN. This is a relatively low value for mill annealed Alloy 600 steam generator tubing and is in line with the large grain size and low carbide density seen in the tube. It is also in agreement with a relatively low tensile strength of Tube R15C28 shown in Part 6-2 of the Discussion.

Table 6-1 Summary of the EDS Analyses of Surface Deposits on Tube R15C28
 Weight percent
 (The concentrations are rounded off to the nearest full percent for clarity)

Element	TSP1 crevice region Spot 1	TSP1 crevice region Spot 2 (thicker deposit)	TSP2 crevice region Spot 1	TSP2 crevice region Spot 2 (thicker deposit)	TSP2 crevice region Spot 3 (particle)
O	27	36	22	26	39
Fe	27	23	13	38	3
Ni	28	9	40	17	1
Cr	9	<1	16	4	-
Ca	<1	9	<1	2	<1
Mg	1	5	<1	1	-
Al	<1	<1	<1	<1	-
P	<1	6	<1	<1	-
Zn	3	3	2	4	1
Pb	1	<1	2	1	-
Si	1	4	1	3	<1
Mn	-	2	<1	2	-
Cu	<1	<1	<1	2	-
S	-	-	-	-	2
Ba	-	-	-	-	53

Table 6-2 Comparison of Kewaunee Field EC and Laboratory DE Results For Tube R15C28

Location	Field E/C	Lab DE
TST	Bobbin: NDD with 5.17V dent 3-Coil: NDD	No Data
TSP1	Bobbin: 1.14V Ind, <20% deep 3-Coil: 0.50V volumetric Ind (0.3"x150 ^o)	Predominantly shallow axial IGSCC with all or most of the short microcracks interconnected by intergranular corrosion. The corrosion occurs in a patch that covers half of the TSP crevice region. SEM fractography of the burst opening showed a 0.368 inch long intergranular corrosion macrocrack that averaged 17% deep with a maximum depth of 30%. Average D/W ratio = 6 and the mid-crevice crack density is moderate.
TSP2	Bobbin: 1.49V Ind, <20% deep 3-Coil: 0.57V volumetric Ind (0.3"x190 ^o)	Predominantly shallow axial IGSCC with all or most of the short microcracks interconnected by intergranular corrosion. The corrosion occurs in a patch that covers nearly all of the TSP crevice region. SEM fractography of the burst opening showed a 0.480 inch long intergranular corrosion macrocrack that averaged 16% deep with a maximum depth of 31%. Average D/W ratio = 9 and the mid-crevice crack density is high.

CONCLUSIONS

The first support plate (TSP1) and the second support plate (TSP2) regions of cold leg Tube R15C28 from Steam Generator B of Kewaunee both had shallow, but extensive axial intergranular stress corrosion cracking (IGSCC) with some intergranular cellular corrosion (ICC) components. All corrosion was confined to the crevice regions and was of OD origin. This corrosion was detected by both field and laboratory eddy current tests, including a call of its extensive (volumetric) nature.

Both TSP regions experienced only a minor deterioration in burst strength, with the TSP1 region having the more significant decrease, 94% of the nondegraded free span section of the pulled tube. Both TSP regions burst well above safety limitations required by R.G. 1.121. Each of the two burst opening cracks contained an intergranular macrocrack composed of a large number of intergranular microcracks joined together by intergranular ledges. The TSP1 region burst macrocrack averaged 17% throughwall deep over a length of 0.368 inch, with a maximum depth of 30%. The TSP2 region burst macrocrack averaged 16% deep over a length of 0.480 inch, with a maximum depth of 31% throughwall. Metallography showed that the area of corrosion was more extensive in the TSP2 region than in the TSP1 region. Similar trends were noted with respect to crack density, as a high crack density was present in the TSP2 region (140 cracks around the circumference) and a moderate crack density was found in the TSP1 region (75 cracks around the circumference).

ANSTEC
APERTURE
CARD

Also Available on
Aperture Card

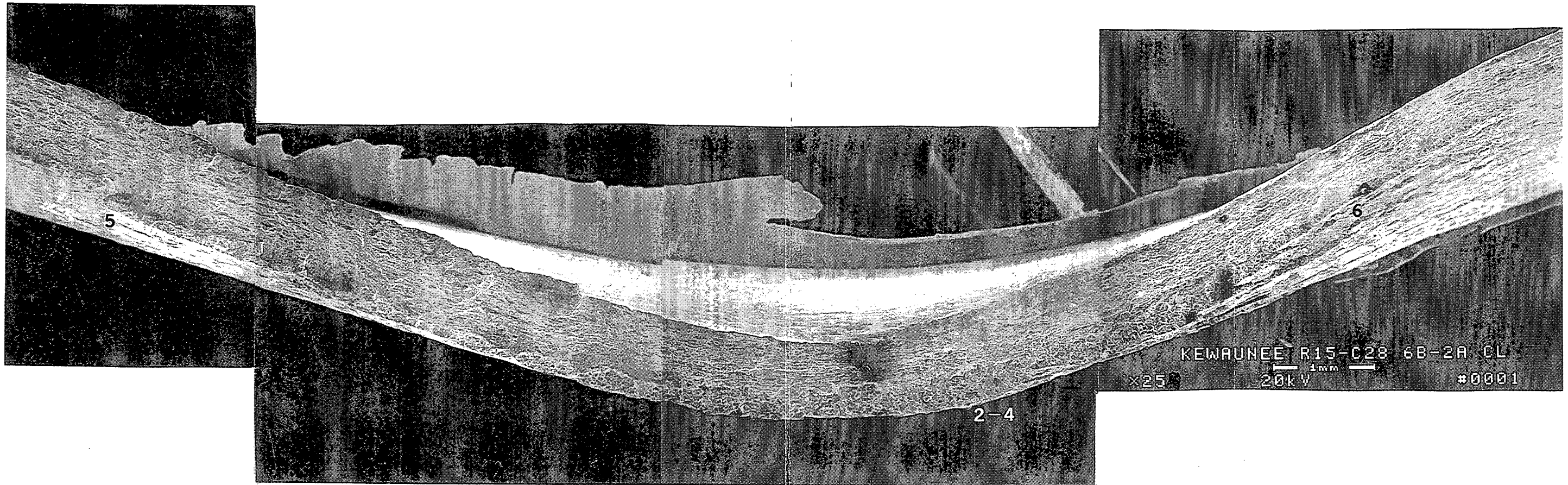


Figure 4-33 TSP2 crevice region Specimen 6B-2A of Tube R15C28. Top view of the opened burst fracture. Areas 2 through 6 of the fracture are shown at higher magnifications in Figures 4-34 through 4-36. Areas 5 and 6 mark the ends of the intergranular corrosion cracking on the OD which started the burst fracture.

9709080028-03

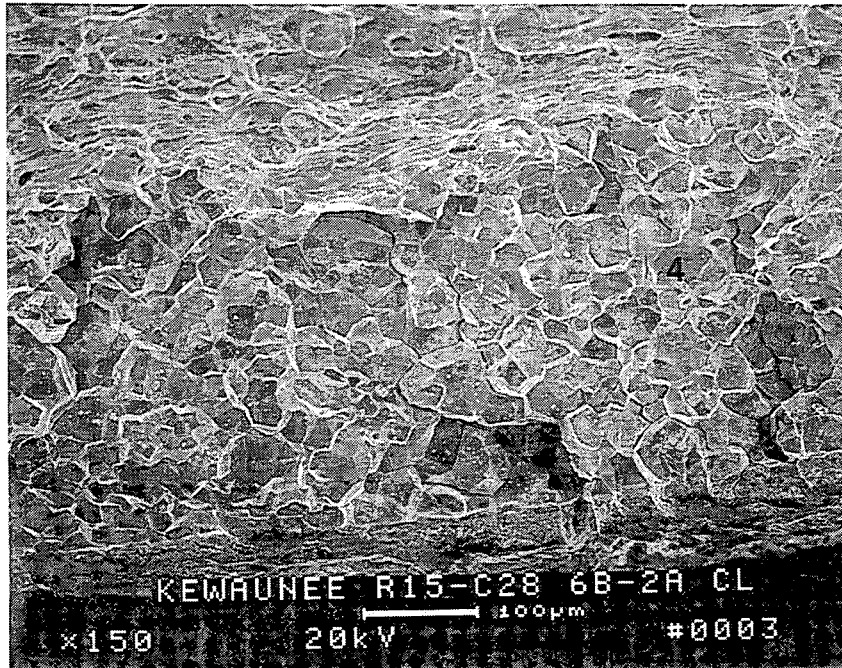
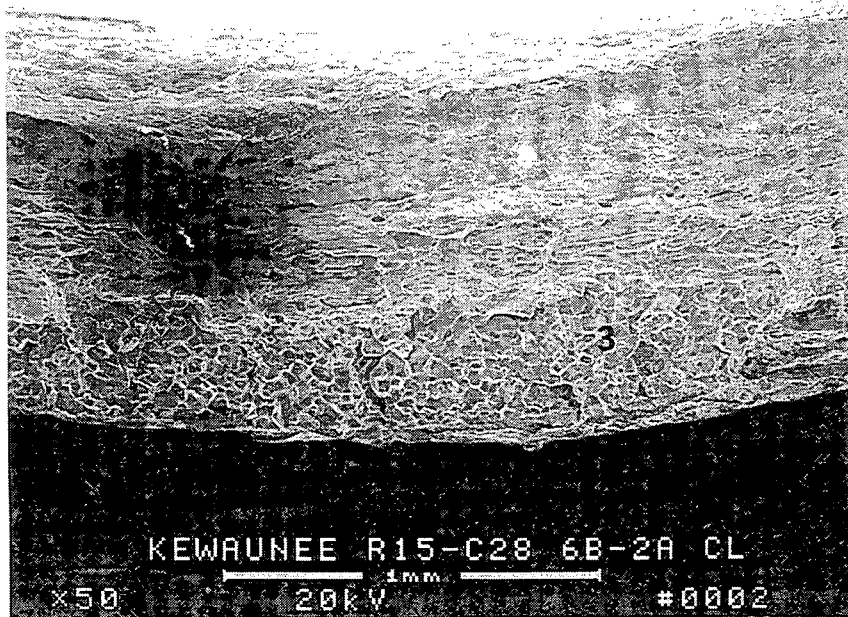


Figure 4-34 TSP2 crevice region Specimen 6B-2A of Tube R15C28. Areas 2 and 3 from Figure 4-33, showing the topography of the burst fracture at the location of the deepest corrosion penetration (31% throughwall).

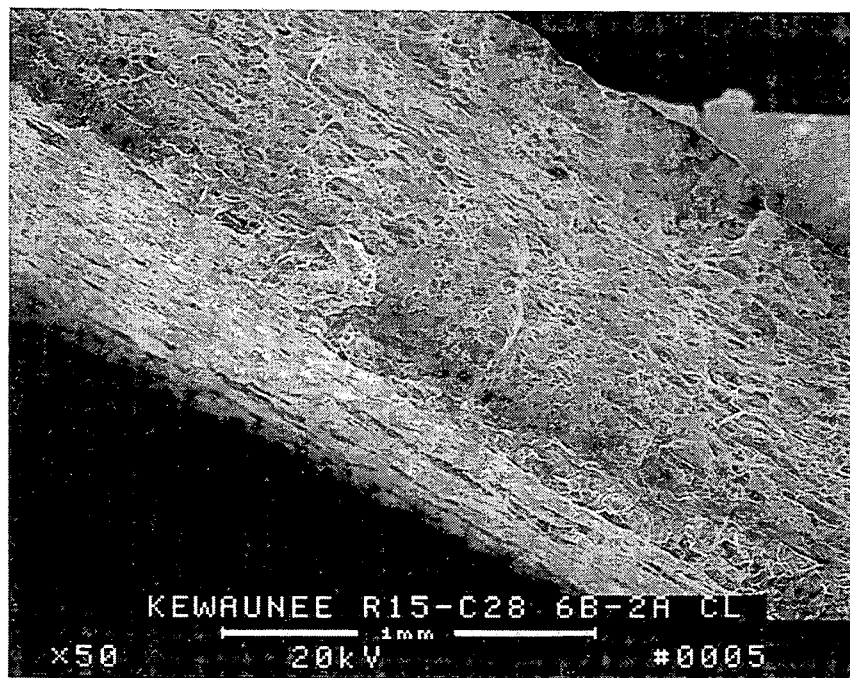
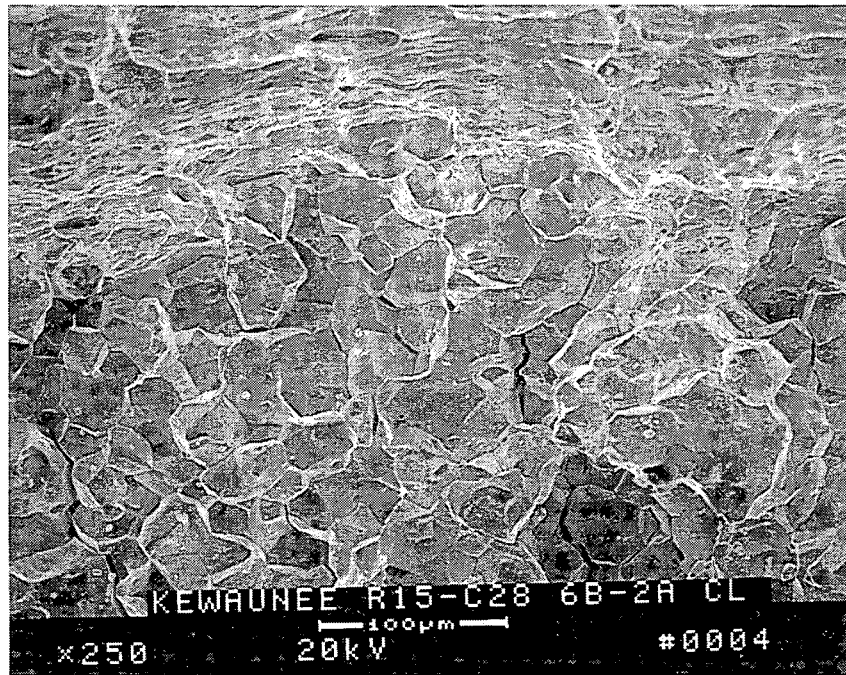


Figure 4-35 TSP2 crevice region Specimen 6B-2A of Tube R15C28. Upper photograph: Area 4 from Figure 4-34 showing the boundary between the field corrosion crack at the point of deepest penetration and the laboratory fracture produced during the burst test.

Lower photograph: Area 5 from Figure 4-33 showing the left end of field corrosion cracking on the burst test fracture.

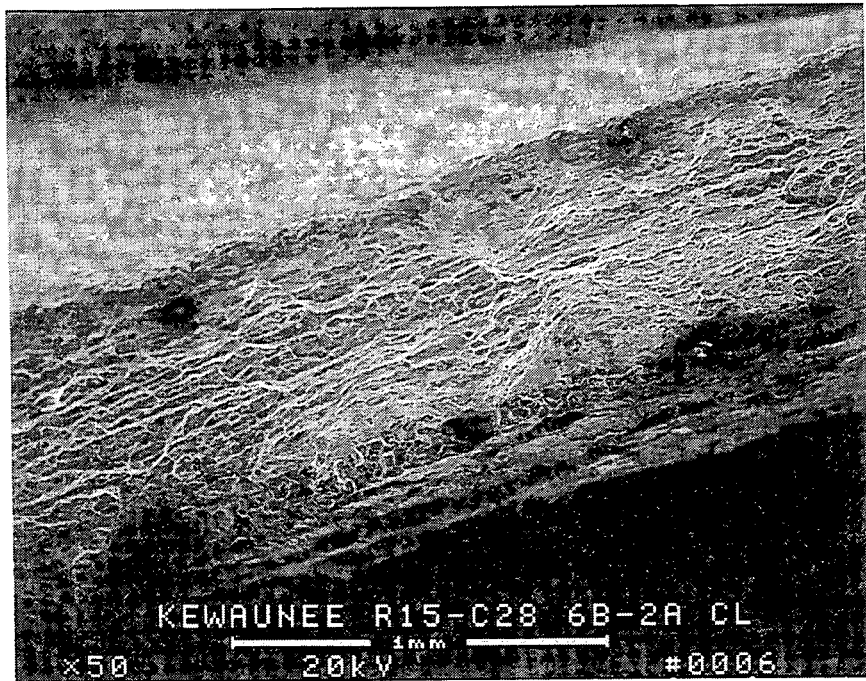


Figure 4-36 TSP2 crevice region Specimen 6B-2A of Tube R15C28. Area 6 from Figure 4-33 showing the right end of field corrosion cracking on the burst test fracture.

ANSTEC
APERTURE
CARD

Also Available on
Aperture Card

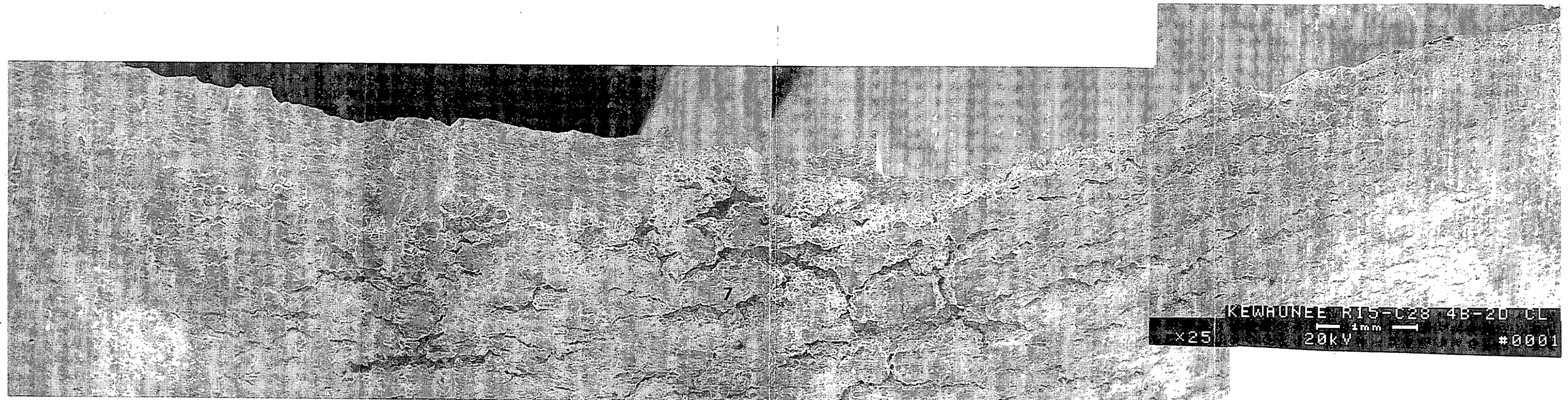


Figure 4-6 TSP1 crevice region Specimen 4B-2D of Tube R15C28. Side view of the opened burst fracture showing OD corrosion cracks opened wider by the burst test. Area 7 on the OD surface is shown at progressively higher magnifications in Figures 4-7 through 4-9.

9709080028-02

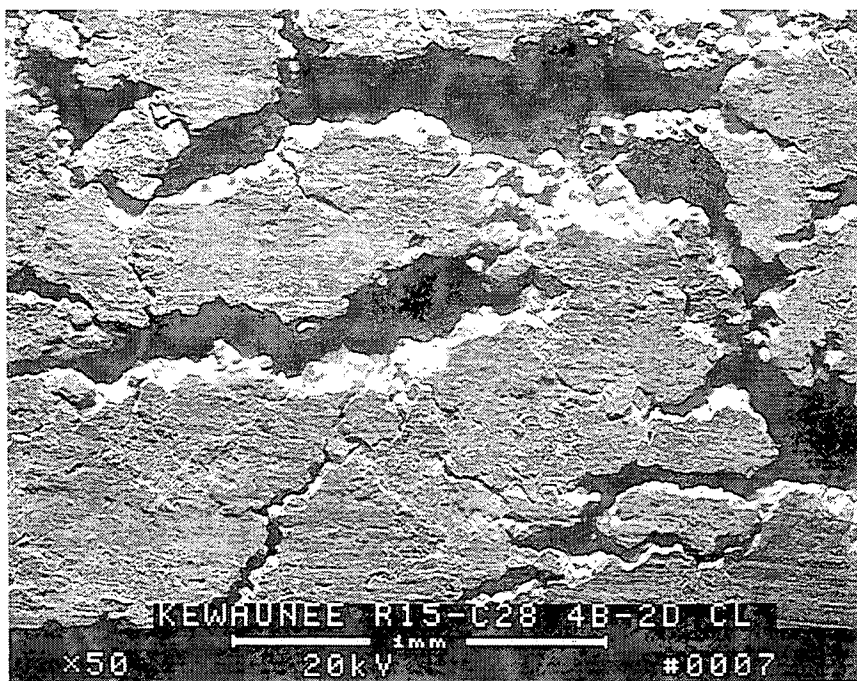


Figure 4-7 TSP1 crevice region Specimen 4B-2D of Tube R15C28. Side view of the opened burst fracture showing OD corrosion cracks opened wider by the burst test. Area 7 on the OD surface from Figure 4-6, shown at a higher magnification.

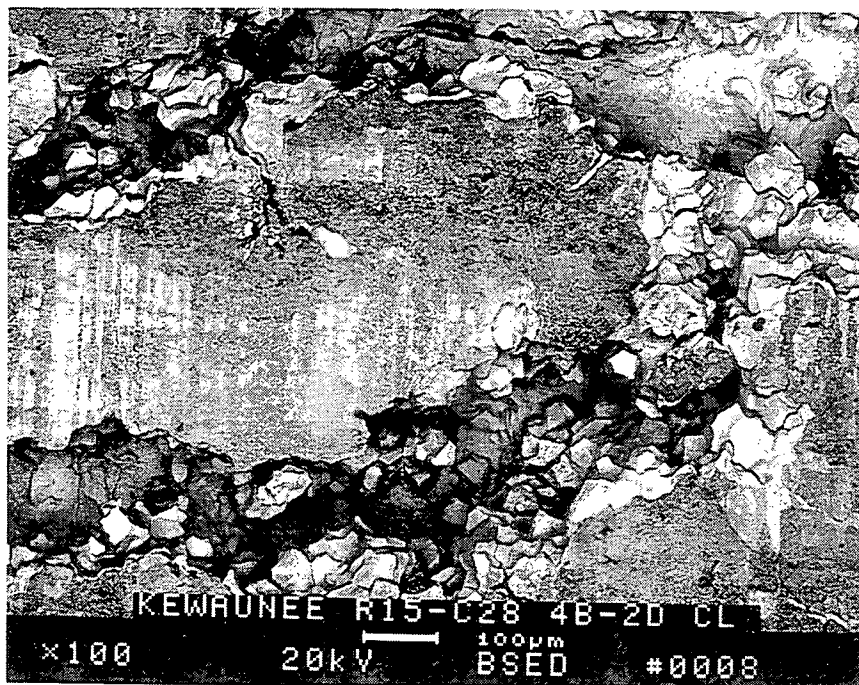
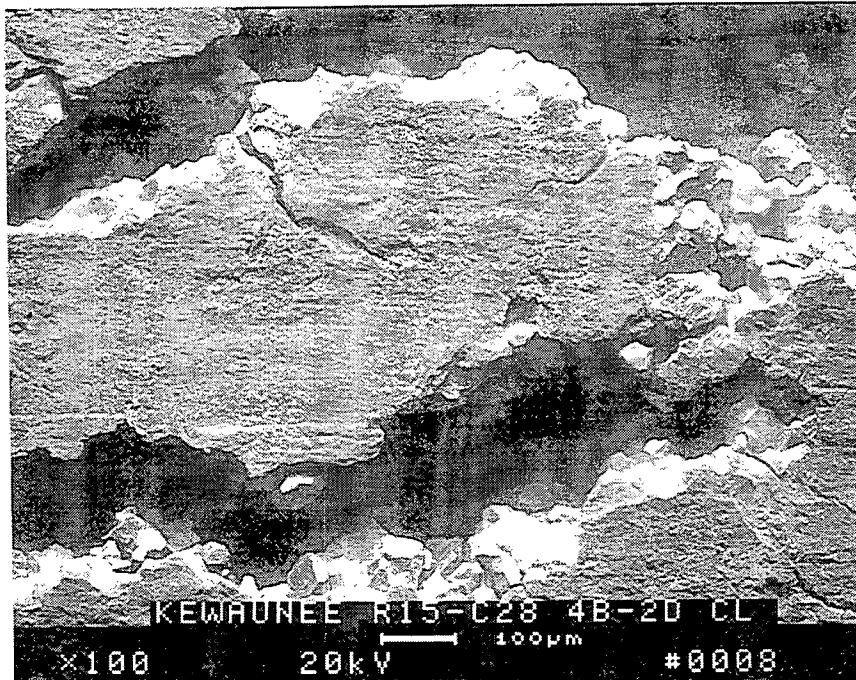


Figure 4-8 TSP1 crevice region Specimen 4B-2D of Tube R15C28. Side view of the opened burst fracture showing OD corrosion cracks opened wider by the burst test. Area 7 on the OD surface from Figure 4-6, shown at a higher magnification. Upper photograph: reflected electron image. Lower photograph: backscattered electron image of the same area.



Figure 4-9 TSP1 crevice region Specimen 4B-2D of Tube R15C28. Side view of the opened burst fracture showing OD corrosion cracks opened wider by the burst test. Area 7 on the OD surface from Figure 4-6, shown at a higher magnification. Upper photograph: reflected electron image. Lower photograph: backscattered electron image of the same area.

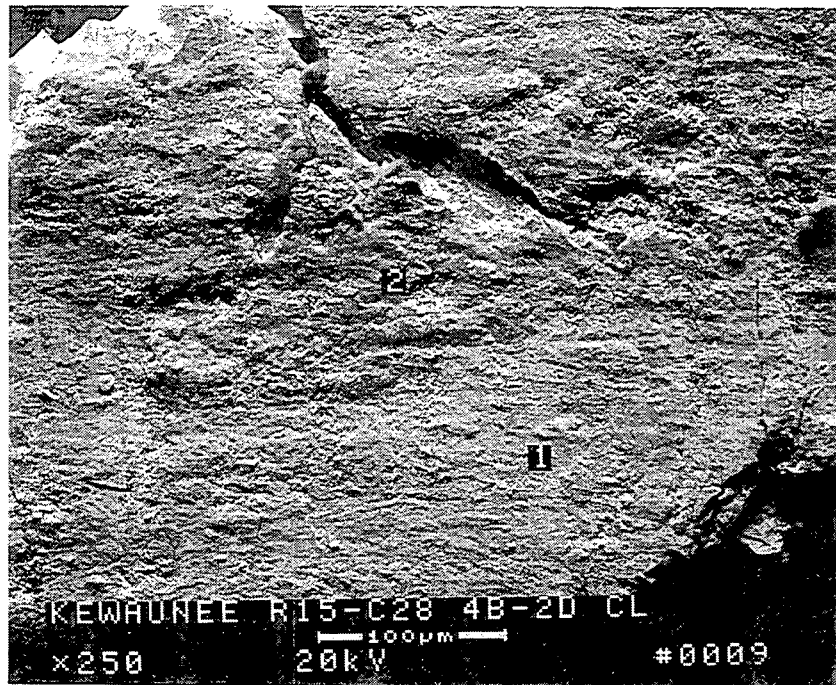
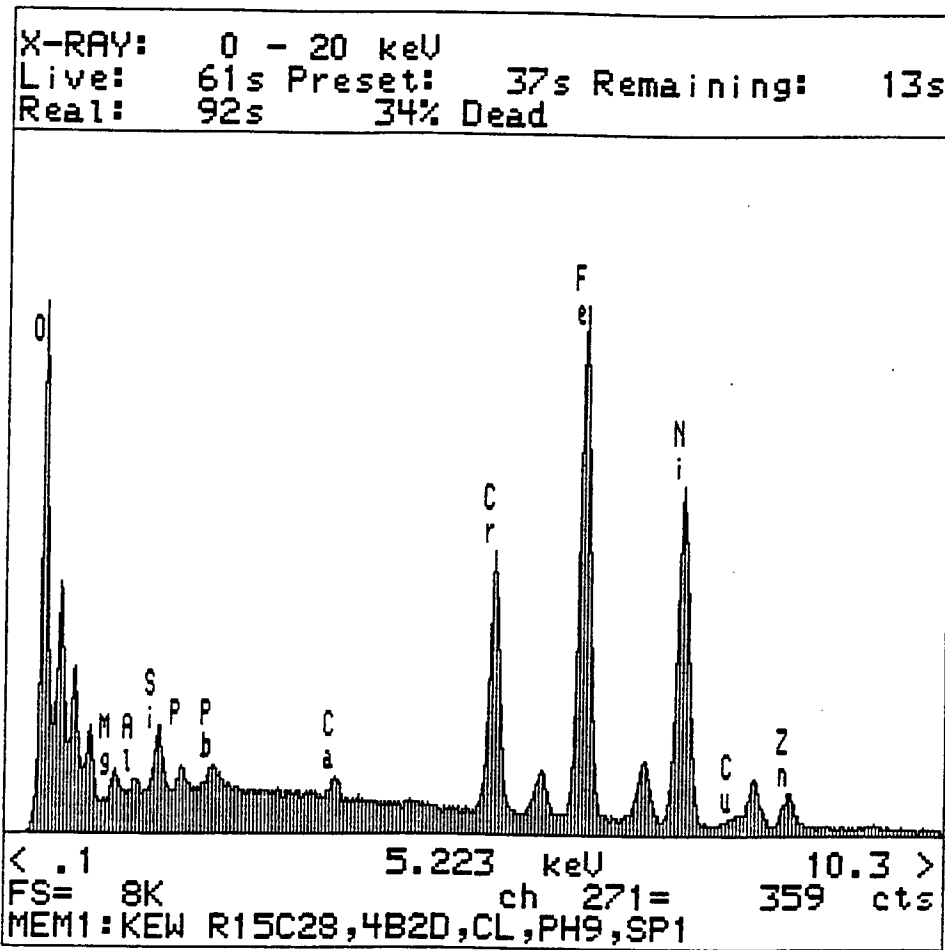


Figure 4-10 TSP1 crevice region Specimen 4B-2D of Tube R15C28. Side view of the opened burst fracture showing OD corrosion cracks opened wider by the burst test. Higher magnification photograph of Area 7 on the OD surface from Figure 4-6, showing the locations of Spots 1 and 2 which were analyzed using the energy dispersive X-ray spectroscopy (EDS) technique. The results of the analyses are shown in Figures 4-11 and 4-12.



ELMT	%ELMT	+-	Error	ATOM. %
O K	26.882	+-	.300	55.770
MgK	1.171	+-	.146	1.598
P K	.466	+-	.059	.500
CaK	.374	+-	.037	.310
ZnK	3.240	+-	.197	1.645
PbM	1.277	+-	.162	.205
AlK	.211	+-	.061	.259
SiK	1.227	+-	.055	1.450
CrK	9.407	+-	.129	6.005
FeK	26.897	+-	.245	15.986
NiK	27.930	+-	.333	15.791
CuK	.920	+-	.189	.480
TOTAL	100.000			100.000

Figure 4-11 TSP1 crevice region Specimen 4B-2D of Tube R15C28. Results of the EDS analysis of Spot 1, Figure 4-10, on the OD surface at Area 7 from Figure 4-6.

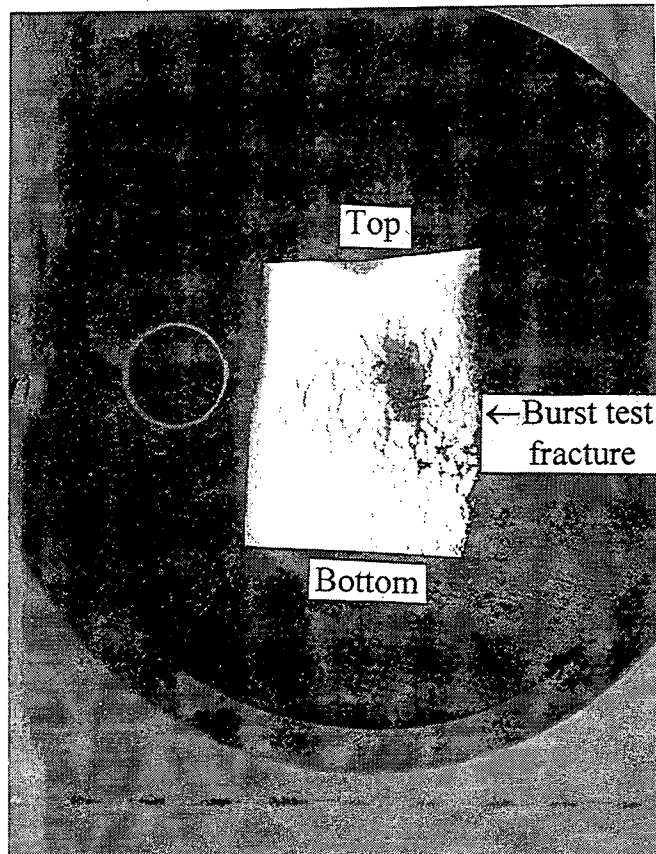


Figure 4-13 TSP1 crevice region Specimen 4B-2C of Tube R15C28. Radial metallographic sample after flattening and polishing to a depth of 0.001 inch below the OD surface. Mount M2161. Mag. 3.25X.



Figure 4-14 TSP1 crevice region Specimen 4B-2C of Tube R15C28. Radial metallographic sample after flattening and polishing to a depth of 0.001 inch below the OD surface. This montage is a higher magnification mirror image of Figure 4-13 because of the reversed optics of the two cameras. Mount M2161. Mag. 16X.

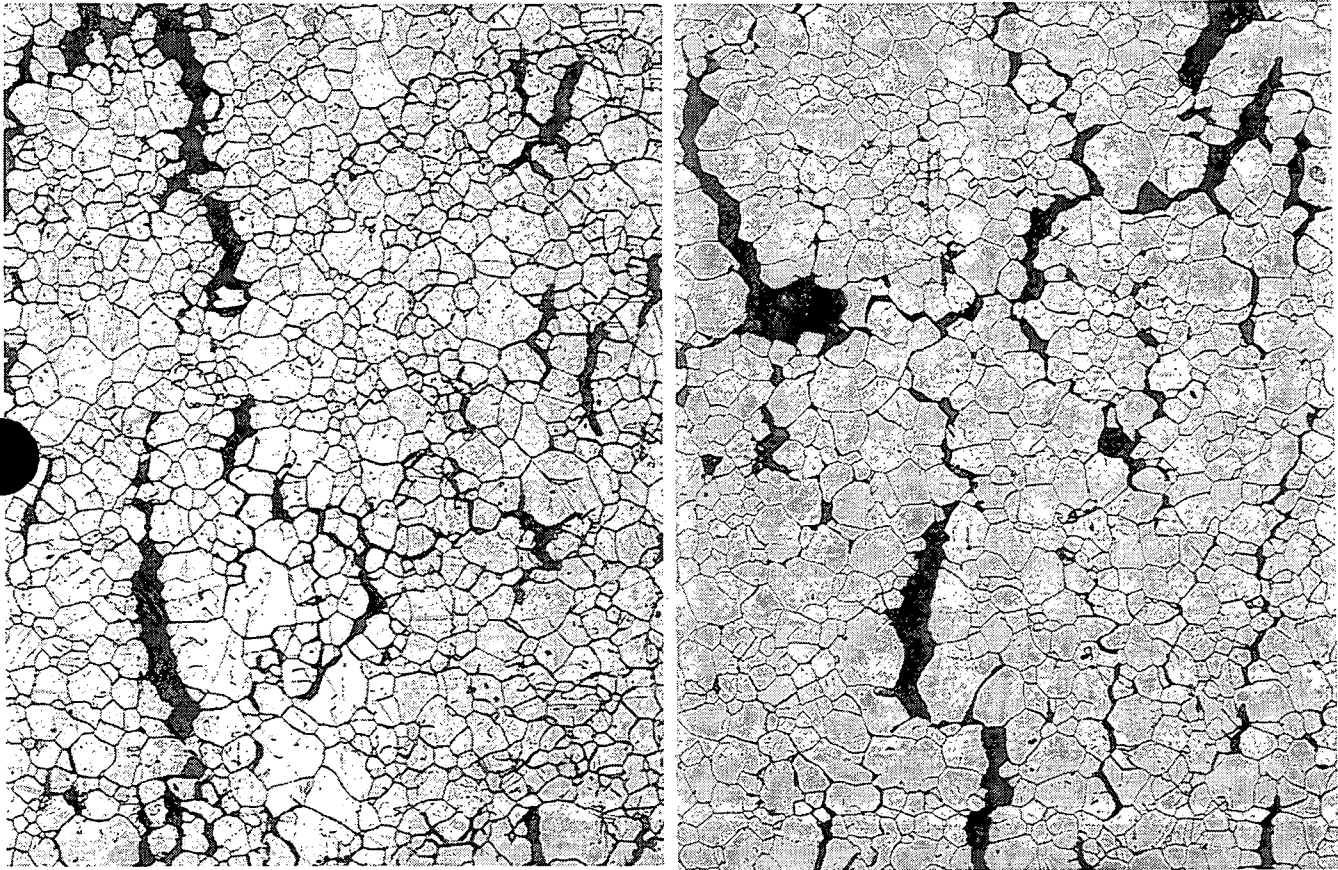


Figure 4-15 TSP1 crevice region Specimen 4B-2C of Tube R15C28. Radial metallographic sample after flattening and polishing to a depth of 0.001 inch below the OD surface. Examples of the corrosion crack pattern at this level of grinding and polishing. Mount M2161. Mag. 100X.

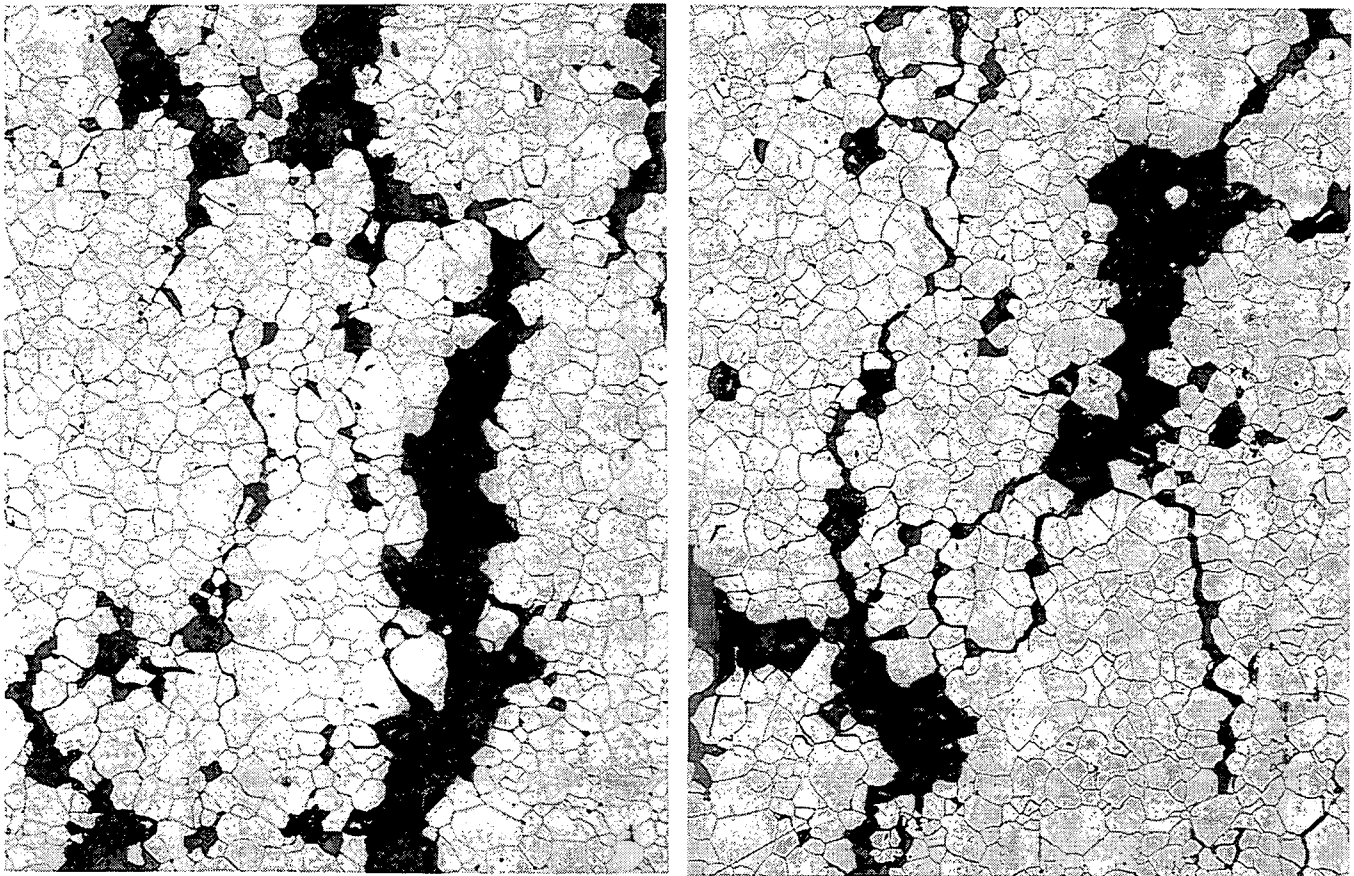


Figure 4-16 TSP1 crevice region Specimen 4B-2C of Tube R15C28. Radial metallographic sample after flattening and polishing to a depth of 0.001 inch below the OD surface. Examples of the corrosion crack pattern at this level of grinding and polishing. Mount M2161. Mag. 100X.

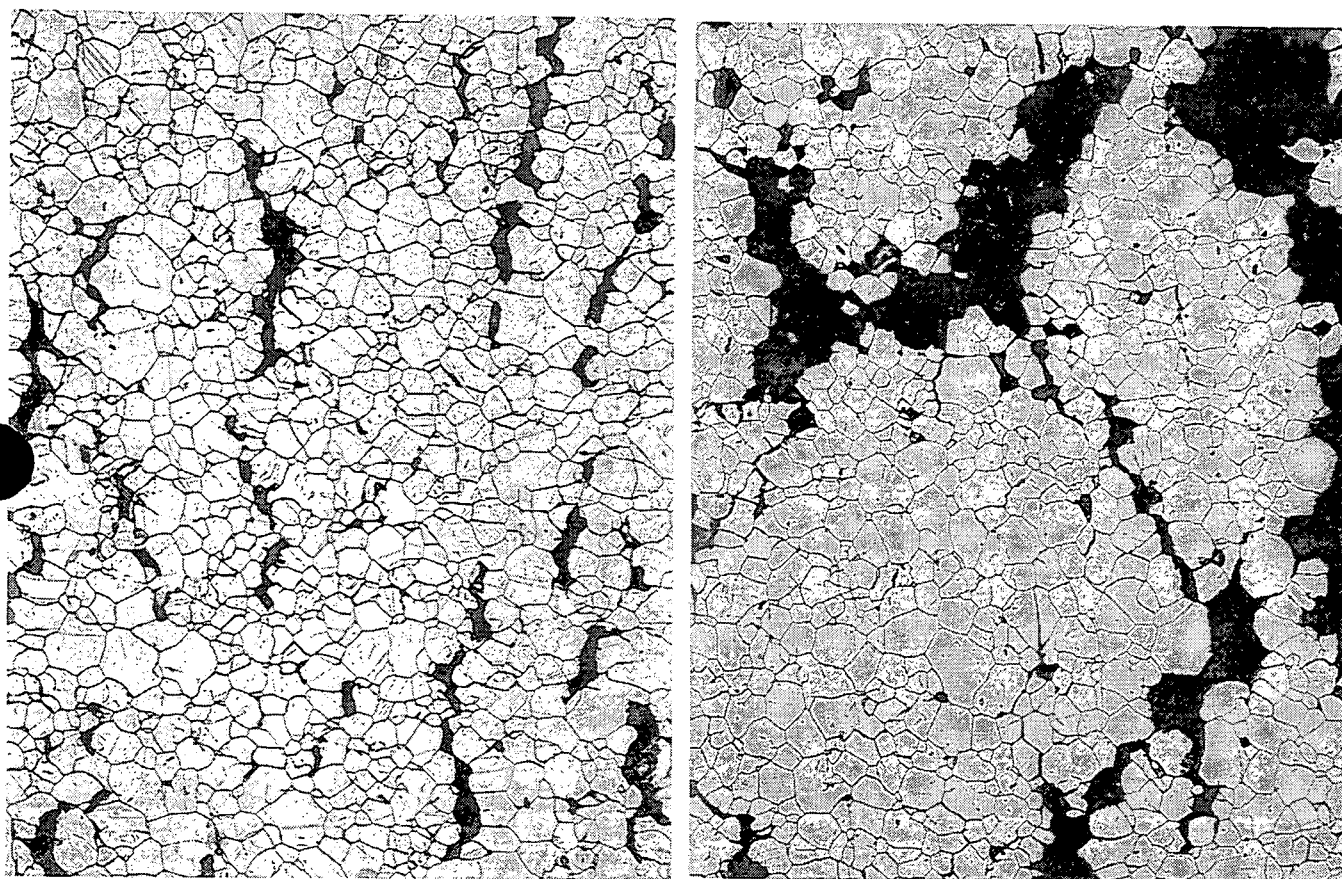


Figure 4-17 TSP1 crevice region Specimen 4B-2C of Tube R15C28. Radial metallographic sample after flattening and polishing to a depth of 0.001 inch below the OD surface. Examples of the corrosion crack pattern at this level of grinding and polishing. Mount M2161. Mag. 100X.

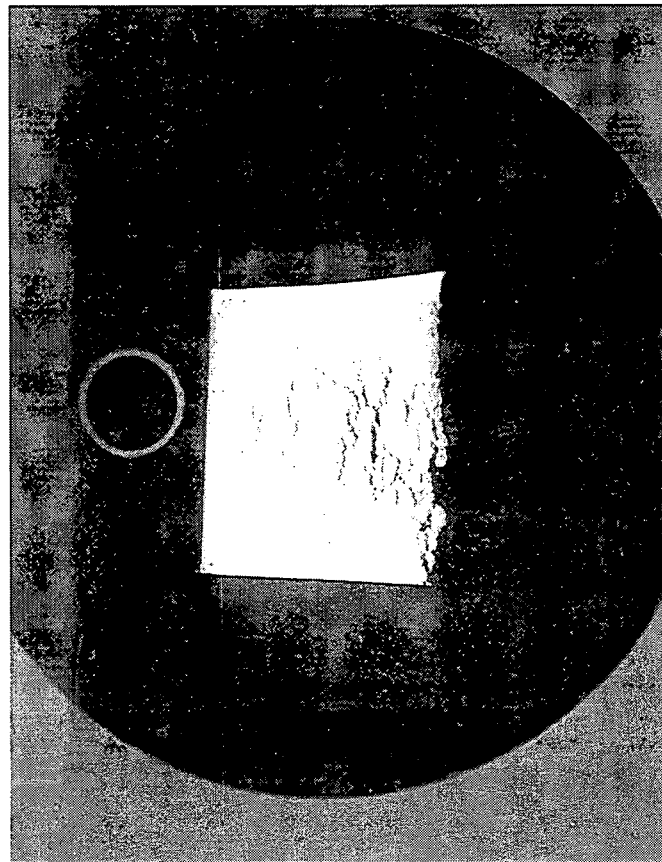


Figure 4-18 TSP1 crevice region Specimen 4B-2C of Tube R15C28. Radial metallographic sample after flattening and polishing to a depth of 0.005 inch below the OD surface. Mount M2161. Mag. 3.25X.

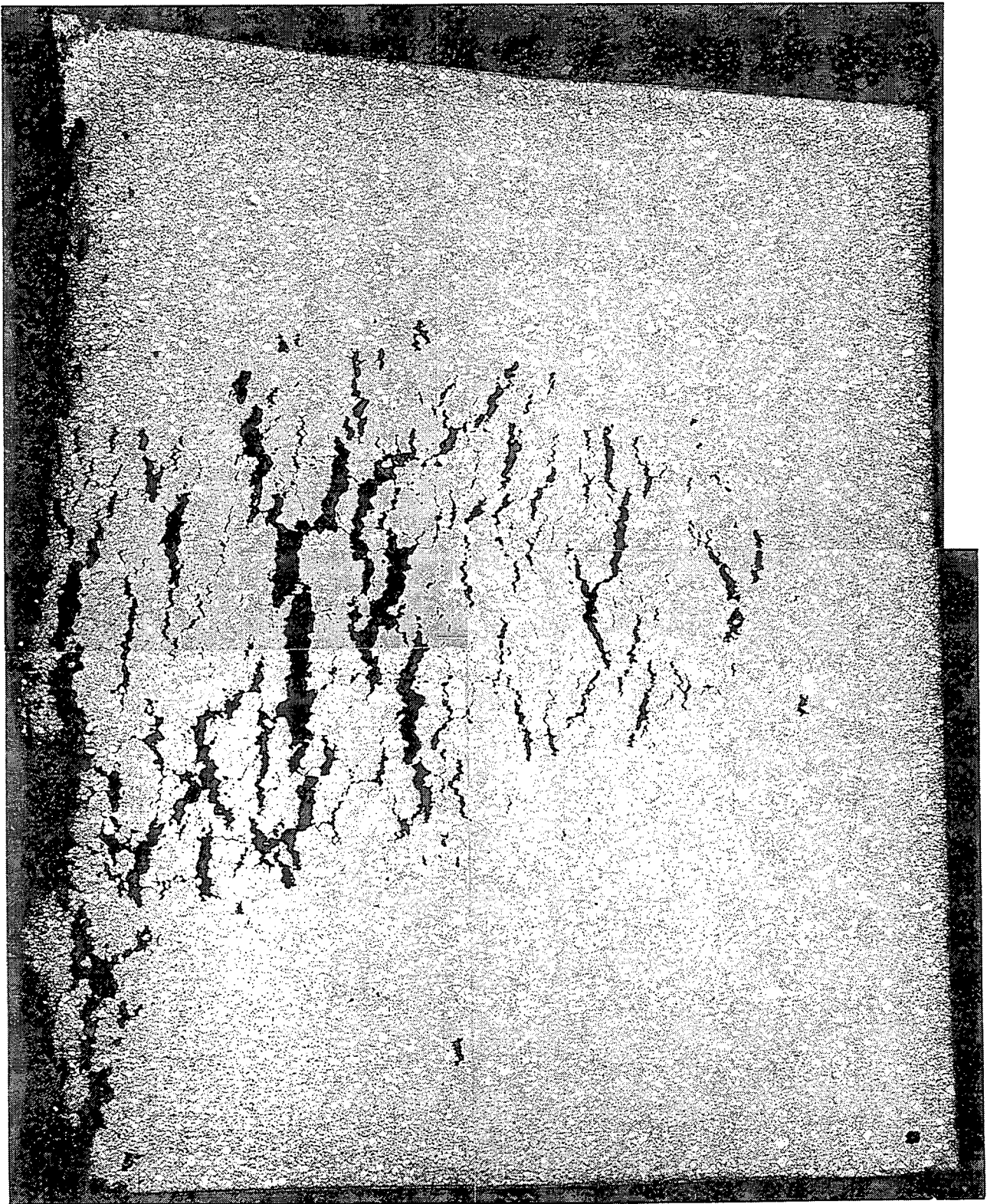


Figure 4-19 TSP1 crevice region Specimen 4B-2C of Tube R15C28. Radial metallographic sample after flattening and polishing to a depth of 0.005 inch below the OD surface. This montage is a higher magnification mirror image of Figure 4-18 because of the reversed optics of the two cameras. Mount M2161. Mag. 16X.

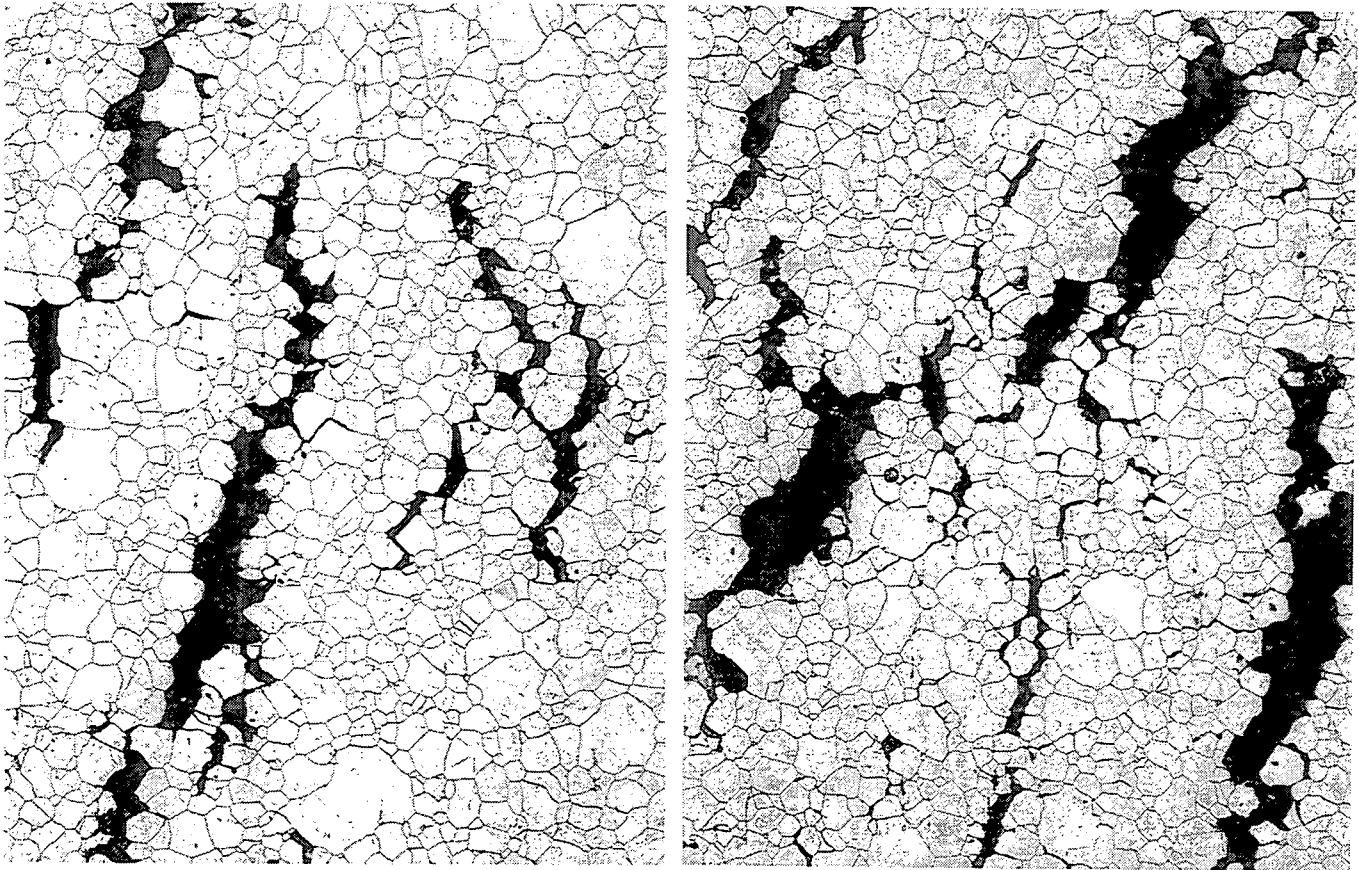


Figure 4-20 TSP1 crevice region Specimen 4B-2C of Tube R15C28. Radial metallographic sample after flattening and polishing to a depth of 0.005 inch below the OD surface. Examples of the corrosion crack pattern at this level of grinding and polishing. Mount M2161. Mag. 100X.

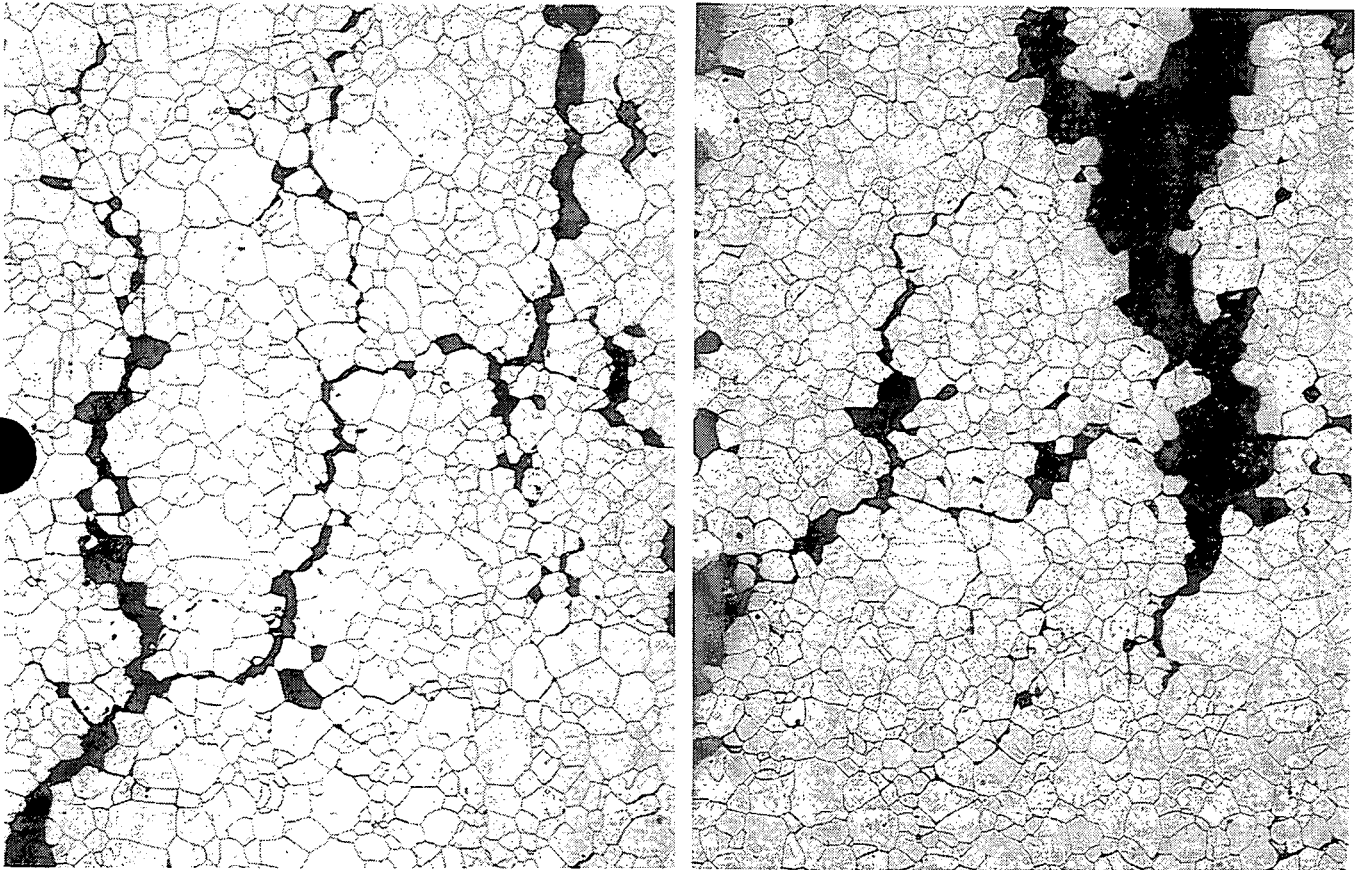


Figure 4-21 TSP1 crevice region Specimen 4B-2C of Tube R15C28. Radial metallographic sample after flattening and polishing to a depth of 0.005 inch below the OD surface. Examples of the corrosion crack pattern at this level of grinding and polishing. Mount M2161. Mag. 100X.

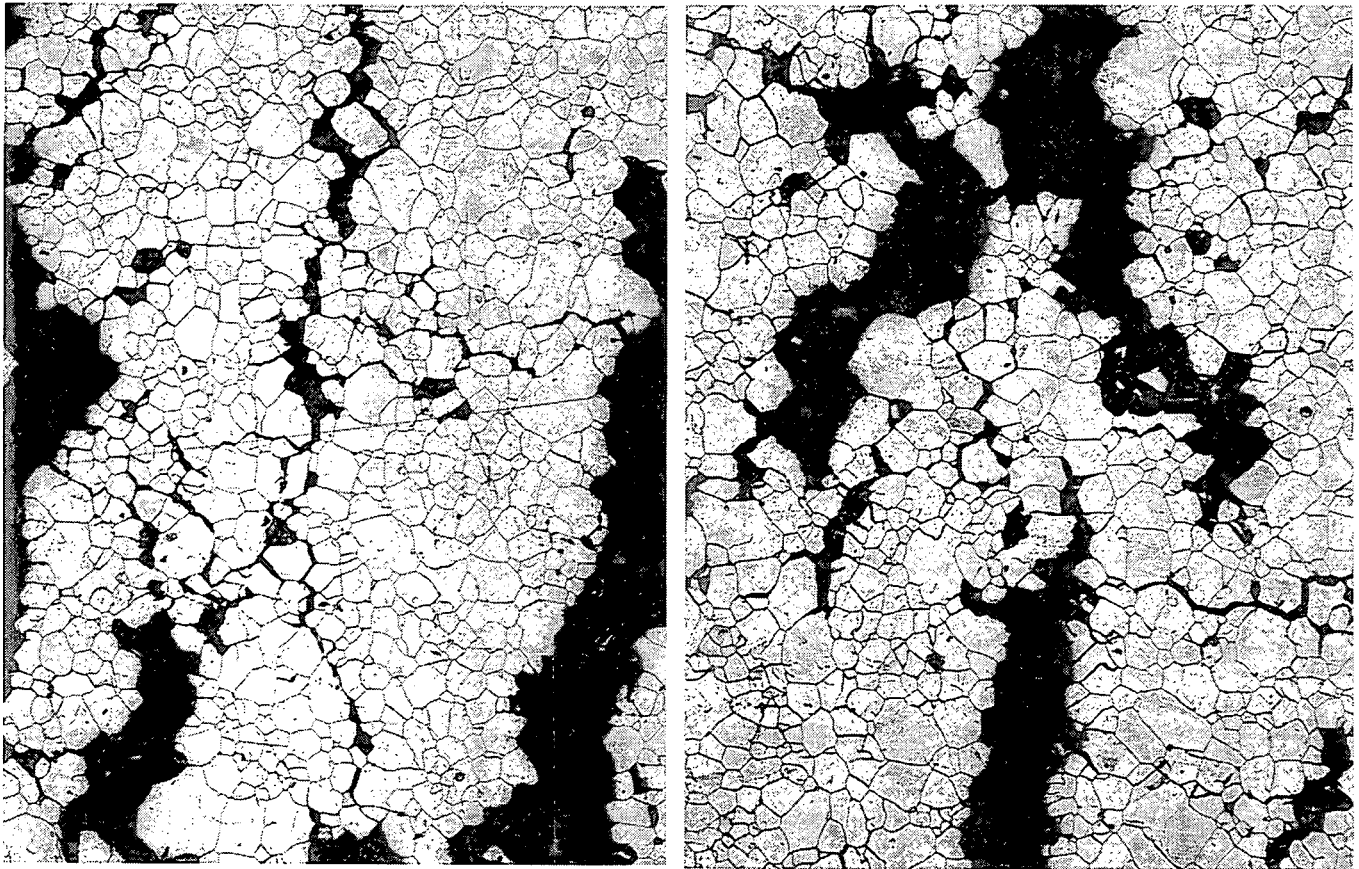


Figure 4-22 TSP1 crevice region Specimen 4B-2C of Tube R15C28. Radial metallographic sample after flattening and polishing to a depth of 0.005 inch below the OD surface. Examples of the corrosion crack pattern at this level of grinding and polishing. Mount M2161. Mag. 100X.

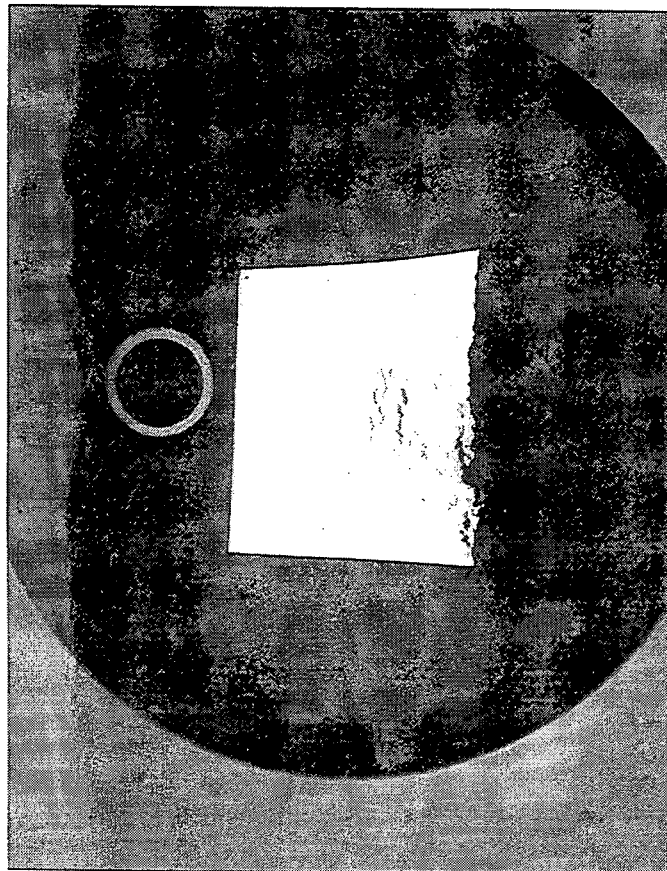


Figure 4-23 TSP1 crevice region Specimen 4B-2C of Tube R15C28. Radial metallographic sample after flattening and polishing to a depth of 0.010 inch below the OD surface. Mount M2161. Mag. 3.25X.

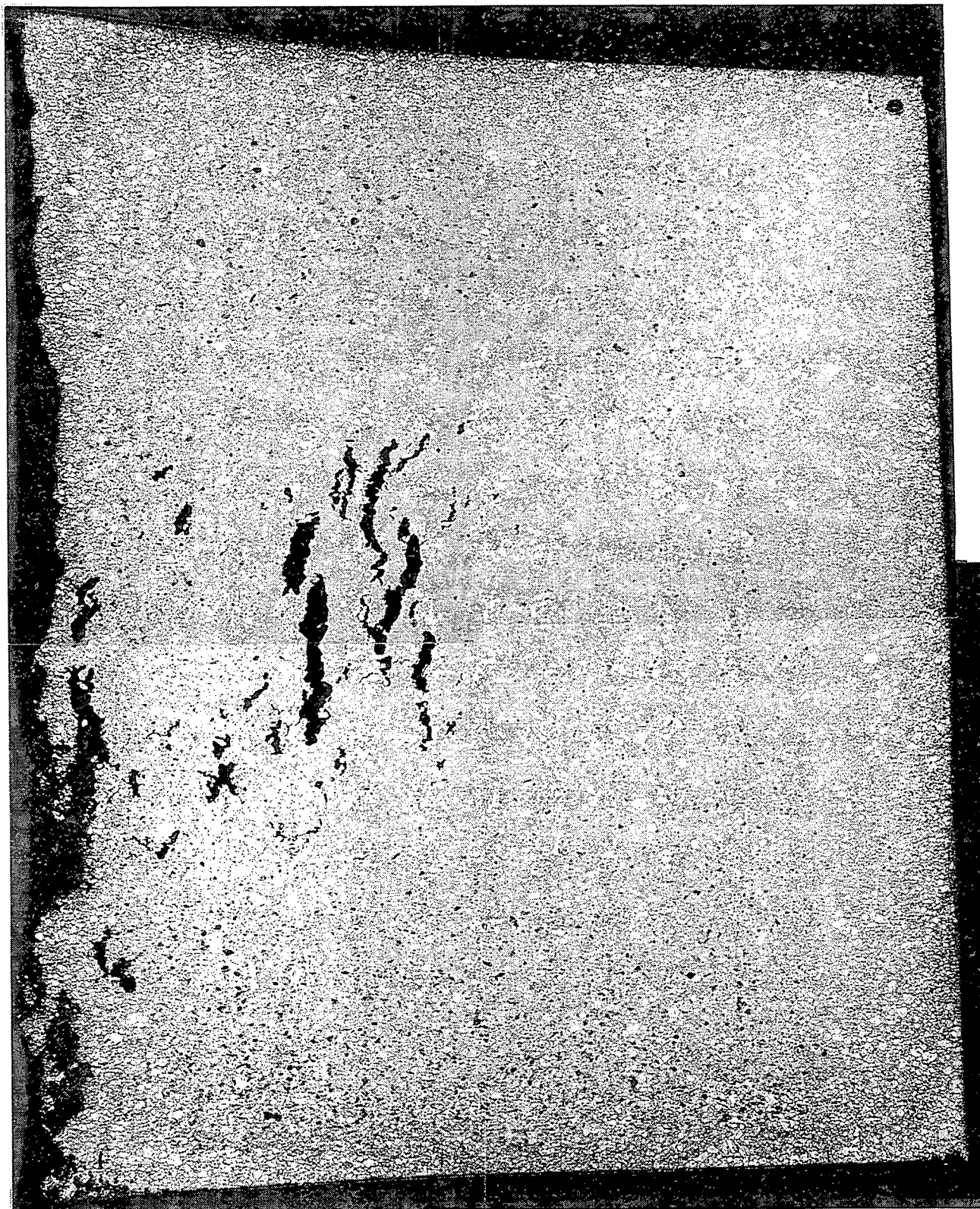


Figure 4-24 TSP1 crevice region Specimen 4B-2C of Tube R15C28. Radial metallographic sample after flattening and polishing to a depth of 0.010 inch below the OD surface. This montage is a higher magnification mirror image of Figure 4-23 because of the reversed optics of the two cameras. Mount M2161. Mag. 16X.

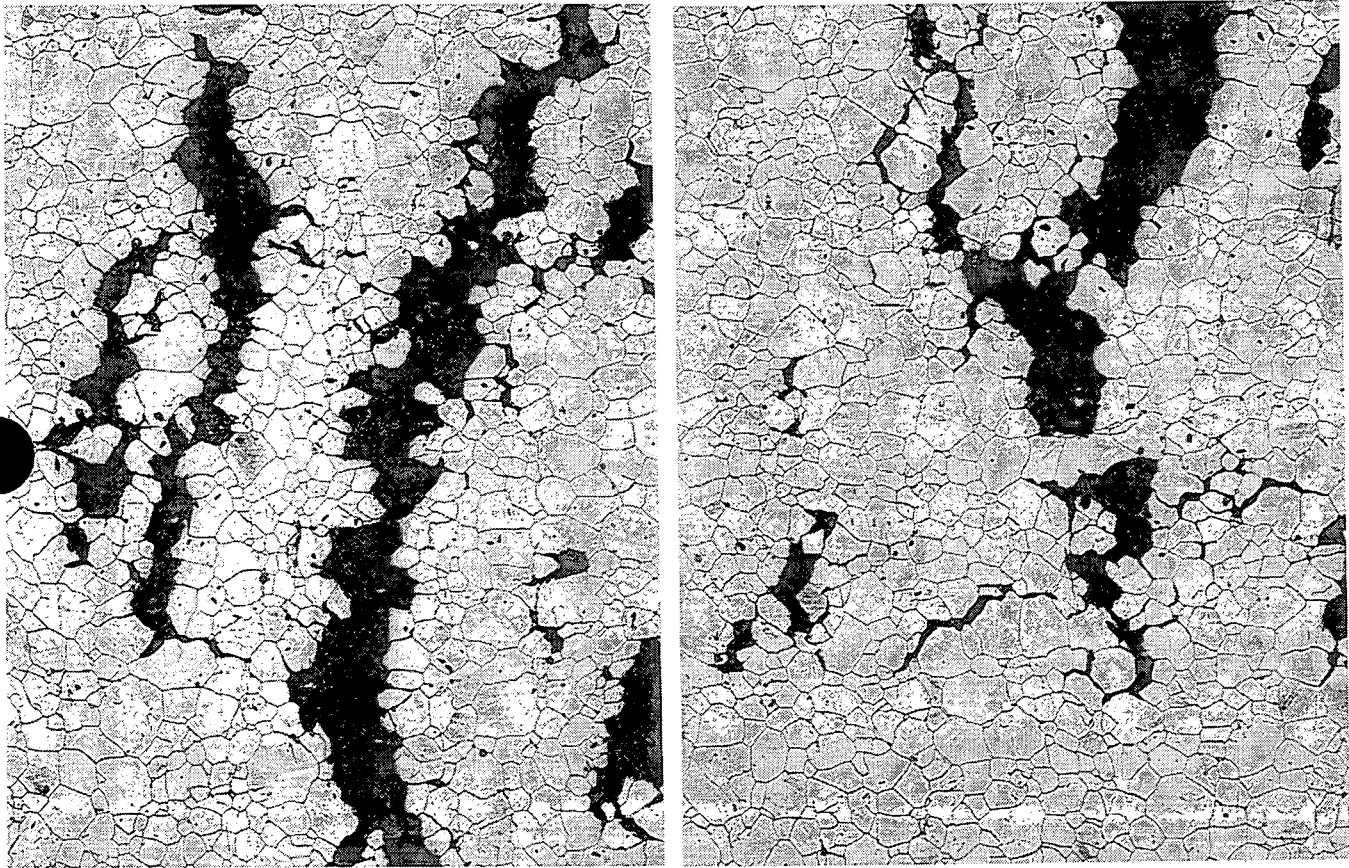


Figure 4-25 TSP1 crevice region Specimen 4B-2C of Tube R15C28. Radial metallographic sample after flattening and polishing to a depth of 0.010 inch below the OD surface. Examples of the corrosion crack pattern at this level of grinding and polishing. Mount M2161. Mag. 100X.

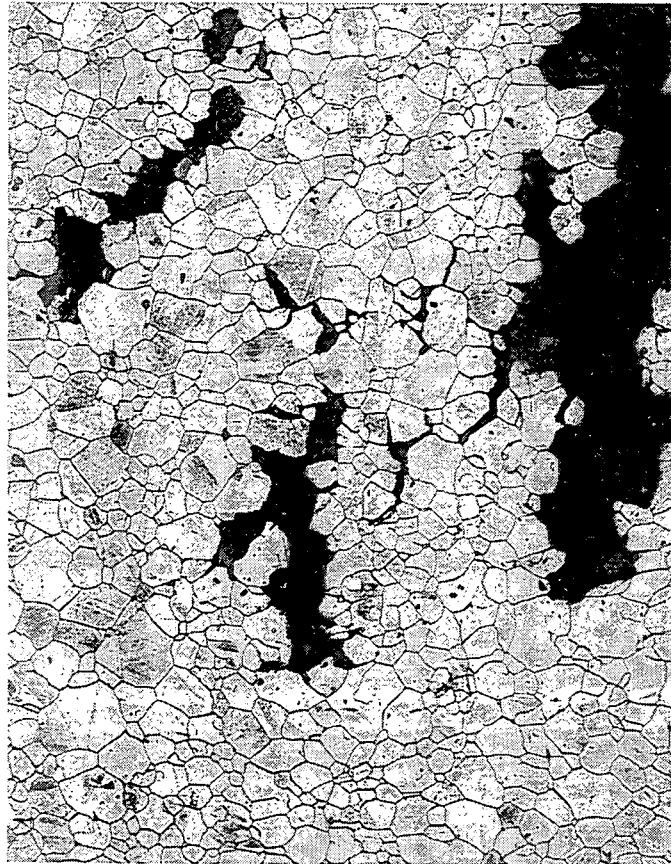


Figure 4-26 TSP1 crevice region Specimen 4B-2C of Tube R15C28. Radial metallographic sample after flattening and polishing to a depth of 0.010 inch below the OD surface. Example of the corrosion crack pattern at this level of grinding and polishing. Mount M2161. Mag. 100X.

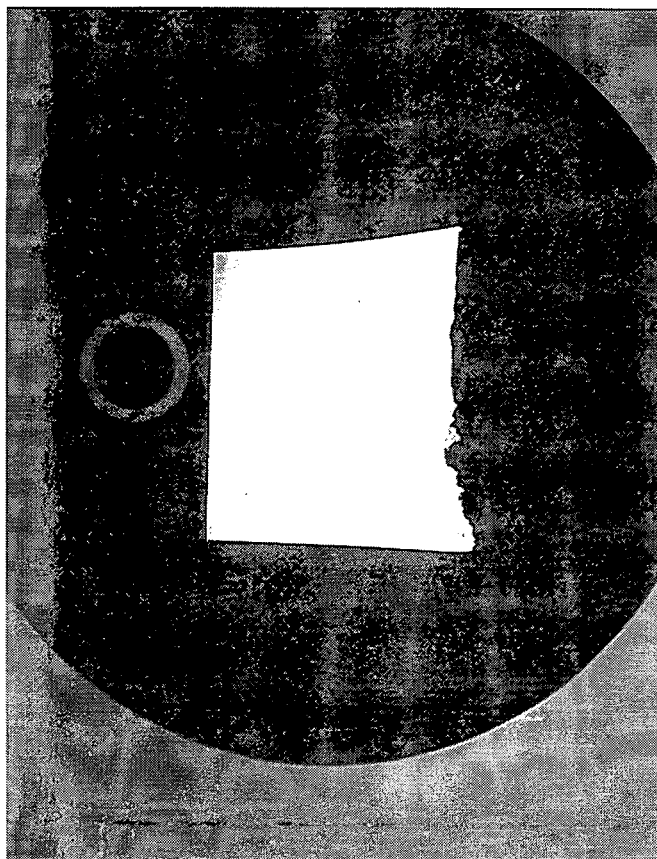


Figure 4-27 TSP1 crevice region Specimen 4B-2C of Tube R15C28. Radial metallographic sample after flattening and polishing to a depth of 0.015 inch below the OD surface. Note the absence of cracks at this level. Mount M2161. Mag. 3.25X.

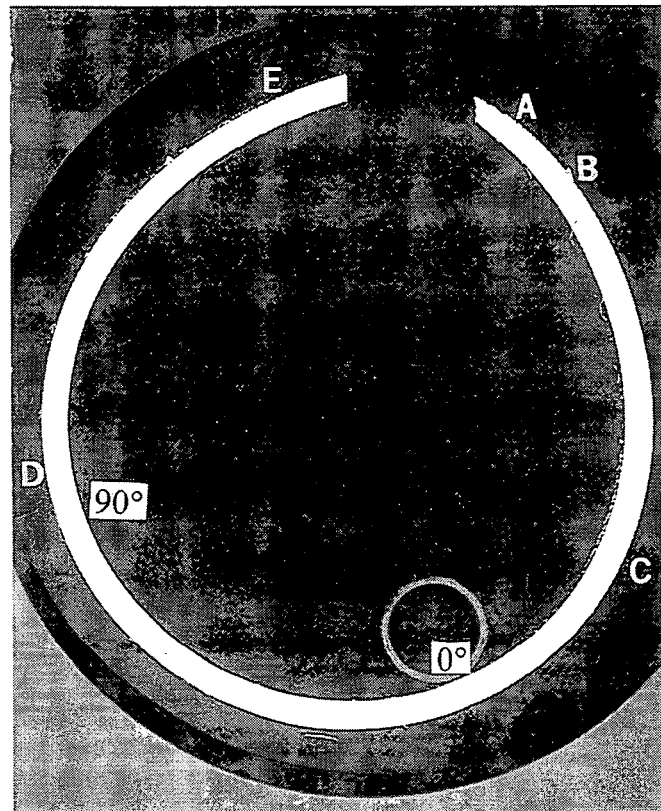


Figure 4-28 TSP1 crevice region Specimen 4B-2B of Tube R15C28. Transverse metallographic sample. Areas A through E are shown at a higher magnification in Figures 4-29 through 4-31. Mount M2160. Mag. 3.25X.

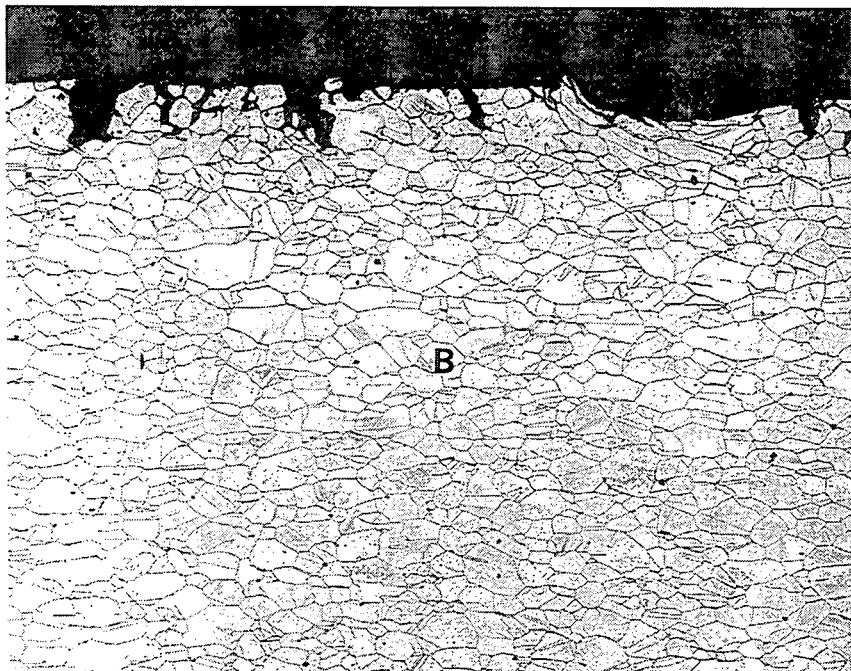
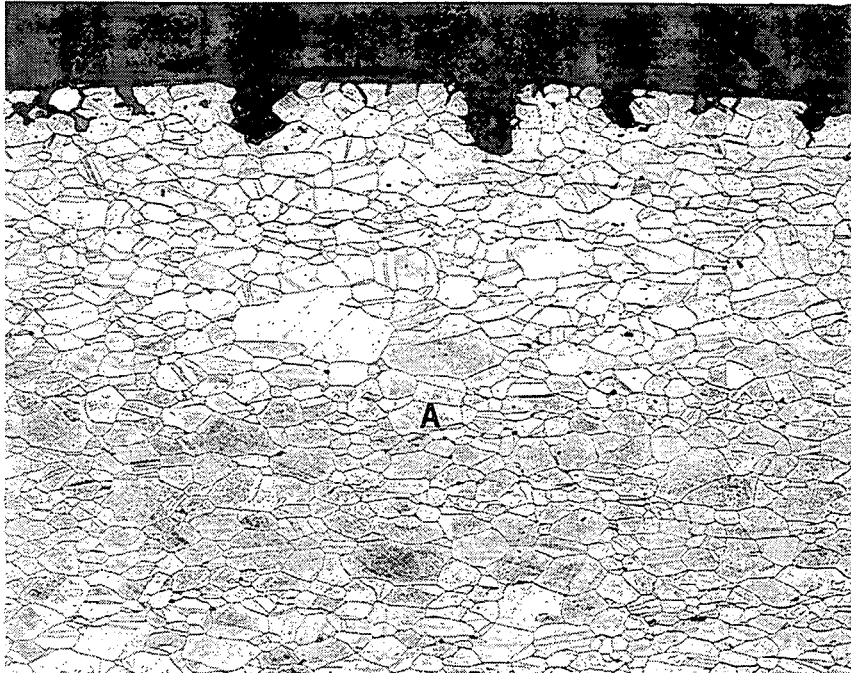


Figure 4-29 TSP1 crevice region Specimen 4B-2B of Tube R15C28. Transverse metallographic sample. Areas A and B from Figure 4-28 showing OD surface cracks at a higher magnification. Mount M2160. Mag. 100X.

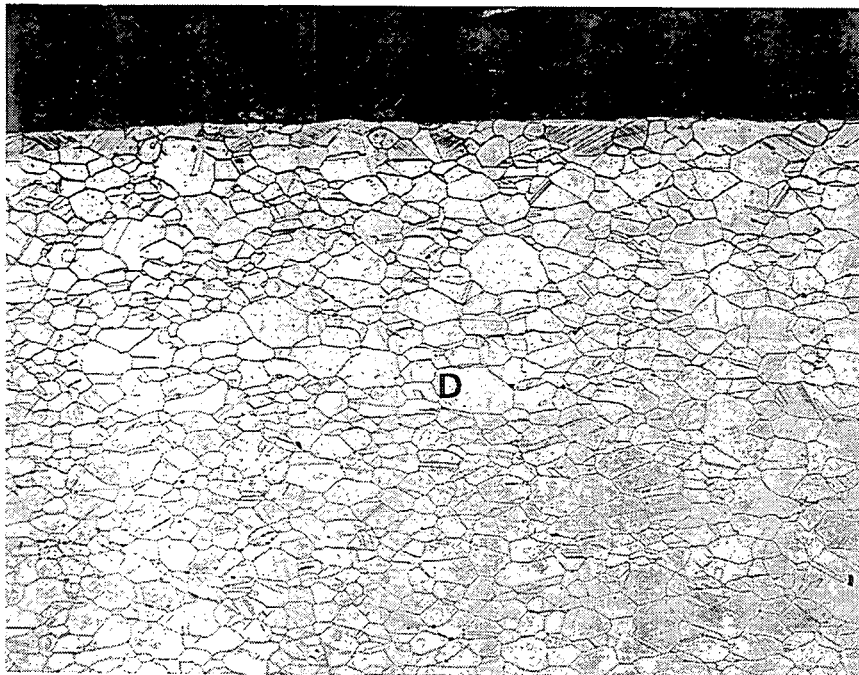
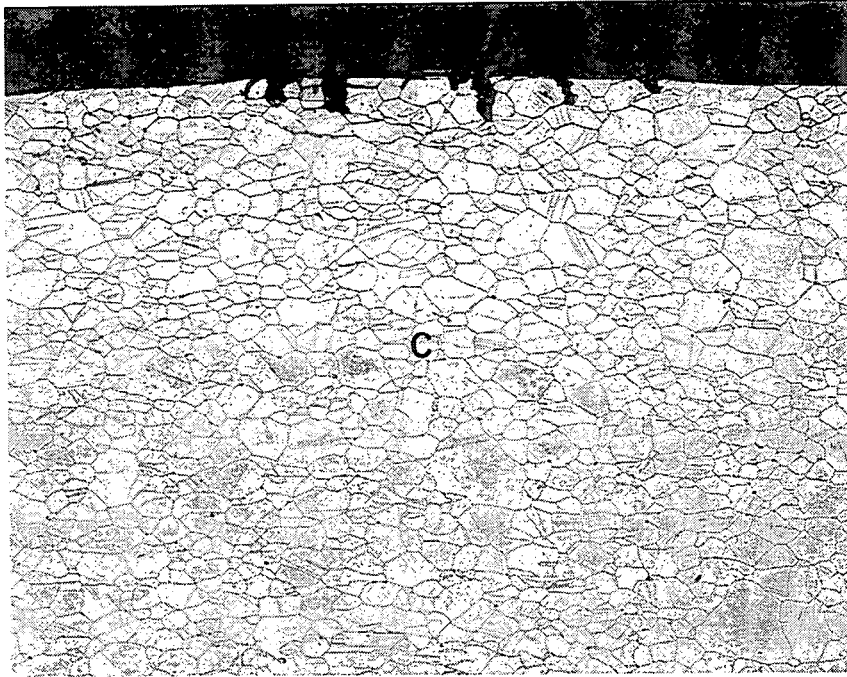


Figure 4-30 TSP1 crevice region Specimen 4B-2B of Tube R15C28. Transverse metallographic sample. Areas C and D from Figure 4-28 showing OD surface cracks at a higher magnification. Mount M2160. Mag. 100X.

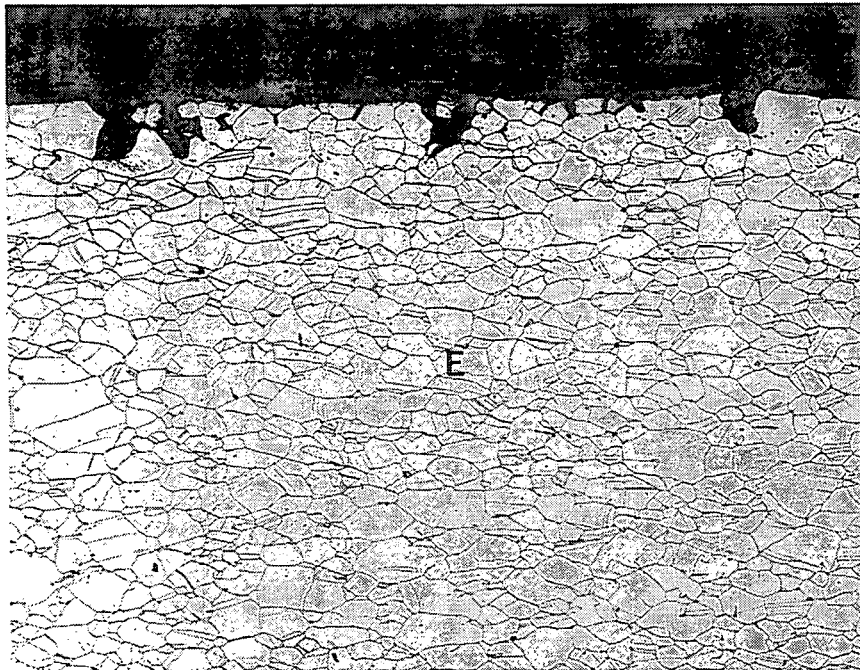


Figure 4-31 TSP1 crevice region Specimen 4B-2B of Tube R15C28. Transverse metallographic sample. Area E from Figure 4-28 showing OD surface cracks at a higher magnification. Mount M2160. Mag. 100X.

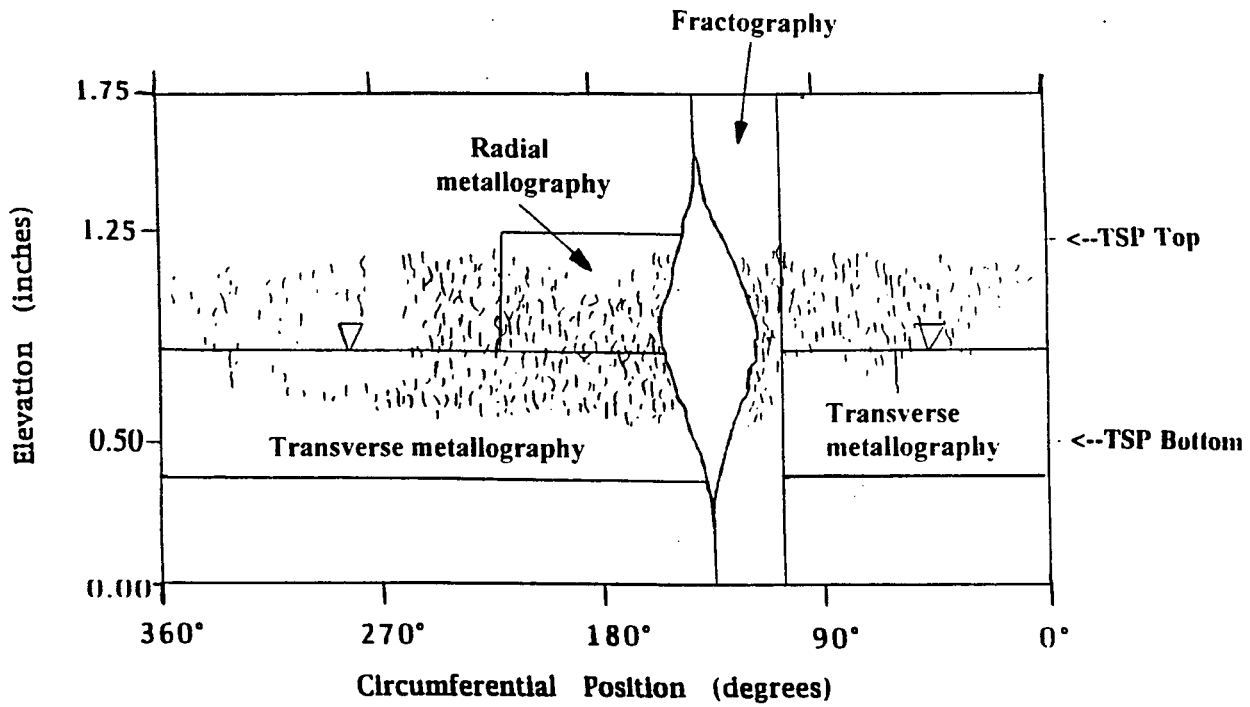


Figure 4-32 TSP2 crevice region Specimen 6B of Tube R15C28. Sketch showing the locations of the fractographic and metallographic samples used in the study of the crack distribution and morphology.

ANSTEC
APERTURE
CARD

Also Available on
Aperture Card

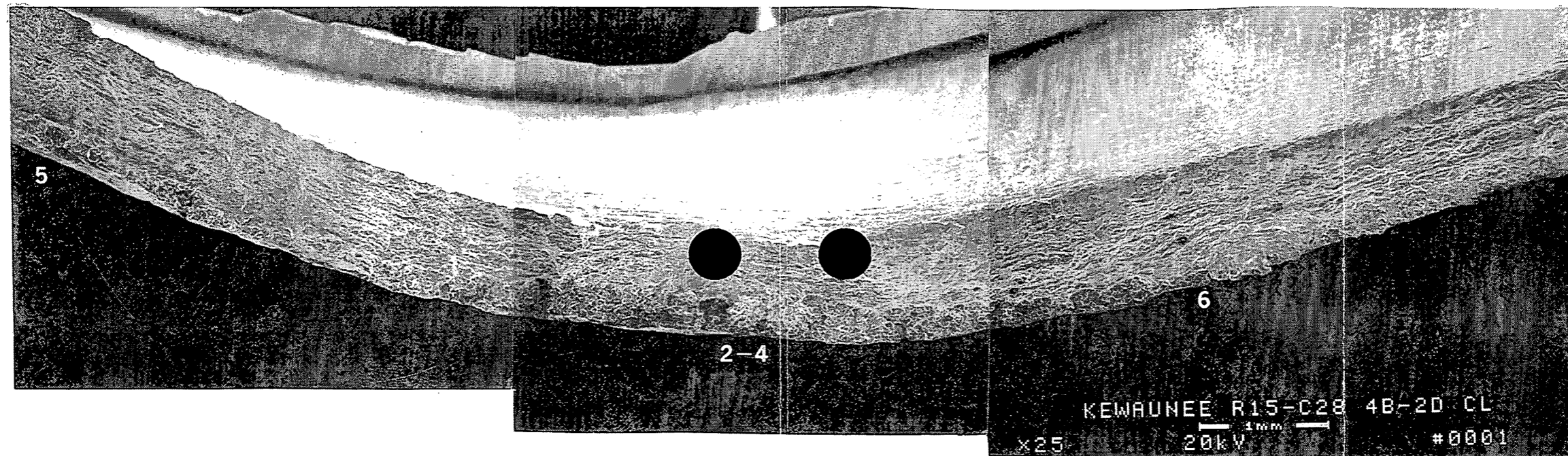


Figure 4-2 TSP1 crevice region Specimen 4B-2D of Tube R15C28. Top view of the opened burst fracture. Areas 2 through 6 of the fracture are shown at higher magnifications in Figures 4-3 through 4-5. Areas 5 and 6 mark the ends of the intergranular corrosion cracking on the OD which started the burst fracture.

9709080028-01

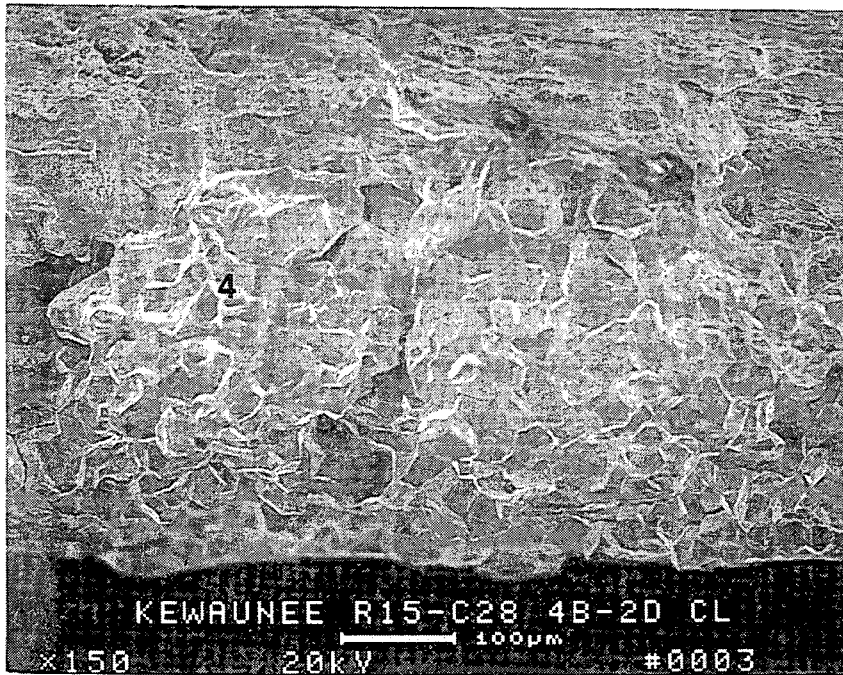
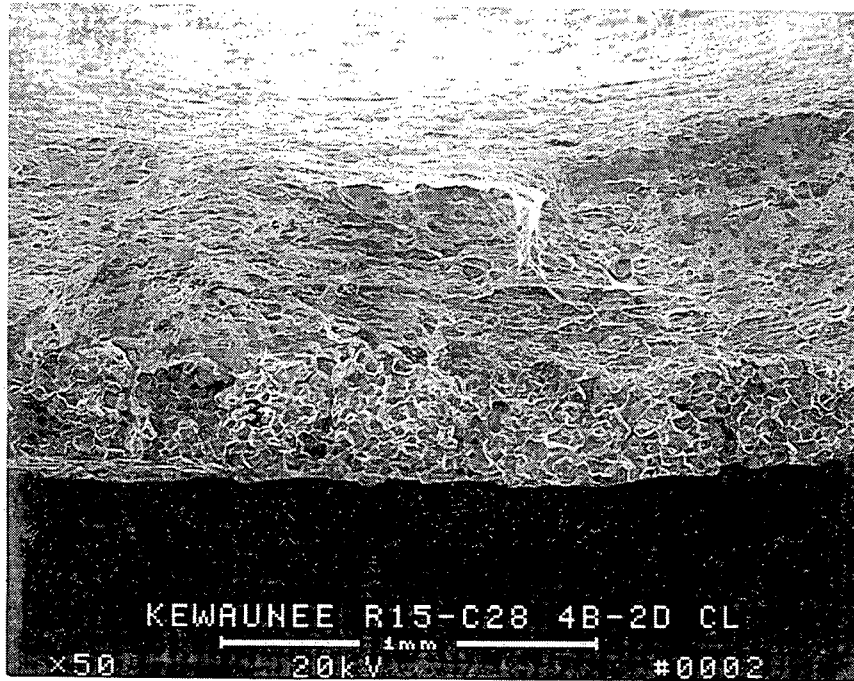


Figure 4-3 TSP1 crevice region Specimen 4B-2D of Tube R15C28. Areas 2 and 3 from figure 4-2, showing the topography of the burst fracture at the location of the deepest corrosion penetration (30% throughwall).

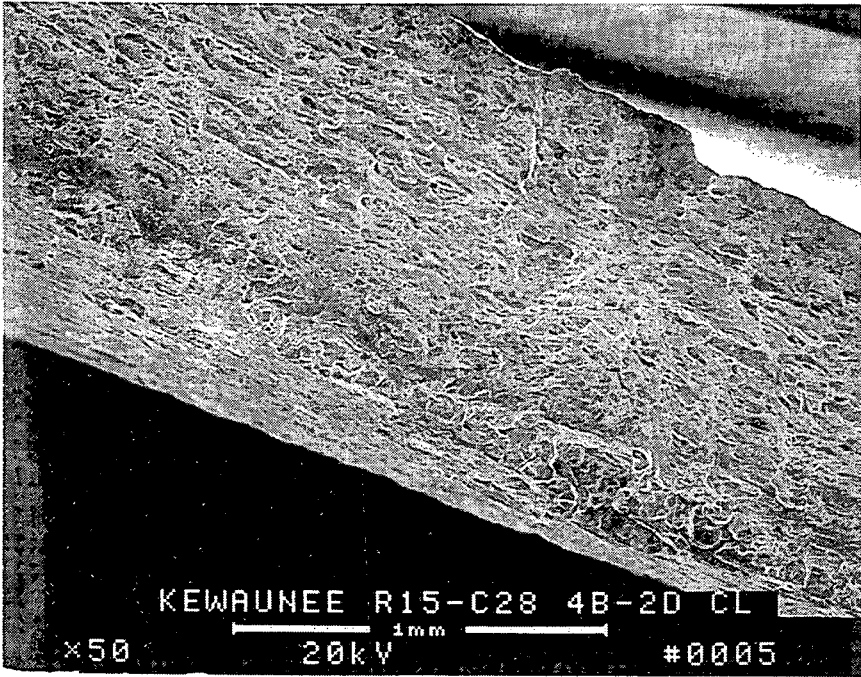
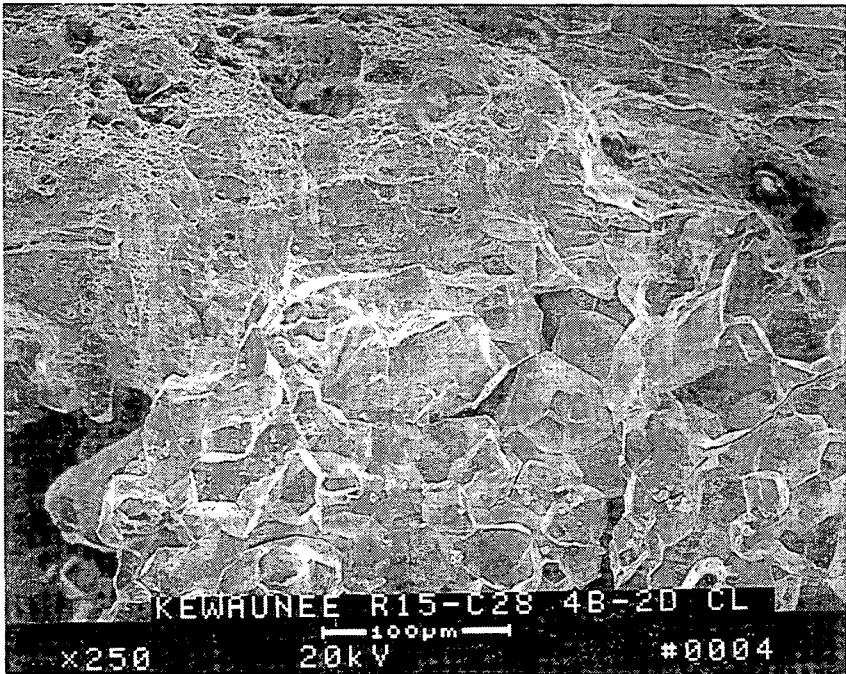


Figure 4-4 TSP1 crevice region Specimen 4B-2D of Tube R15C28. Upper photograph: Area 4 from Figure 4-3 showing the boundary between the field corrosion crack at the point of deepest penetration and the laboratory fracture produced during the burst test.

Lower photograph: Area 5 from Figure 4-2 showing the left end of field corrosion cracking on the burst test fracture.

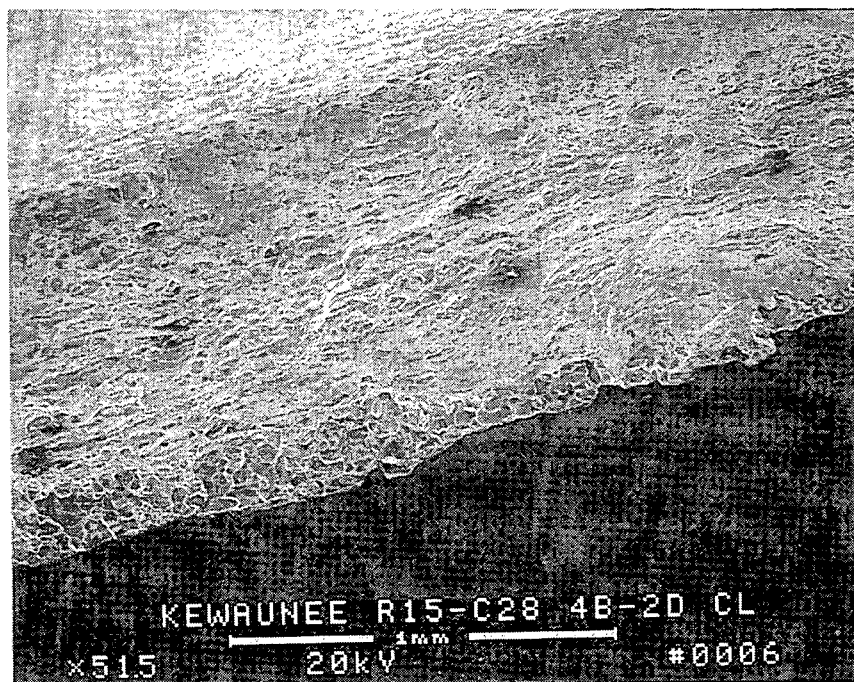


Figure 4-5 TSP1 crevice region Specimen 4B-2D of Tube R15C28. Area 6 from Figure 4-2 showing the right end of field corrosion cracking on the burst test fracture.